Universidade do Minho
Escola de Engenharia

Filipe Tiago de Matos

Seismic behavior assessment of CLT buildings applying current regulation approaches

Novembro de 2020

Seismic behavior assessment of CLT buildings applying current regulation approaches
Filipe Tiago de Matos
UMinho | 2020

Universidade do Minho
Escola de Engenharia

Filipe Tiago de Matos

Seismic behavior assessment of CLT buildings applying current regulation approaches

Tese de Doutoramento
Engenharia Civil

Trabalho realizado sob a orientação do
Professor Doutor Jorge Manuel Gonçalves Branco
Professor Doutor Patrício António Almeida Rocha

Novembro de 2020

DIREITOS DE AUTOR E CONDIÇÕES DE UTILIZAÇÃO DO TRABALHO POR TERCEIROS

Acknowledgments

I want to express my gratitude to all those who have helped me throughout these years, without whom this Ph.D. thesis would not have been possible.

My sincere gratitude to my supervisors, Professor Jorge M. Branco and Professor Patricio Rocha, mentors of all work, who shared all the availability and dedication to the success of this work.

I also want to express my gratitude to the technicians of the Structures Laboratory of the Civil Engineering Department at the University of Minho for the time and dedication given during the experimental campaigns. In particular, Marco and Mr. Matos, who also provided discussions and experience, not forgetting the friendship given over these years.

In particular, I am grateful to Dr. Mario Marques for the time available and for sharing all the knowledge, enlightening me various points of research.

To all PhD students and post-doc colleagues in the Civil Engineering Department of University of Minho, with special affection to timber group, Hélder Sousa, Maxime Verbist, Leonardo Rodrigues and Elisa Poletti; office mates Cristina, Abide, Elisabete and Pilar; and last but not less important to Luís Carlos, Luís Miguel, Chandan, João and Joana.

I want to dedicate this thesis to all my family, close friends, and my goddaughter Alice. To my parents Rui Matos and Maria Tiago and brother Hugo Matos for their continued support in life, where they always supported me in everything; to long-time friends, where I hope not to forget any: André, Bruno Costa, Pedro Sousa, Emanuel, Pedro Aires, Sara Leitão, Bruno Abadesso, Adão, Bruno Miguel, Carolina, Rita, João, Sónia, Sara Vaz, Diogo, Helena, Hélder and Flávio; to the friends I won in my degree in Viana do Castelo, José, Carlos Gonçalves, Fábio, Pedro, Miguel, Carlos Ferreira, Nelson, Guilherme, Vasco, Luís and Filipe.

Lastly, I would like to acknowledge the financial support provided by Stora Enso Wood Products company.

STATEMENT OF INTEGRITY

I hereby declare having conducted this academic work with integrity. I confirm that I have not used plagiarism or any form of undue use of information or falsification of results along the process leading to its elaboration.

I further declare that I have fully acknowledged the Code of Ethical Conduct of the University of Minho.

University of Minho, 24 November 2020

Name: **Filipe Tiago de Matos**

Signature:

Resumo

Na procura de novas soluções de utilização de materiais à base de madeira, naturais e totalmente renováveis, e com o objetivo de aplicar a construção em madeira em diferentes sistemas estruturais, a Madeira Lamelada Colada Cruzada (MLCC) oferece uma solução, alternativa ao betão armado, de excelente qualidade. A MLCC é um painel multicamadas, inicialmente desenvolvido na Suíça na década de 1990, que apresenta potencialidades para a sua utilização em paredes e pavimentos estruturais. Por se tratar de um material relativamente recente, existe ainda uma grande carência de conhecimento das condições para a sua utilização.

Deste vazio de conhecimento resultou a motivação para o presente trabalho que estuda o comportamento de estruturas em MLCC, à ação sísmica através da análise *pushover*. Para concretizar este objetivo, apresenta-se; inicialmente, uma campanha experimental realizada aos conetores metálicos típicos da construção MLCC, cujo resultado passou pela aferição do comportamento de cada um dos conetores a cargas monotónicas e cíclicas; de seguida, apresenta-se uma campanha experimental a um edifício MLCC de 2 andares, à escala real, testado em plataforma, com o objetivo de analisar a resposta global da estrutura, com principal foco no desempenho das paredes paralelas à resposta da estrutura; caracterizar os respetivos mecanismos de rotura; e o desempenho das conexões entre painéis e conetores metálicos.

Numa segunda fase, os resultados experimentais foram usados para a calibração de um modelo numérico, (programa comercial de elementos finitos Dlubal RFEM) do edifício ensaiado em laboratório. Neste processo foram estudadas diferentes curvas experimentais dos conetores metálicos e foi avaliada a influência do atrito na interface de ligação entre painéis. Depois da aferição dos resultados obtidos, e tendo em conta um dos objetivos principais deste trabalho, realizou-se a análise *pushover* com a aplicação do método N2 em dois casos de estudo, aferindo os resultados obtidos para diferentes espectros de resposta elásticos. Por fim, propõe-se algumas recomendações que poderiam vir a ser consideradas na regulamentação, nomeadamente, no Eurocódigo 8, para melhor adequar a sua utilização ao projeto sísmico de estruturas MLCC.

Palavras-chave: Comportamento sísmico, Estruturas MLCC, Eurocódigo 8, Segurança estrutural.

Abstract

In the search for new solutions using wood-based materials, therefore, natural and renewable, and aiming to take timber construction to different structural systems, more demanding, Cross Laminated Timber (CLT), is an interesting alternative to concrete. CLT is a multi-layered shell product designed in Switzerland, in the early 1990s. The panels are prefabricated and have many advantages for both walls and floors. Being a relatively recent material, it is completely omitted on current European regulation.

Therefore, with the lack of information, the present work studies the seismic action to CLT buildings, through the pushover analysis defined in regulation EC8. To contextualize this objective, presents, initially, an experimental campaign carried out for the typical metal connectors of the CLT construction, where the result was to analyze the behavior of each connector to monotonic and cyclic loads. The following is an experimental campaign to a 2-story full-scale CLT platform-type building, where the objectives were to analyze the 3-D system performance, with the main focus on the performance of the shear walls, failure mechanisms, and performance of connections between panels and metal connectors.

In a second phase, the experimental results have been used for the calibration of a numerical model (Dlubal RFEM commercial finite element program) for the experimentally tested building. The finite element models have been studied with different experimental curves of the metal connectors, where the presence of friction has been considered and analyzed. After validation of the obtained results, and taking into account one of the main objectives of this work, the pushover analysis was performed with the application of the N2 method for two study cases, where different elastic response spectra have been considered. Finally, recommendations have been proposed for the seismic design of CLT structures, which could be contributing to the new generation of Eurocode 8.

Keywords: Seismic Behaviour, CLT structures, Eurocode 8, Structural Safety.

Table of Contents

List of Figures

List of Tables

Chapter 1

Introduction

1.1 Context of the research

Cross Laminated Timber (CLT) is a multi-layered shell product developed in Switzerland, in the early 1990s, where it has been created in search of new solutions using wood-based materials, aiming to take timber construction to different structural systems. Being a relatively recent material, it is completely omitted on current European regulation, like EC5 [1]. However, the research activities have increased drastically, and several CLT handbooks or state-of-the-art have been prepared for different markets, e.g., Canadian [2], US [3] and European [4].

Looking at the subject of this research, seismic analysis is considered one of the most important subjects for Civil Engineering, in which it has developed seriously in recent years. Therefore, being an action of Nature, it is indispensable to quantify it, where the design methods, whether by numerical or analytical methods, continue to have high uncertainties.

This thesis focuses on the seismic behavior assessment of CLT buildings, through experimental and numerical approaches. Experimental evaluations are extremely important for the validation of numerical methods, being the main ones responsible for creating a reliable design. Thus, in the first phase, two experimental analyses were carried out. One for typical metal connectors, highlighting the application and analysis of a proposal for the revision of the EN 12512 [5] and the other for a 2-story CLT platform type building.

On the other hand, in the numerical approach, the first step was to develop a finite element model that could be easily applied in commercial software, where the objective was to predict the response of the experimentally analyzed building. To predict the building responses, a pushover analysis has been applied to two examples, in which the performance of the structures has been quantified through the methodology of Annex B of Eurocode 8, better known as the N2 method.

1.2 General objectives

This work addresses a seismic behavior assessment of CLT buildings applying current state-of-the-art approaches. The main objective is to study the behavior of structures subjected to lateral quasi-static actions, where the focus was mainly on the creation of a seismic design methodology with an accessible application, without creating many complexities. In the same context, the new proposal

under the review of chapter 8 of Eurocode 8 seeks to provide more detail for the design of timber structures. Therefore, for CLT structures, the objectives of this study are:

- Evaluation of the behavior of metal connectors applying the new proposal of EN 12512;
- To assess the seismic behavior of CLT buildings aiming the analysis of the 3D system performance when subjected to lateral loads;
- Creation of a simplified finite element methodology to perform pushover analysis;
- Finally, to propose recommendations for the implementation of pushover analysis to CLT buildings in the new generation of Eurocode 8.

1.3 Outline and thesis overview

The thesis can be separated into two different approaches: experimental and numerical, as shown in Figure 1.1. The experimental approach has applied for the study of the real behavior of CLT buildings and each component under lateral loads. On the other hand, the numerical approach has used for the prediction of the real behavior of CLT buildings and the application of the pushover analysis with the help of the N2 method. In terms of the document, the chapters are separated as follows:

- In chapter 1, the general context of the research is presented. Moreover, the objectives of each chapter are described;
- In chapter 2, a literature review of relevant topics of CLT construction is presented. First, it presents the CLT material, the most remarkable buildings in the world, and the typical connections of CLT construction. Then, focusing on the seismic analysis, an experimental analysis performed on CLT buildings, shear walls, and metal connectors are presented and analyzed. Last but not least, numerical predictions of buildings analyzed experimentally are described;
- In Chapter 3, an experimental campaign is presented regarding the assessment of typical metal connectors used in CLT buildings. Special attention has been given to the validation of the Setup carried out at the University of Minho and the proposal for a revision of standard EN 12512. Besides, the presence of an acoustic layer in the metal connectors and the study of a new configuration of the uplift connector have been studied;

- In Chapter 4, an experimental campaign for a real-scale 2-story CLT building under lateral loads is described and discussed. The analysis performed for longitudinal and transverse directions, where special attention has been given to the 3D performance system;
- In Chapter 5, the methodology proposed to predict the experimental results of the CLT building tested in chapter 4 is described. For the development of the methodology, special attention has been given to the experimental analysis on the metal connectors described in chapter 3. The prediction and comparison with the experimental analysis have been performed for different force-displacement curves of the metal connectors, where the influence of friction has been also discussed;
- In Chapter 6, a numerical evaluation of two examples is described. For this purpose, a pushover analysis has been applied with the help of the N2 method. The study was performed for different structural assemblies and a different number of floors. Besides, different geographic locations and different elastic spectra with distinct seismic actions have been selected;
- Finally, in Chapter 7, recommendations and conclusions are summarized. Moreover, some suggestions for future actions are proposed.

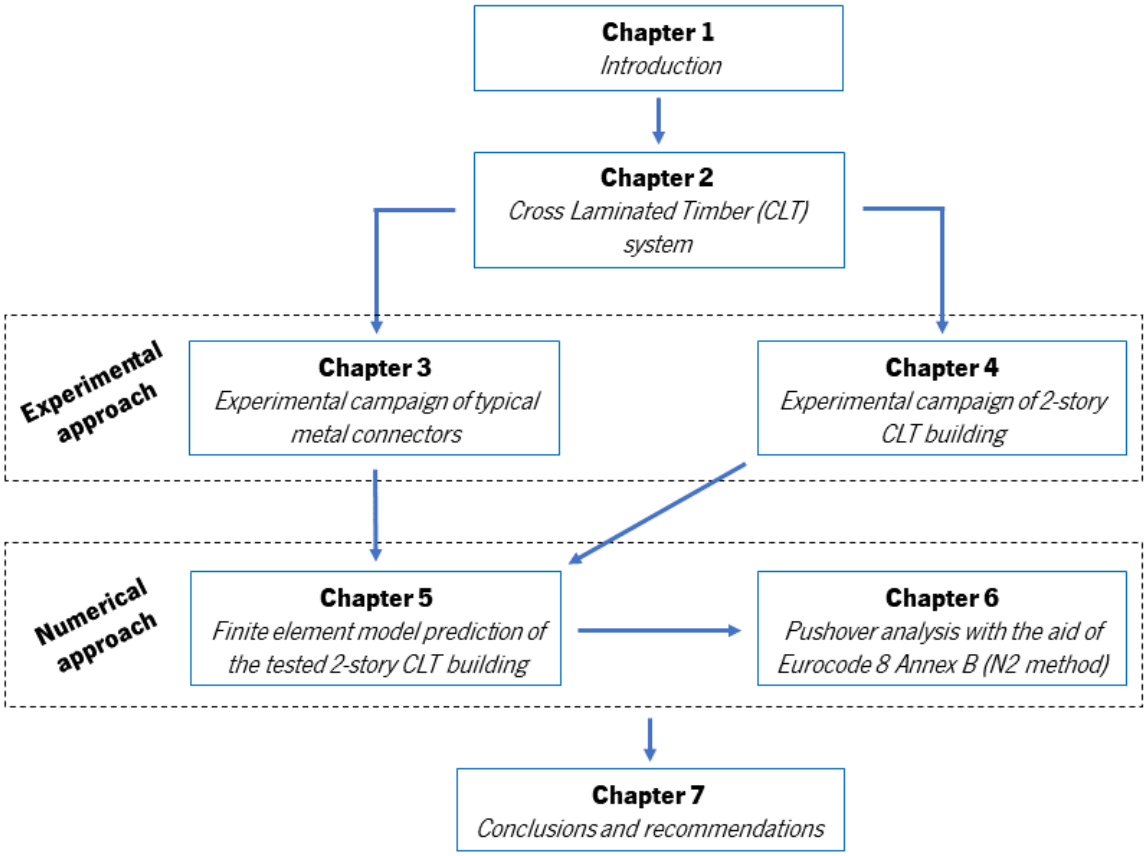

Figure 1.1 – Schematic overview of the thesis.

Chapter 2

Cross Laminated Timber (CLT) system

Wood is considered the oldest building material, played a prominent role in human life. However, over time and with the arrival of concrete and steel, wood lost importance in the construction field. It was considered an easily flammable material with low durability and, therefore, it was surpassed by other materials with smaller risks.

Wood as a building material offers an excellent good ratio of weight-resistance and a reduced environmental impact (structural product obtained from sustainable and renewable resources) when compared to the other materials, like concrete and steel (see Figure 2.1). Regarding the durability of the material, maintenance is essential.

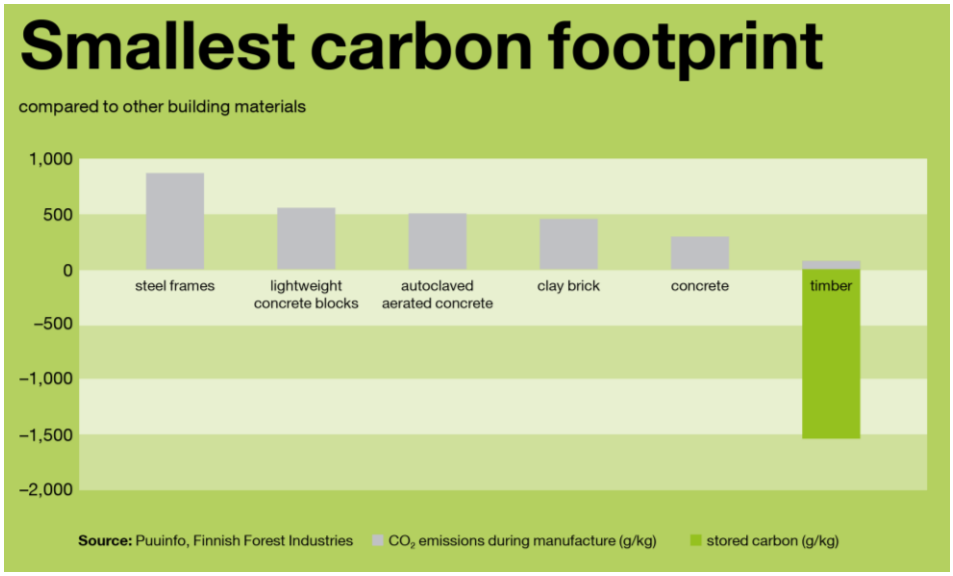

Figure 2.1 – Carbon footprint of building materials [6].

In the search for new solutions using wood-based materials, and aiming to take timber construction to different structural systems, a new material was created, Cross Laminated Timber (CLT) (see Figure 2.2).

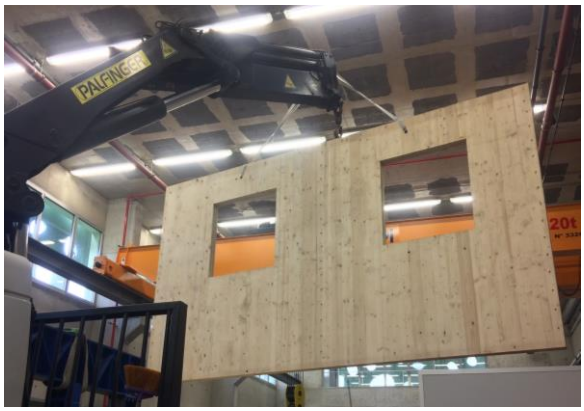

Figure 2.2 – Cross Laminated Timber panels.

Cross Laminated Timber (CLT) is a multi-layered product, designed in Switzerland in the early 1990s, that offer strength, stiffness, and stability. It is a competitive replacement for traditional structural materials such as steel, concrete and masonry. The most common wood species used is the spruce, where each lamella is glued to each other with a non-toxic and environmentally friendly adhesive. To obtain the strength required, each lamella is positioned perpendicularly to the one below, where after it will be hydraulically pressed to form the material (see Figure 2.3).

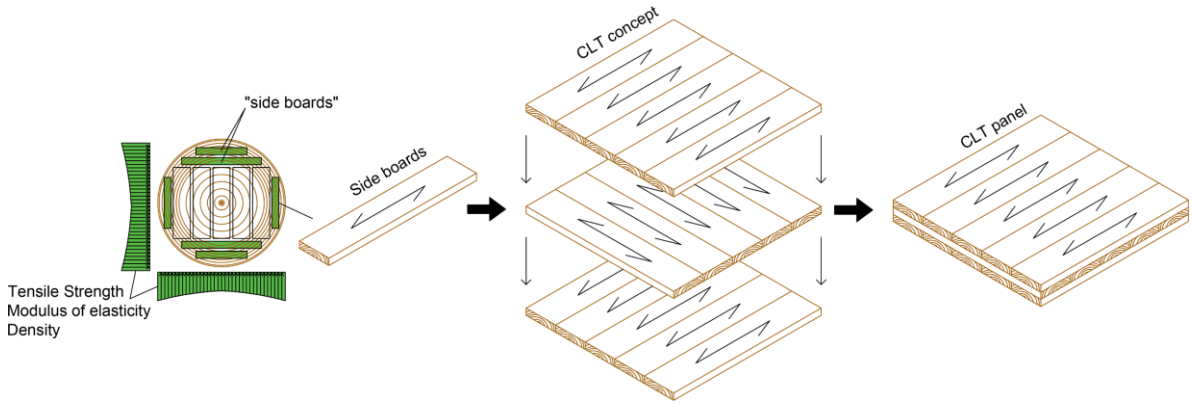

Figure 2.3 – CLT concept from the wood selection to the panel [2, 7].

The density of CLT material is approximately 400 kg/m^3 in the case of spruce [8, 9]. However, the value may vary: for example, Stora Enso Wood Products presents a value of 470 kg/m^3 [6] because of the product requirements (e.g. timber, adhesives, end joints and laminations, and glue line integrity) [10]. Panels can be applied to both walls and floors, and the windows and doors openings can be pre-cut at the factory.

Currently there are several examples of applying these panels, mostly around Europe, USA, and Australia. The most remarkable examples are: Stadthaus building with 8-story of timber and 1-story of concrete (see Figure 2.4a); Forté building with 9-story of timber and 1-story of concrete (see Figure 2.4b); Bridport House building of 8-story (see Figure 2.4c); The Treet with 14-story of timber and 1-story of concrete (see Figure 2.4d); Dalston Lane with 9-story of timber and 1-story of concrete (see Figure 2.4e); and, more recently, the 25 king with 9-story of timber and 1-story of concrete (see Figure 2.4f). Some of them are not exclusively in CLT but also with Glulam (glued laminated timber).

(a) Stadthaus in 2008 (United Kingdom) [11]

(b) Forté building in 2012 (Australia) [12]

(c) Bridport House in 2011 (United Kingdom) [13]

(d) The Treet in 2015 (Norway) [14]

(e) Dalston Lane in 2016 (United Kingdom) [15]

(f) 25 king in 2018 (Australia) [16]

Figure 2.4 – Remarkable buildings made of CLT.

2.1 Structural material

As a structural element, the CLT panel must have at least three layers, with the orientation of each layer is stacked crosswise. However, to obtain specific structural capacities, consecutive layers with the same direction may exist. Panel dimensions vary by manufacturer but are usually limited due to transportation. The panel can be installed as a floor or wall, in which the orientation is defined according to the structural case (see Figure 2.5).

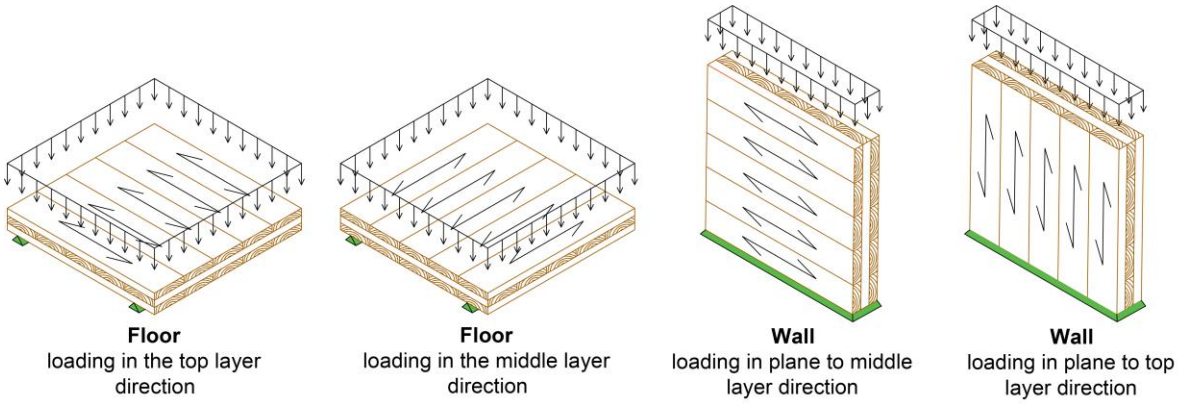

Figure 2.5 – Loading on CLT panels [2, 17].

The panel offers resistance in both directions, but the major strength direction is on the external layer direction. However, it is important to note that the panel strength is mainly limited by the "Rolling-shear" behavior between opposite layers interface that presents low resistance because of its constructive anisotropy. To exemplify this behavior, Figure 2.6 shows the different shapes of stresses for the major and minor strength direction of the panel.

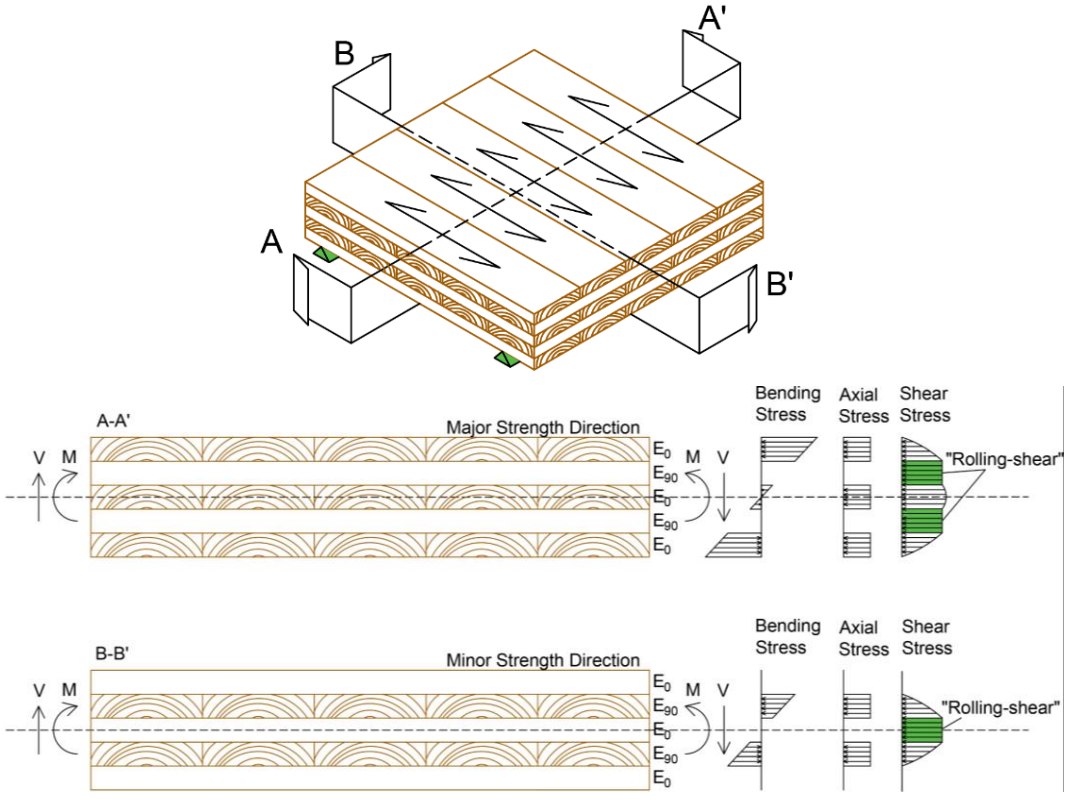

Figure 2.6 – Bending, axial, and shear stresses of a CLT element (5-layers) [2, 18].

Regarding the mechanical properties of the CLT panel, some of the properties may differ from manufacturer to manufacturer, as consequences of differences in the production process (see Table 2.1). Concerning the boards used to make the panels, they mainly have C24 strength (see EN 338:2009 [19]).

Table 2.1 – Properties (N/mm²) of CLT with C24 boards from main manufacturers [6, 20, 21].

Manufacturer		Binderholz	Stora Enso	KLH
Modulus of Elasticity				
Parallel to the grain direction	$E_{0, mean}$	12000	12500	12000
Shear Modulus				
Parallel to the grain direction	G_{mean}	690.0	690.0	690.0
Perpendicular to the grain direction	$G_{r, mean}$	50.0	50.0	50.0
Bending Strength	$f_{m, k}$	18.0/24.0	24.0	24.0
Tensile Strength				
Perpendicular to the grain direction	$f_{t, 0, k}$	10.2/14.0	14.0	16.5
Compression Strength				
Perpendicular to the grain direction	$f_{c, 0, k}$	21.0	21.0	24.0
Shear Strength				
parallel to the grain direction	$f_{v, k}$	2.5	4.0	2.7

2.2 Connections

The metal connections between the different CLT panels are crucial to ensure an adequate overall behavior of the system, keeping the different structural elements connected, while the local behavior of joints is fundamental to assure the deformability, ductility, and energy dissipation capacities needed. In these circumstances, depending on the location of the panels and their structural behavior, Figure 2.7 shows the different typical connection regions of the CLT construction [2].

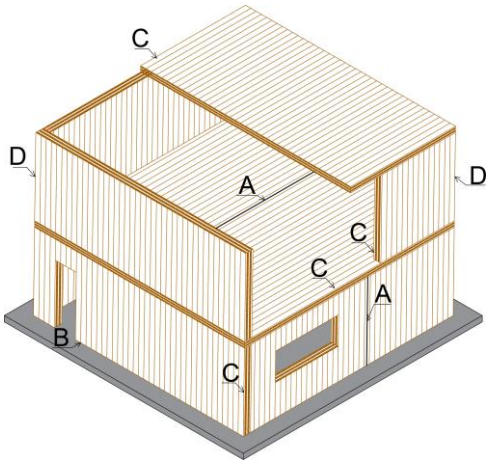

Figure 2.7 – Typologies of connection in CLT structures [2].

The typology referenced as A (see Figure 2.7), it is related to segmented walls or floors, where they are usually carried out due to transport limitations. Thus, to ensure the continuity of the panels, can be introduced a wooden spline (Plywood or Laminated Veneer Lumber) inserted in the middle (see Figure 2.8a) or into the upper (see Figure 2.8b) of the section, making a half-lapped joint in the panels (see Figure 2.8c) or even the insertion of a wooden spline in the upper and lower part (see Figure 2.8d).

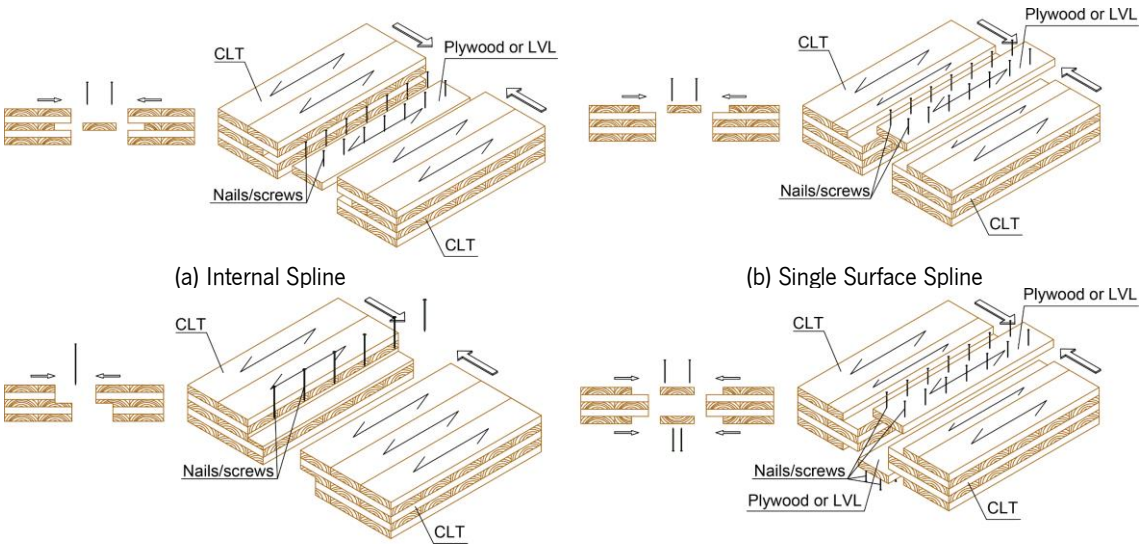

Figure 2.8 – Typical connections of segmented walls and floors [2].

In terms of the connection between concrete elements and CLT walls referenced as B (see Figure 2.7), in the case of a concrete base (CLT constructions in height it is common to perform the 1st floor on concrete), an angle metal bracket can be inserted (see Figure 2.9a). However, in the case of the existence of a concrete beam, a vertical metal bracket can be introduced into the wall (see Figure 2.9b). To protect the wood and ensure the durability of the panels, it can be inserted into an SCL layer (structural composite lumber), as can be seen in see Figure 2.9 (blue layer).

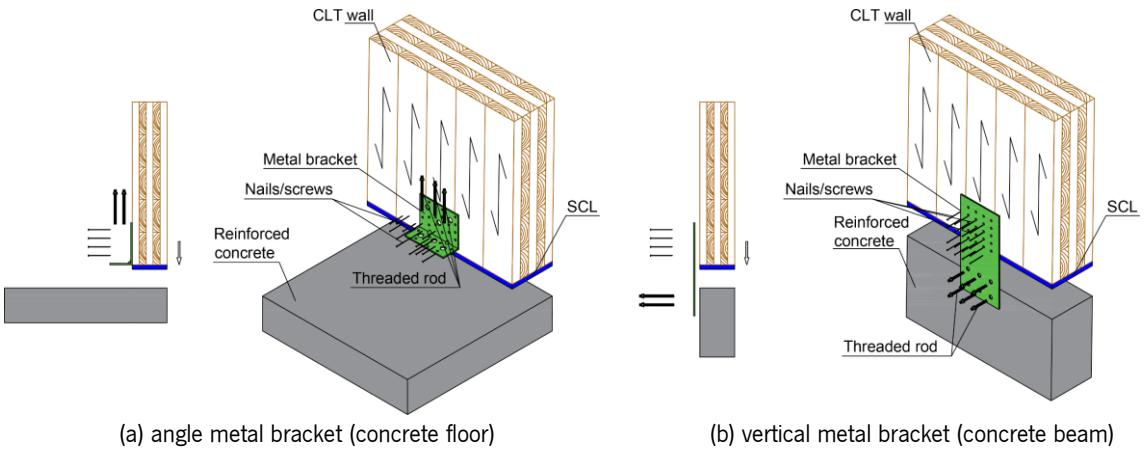

Figure 2.9 – Typical connections of the concrete-CLT wall [2].

On the other hand, in the existence of a CLT element as a floor, referenced as C (see Figure 2.7), it can be connected by screws or nails to the lower wall and connected through a metal bracket to the upper wall (see Figure 2.10a). In this case, the connection can also be performed by introducing two metal brackets, one in the upper part and another in the lower part, as can be seen in Figure 2.10b. In a roof situation, the same construction process can be performed excluding the top wall connection.

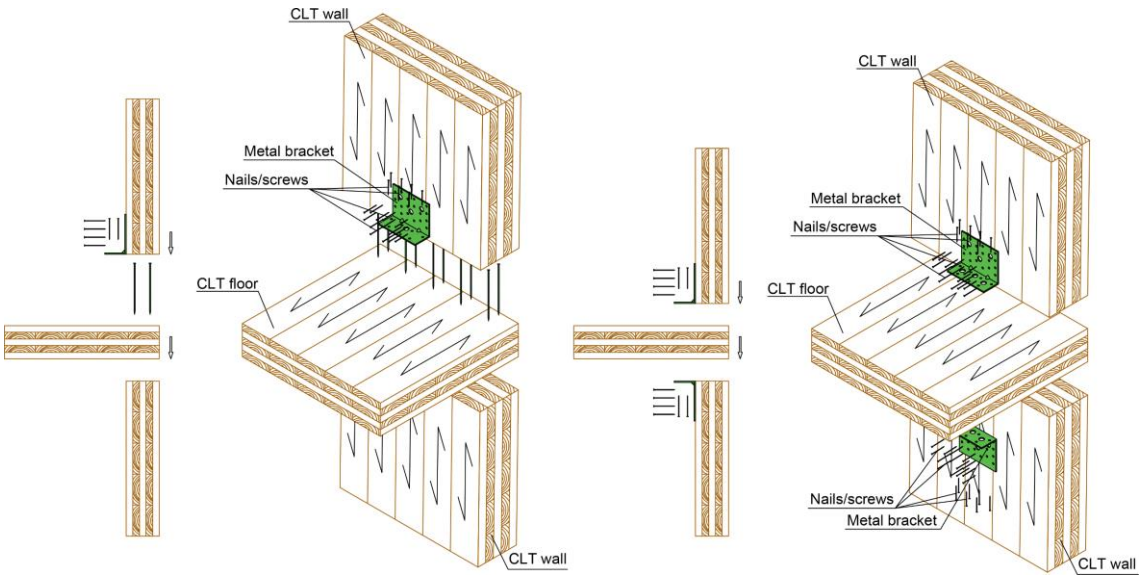

(a) metal bracket and self-tapping screws (b) metal bracket

Figure 2.10 – Typical connections wall-floor-wall [2].

Finally, concerning the connections of corners and crossings of walls, referenced as D (see Figure 2.7), it can be screwed at the intersection, whether horizontal (see Figure 2.11a) or inclined (see Figure 2.11b). Furthermore, the connection can also be made through the introduction of metal brackets, as can be seen in Figure 2.11c and Figure 2.11d.

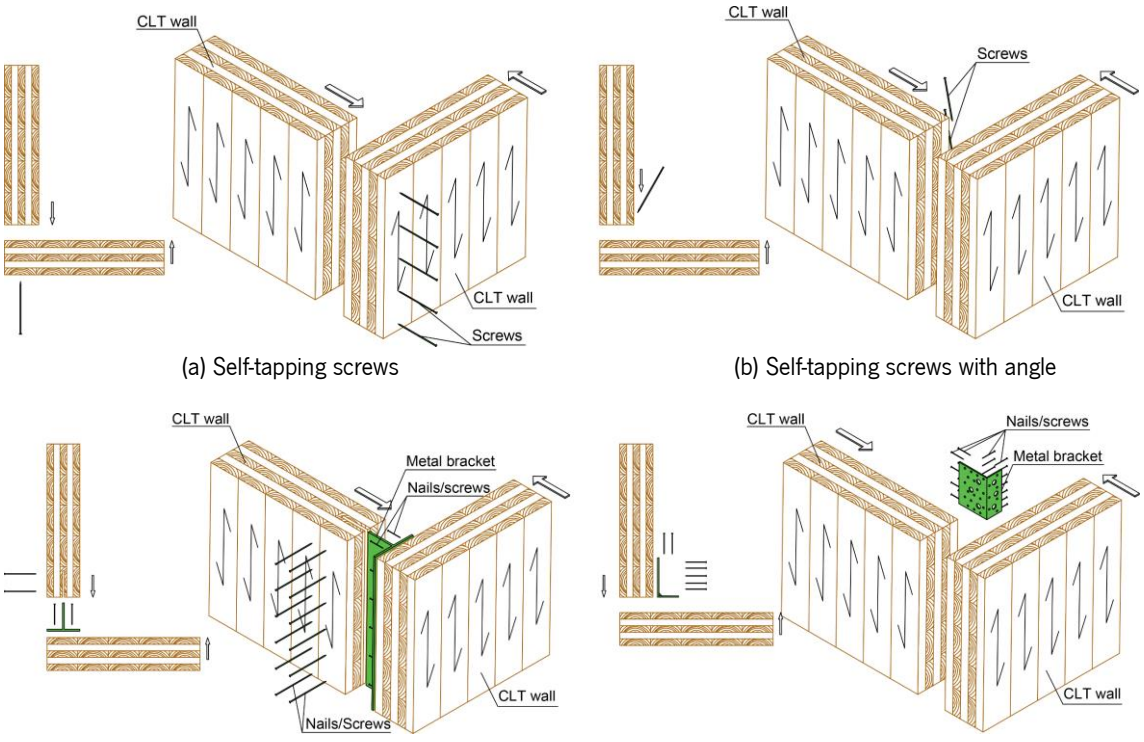

(a) Self-tapping screws (b) Self-tapping screws with angle

(c) Concealed metal bracket (d) Internal metal bracket

Figure 2.11 – Typical connection of corners and crossings walls [2].

2.3 Seismic resistance

Looking into the field of seismic resistance, several research projects have been developed to understand the performance of timber buildings. The first steps were taken by analyzing the behavior of light-frame structures (they represent the most common structures in the world at the time). The real-scale shaking table tests resulted in a good energy dissipation, where it was possible to verify that most of the plastic deformations were concentrated in the metal connectors angle brackets and hold-downs and in the sheathing-to-framing joints. In this way, to take seismic performance to another level, the focus at this time is the seismic analysis of CLT buildings, where presents greater in-plane stiffness and higher load-carrying capacity [22]. Therefore, the following are described the dynamic tests on real-scale CLT buildings, quasi-static CLT buildings, 2D CLT shear walls, metal connectors, and the numerical models.

2.3.1 Dynamic tests on real-scale CLT buildings

Among the tests performed on a shaking table, it is important to point out the SOFIE project, in which: a three-story building (see Figure 2.12a); with 7 m x 7 m in plan and 10 m of total height, including the roof, was tested with three different configurations (variation of openings as can be seen in Figure 2.12b). The building was subjected to a series of 26 earthquakes, (including the 1995 great Hanshin-Awaji earthquake in Kobe), at the NIED Laboratory, in Tsukuba, in July 2006. The building resisted 15 destructive earthquakes without any serious damage and no significant torsion was recorded [23].

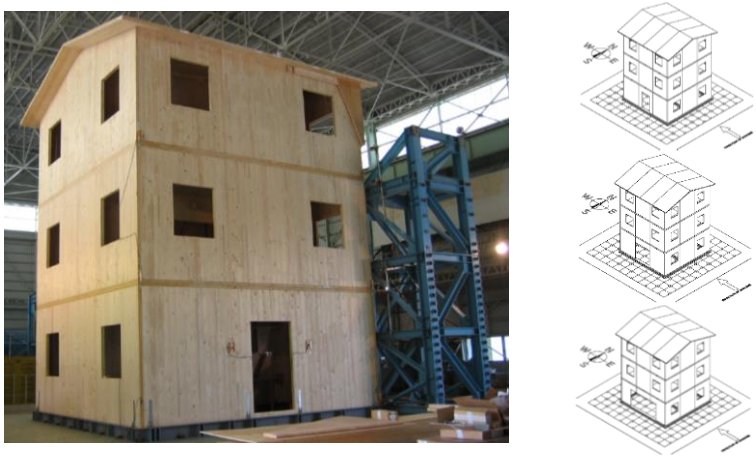

(a) (b)

Figure 2.12 – Panoramic image (a) and the different configurations tested (b) of the 3-story building [23].

Another high building with seven stories was tested, in 2007, at the shaking table of the E-Defense laboratory in Miki, Japan. The building with 13.44 m x 7.68 m and a total height of 23.2 m (see Figure 2.13), was submitted to: the Hanshin-Awaji earthquake in Kobe; the Italian earthquake of Nocera Umbra;

and the Kashiwazaki of the Japanese west coast. The walls of the building had 142 mm on the 1st and 2nd stories, 125 mm on the 3rd and 4th, and 85 mm in the others, including the roof. In terms of the floors, all contained 142 mm of thickness. The tests performed provided excellent results, as the building behaved very well on large-scale earthquakes, with very low structural damage [24].

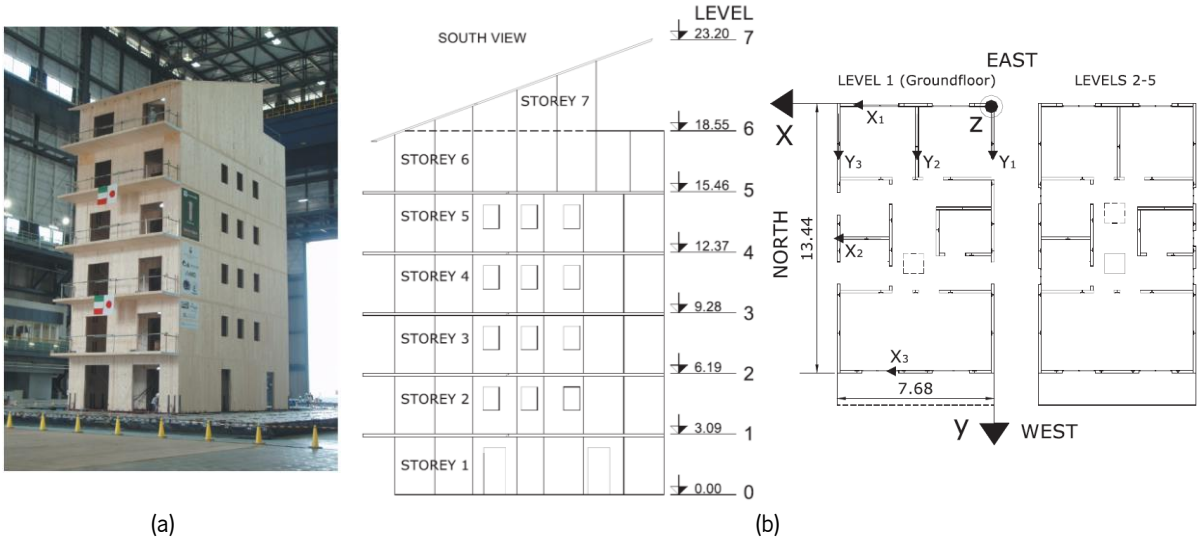

(a) (b)

Figure 2.13 – Panoramic image (a) and plans (b) of 7-story CLT building [24, 25].

More recently, another CLT full-scale building was tested on the shaking table of the National Laboratory for Civil Engineering (LNEC), in Portugal. In the scope of a SERIES project aimed to evaluate multi-stories timber buildings, researchers from the Graz University, the National Laboratory of Civil Engineering (LNEC), the University of Trento, and the University of Minho, tested a three-story CLT building with 5.17 m x 6.76 m in plan and 7.74 m of total height, including the roof (see Figure 2.14). The walls had a thickness equal to 100 mm (3-layers); the floors had 150 mm (5-layers) and the roof 99 mm (3-layers). The main metal connectors were angle brackets (AE116 Simpson Strong-Tie) and hold-downs (HTT22 Simpson Strong-Tie) with the corresponding nails and screws. The building has been subjected to 32 seismic tests, with the maximum ground acceleration of 0.5 g. At the end of these tests, the building presented reduced damages (located in some connections and walls) with a decrease of the fundamental frequency from 3.98 Hz to 3.75 Hz (around 5.8%) [26].

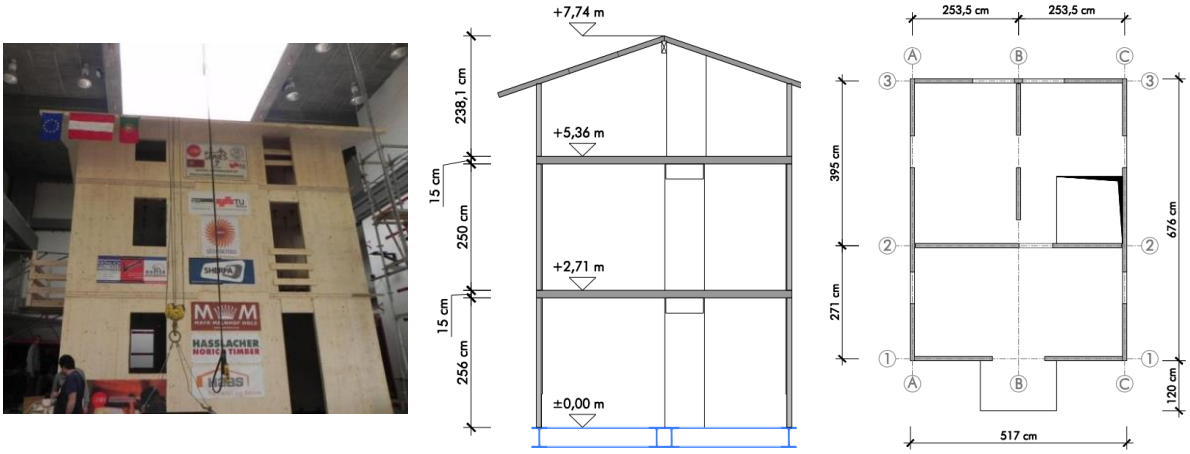

(a) (b)

Figure 2.14 – Panoramic image (a) and plans (b) of the 3-story building tested at the LNEC [26]

2.3.2 Quasi-static CLT buildings

Using a different approach, based on quasi-static tests, Popovski and Gavric [6, 7] analyzed a CLT building with 6.0 m x 4.8 m in plan and a height of 4.8 m (see Figure 2.15). Most of the connections used were angle brackets (BMF 116x48x3x116) and hold-downs (HTT4), but their number and location varied on each test performed. The specimen was tested under monotonic and cyclic lateral loading in five different tests.

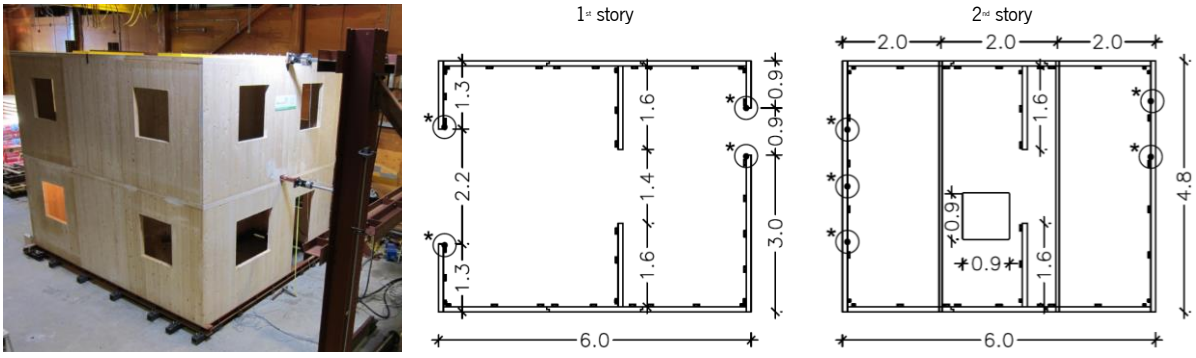

(a) (b)

Figure 2.15 – Panoramic image (a) and plans (b) of a quasi-static tested 2-story building [27, 28].

All the tests showed that the main failure mechanisms were the nails of the angle brackets at the bottom of the 1st-floor story, as a consequence of sliding and rocking (uplift) deformations of the walls (see Figure 2.16). Before the tests, the building registered a 13.5 Hz (E-W) and 11 Hz (N-S) fundamental frequency. After all the tests, the values decreased to 10.13 Hz and 7.63 Hz, respectively [27, 28].

Figure 2.16 – Main failure mechanisms of a quasi-static building tested [27, 28].

In the same way, two CLT buildings were analyzed with a different application of CLT panels. In plan and height, both buildings presented 6.0 m x 4.0 m with 5.82 m of height, but with different CLT panels around the openings. While in one building, the openings were cut directly on the CLT panels (see Figure 2.17a and Figure 2.17b), in the other, the openings were materialized trough segments (see Figure 2.17c). It is also important to note that buildings only featured hydraulic jacks on the 2nd floor.

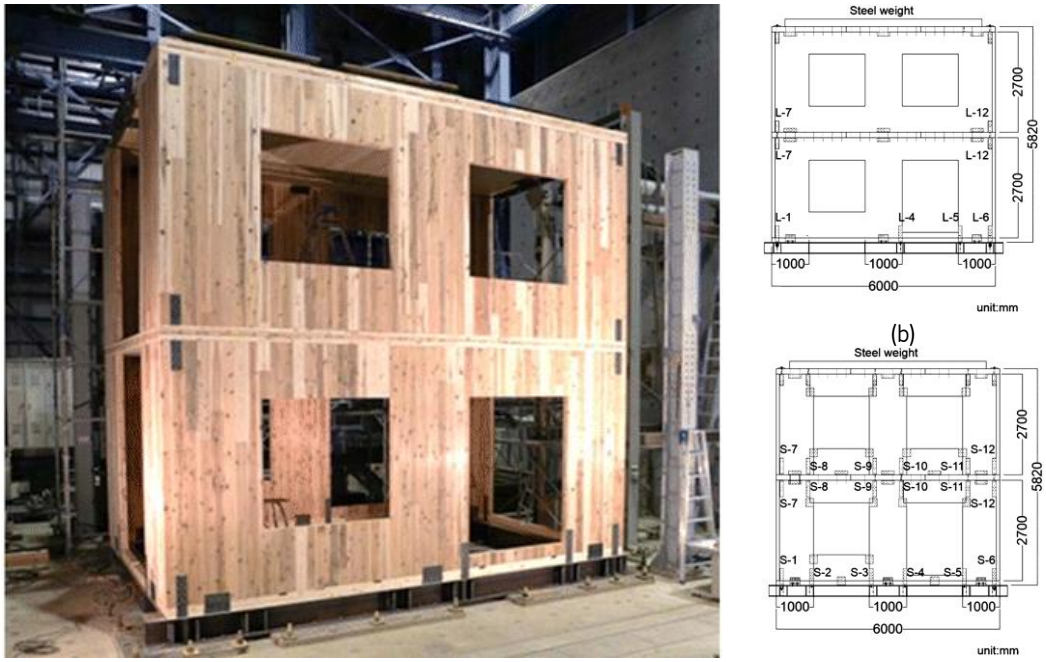

Figure 2.17 –Panoramic image (a) and facade of the building with openings cut directly on the CLT panels (b) and facade of the building with openings trough segments (c) [29].

The results presented a greater stiffness for the structure without segmentation of the panels, and it was possible to see cracks at the corners of the openings (see Figure 2.18a). On the other hand, with segmented walls, the structure presented a high deformation caused by the rotation of each wall panel (see Figure 2.18b) [29].

(a) (b)

Figure 2.18 – Failure mechanisms of a quasi-static building tested [29].

2.3.3 2D CLT shear walls

Based on the results presented for the shaking table tests, we might conclude that, in these cases, the resistance to lateral loads is mostly related to the shear walls. Thus, several configurations of the panels were studied to evaluate the response of each panel. Namely, in the SOFIE project, four different configurations of walls (see Figure 2.19a) were studied under quasi-static loading, where the influence of the metal connectors (in contact with the foundation and CLT panels), openings and the vertical loads were taken into account. The results showed that connectors have a great influence on the structural response, where the metal connectors guarantee ductility and energy dissipation. Regarding the mechanisms of failure, the damage was mainly located on metal connectors (see Figure 2.19b), where the configuration with door opening showed a local failure of wood in compression (see Figure 2.19c)[30].

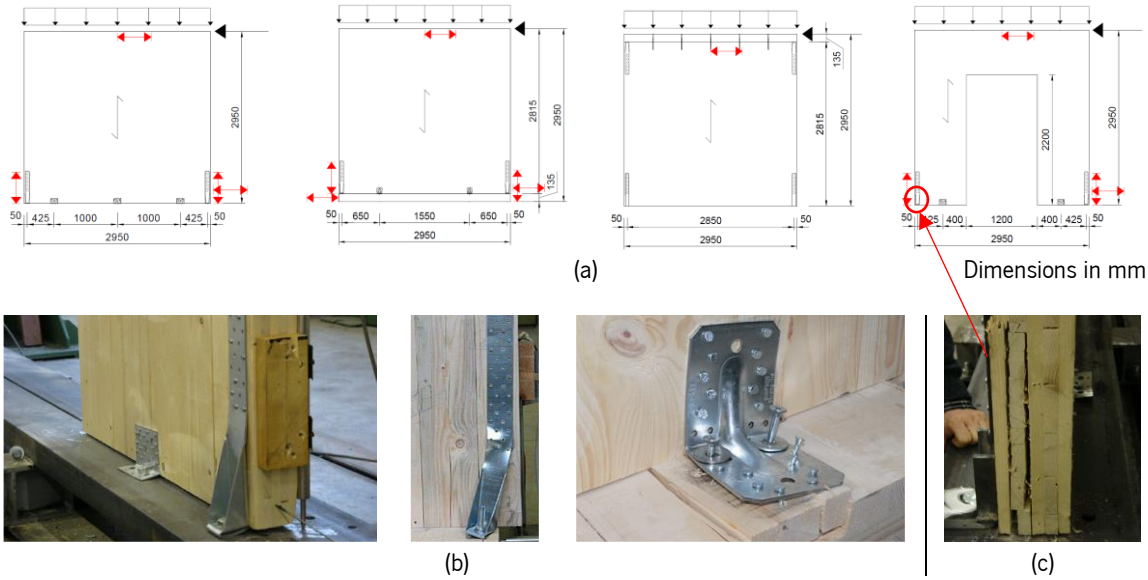

Figure 2.19 – Wall Configurations (a) and failure modes of the walls tested (b and c) [30].

In another study to analyze the influence of openings, two configurations with a single difference (see Figure 2.20), the opening of a window, and door (41% of the entire panel) were studied. The results

obtained showed a significant reduction of the shear stiffness, but at the level of the load capacity, did not obtain much difference (see Figure 2.21) [31].

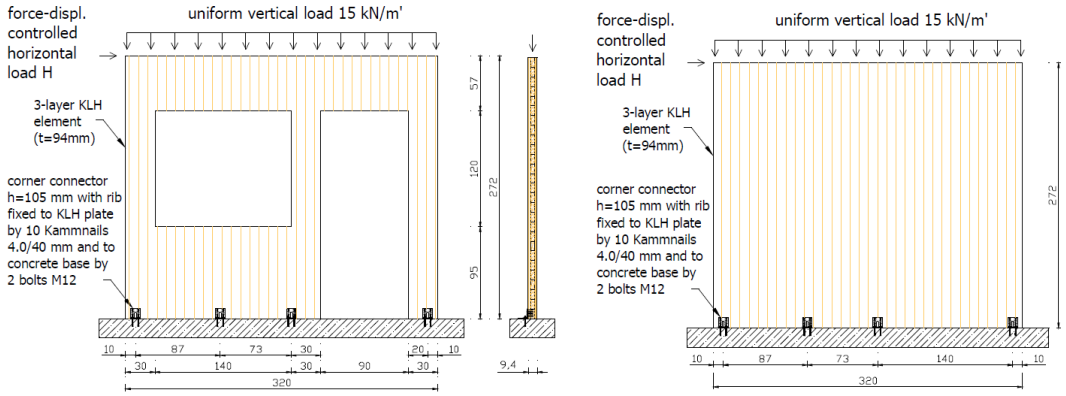

Figure 2.20 – Configurations (a) of the tested walls [31].

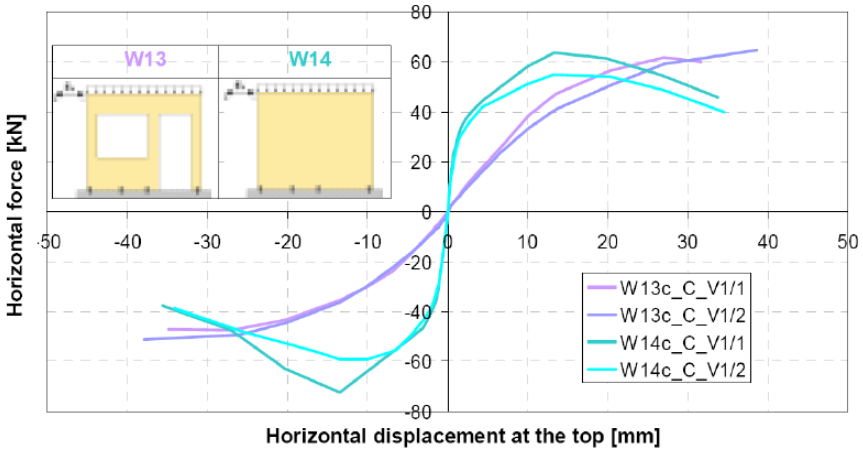

Figure 2.21 – Main results of the tests [31].

Similarly, with different walls ratio, a series of 12 CLT wall configurations were tested at FPInnovation-Forintek in Vancouver. The goal was to investigated different types of wall configurations (see Figure 2.22a) with different angle brackets (see Figure 2.22b) and fasteners (see Figure 2.22c). The effects of openings on the panels and wood and steel support were also investigated.

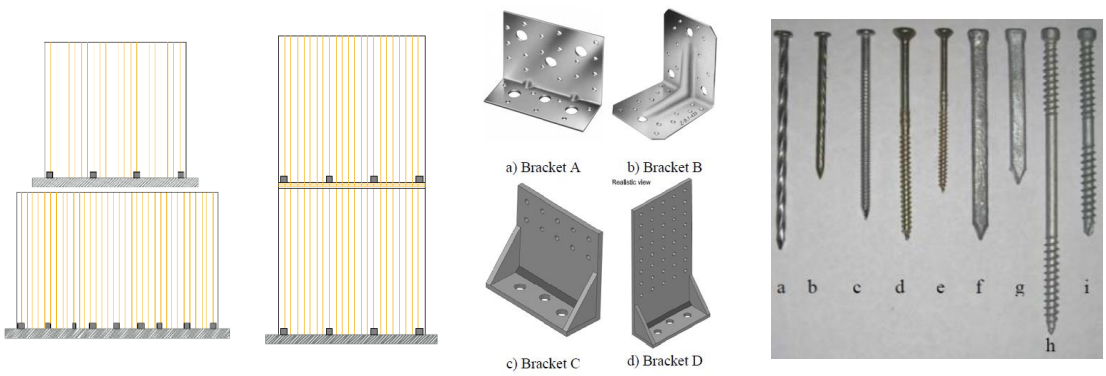

(a) (b) (c)

Figure 2.22 – Wall configurations (a), metal brackets (b) and fasteners (c) used on the walls analyzed [32].

The results showed that the CLT walls containing angle brackets and hold-downs at each end of the wall, improved performance under lateral loads. On the other hand, the use of diagonal screws to connect CLT floors and CLT walls can reduce the wall ductility [32].

Within the process to contribute to European construction practice, two research studies were performed at the University of Kassel and TU Graz. The University of Kassel studied a wall configuration (twelve walls with dimensions 2.50 m × 2.50 m), where the variables mainly focused on support conditions, vertical loads, and loading protocol. However, the presence of an elastomeric interlayer (sylodyn) and plastic interlayer (PE) was also studied to observe the influence of friction. On the other hand, Graz University of Technology Institute of Timber Engineering and Wood Technology studied five wall configurations, where the influence of various connections and vertical loads on monotonic and cyclic behavior were the main variables of the study. However, for both investigations, the contribution to the total deflection of each wall was also analyzed. In this way, the main conclusions of the two research studies are relative to the layers introduced for testing the influence on friction. The results showed that the elastomeric interlayer (sylodyn) increases the friction at the interface between the wall and the floor, while the plastic interlayer (PE) reduces the friction between panels. In terms of lateral deflection, the sliding and rocking affect the damping capacity of the wall element, where the rocking always presents higher percentages [33].

Another experimental program was conducted at IVALSATrees and Timber Institute on CLT walls with different anchoring systems and different types of joints between adjacent panels. Three wall configurations were studied (see Figure 2.23a), under cyclic tests according to EN 12512:2001 [34]. The results showed that the layout and design of joints are critical to the overall behavior of the structural system. However, the number of screws in joints between segmented walls influenced the kinematic behavior of CLT walls [35].

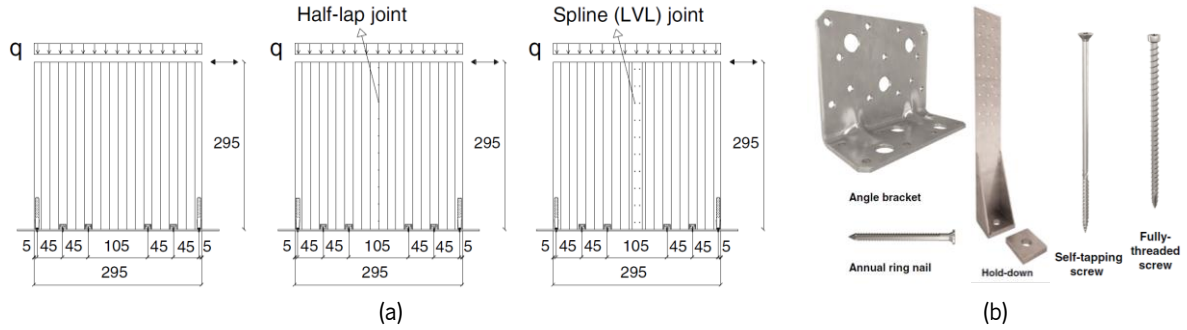

Figure 2.23 – Configurations (a) and connections (b) used on the walls analyzed [35].

Finally, with special attention to the distribution of forces in each metal connector (angle brackets WB100 and hold-downs WHT340) installed on the floor, six full-scale shear walls were studied under cyclic loads

(see Figure 2.24). In general, the results show a clear transition between elastic and inelastic response, where the vertical loads imposed on the panels influenced the stiffness and ultimate force of CLT walls. Concerning the metal connectors, each hold-down contributed around 5% of shear resistance of the panel and the angle brackets around 35% [36].

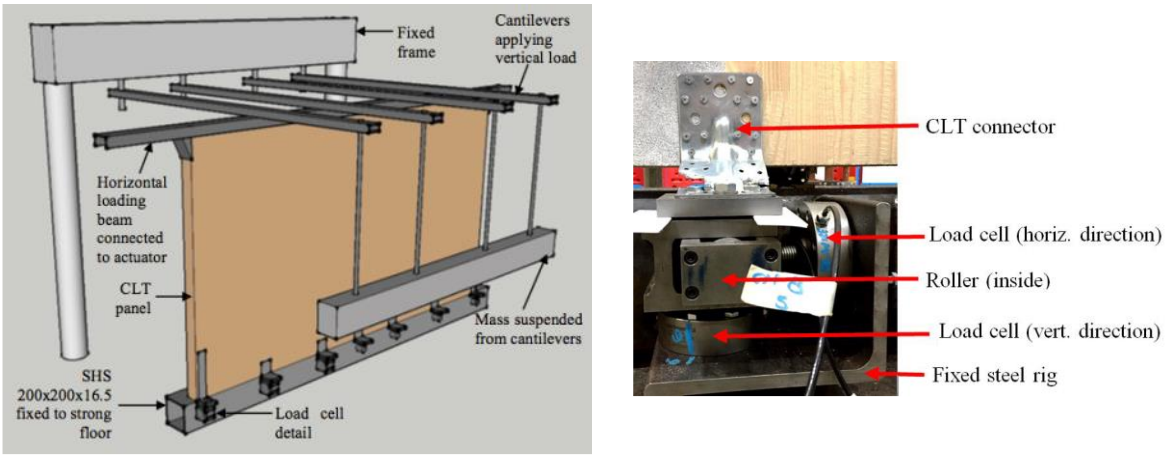

(a) (b)

Figure 2.24 – Configuration of the walls (a) and load cell installed on angle bracket metal connector (b) [36].

2.3.4 Metal connectors

The several experimental campaigns carried out on buildings and shear walls demonstrated that metal connectors (hold-downs and angle brackets) play an extremely important role in the response under lateral loads. Therefore, any contribution to increasing the knowledge on the behavior of the metal connector is valuable, and, in particular, all experimental analyses will allow further numerical analyses.

For example, an experimental campaign was set to assess the behavior of the hold-downs (WHT540 and WHT440) and angle brackets (BMF90x116x48x3 and BMF100x100x90x3) used in the buildings (3-story [23] and 7-story CLT building [24, 25]) of SOFIE project, under monotonic and cyclic loads, following the loading protocol according to EN 12512:2001 [34]. However, it is important to note that the hold-downs tested were not the same as those used, but similar. To test the connectors under shear and tension (pull-out), two configurations have been carried out (see Figure 2.25). The tests were performed with a steel and timber base, to represent the behavior on the foundation and between CLT floors, respectively [37, 38].

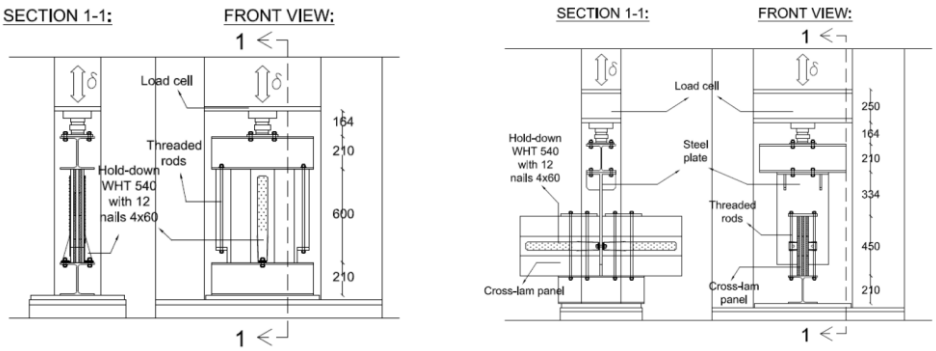

(a) (b)

Figure 2.25 – Test setup for (a) tension and (b) shear loads [37, 38].

Regarding the results, the angle brackets showed significant stiffness and strength capacity in both directions. In terms of failure, the angle bracket under lateral loading failed on the combination of bending and withdrawn of the nails on the vertical steel plate (see Figure 2.26a). On the other hand, tension failed on the steel around the threaded rod for steel base and failed through pull-out of the nails present in the horizontal plate for timber base (see Figure 2.26b).

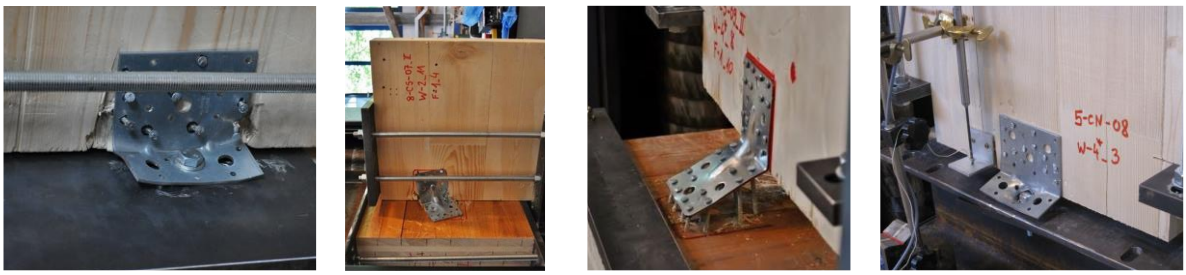

(a) (b)

Figure 2.26 – Failure of the angle brackets loaded in shear (a) and tension (b) [37, 38].

As expected, the shear strength of hold-downs is much lower than the tensile strength. The failure in tension occurred in the nails, mainly by the combination of withdrawal and bending of the fasteners (see Figure 2.27a). On the other hand, under shear loads, due to the buckling of the steel metal (high displacement values), it occurred in the region of the plate that does not have nails. (see Figure 2.27b). As a general conclusion, it was found that the concentration of forces and deformation occurs in a relatively small region.

(a) (b)

Figure 2.27 – Failure of the hold-downs loaded in tension (a) and shear (b) [37, 38].

In another experimental campaign promoted by Simpson Strong-Tie, angle bracket (AE116) has been evaluated under shear and tension loading for timber and steel base. In those tests, the loading protocol followed an approximation of ISO 16670 [39] and EN 26891 [40]. In terms of failure mechanisms, they were identical to those identified in the analyzed connectors of the SOFIE project, as shown in Figure 2.28. The results obtained showed very encouraging results, where, on the other hand, as the loading protocol was performed through the approximation of two standards, the test results did not show great accuracy for the highest loads achieved [41].

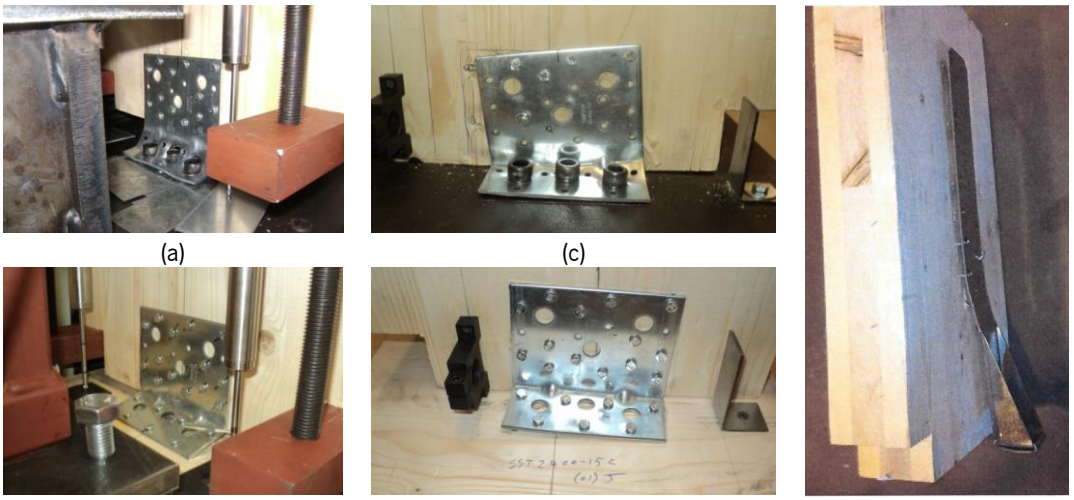

(a) (c)

(b) (d) (e)

Figure 2.28 – Failure mechanisms on angle brackets AE116 (a, b, c and d) and hold-downs HTT22 (e).

In the case of hold-downs, all experiments performed by the diverse authors and within various research projects showed that this kind of connectors only presents axial strength. In fact, in practice, it is assumed that hold-downs only contribute to the response of the structure through the axial strength. Most of the research efforts about hold-downs are concentrated in the analysis of this behavior. However, Luca Pozza et al. conducted an experimental campaign, aimed to analyze in detail the axial-shear interaction of the WHT 540 hold-down connector (see Figure 2.29). The results showed that the axial-shear interaction up to 7.5 mm is not important, but, for higher displacement values, can be significant [42].

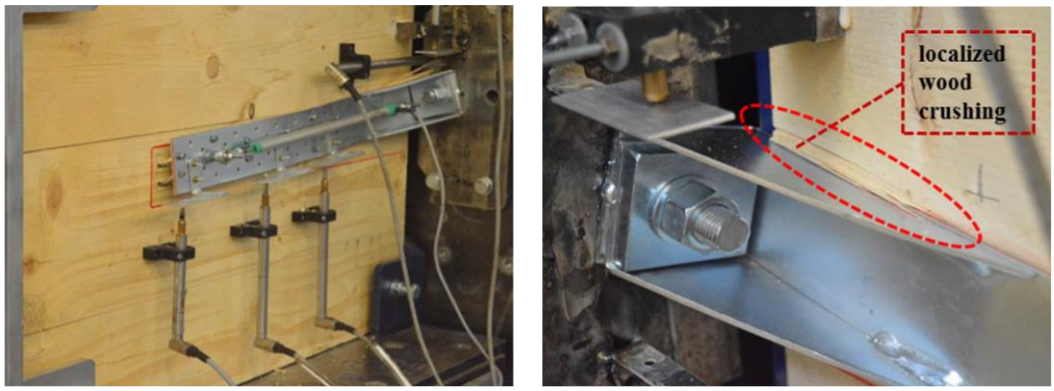

Figure 2.29 – Failure mechanisms of the hold-downs WHT 540 analyzed under axial-shear interaction [42].

2.3.5 Numerical models of CLT buildings

With the experimental research carried out on the CLT buildings and each of the important components (mostly CLT panels and metal connectors angle brackets and hold-downs) analyzed, this phase is relative to the numerical model prediction of finite element method, the experimentally analyzed buildings within the SOFIE project. A numerical model of the 3-story building evaluated within the SOFIE project was performed through the commercial software SAP2000 [43] (see Figure 2.30a). Linear elastic shell elements were used to represent the CLT panels, diagonal truss elements to represent angle brackets, and vertical truss elements to represent hold-downs (see Figure 2.30b). However, it is important to point out that friction contribution has also been studied [44].

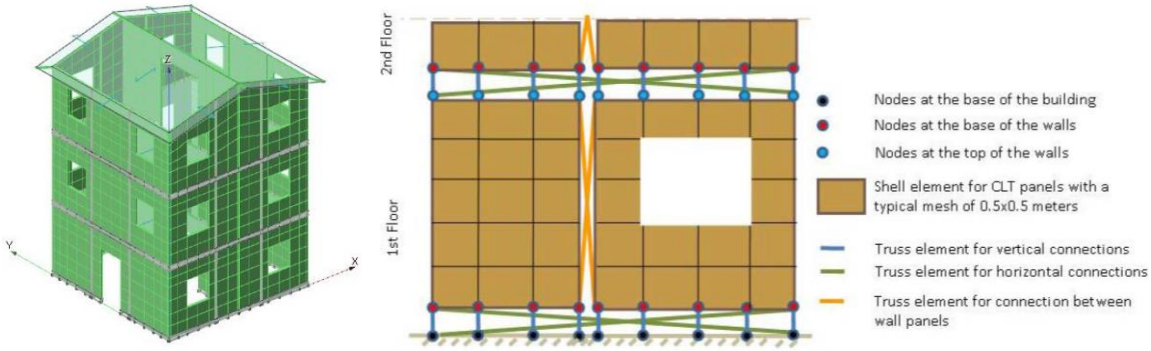

(a) (b)

Figure 2.30 – (a) Wall schematization used and (b) numerical model of 3-story building [44].

Comparing the experimental campaign with the numerical model, the results of the frequency showed good agreement between them, but, on the other hand, in terms of maximum displacements, the model showed higher values. Regarding the model with and without the contribution of friction, the model with friction always presents values closer to tests.

For the 7-story building also evaluated in the SOFIE project (Dujic et al. [45]), SAP2000 [43] model was created to predict the response of the building (see Figure 2.31a). As in the previous numerical model, CLT elements have been defined as shell elements and the main metal connectors through spring elements (diagrams of envelope curves of experimental campaigns). Proceeding to the numerical analysis, the algorithm did not reach convergence, mainly because of the descending parts of the envelope curves (green color in Figure 2.31b and Figure 2.31c). In consequence, two more simplifications were made: first, the descending parts were changed into a constant deformation (see Figure 2.31b and Figure 2.31c); and, the values of secant stiffness of the brackets were inserted into the metal connectors [45].

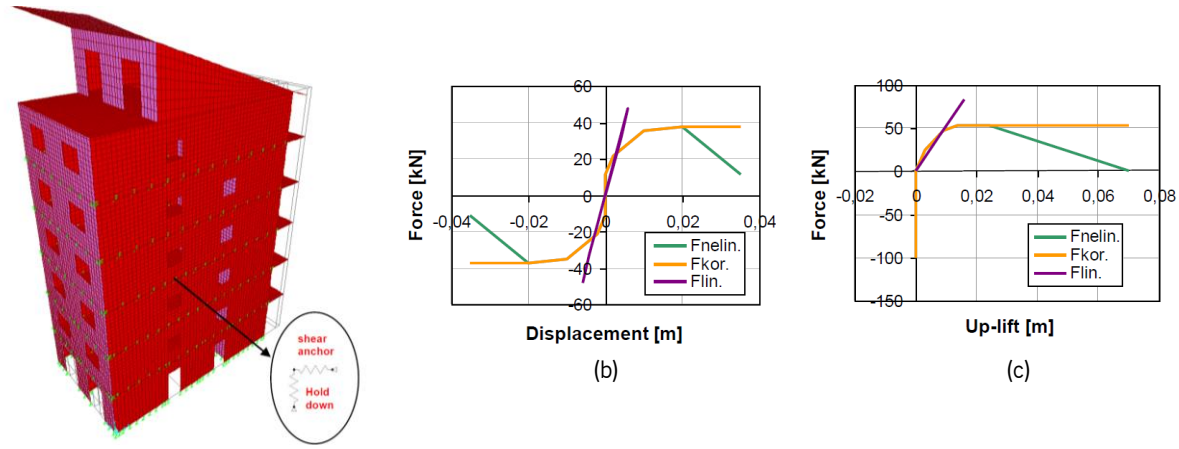

(a) (b) (c)

Figure 2.31 – (a) Numerical model of 7-story building and diagrams used on angle brackets (b) and hold-downs (c) [45].

As a conclusion of the comparison between the numerical model and the experimental campaign, it can be said that this model presents good results, in which the numerical model showed higher amplitudes (see Figure 2.32). However, it is important to note that due to the lack of data on horizontal displacements caused by the uplifts of CLT panels in the experimental campaign, the differences could be much smaller.

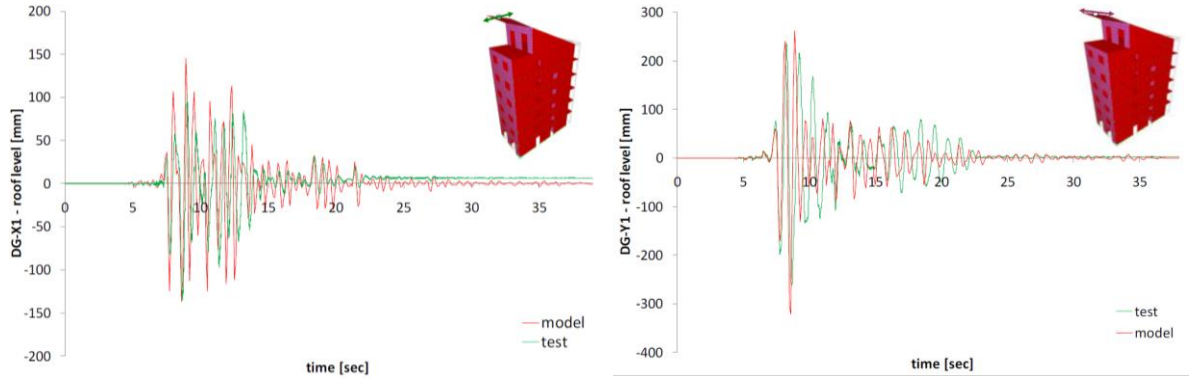

(a) (b)

Figure 2.32 – Comparison between the numerical model and experimental tests in (a) X direction and (b) Y direction.

Rinaldin and Fragiacomo [46] also predicted the response of those both buildings (see Figure 2.33), but in this case, using an advanced FE model, where the proposed model was implemented in different software packages: Abaqus, OOFEM and OpenSees. CLT panels have been defined as linear elastic shell elements, while all-metal connectors were defined as a tri-linear backbone curve, in which the curves have been calibrated through experimental cyclic tests. However, it is important to note that the proposed numerical model allows knowing more details of the analysis compared to the numerical models performed in SAP2000, which highlights the implementation of complex 3D buildings, strength and stiffness degradation, and performed dynamic analyses with minor convergence issues [46].

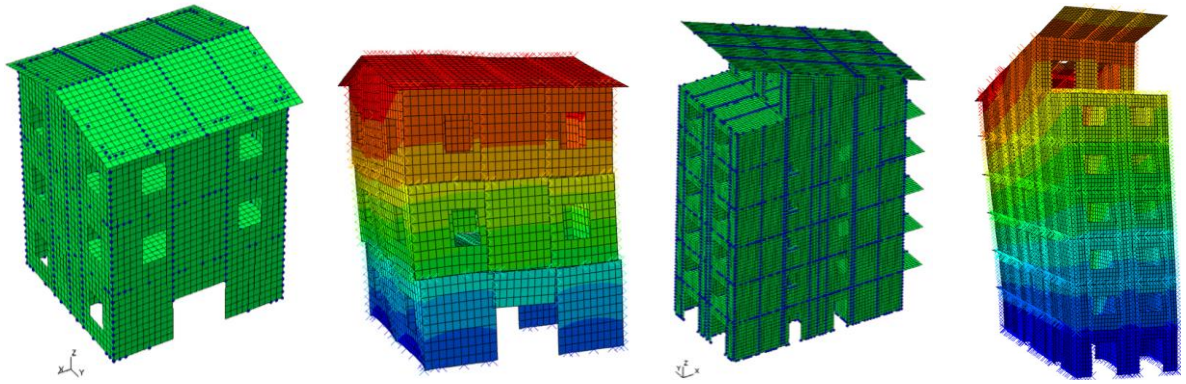

(a) (b)

Figure 2.33 – Numerical model and deformed shape of the 1st vibration mode of a (a) 3-story and (b) 7-story building.

The results showed for both cases (3-story and 7-story building) errors about 20% concerning acceleration and 7% for the displacement reached on the roof. However, it is important to note that the friction coefficient (μ=0.6) provides the best fit of the experimental results. To conclude, as expected, the results obtained in this advanced FE model presents more promising results, but present high modeling complexities [46].

Chapter 3

Experimental campaign of typical metal connectors

3.1 Introduction

CLT panels have shown high in-plane stiffness and the metal connectors have demonstrated a high influence on flexibility and, therefore, higher stiffness, strength, stability, and ductility when subjected to seismic loads. Connectors represent the main responsible for the transfer of forces to the foundation, where the angle brackets are the main responsible for shear strength and the hold-downs for tension strength. Under these circumstances, a detailed analysis of each connector will be important to predict the seismic behavior of CLT structures.

In the process of characterizing the real behavior of metal connectors, two experimental campaigns were carried out. The experimental campaigns fulfilled at the University of Minho (UM) and Simpson Strong-Tie (SST), where UM tested the angle bracket AE116 and the hold-downs HTT22 and HTT22E and SST tested the angle brackets AB+plate and ABAI. The tests carried out at UM had as their first goal the validation of the test setups performed, and with that, the analysis of the current [34] and the proposal for the revision of the European standard EN 12512 [5]. Beyond these, a comparison between HTT22 and HTT22E was carried out, where the difference between the connectors is in the holes for the nails. On the other hand, the AB+plate and ABAI connectors testes by SST had as the primary goal of the study of the influence of an acoustic layer (Sylodyn [47]).

3.2 Experimental program

To contribute to the study of the principal metal connectors used in CLT structures, two experimental programs composed of thirty-five tests on angle brackets AE116, AB+plate, and ABAI and hold-downs HTT22 and HTT22E have been carried out. As mentioned, the connectors AE116, HTT22, and HTT22E have been tested at the University of Minho while connectors AB+plate and ABAI were tested in the laboratory of Simpson Strong-Tie. Here, at the University of Minho, five tests under monotonic loading and eighteen under cyclic loading were performed, while at Simpson Strong-Tie twelve tests under cyclic loading were carried out. All angle brackets were studied under lateral and tension loading for two kinds of supports (CLT panel to simulate a connection of the wall to the CLT floor and a steel plate simulating the interaction CLT with the foundation), except for the angle brackets AB+plate and ABAI that were only studied for CLT support. Regarding the hold-downs, they were analyzed only under tension, due to the

weak capacity in shear loads of this metal connector (buckling of the metallic flanges) [48]. Even more, due to the similarity of results between supports that has been verified in preliminary tests, hold-downs were only analyzed with CLT support.

In terms of dimensions of the CLT panels under shear and with a CLT support, used 360 x 360 mm for both panels and, under tension, the vertical panel with 360 x 750 mm and the support 360 x 360 mm. For the steel support case, the only difference was related to the change of support, from CLT panel to steel plate. In the Simpson Strong-Tie experimental campaign, the only change was given by the vertical panel under tension loading, where it had 360 x 400 mm. In terms of thickness, the CLT used for the support had 120 mm (3 layers 40 mm) and 100 mm for vertical panel (5 layers 20 mm) for analyzing the AE116, HTT22 and HTT22E connectors, while for analyzing the AB+plate and ABAI were 100 mm for both cases. Table 3.1 presents a summary of the test program that was carried out, with a description of each specimen, the fixation to the base used and the loading protocol applied, while Figure 3.1 presents the specimens and their main details.

Table 3.1 – Description of the specimens tested.

Connector	Nº Tests	Loading	Fixation to the base	Setup/performed	Test direction
AE116	1	Monotonic	Steel plate	**University of Minho** Loading protocol according to the proposal for the revision of the EN 12512 [5]	Shear (Figure 3.1a)
	3	Cyclic			
	1	Monotonic	CLT 120 L3s		Shear (Figure 3.1b)
	3	Cyclic			
	1	Monotonic	Steel plate		Tension (Figure 3.1c)
	3	Cyclic			
	1	Monotonic	CLT 120 L3s		Tension (Figure 3.1d)
	3	Cyclic			
HTT22	1	Monotonic	CLT 120 L3s		Tension (Figure 3.1e)
	3	Cyclic			
HTT22E	3	Cyclic	CLT 120 L3s		Tension (Figure 3.1f)
ABAI	3	Cyclic	CLT 100 L3s	**Simpson Strong-Tie** Loading protocol according to ISO 16670:2003 [39] & EN 26891:2001 [40]	Shear (Figure 3.1g)
	3	Cyclic	CLT 100 L3s		Tension (Figure 3.1i)
AB+plate	3	Cyclic	CLT 100 L3s		Shear (Figure 3.1h)
	3	Cyclic	CLT 100 L3s		Tension (Figure 3.1j)

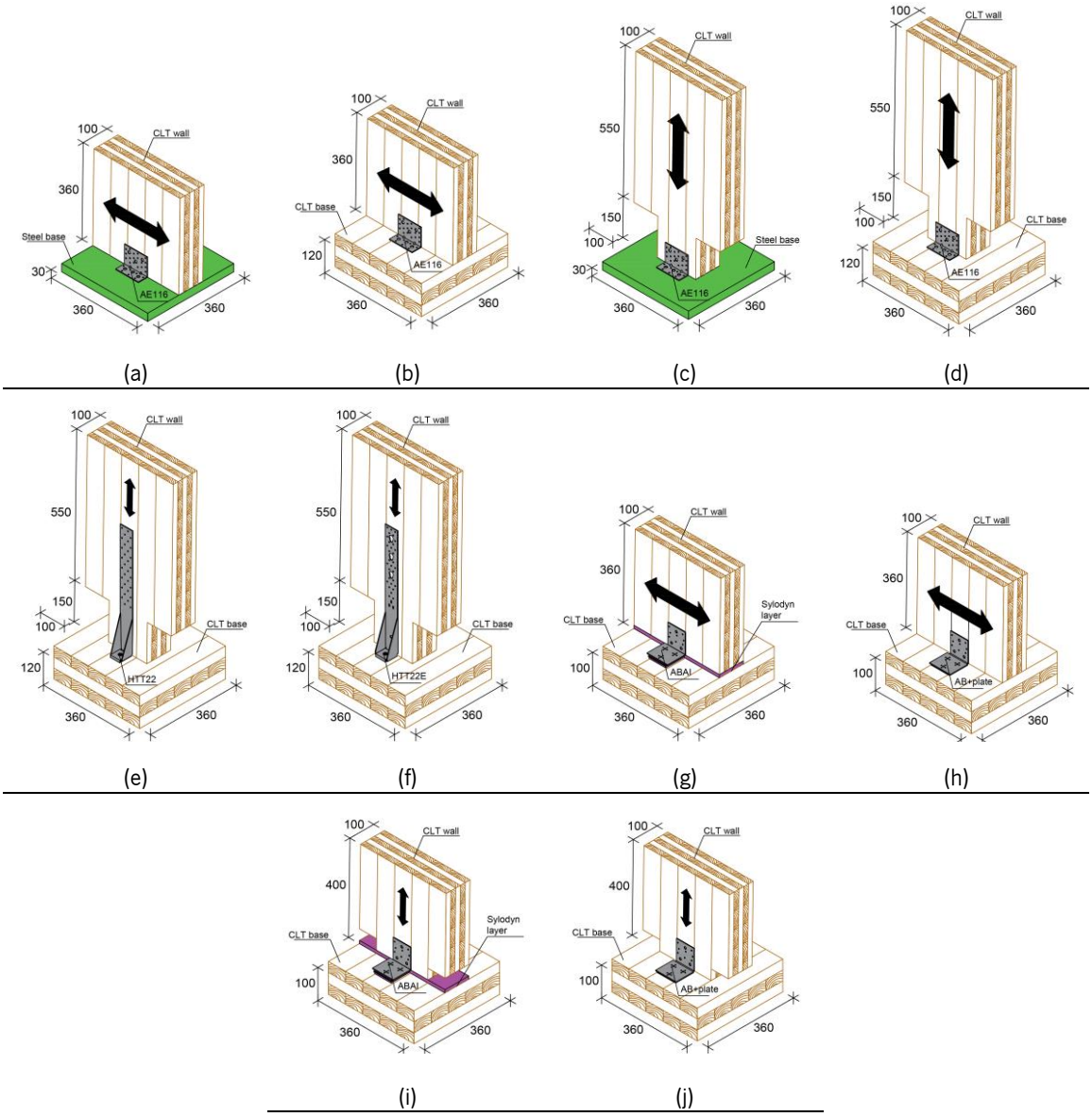

Figure 3.1 – Details of the specimens (dimensions in mm).

About the fasteners used on the connectors, the angle brackets AE116 have been fixed with 14 CNA Annular ring nails (flange A) and two threaded roads of Ø12 (flange B) for the case of the steel support and, with 14 (flange A) + 7 (flange B) CNA Annular ring nails for the CLT support case. The hold-downs used one threaded road of Ø16 mm (flange B) and 15 CNA Annular ring nails (flange A) for all cases. However, it is important to note that in the HTT22E case, the different holes of the lower three nails (see Figure 3.2) have always been inserted to verify strength changes. Finally, connectors AB+plate and ABAI presented 8 CNA Annular ring nails (flange A) and 3 SDS (flange B). Table 3.2 and Figure 3.2 summarizes the different types of fasteners and the number used on each connector studied.

Table 3.2 – Connectors and fasteners used in the tests.

Specimen	Type	Reference	Description
[CLT-to-Steel]	Angle bracket	AE116	14 × CNA4.0×60 (A) 2 × M12 (B)
[CLT-to-CLT]	Angle bracket	AE116	14 × CNA4.0×60 (A) 7 × CNA4.0×60 (B)
		ABAI	8 × CNA4.0×60 (A) 3 × SDS6.4×50 (B)
		AB+plate	8 × CNA4.0×60 (A) 3 × SDS6.4×50 (B)
	Hold-down	HTT22	14 × CNA4.0×60 (A) 1 × M16 (B)
		HTT22E	14 × CNA4.0×60 (A) 1 × M16 (B)

M12 - Threaded road Ø12 (8.8 Grade); M16 - Threaded road Ø16 (8.8 Grade)

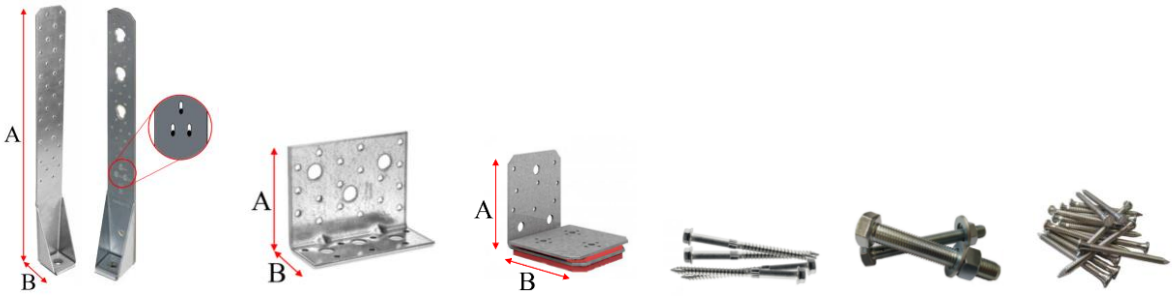

HTT22 & HTT22E | AE116 | ABAI & AB+plate | SDS6.4×50 | M12 & M16 | CNA4.0×60

Figure 3.2 – Connectors and fasteners used in the tests.

3.3 Test procedures

Two loading procedures were applied to the specimens analyzed. Through a monotonic test it is possible to assess: the maximum of the elastic force; the elastic stiffness; the elastic and ultimate displacement; and, the ductility. Moreover, they allow quantifying the yielding displacement. On the other hand, the cyclic test provides a clearer view of the response of the connectors, allowing the study of the metal connector ability to dissipate energy as well as the degradations caused by cyclic loading.

3.3.1 Monotonic tests

Monotonic tests were conducted by the standard EN 26891 [40]. The method consisted of applying two loading patterns, one in force control and the other in displacement control. A constant rate of 20% of the estimated maximum load (F_{est}) per minute for the first and a constant rate of 0.085 mm/s for the second. However, it is essential to note that the first pattern included a pre-load, where it was kept for 30 seconds at 40% and 10% of the estimated maximum load (F_{est}), as shown in Figure 3.3.

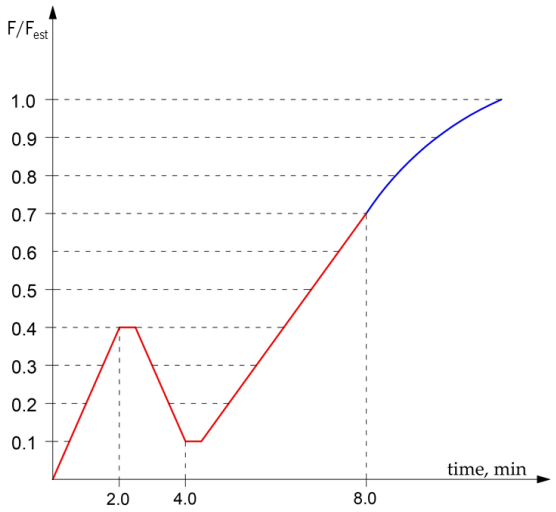

Figure 3.3 – Loading procedure defined by EN26891 for monotonic tests.

For the quantification of different mechanical parameters and definition of the bilinear curve, the current version of the standard EN 12512:2001 [34] defines the initial stiffness (k) through the slope of the trend line of the force-displacement curve between 10% and 40% of maximum force (F_{max}), and the post-elastic stiffness (K_p) is quantified through 1/6 of the initial stiffness (k). On the other hand, in the new proposal of this standard [5], the elastic stiffness (k_m) is always quantified through the slope of the trend line of the force-displacement curve between 10% and 40% of maximum force ($F_{max,\,m}$). The yielding displacement ($V_{y,EEEP,\,m}$) and yielding load ($F_{y,EEEP,m}$) are obtained through the equal areas of the load-displacement curve and the Equivalent Energy Elastic-Plastic (EEEP) curve, as can be seen in Figure 3.4. At the level of ultimate displacement ($V_{u,EEEP,m}$), the value is given by the minimum value of displacement between: (i) failure; (ii) 80% of the maximum load after the maximum load reached; or, (iii) 30 mm

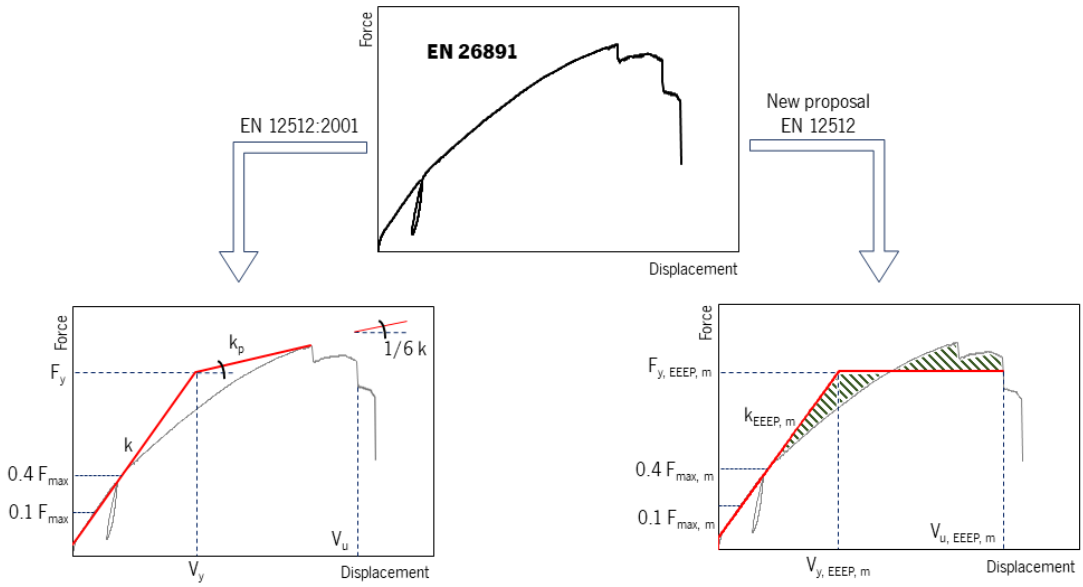

Figure 3.4 –Comparison between the current and the new proposal of the standard EN 12512 for a monotonic test performed following EN 26891.

3.3.2 Cyclic tests

Regarding the definition of the cyclic test load protocol and, as the proposal of the standard EN 12512 [5] still presents a discussion about the displacement rate, the intermediate values that the standard presented in 2018 [5] were assumed. Thus, with the definition of the yielding displacement on the monotonic test, it was defined 0.275 mm/s up to the value of the yielding displacement (see 1st pattern of Figure 3.5) and 1.25 mm/s until failure (see 2nd pattern of Figure 3.5). Regarding the number of cycles, one cycle was defined until yielding displacement (see 1st pattern of Figure 3.5) and three cycles until failure (see 2nd pattern of Figure 3.5) according to the proposal for the revision of the EN 12512 [5] in 2018. However, it is important to note that the most recent proposal of the standard (2019) [5], no longer presents one cycle until yielding displacement, but up to 60% of yielding displacement.

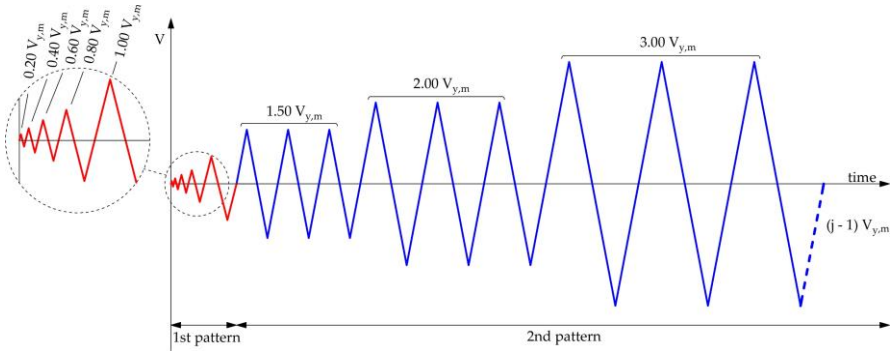

Figure 3.5 – Loading procedure defined by EN 12512 [5] for cyclic tests in 2018.

With the obtained experimental load-displacement curves, it is possible to quantify the energy dissipation and the strength degradation observed during each test. In this context, these two parameters obtained change between the new proposal [5] and the current version [34], where the equivalent viscous damping ratio is quantified through one cycle and not only half of the cycle, as shown in Figure 3.6.

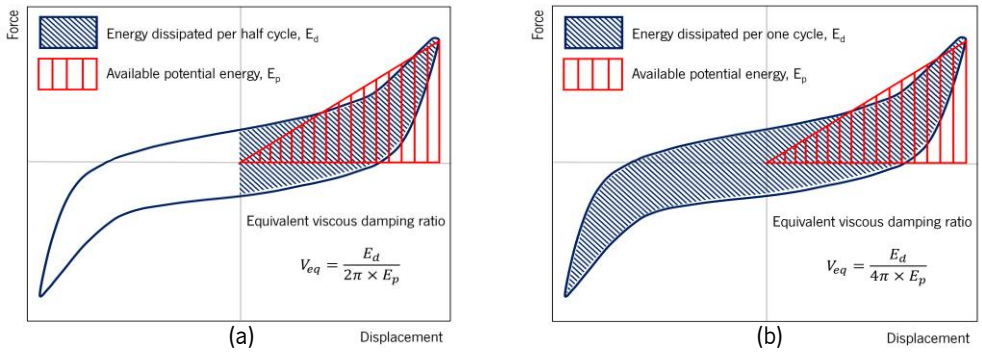

Figure 3.6 – Definition of equivalent viscous damping ratio according to the current (a) and the new proposal (b) of the standard EN 12512.

Regarding the degradation factor, which represents a load reduction factor between the 1st Load Envelope Curve (1st LEC) and 3rd Load Envelope Curve (3rd LEC), the new proposal does not recommend values less than 0.6, while the current version says nothing about it. For the quantification of the different parameters and definition of the bilinear curve, the methodology is the same as that mentioned above for the monotonic tests: being quantified through the 1st Load Envelope Curve (1st LEC), as can be seen in Figure 3.7. To define the ultimate displacement, besides those reported for monotonic tests, it can be given by the minimum value of degradation factor (0.6). However, it is important to note that the 3rd Load Envelope Curve (3rd LEC) can be crucial for the quantification of the ultimate displacement. On the other hand, the strength degradation and the 1st LEC can only be quantified if the total number of cycles is applied to the step.

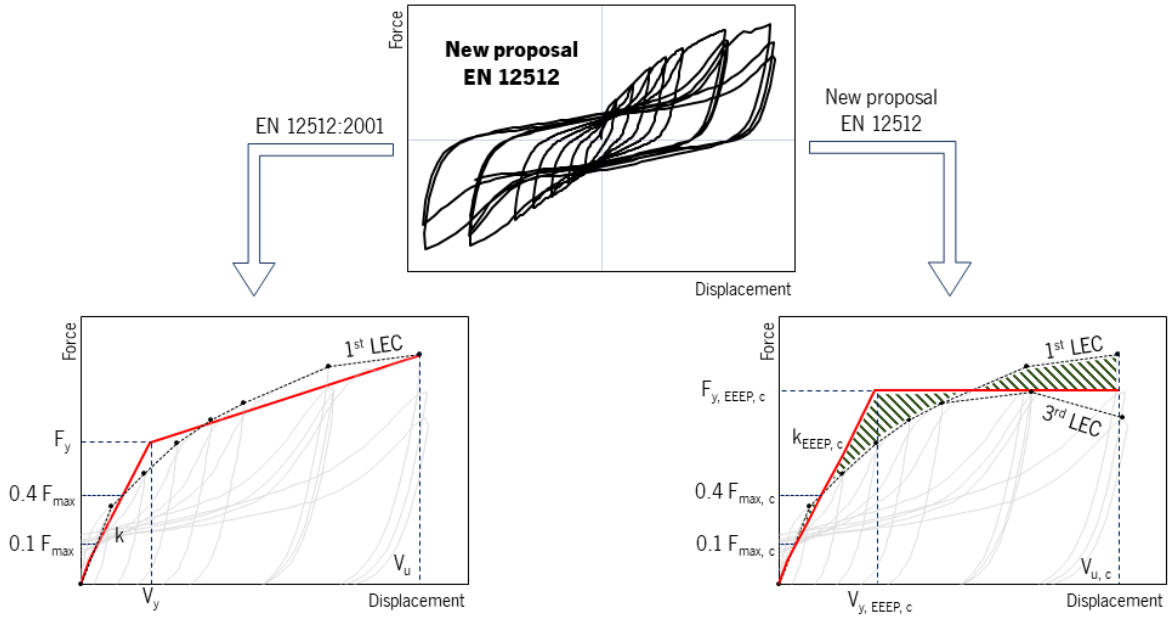

Figure 3.7 – A brief comparison between the current and the new proposal of the standard EN 12512 for cyclic tests.

3.3.3 Tests Setups and Instrumentation

To analyze the metal connectors under lateral (see Figure 3.8a) and tension (see Figure 3.8b) loads, two test setups have been planned. The design of the test setups has been based on experimental campaigns performed by Gavric et al. [48] and Simpson Strong-Tie. In these circumstances, particular attention was given to the application of a cyclic loading procedure through the introduction of steel plates and steel rods. However, mainly for the shear setup, two metal plates were designed to prevent specimen rotation (see Figure 3.8a number 6.). However, it is important to note that the steel plates had no direct contact with the specimen. Teflon tape was inserted between the CLT panel and the steel plates to minimize the

effects of friction on the final results. Panoramic images and plans of the setups with their main details are presented in Figure 3.8.

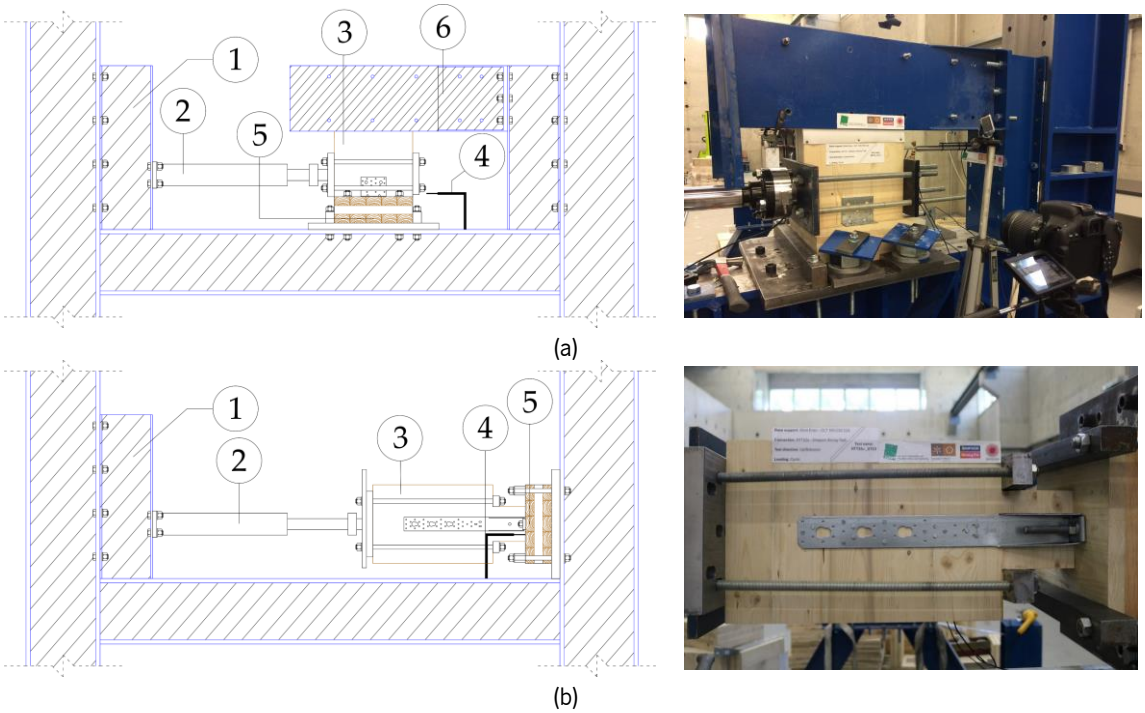

1. Steel frame;
2. Load Cell;
3. Specimen;
4. Measuring devices;
5. Timber or steel support;
6. Steel plate to avoid specimen rotation.

Figure 3.8 – Panoramic images and details of the test setups for lateral (a) and tension (b) loads.

For instrumentation, to ensure in-plane, rotation, and possible base uplift measurements, a load cell with a maximum capacity of 100 kN and four linear voltage displacement transducers (LVDTs) were placed for each setup (Figure 3.9).

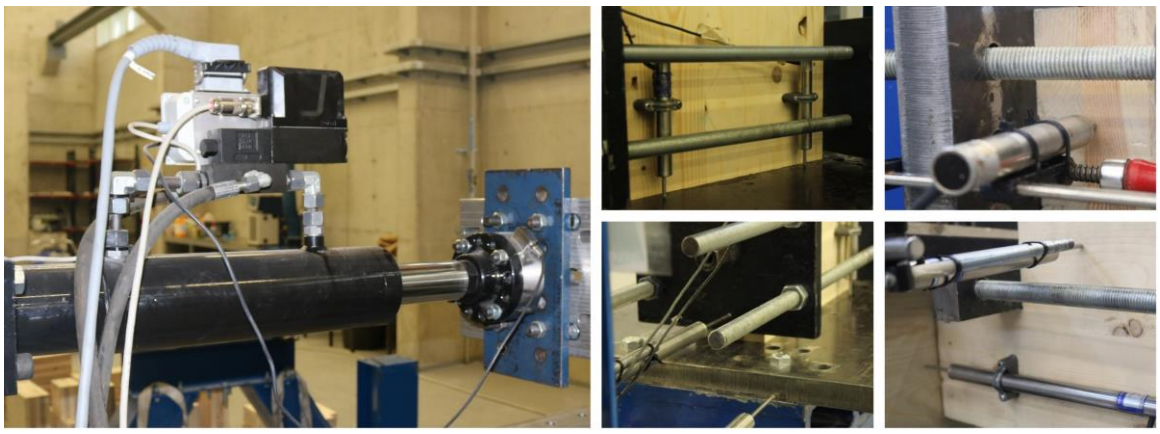

(a) (b) (c)

Figure 3.9 – Load cell (a) and measuring devices used in lateral (b) and tension (c) loads tests.

3.4 Results

The main results obtained from the experimental program performed at the University of Minho (UM) and Simpson Strong-Tie (SST) will be here described and discussed. Briefly, thirty-five specimens were tested, five under monotonic loading and thirty under cyclic loading. The results were separated into five groups:

1. Angle brackets AE116 under lateral loads;
2. Angle brackets AE116 under tension loads;
3. Hold-downs HTT22 and HTT22E under tension loads;
4. Angle brackets AB+plate and ABAI under lateral loads;
5. Angle brackets AB+plate and ABAI under tension loads.

To describe the behaviour of the metal connectors, the new proposal, in the revision of the standard EN 12512 [5], has been applied to the quantification of: elastic stiffness (k); yielding load ($F_{y,EEEP}$); yielding displacement ($V_{y,EEEP}$); strength degradation ($\beta_{sd,c}$); ductility (D_{EEEP}); and, equivalent viscous damping ratio (V_{eq}). However, it is important to note that, the angle brackets AE116 and hold-downs HTT22 previously analyzed by Simpson Strong-Tie have been added to the analysis for validation of the test setups used at the University of Minho. For a better analysis of the results, the average curves for the tests performed at the University of Minho and Simpson Strong-Tie are highlighted and the others with transparency.

3.4.1 Angle brackets AE116 under lateral loads

This group consists of angle brackets AE116 Simpson Strong-Tie under lateral loads. Figure 3.10 shows the experimental force-displacement loops, obtained from the experimental campaign performed at the University of Minho (UM), using a steel plate as the ground support. Three specimens, cyclic 1, cyclic 2, and cyclic 3, have been tested.

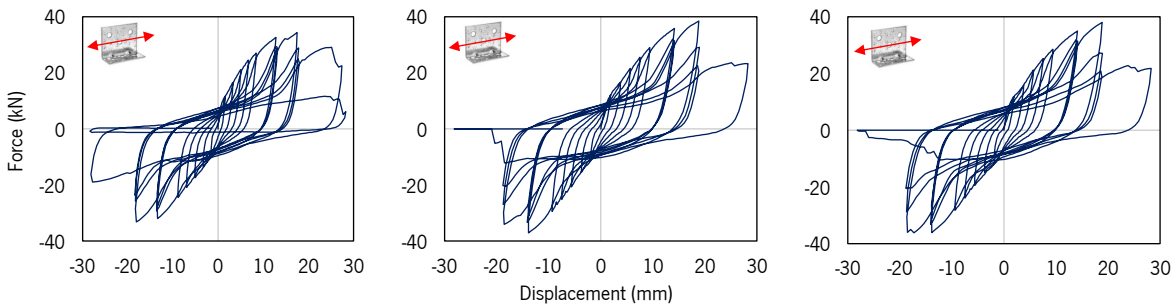

Figure 3.10 – Experimental force-displacement loops obtained in the case of angle brackets AE116 with a steel plate support.

Analyzing the Load Envelope Curves (LECs) of the experimental tests and applying to the new proposal of EN 12512 [5], Figure 3.11 shows the 1st Load Envelope Curves (1st LECs) and the Equivalent Energy Elastic-Plastic (EEEP) curves while Table 3.3 summarized the main parameters obtained. However, it is important to note that no curve exhibits a behavior after maximum force because the experimental tests did not reach the total number of cycles of the step, as shown in Figure 3.10.

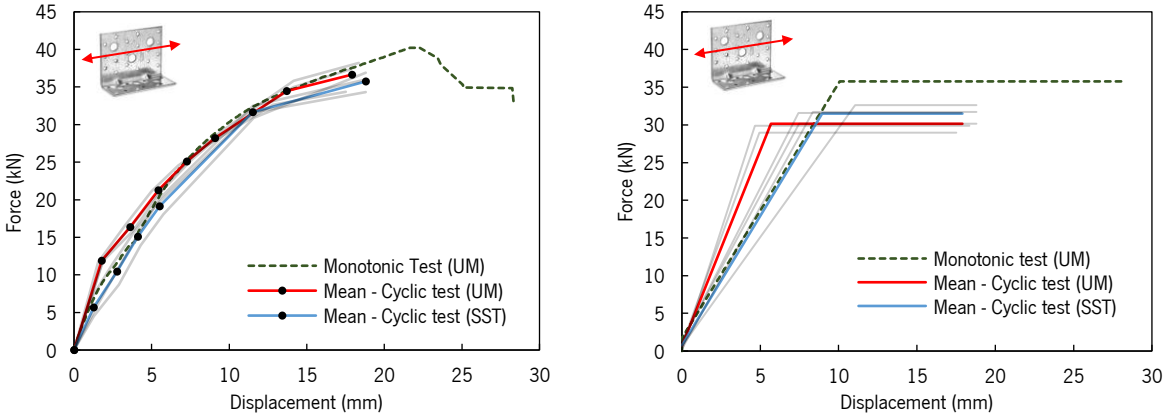

Figure 3.11 – Force versus displacement curves: (a) 1st Load Envelope Curves (1st LECs); (b) Equivalent Energy Elastic-Plastic (EEEP) curves.

Table 3.3 – Results of the angle brackets AE116 under lateral loads and with a steel plate support.

Specimen	F_{max} (kN)	K_{EEEP} (N/mm)	$F_{y,EEEP}$ (kN)	$V_{y,EEEP}$ (mm)	$V_{u,EEEP}$ (mm)	$V_{eq,c}$ (%)	$\beta_{sd,c}$	D_{EEEP}
Monotonic (UM)	40.3	3383	35.8	10.1	28.3	-	-	2.8
Cyclic 1 (UM)	34.4	5678	29.0	4.9	17.5	4.2	0.73	3.5
Cyclic 2 (UM)	38.2	6418	29.9	4.7	18.4	4.1	0.60	3.9
Cyclic 3 (UM)	37.4	4081	31.6	7.4	17.8	3.6	0.60	2.4
$CoV_{UM,c}$ (%)	4.5	18.1	3.6	21.9	1.9	6.1	9.6	19.8
Cyclic 1 (SST)	36.0	3765	31.7	8.4	17.5	6.0	0.81	2.3
Cyclic 2 (SST)	34.3	3860	30.2	7.5	18.4	4.2	0.81	2.5
Cyclic 3 (SST)	36.4	2892	32.6	11.1	17.8	4.9	0.88	1.7
$CoV_{SST,c}$ (%)	2.5	12.4	3.2	17.0	1.9	15.1	3.8	15.8
$CoV_{global,c}$ (%)	4.0	27.2	4.1	29.4	1.9	17.7	14.3	28.3

(UM) Performed at the University of Minho; (SST) Performed by Simpson Strong-Tie.

The analysis of Figure 3.11 and Table 3.3 shows that the cyclic results obtained by the University of Minho have good proximity when compared to the experimental performed by Simpson Strong-Tie. Regarding the coefficient of variation of 27.2% in the elastic stiffness (k) and 29.4% in yielding displacement ($V_{y,EEEP}$), it may be related to the loading procedure adopted in the new proposal of the standard. However, it is important to note that, the tests performed at the University of Minho obtained greater degradation. In the same way, considering a CLT ground support, Figure 3.12 shows the experimental force-displacements loops obtained from the experimental campaign performed at the University of Minho.

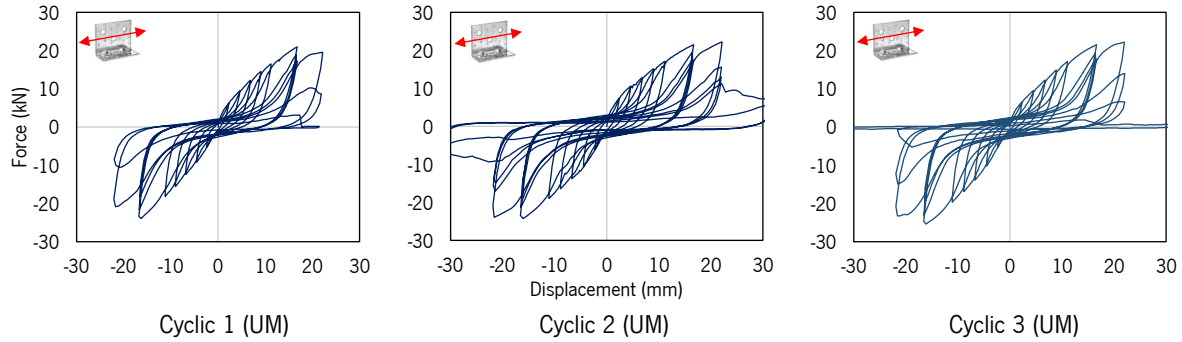

Figure 3.12 – Experimental force-displacement loops obtained in the case of angle brackets AE116 and a support made of CLT.

Using the obtained Load Envelope Curves, applying the new proposal of standard EN 12512 [5], Figure 3.13 shows the 1st Load Envelope Curves (1st LECs) and the Equivalent Energy Elastic-Plastic (EEEP) curves and Table 3.4 summarizes the main mechanical parameters obtained through each test.

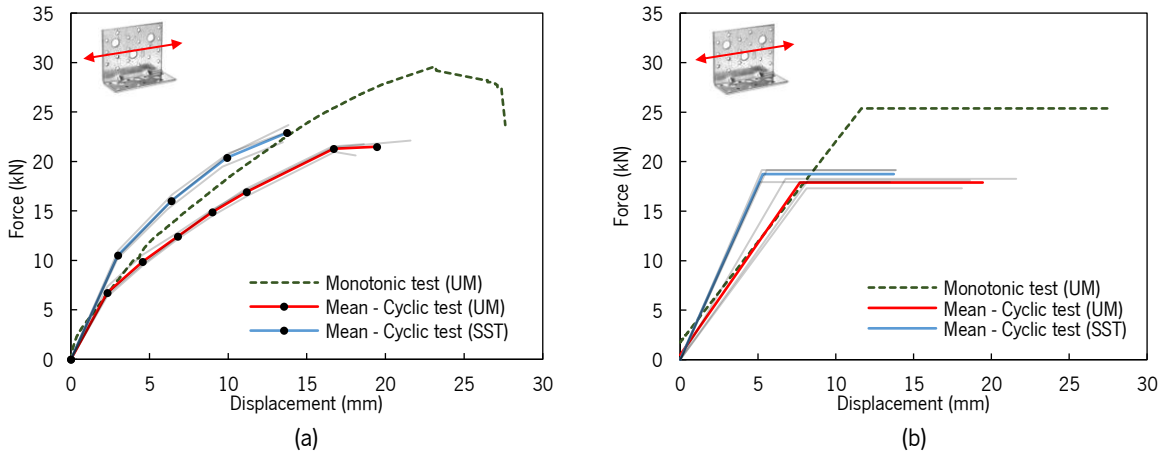

Figure 3.13 – Force versus displacement curves: (a) 1st Load Envelope Curves (1st LECs); (b) Equivalent Energy Elastic-Plastic (EEEP) curves applying the new proposal of the standard EN 12512 [5].

Table 3.4 – Results of the angle brackets AE116 under lateral loads and a support made of CLT.

Specimen	F_{max} (kN)	K_{EEEP} (N/mm)	$F_{y,EEEP}$ (kN)	$V_{y,EEEP}$ (mm)	$V_{u,EEEP}$ (mm)	$V_{eq,c}$ (%)	$\beta_{sd,c}$	D_{EEEP}
Monotonic (UM)	29.6	2027	25.4	10.7	27.6	-	-	2.6
Cyclic 1 (UM)	21.0	2064	17.3	8.1	18.1	5.2	0.60	2.2
Cyclic 2 (UM)	22.1	2644	18.3	6.8	21.6	4.8	0.60	3.2
Cyclic 3 (UM)	21.8	2140	18.1	8.2	18.6	5.0	0.60	2.3
$CoV_{UM,c}$ (%)	2.2	11.3	2.3	8.5	7.9	2.7	0.0	17.3
Cyclic 1 (SST)	23.0	3654	19.2	5.2	13.9	5.2	0.84	2.6
Cyclic 2 (SST)	23.7	3442	19.1	5.6	13.8	4.6	0.86	2.5
Cyclic 3 (SST)	21.9	3504	17.9	5.1	13.5	4.0	0.83	2.6
$CoV_{SST,c}$ (%)	3.1	2.5	3.0	3.5	1.3	11.0	1.4	2.7
$CoV_{global,c}$ (%)	4.0	22.5	3.6	19.9	18.4	8.7	16.9	12.3

(UM) Performed at the University of Minho; (SST) Performed by Simpson Strong-Tie.

Analyzing Figure 3.13 and Table 3.4, it is possible to verify again the proximity of the results obtained inboth experimental campaigns considered (UM and SST). The values of yielding displacement (V_y) and ductility (D) are closer than the previous analysis using a steel plate on support. This proximity is given

by the highest elastic stiffness followed by the lowest ultimate displacement of the tests performed by SST.On the other hand, the lowest elastic stiffness followed by the most significant ultimate displacement (V_u) of the tests performed at UM. Regarding the ultimate displacement (V_u), the tests performed at the University of Minho (UM) were always given by the strength degradation of 0.4. The failure, as can be seen in Figure 3.14 and Figure 3.15, for both cases (CLT and steel base supports) occurred by the combination of bending and withdrawn of the nails. For the tests with steel base occurred in the vertical steel plate (A), and for the CLT base tests on the horizontal steel plate (B). However, the angle brackets were slightly bent (see Figure 3.14) in the case of steel base support while in the case of the CLT ground support, the angle brackets were virtually undamaged (see Figure 3.15).

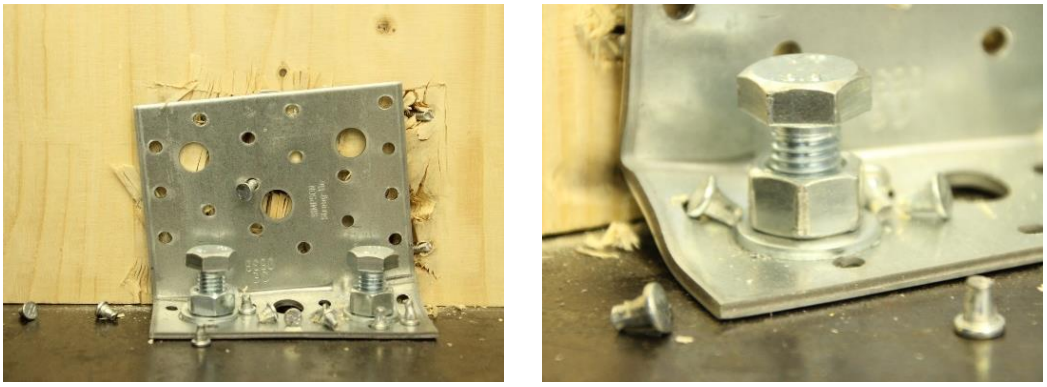

Figure 3.14 – Failure of the angle brackets AE116 under lateral loads with a steel plate support.

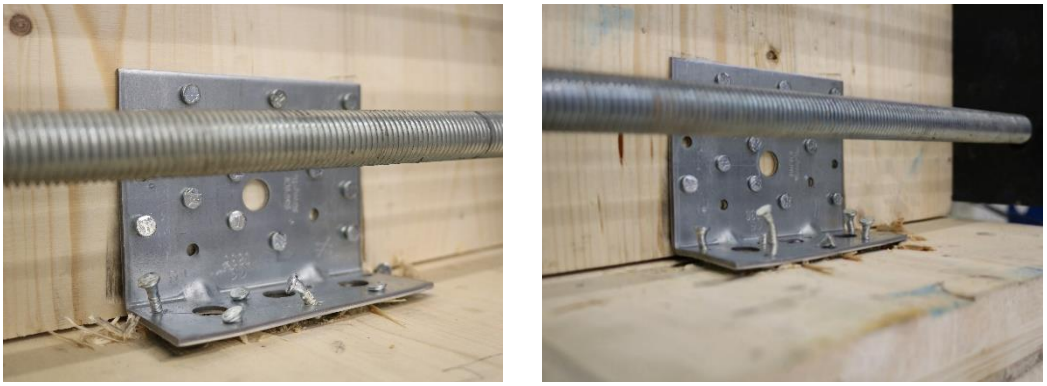

Figure 3.15 – Failure of the angle brackets AE116 under lateral loads and support made of CLT.

3.4.2 Angle brackets AE116 under tension loads

For the same metal connector, now, it consists of the analysis of their response under tension loads with a steel plate support. Figure 3.16 shows the experimental force-displacement loops obtained from the experimental campaign performed at the University of Minho (UM).

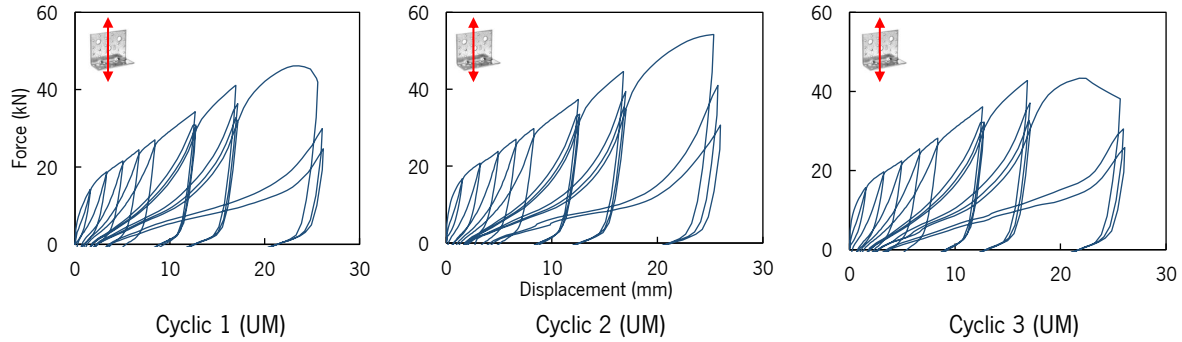

Figure 3.16 – Experimental force-displacement loops obtained in the case of angle brackets AE116 and a steel plate support.

Applying the new proposal of the standard EN 12512 [5] on the force-displacement loops: Figure 3.17 shows the 1st Load Envelope Curves (1st LECs), and the Equivalent Energy Elastic-Plastic (EEEP) curves; and, Table 3.5 summarizes the mechanical parameters obtained. However, it is important to point out that, as the last point of the cyclic test 1 and 2 performed by Simpson Strong-Tie did not obtain a great response due to the loading procedure inserted, the last point of the mean curve was admitted equal to the one of cyclic test 3.

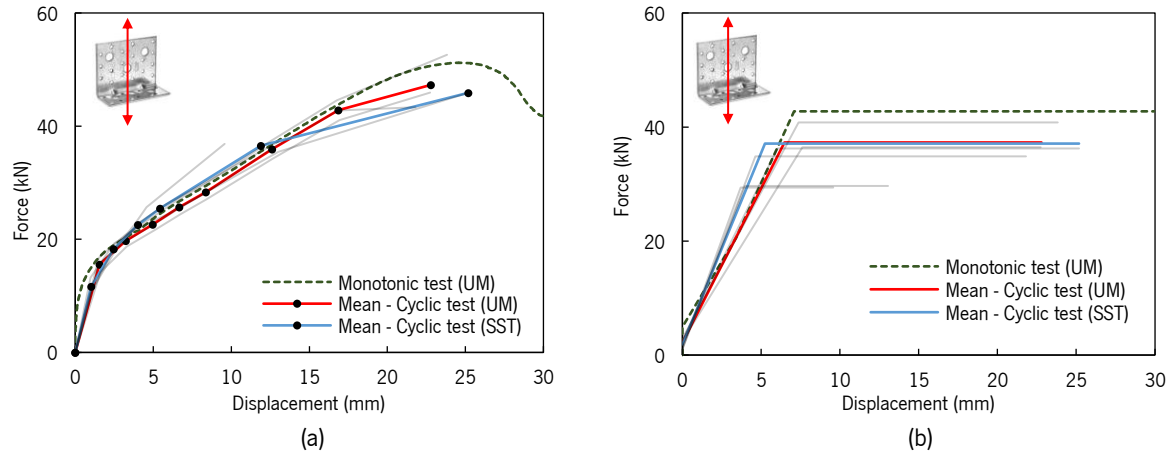

Figure 3.17 – Force versus displacement curves: (a) 1st Load Envelope Curves (1st LECs); (b) Equivalent Energy Elastic-Plastic (EEEP) curves.

Table 3.5 – Results of the angle bracket AE116 under tension loads and a steel plate support.

Specimen	**F_{max} (kN)**	**K_{EEEP} (N/mm)**	**$F_{y,EEEP}$ (kN)**	**$V_{y,EEEP}$ (mm)**	**$V_{u,EEEP}$ (mm)**	**$V_{eq,c}$ (%)**	**$\beta_{sd,c}$**	**D_{EEEP}**
Monotonic (UM)	51.2	4581	42.8	7.1	30.0	-	-	4.2
Cyclic 1 (UM)	45.9	4465	36.4	7.6	22.7	16.5	0.60	3.0
Cyclic 2 (UM)	52.6	5149	40.8	7.4	23.8	18.8	0.60	3.2
Cyclic 3 (UM)	43.3	7263	34.9	4.6	21.8	16.7	0.67	4.7
$CoV_{UM,c}$ (%)	8.3	21.2	6.7	20.7	3.6	5.8	5.3	20.9
Cyclic 1 (SST)	36.9	7663	29.4	3.7	9.6	20.5	0.89	2.6
Cyclic 2 (SST)	37.3	7208	29.7	4.0	13.1	17.8	0.87	3.3
Cyclic 3 (SST)	45.9	5569	36.2	6.0	25.2	15.3	0.75	4.2
$CoV_{SST,c}$ (%)	10.4	13.2	10.0	22.8	42.0	11.8	7.5	19.3
$CoV_{global,c}$ (%)	12.4	19.5	11.6	28.1	30.3	9.5	16.2	20.7

(UM) Performed at the University of Minho; (SST) Performed by Simpson Strong-Tie.

By observing Figure 3.17 and Table 3.5, despite the brittle failure observed in cyclic tests 1 and 2 performed by SST, it is possible to verify again the proximity of the results obtained in both experimental campaigns (UM and SST). As expected, high coefficients of variation were obtained to yielding (28.1%) and ultimate displacement (30.3%). As for the monotonic test performed, it presented results similar to the cyclic tests performed, where the ultimate displacement was given by the largest displacement allowed by the standard. In the case of support made of CLT, Figure 3.18 shows the experimental force-displacements loops obtained from the experimental campaign performed at the University of Minho (UM).

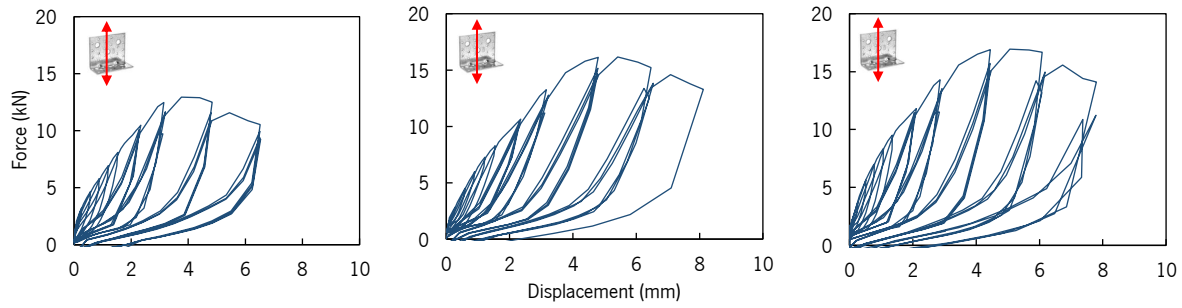

Figure 3.18 – Experimental force-displacement loops obtained from angle brackets AE116 with CLT support.

With the obtained force-displacement loops and applying the new proposal for the standard EN 12512 [5], Figure 3.19 was built to shows the 1st Load Envelope Curves (1st LECs) and the Equivalent Energy Elastic-Plastic (EEEP) curves and Table 3.6 summarizes the main mechanical parameters obtained.

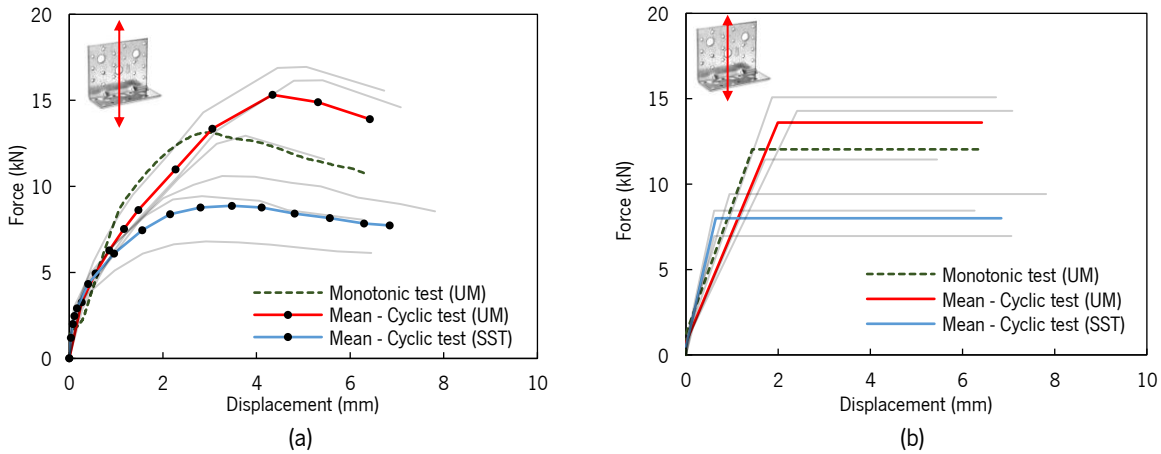

Figure 3.19 – Force versus displacement curves: (a) 1st Load Envelope Curves (1st LECs); (b) Equivalent Energy Elastic-Plastic (EEEP) curves.

Table 3.6 – Results of the angle bracket AE116 under tension loads andCLT support.

Specimen	F_{max} (kN)	K_{EEEP} (N/mm)	$F_{y,EEEP}$ (kN)	$V_{y,EEEP}$ (mm)	$V_{u,EEEP}$ (mm)	$V_{eq,c}$ (%)	$\beta_{sd,c}$	D_{EEEP}
Monotonic (UM)	13.1	6332	12.0	1.4	6.4	-	-	4.4
Cyclic 1 (UM)	12.9	6314	11.4	1.7	5.5	22.5	0.78	3.2
Cyclic 2 (UM)	16.2	5634	14.3	2.4	7.1	28.6	0.85	2.9
Cyclic 3 (UM)	16.9	7658	15.1	1.9	6.7	21.9	0.81	3.6
$CoV_{UM,c}$ (%)	11.3	12.9	11.5	14.9	10.9	12.4	3.5	8.5
Cyclic 1 (SST)	9.4	12827	8.4	0.6	6.3	28.6	0.88	10.3
Cyclic 2 (SST)	7.6	10822	7.0	0.6	7.1	40.9	0.88	11.6
Cyclic 3 (SST)	10.6	8905	9.4	0.9	7.8	59.0	0.88	8.3
$CoV_{SST,c}$ (%)	13.5	14.8	12.2	22.1	9.0	29.1	0.3	13.8
$CoV_{global,c}$ (%)	27.9	28.9	27.2	50.1	11.0	38.6	4.6	53.3

(UM) Performed at the University of Minho; (SST) Performed by Simpson Strong-Tie.

As one might expect, as the angle bracket with CLT base support presents poor behavior under tension loads, the differences between experimental campaigns were high, as can be seen in Figure 3.19 and Table 3.6. Regarding the failure of the specimens, it can be divided into two distinct cases. When a steel has used as support, the failure mode was located on the steel support (see Figure 3.20). On the other hand, when a CLT has used as support, the failure was given by the pullout of the nails inserted in the CLT element (see Figure 3.21).

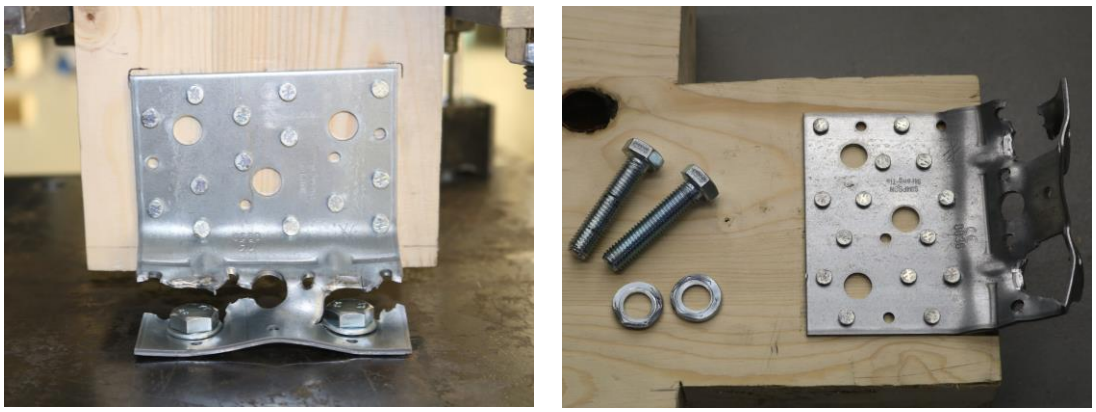

Figure 3.20 – Failure of the angle brackets under tension loads fixed to a steel plate support.

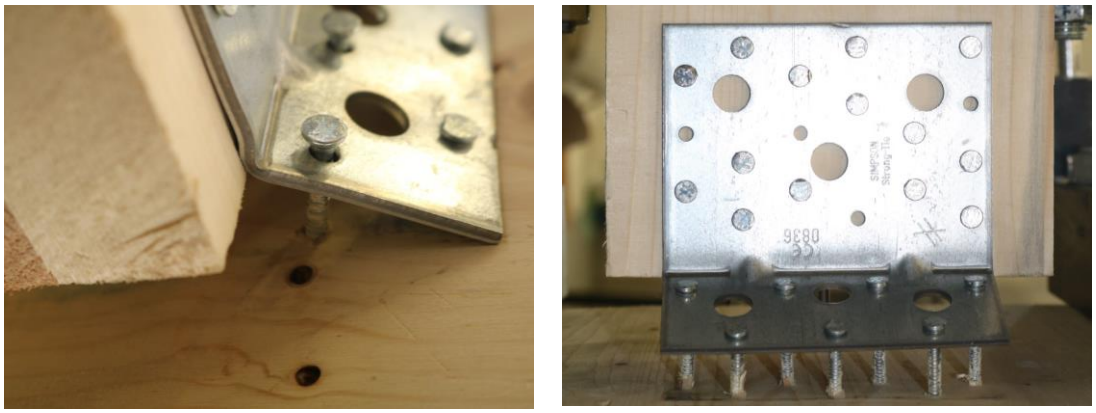

Figure 3.21 – Failure of the angle brackets under tension loads fixed to CLT support.

3.4.3 Hold-downs HTT22 and HTT22E under tension loads

The connectors hold-downs HTT22 and HTT22E are similar. The difference between them is the nail configuration and different holes presented by HTT22E. In this work only, the support made with CLT was analyzed. The decision was made considering the similarity of the tests results carried out by SST, for CLT and steel support. In this way, Figure 3.22 shows the experimental force-displacements loops obtained from the experimental campaign performed at the University of Minho (UM) for the hold-downs HTT22.

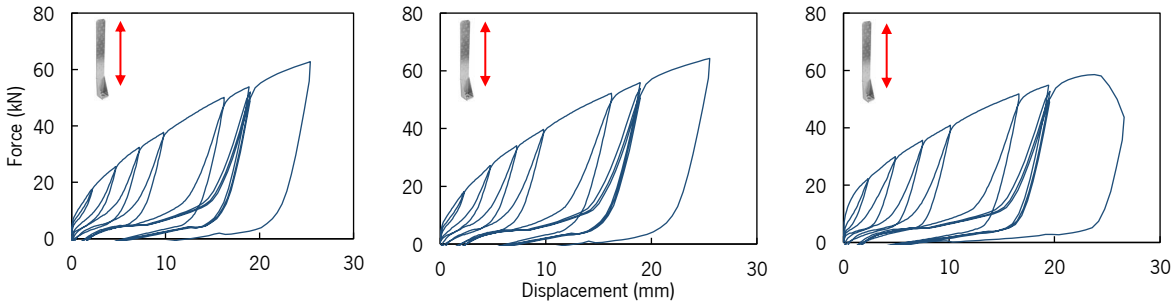

Figure 3.22 – Experimental force-displacement loops obtained from hold-downs HTT22 fixed to a CLT support.

Like angle brackets, using the obtained force-displacements loops and applying the proposal of standard EN 12512 [5], Figure 3.23 was built to shows the 1st Load Envelope Curves (1st LECs) and the Equivalent Energy Elastic-Plastic (EEEP) curves.Table 3.7 summarizes the main mechanical parameters obtained.

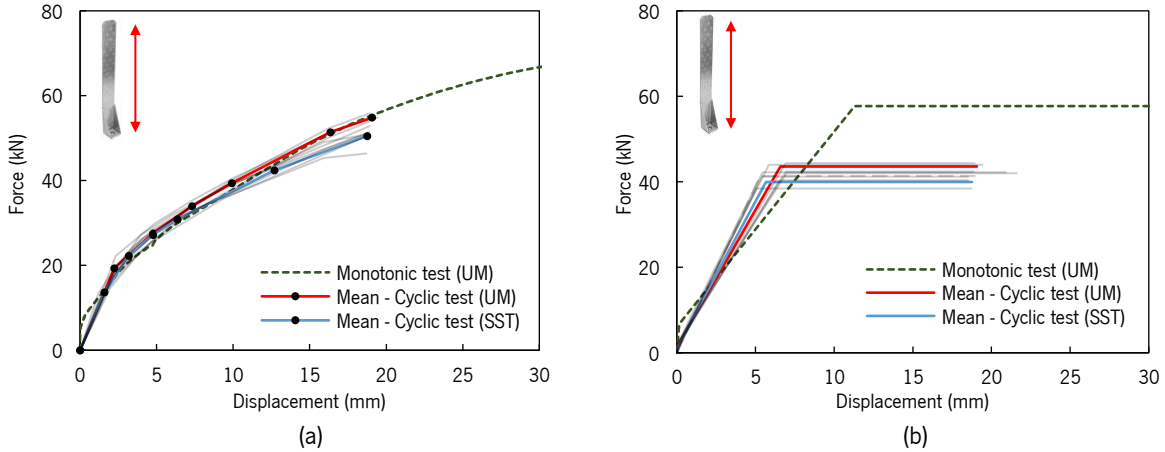

Figure 3.23 – Force versus displacement curves: (a) 1st Load Envelope Curves (1st LECs); (b) Equivalent Energy Elastic-Plastic (EEEP) curves.

Table 3.7 – Results of the hold-downs HTT22 under tension loads fixed to CLT support.

Specimen	F_{max} (kN)	K_{EEEP} (N/mm)	$F_{y,EEEP}$ (kN)	$V_{y,EEEP}$ (mm)	$V_{u,EEEP}$ (mm)	$V_{eq,c}$ (%)	$\beta_{sd,c}$	D_{EEEP}
Monotonic (UM)	67.9	3950	57.7	11.3	30.0	-	-	3.1
Cyclic 1 (UM)	53.8	5870	42.4	6.9	18.9	20.4	0.91	2.7
Cyclic 2 (UM)	55.9	6205	44.4	6.9	18.9	20.8	0.88	2.7
Cyclic 3 (UM)	54.8	7293	44.0	5.9	19.4	18.0	0.90	3.3
$CoV_{UM,c}$ (%)	1.5	9.4	2.0	7.8	1.3	6.2	1.6	9.7
Cyclic 1 (SST) [a]	51.5	5731	42.0	7.0	21.6	24.6	0.75	3.1
Cyclic 2 (SST) [a]	52.9	7869	41.0	5.2	18.9	26.2	0.87	3.6
Cyclic 3 (SST) [a]	51.4	7423	42.2	5.5	20.9	26.5	0.75	3.8
$CoV_{SST,c}$ (%)	1.3	13.1	1.3	13.2	5.5	3.2	7.2	8.8
Cyclic 1 (SST) [b]	50.7	7476	41.2	5.4	18.5	18.7	0.60	3.4
Cyclic 2 (SST) [b]	50.7	6017	40.4	6.5	18.5	18.0	0.87	2.8
Cyclic 3 (SST) [b]	46.4	7485	38.4	5.1	18.7	21.1	0.74	3.7
$CoV_{SST,c}$ (%)	4.1	9.9	2.9	11.1	0.5	6.9	14.9	10.9
$CoV_{global,c}$ (%)	5.1	11.6	4.1	12.5	5.4	14.7	12.1	12.4

(UM) Performed at the University of Minho; (SST) Performed by Simpson Strong-Tie; a) Steel plate support; b) CLT support.

The analysis of Figure 3.23 and Table 3.7 shows the proximity of all cyclic results, where the coefficient of variation is always lower than 15%. As for the monotonic test performed, it presented lower elastic stiffness with higher load capacity compared to cyclic tests, where the ultimate displacement (V_u) was given by the largest displacement allowed by the standard (30 mm). In the case of the hold-down HTT22E, Figure 3.24 shows the experimental force-displacements loops obtained from the experimental campaign performed at the University of Minho (UM).

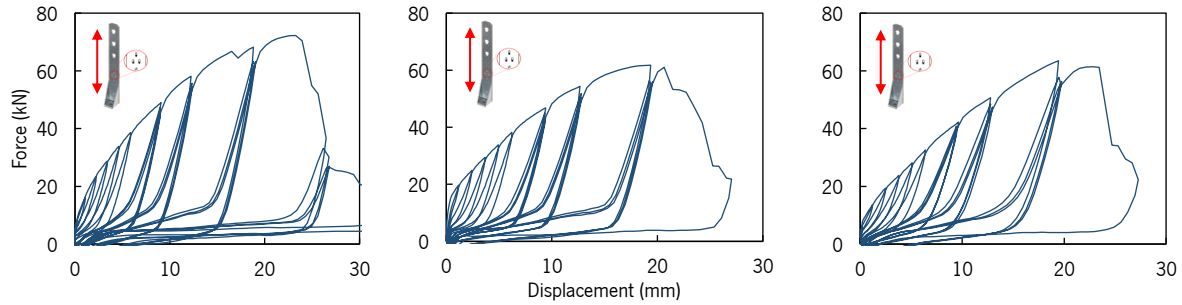

Figure 3.24 – Experimental force-displacement loops obtained in the case of hold-downs HTT22E and a CLT support.

Applying the new proposal of the standard EN 12512 [5], Figure 3.25 shows the 1st Load Envelope Curves (1st LECs) and the Equivalent Energy Elastic-Plastic (EEEP) curves and Table 3.8 the main mechanical parameters obtained. Also, for a better analysis of the differences between the hold-downs considered, the average curve of HTT22 was added in Figure 3.25.

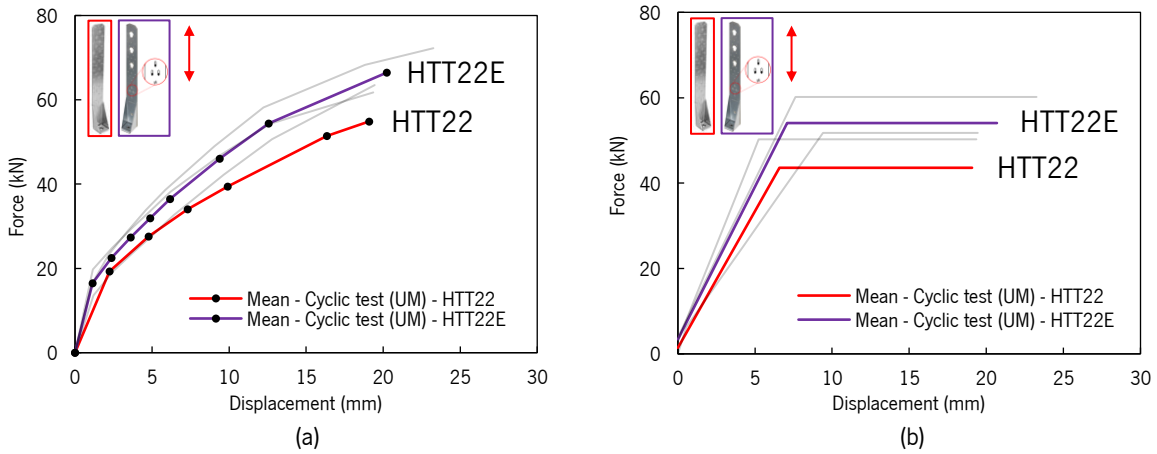

Figure 3.25 – Force versus displacement curves: (a) 1st Load Envelope Curves (1st LECs); (b) Equivalent Energy Elastic-Plastic (EEEP) curves.

Table 3.8 – Results of the hold-downs HTT22E under tension loads and CLT support.

Specimen	$F_{max,c}$ (kN)	$K_{EEEP,c}$ (N/mm)	$F_{y,EEEP,c}$ (kN)	$V_{y,EEEP,c}$ (mm)	$V_{u,EEEP,,c}$ (mm)	$V_{eq,c}$ (%)	$\beta_{sd,c}$	D_{EEEP}
Cyclic 1 (UM)	72.2	7383	60.2	7.6	23.3	21.5	0.92	3.1
Cyclic 2 (UM)	61.7	9042	50.3	4.9	19.4	23.3	0.92	3.9
Cyclic 3 (UM)	63.5	5136	51.8	8.7	19.4	22.1	0.88	2.2
$CoV_{UM,c}$ (%)	7.0	22.3	8.1	22.6	8.8	3.3	2.0	22.8

The analysis of Figure 3.25 and Table 3.8 show the increase of the load-carrying capacity of the HTT22E around 21% higher in comparison to the hold-downs HTT22. Regarding the failure, both hold-down connectors showed the same failure, which occurred on a combination of bending and withdrawn of the nails, as can be seen in Figure 3.26 and Figure 3.27. However, the behavior of the three nails with the new configuration (see Figure 3.27), can be the reason for the highest resistance of the connector, where the different openings of the nail holes seems to allow higher energy dissipation.

Figure 3.26 – Failure of the hold-downs HTT22 under tension loads.

Figure 3.27 – Failure of the hold-downs HTT22E under tension loads.

3.4.4 Angle brackets AB+plate and ABAI under lateral loads

In the case of the connectors analyzed by the Simpson Strong-Tie campaign, AB+plate and ABAI have the same configuration, but the difference is given by an acoustic layer (sylodyn [47]) in the ABAI connector. Thus, the main objective is to assess the influence of the acoustic layer presence under lateral loads. In this way, Figure 3.28 and Figure 3.29 shows the experimental force-displacement loops obtained from the experimental campaign performed by Simpson Strong-Tie (SST) for the angle brackets AB+plate and ABAI, respectively.

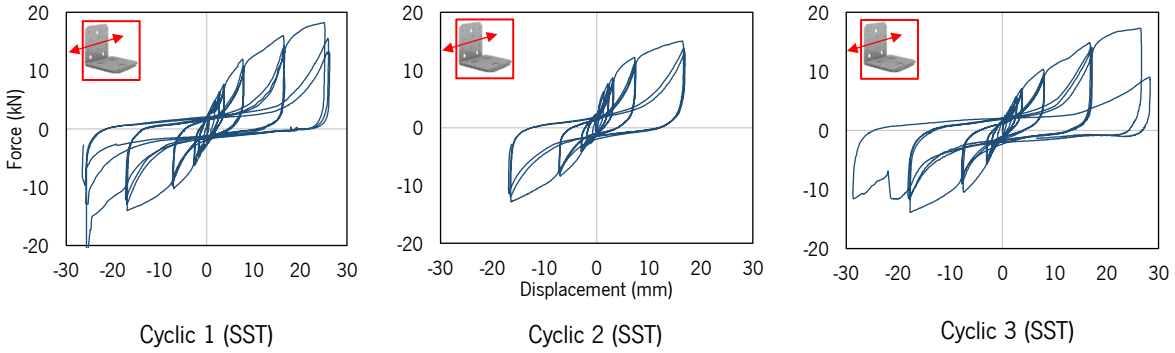

Figure 3.28 – Experimental force-displacement loops obtained from angle brackets AB+plate fixed to a CLT support.

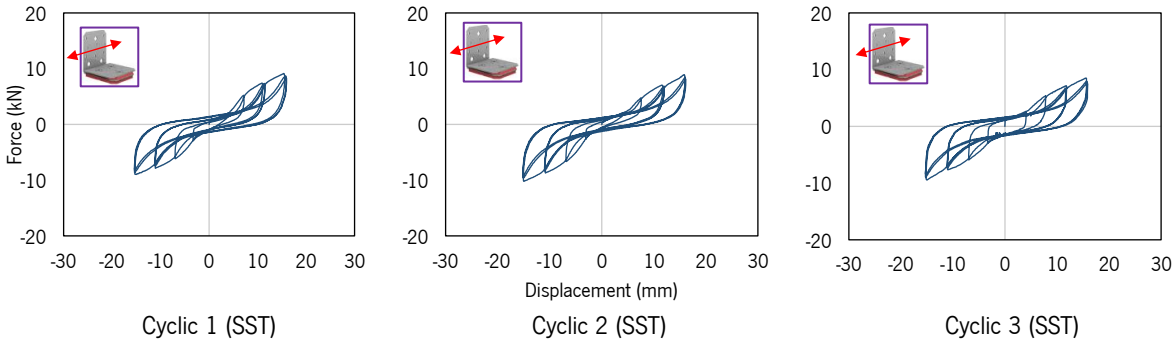

Figure 3.29 – Experimental force-displacement loops obtained from angle brackets ABAI fixed to a CLT support.

Based on the force-displacement loops and applying the new proposal of standard EN 12512 [5], Figure 3.30 shows the 1st Load Envelope Curves (1st LECs) and the Equivalent Energy Elastic-Plastic (EEEP) curves. Table 3.9 shows the main mechanical parameters obtained.

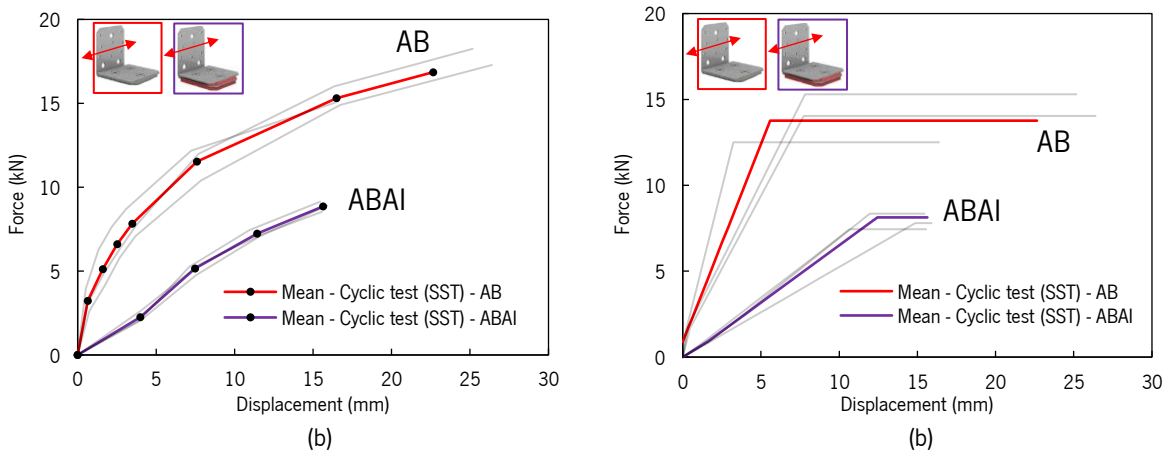

Figure 3.30 – Force versus displacement curves: (a) 1st Load Envelope Curves; (b) Equivalent Energy Elastic-Plastic curves.

Table 3.9 – Results of the angle brackets AB+plate and ABAI under lateral loads fixed to a CLT support.

Specimen	$F_{max,c}$ (kN)	$K_{EEEP,c}$ (N/mm)	$F_{y,EEEP,c}$ (kN)	$V_{y,EEEP,c}$ (mm)	$V_{u,EEEP,c}$ (mm)	$V_{eq,c}$ (%)	$\beta_{sd,c}$	D_{EEEP}
AB - Cyclic 1 (SST)	18.2	1812	15.3	7.2	25.2	4.6	0.72	3.5
AB - Cyclic 2 (SST)	15.0	3612	12.5	3.0	16.4	4.6	0.87	5.5
AB - Cyclic 3 (SST)	17.3	1700	14.0	7.2	26.4	4.3	0.61	3.7
$CoV_{SST,c}$ (%)	8.0	36.9	8.2	34.0	19.7	3.1	14.5	20.9
ABAI - Cyclic 1 (SST)	9.1	729	8.4	12.6	15.5	4.7	0.90	1.2
ABAI - Cyclic 2 (SST)	8.9	527	7.8	14.9	15.9	4.9	0.90	1.1
ABAI - Cyclic 3 (SST)	8.5	704	7.4	10.8	15.6	3.7	0.90	1.4
$CoV_{SST,c}$ (%)	2.8	13.8	4.7	13.3	1.2	12.1	0.1	12.4

The analysis of Figure 3.30 and Table 3.9, as expected, shows the decrease of the load-carrying capacity of the ABAI connector compared to the AB+plate without the acoustic layer. The failure of the specimens occurred on rotation and combination of bending and withdrawn of the nails, as can be seen in Figure 3.31 and Figure 3.32. It is important to note that the screws SDS (see Figure 3.2) on angle bracket ABAI has been pullout (see Figure 3.32), where the main reason is related to the reduced length of the screw inserted in the CLT base support.

Figure 3.31 – Failure of the angle brackets AB+plate under lateral loads.

Figure 3.32 – Failure of the angle brackets ABAI under lateral loads.

3.4.5 Angle brackets AB+plate and ABAI under tension loads

For the same angle brackets previously analyzed, but now under tension loads. Figure 3.33 (angle bracket AB+plate) and Figure 3.34 (angle bracket ABAI) show the experimental force-displacement loops obtained from the experimental campaign performed by Simpson Strong-Tie (SST).

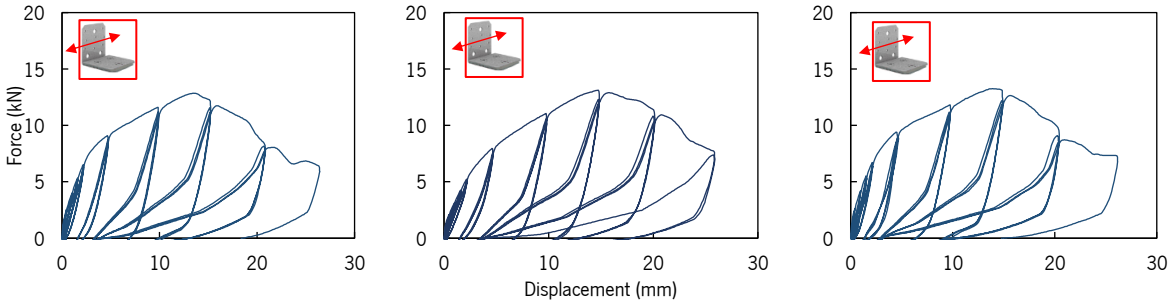

Figure 3.33 – Experimental force-displacement loops obtained from angle brackets AB+plate with CLT support.

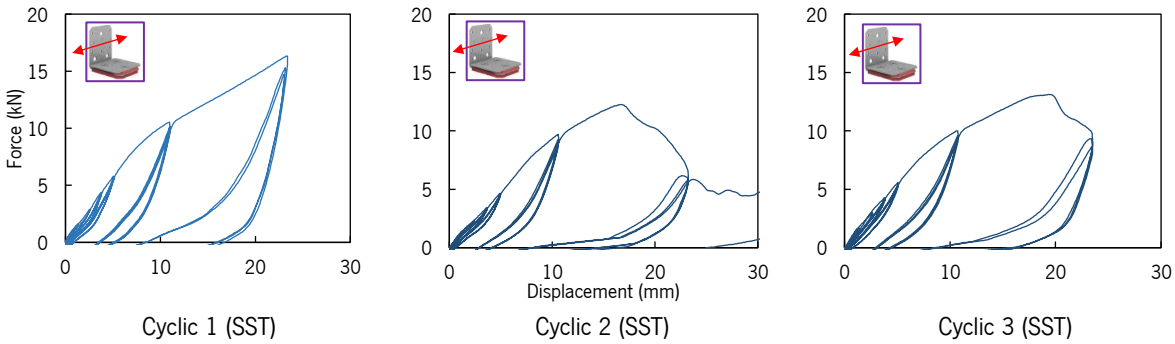

Figure 3.34 – Experimental force-displacement loops obtained from angle brackets ABAI with CLT support.

Using the obtained force-displacement loops and applying the new proposal of the standard EN 12512 [5], Figure 3.35 shows the 1st Load Envelope Curves (1st LECs) and the Equivalent Energy Elastic-Plastic (EEEP) curved and Table 3.10 the main mechanical parameters obtained.

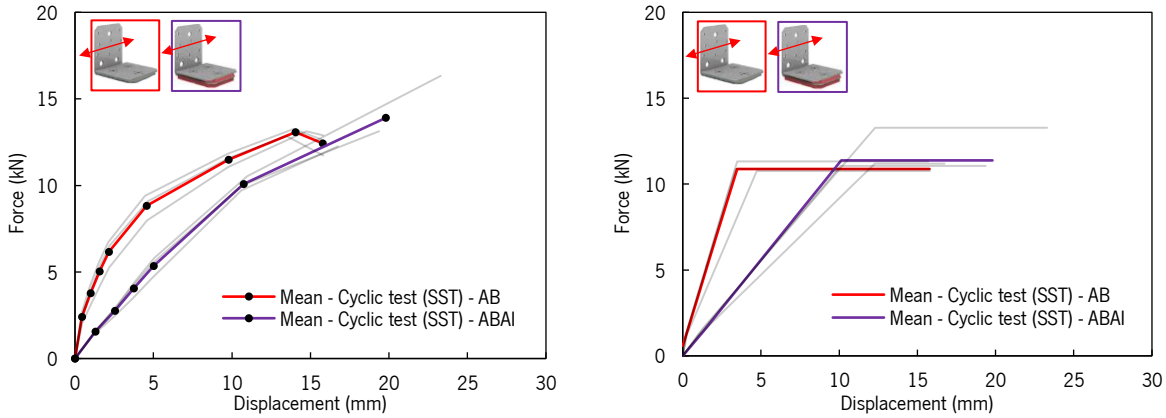

Figure 3.35 – Force versus displacement curves: (a) 1st Load Envelope Curves (1st LECs); (b) Equivalent Energy Elastic-Plastic (EEEP) curves.

Table 3.10 – Results of the angle brackets AB+plate and ABAI under tension loads with CLT support.

Specimen	$F_{max,c}$ (kN)	$K_{EEEP,c}$ (N/mm)	$F_{y,EEEP,c}$ (kN)	$V_{y,EEEP,c}$ (mm)	$V_{u,EEEP,c}$ (mm)	$V_{eq,c}$ (%)	$\beta_{sd,c}$	D_{EEEP}
AB - Cyclic 1 (SST)	12.9	3050	10.9	3.2	15.8	18.9	0.86	5.0
AB - Cyclic 2 (SST)	13.1	2134	10.8	4.4	15.8	21.3	0.90	3.6
AB - Cyclic 3 (SST)	13.3	3063	11.3	3.2	15.7	19.9	0.88	4.9
$CoV_{SST,c}$ (%)	1.3	15.8	2.2	16.0	0.4	5.1	1.7	14.3
ABAI - Cyclic 1 (SST)	16.3	1061	13.3	12.1	23.3	34.7	0.91	1.9
ABAI - Cyclic 2 (SST)	12.3	888	11.2	11.9	16.7	35.3	0.61	1.4
ABAI - Cyclic 3 (SST)	13.1	1081	11.1	10.0	19.4	39.9	0.68	1.9
$CoV_{SST,c}$ (%)	12.6	8.6	8.6	8.5	13.6	6.3	17.8	14.1

By analyzing just Figure 3.35, the decrease of elastic stiffness and the greater ultimate displacements of angle brackets ABAI, was evidenced. According to Table 3.10, it is important to point out the high equivalent viscous damping values and the low ductility values for the angle brackets with the acoustic layer. The failure of the specimens occurred on the pullout of the SDS screws (see Figure 3.2), as can be seen in Figure 3.36 and Figure 3.37.

Figure 3.36 – Failure of the angle brackets AB+plate under tension loads.

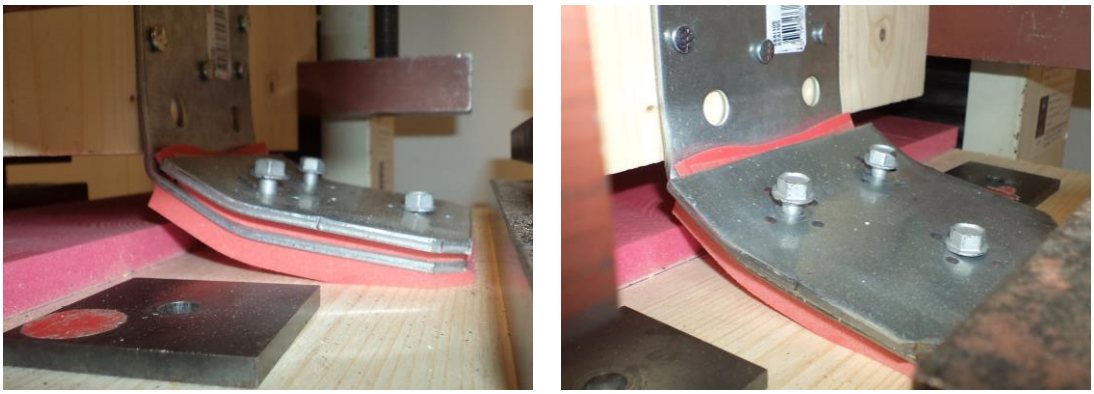

Figure 3.37 – Failure of the angle brackets ABAI under tension loads.

3.5 Discussion of the experimental tests

Presented the results and validated the test setups used in both experimental campaigns (UM and SST), the discussion of the results consists in: the comparison between the current [34] and the new proposal of standard EN 12512 [5] (see Table 3.11); the comparison between the hold-down configurations (see Table 3.12); and, finally, the discussion of the influence of the acoustic layer on angle brackets response (see Table 3.13). The values presented are related to the average of the three cyclic tests performed for each case studied.

Table 3.11 – Results of the cyclic tests applying the current and the new proposal of the standard EN 12512.

Specimen	Standard	K_c (N/mm)	$F_{y,c}$ (kN)	$V_{y,c}$ (mm)	$V_{eq,c}$ (%)	D_c
AE116	EN 12512:2001 [34]	6141	20.6	3.3	15.6	5.4
Lateral loads	*EN 12512 [5]	5392	30.1	5.7	3.9	3.3
Steel base	Δ (%)	12.2	46.0	70.9	74.8	39.4
AE116	EN 12512:2001 [34]	2749	12.1	4.4	20.6	4.9
Lateral loads	*EN 12512 [5]	2282	17.9	7.7	5.0	2.6
CLT base	Δ (%)	17.0	47.5	75.5	75.8	48.2
AE116	EN 12512:2001 [34]	7263	20.1	2.6	17.2	8.4
Tension loads	*EN 12512 [5]	5626	37.4	6.5	8.7	3.6
Steel base	Δ (%)	22.5	86.1	152.0	49.5	56.7
AE116	EN 12512:2001 [34]	12337	7.2	0.6	47.8	7.8
Tension loads	*EN 12512 [5]	6535	13.6	2.0	22.5	3.2
CLT base	Δ (%)	47.0	90.0	235.8	52.8	58.4
HTT22	EN 12512:2001 [34]	8624	25.2	2.9	36.5	6.5
Tension loads	*EN 12512 [5]	6456	43.6	6.6	19.8	2.9
	Δ (%)	25.1	72.7	124.7	45.8	55.2

* proposal for the revision of the European standard EN 12512 [5].

The comparison between the standards come out a difference for all mechanical parameters, where the smallest differences are relative to the elastic stiffness (k_c). It is possible to see higher values of yielding load and yielding displacement, and, on the other hand, lower values of elastic stiffness, equivalent viscous damping, and ductility, applying the new proposal of the EN12512 standard [5] in comparison to the old version [34].

Table 3.12 – Results of the cyclic tests on hold-downs HTT22 and HTT22E

Specimen	$F_{max,c}$ (kN)	K_c (N/mm)	$F_{y,EEEP,c}$ (kN)	$V_{y,EEEP,c}$ (mm)	$V_{eq,c}$ (%)	$D_{EEEP,c}$
HTT22	52.0	6456	43.6	6.6	19.8	2.9
HTT22E	65.8	7187	54.1	5.6	22.3	3.1
Δ (%)	21.0	10.2	19.4	18.4	11.4	5.0

Comparing between hold-downs HTT22 and HTT22E, the new configuration (HTT22E) demonstrates an increase of the load-carrying capacity (see Table 3.12). This increase can be considered reasonable because of the different typology of the holes in HTT22E, where allow higher energy dissipation. In relation to the results, it was evident in maximum force (21.0%), yielding load (19.4%), and yielding displacement (18.4%).

Table 3.13 – Results of the cyclic tests on angle brackets AB+plate and ABAI.

Specimen		$F_{max,c}$ (kN)	K_c (N/mm)	$F_{y,EEEP,c}$ (kN)	$V_{y,EEEP,c}$ (mm)	$V_{eq,c}$ (%)	$D_{EEEP,c}$
Lateral loads	AB+plate	16.9	2375	13.9	5.8	4.5	4.2
	ABAI	8.9	653	7.9	12.8	4.4	1.2
	Δ (%)	89.9	263.6	77.3	54.6	1.0	237.8
Tension loads	AB+plate	13.1	2749	11.0	3.6	20.0	4.5
	ABAI	13.9	1010	11.8	11.3	36.7	1.8
	Δ (%)	5.8	172.3	7.2	68.2	45.3	154.8

Finally, in the case of the angle brackets with (ABAI) and without (AB+plate) acoustic layer, the analysis of Table 3.13 shows that, as expected, the acoustic layer significantly decreases the resistance. Moreover, it is clear the difference in elastic stiffness and ductility for both cases. In general, it is possible to conclude that the acoustic layer reduces the response of this metal connector under cyclic loads.

3.6 Final remarks

In this chapter, the behavior of the shear connectors AE116, AB+plate and ABAI and the uplift connectors HTT22 and HTT22E have been studied. In the experimental campaign conducted at the University of Minho (UM), in the first phase, the validation of the setups was performed by comparing the results with the same connectors analyzed by Simpson Strong-Tie (SST). In the second phase, an analysis between the current and the proposal for the revision of the European standard EN 12512 is presented. Finally, the comparison of the new configuration hole of the connector HTT22 was also studied (HTT22E). For the experimental analysis, besides the validation of the results obtained through the experimental analysis performed at the University of Minho, the presence of an acoustic layer was evaluated.

Regarding the setups performed at the University of Minho, it can be concluded that they have been properly performed, presenting results close to those performed by the Simpson Strong-Tie.

In this way, applying the proposed load protocol in the standard EN 12512, it was possible to visualize a greater degradation of the connectors analyzed at the University of Minho. Comparing the current and the new proposal of the standard EN 12512, it was possible to verify large differences between the obtained values applying those two methodologies, where the smallest difference is relative to the elastic stiffness. The differences can be considered normal, in which the proposal for the new version of the standard presents a different and much more detailed view in relation to the current standard.

In the case of the HTT22 and HTT22E uplift connectors, it was possible to conclude that the new configuration (HTT22E) presents higher resistance, where the new configuration and different opening of the nail holes seems to allow higher energy dissipation.

Finally, comparing the connectors with and without the acoustic layer, the results are rather evident, where the acoustic layer results in a high reduction of the load-carrying capacity of the metal connector. Thus, it can be concluded that the acoustic layer should be avoided in areas with high seismicity.

Chapter 4

Experimental campaign of 2-story CLT building

4.1 Introduction

An experimental program based on quasi-static tests was performed at the University of Minho, by using a 2-story CLT building, with the leading research aim being to analyze the 3D system performance when subjected to lateral loads. The main variables for the experimental program were the analysis of lateral resistance and deformability capacity, global behavior of the structure, and the performance of the connectors (mainly AE116 and HTT22 from Simpson Strong-tie analyzed in chapter 3). The building was designed to obtain a non-symmetric structure, with a clear distinction between the longitudinal (stiffer) axis and the transverse one and assuming that the center of the stiffness had to be different from the center of mass. Moreover, to avoid a possible overlap of effects, it was assumed that the metal connectors would be placed only in the CLT walls working as shear walls in each loading direction, during each test.

4.2 Building description

The building had a plan of 4.5 m x 9.1 m, with two floors, with a total height of 5.04 m. Several partition walls and openings were included (a staircase on the 1st floor and on the external walls), to create an asymmetric structure prone to torsion. The CLT panels were produced and supplied by Stora Enso Wood Products Ltd. These panels were made of spruce (picea abies), with an approximate density of 470 kg/m^3. In terms of thickness, the CLT panels for the walls had 100 mm (5-layers of 20 mm) and the floors' CLT panels had 120 mm (3-layers with 40 mm). Several metal connectors were installed on the structure, mainly angle brackets AE116 (shear resistance) and hold-downs HTT22 (uplift resistance) already studied in detail in chapter 3. However, as they play an important role in final results and to avoid a possible overlapping of effects, the connectors were applied only to the shear walls in each direction tested. A panoramic image and plans of the building, with the location of the main connectors inserted in the tests, are presented in Figure 4.1.

(a)

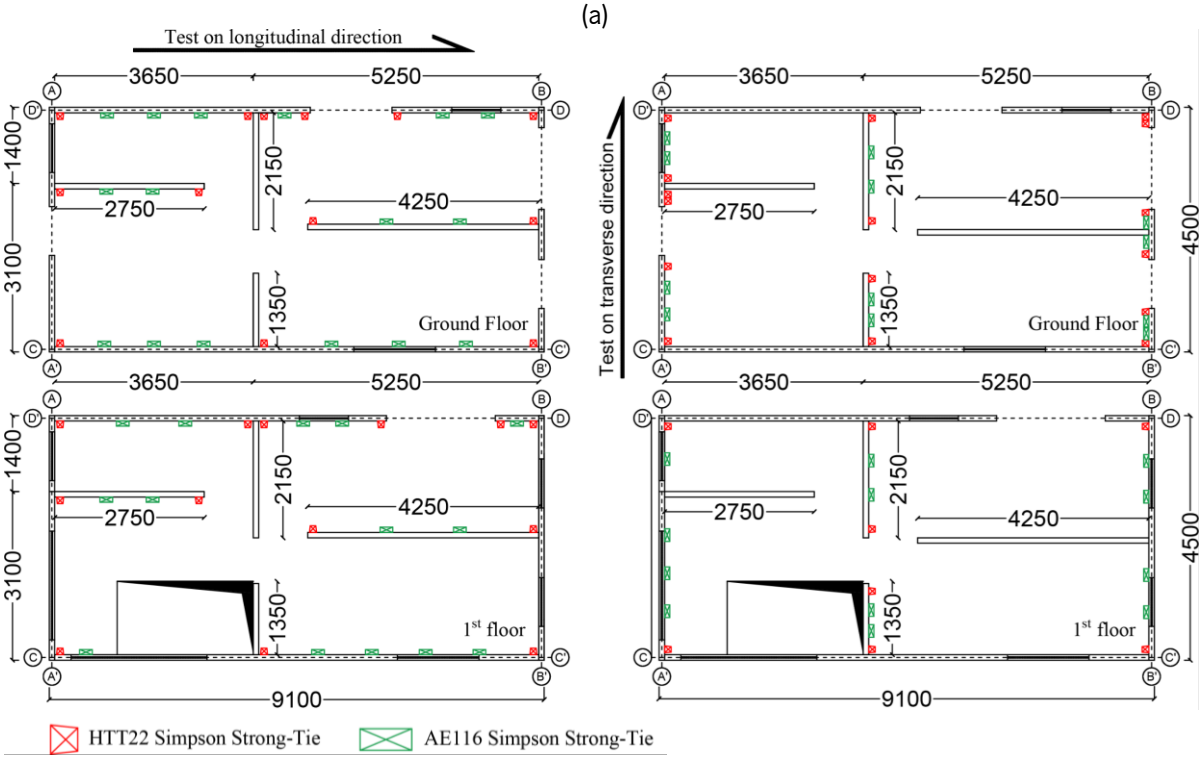

(b) (c)

Figure 4.1 – Panoramic image (a) and building plans, with the location of main connectors in the tests under longitudinal (a) and transversal (b) direction. (dimensions in mm).

The CLT wall panels were connected with LVL (laminated veneer lumber [49]) spline joints, with the introduction of screws to ensure the continuity of the wall. The same connection method was used on floors. Regarding the openings in the walls, several windows and doors were included, as depicted in Figure 4.2. Knowing that the openings can result in structural disorders, the percentage of openings in each façade is shown in Figure 4.2.

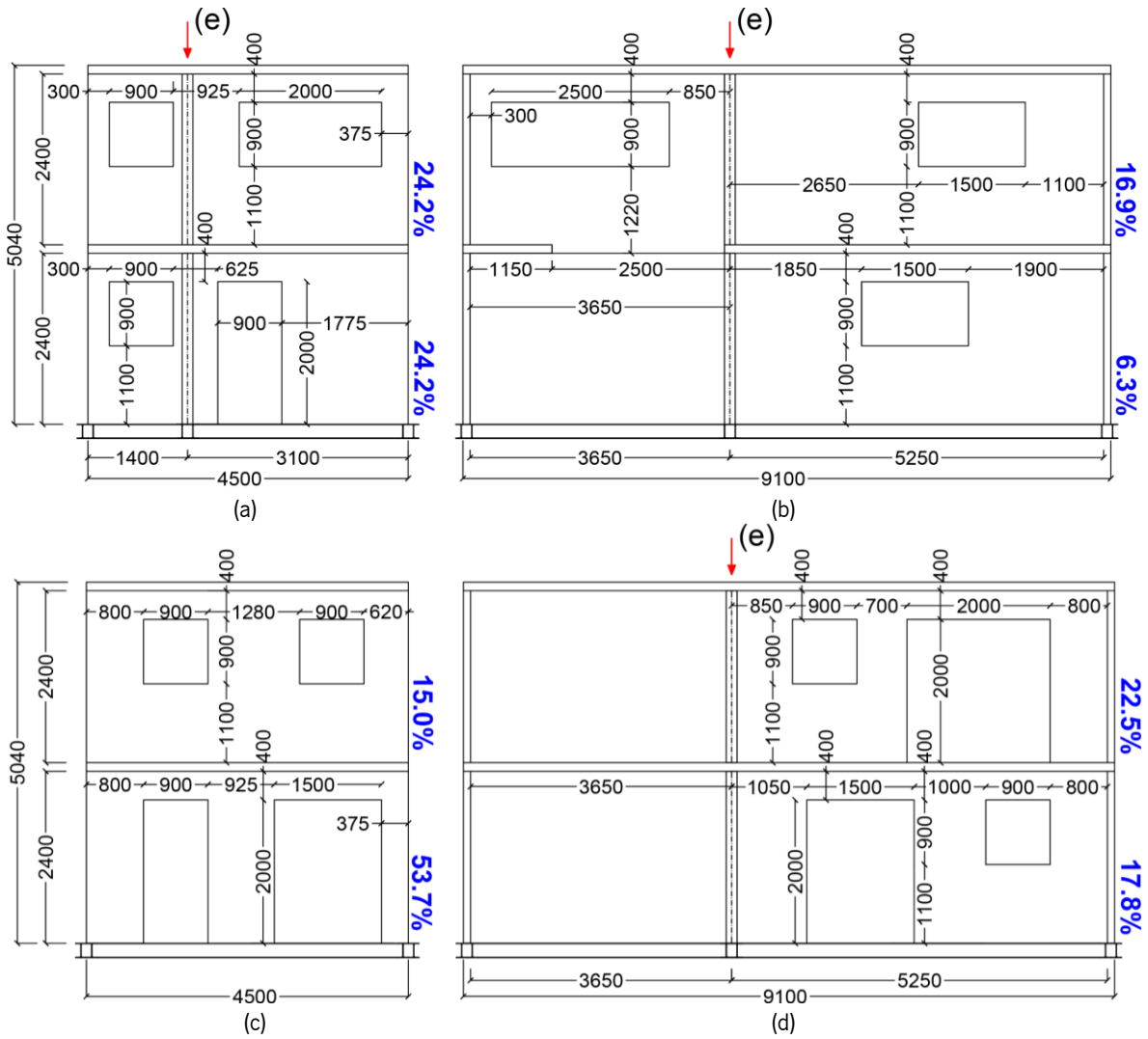

Figure 4.2 – Building façades (dimensions in mm): (a) façade A-A'; (b) façade C-C'; (c) façade B-B'; (d) façade D-D'; (e) spline joint with LVL. (note that the plotted percentage values concern the relative area of the openings within each façade).

In terms of vertical loads, for the representation of a real building, in addition to own weight, the remaining dead loads and the live-loads [50] (combinations of the seismic action of Eurocode 8 [51]) were placed over the building as additional masses, by distributing drums of water over the floors as shown in Figure 4.3. A total of 2 kN/m^2 and a 1.7 kN/m^2 were applied for the first and second floors, respectively.

(a) (b)

Figure 4.3 – Additional masses used in the tests. (a) 1st floor; (b) 2nd floor.

4.3 Setup and Instrumentation

The test setup was based on the need to have two lateral loads, each of the two directions of the CLT building, one on at each floor level. To achieve accurate experimental results, the main concerns of the test setup were: i) to have a rigid steel base to ensure adequate fixation of the building to the reaction floor of the laboratory, including the fixation of the CLT panels of the first floor to the base with angle-brackets (AE116) and hold-downs (HTT22), as already discussed (see Figure 4.4a); ii) a steel structure to place and fix the two hydraulic jacks responsible for applying the lateral loads in both axes of the building (see Figure 4.4b); the hydraulic jacks, placed in the middle of the façades, included one hinge in each extremity, to avoid other deformations and stresses (see Figure 4.4c); iii) a steel plate to ensure that the loads applied by the hydraulic jacks on the CLT floors were correctly distributed (see Figure 4.4d).

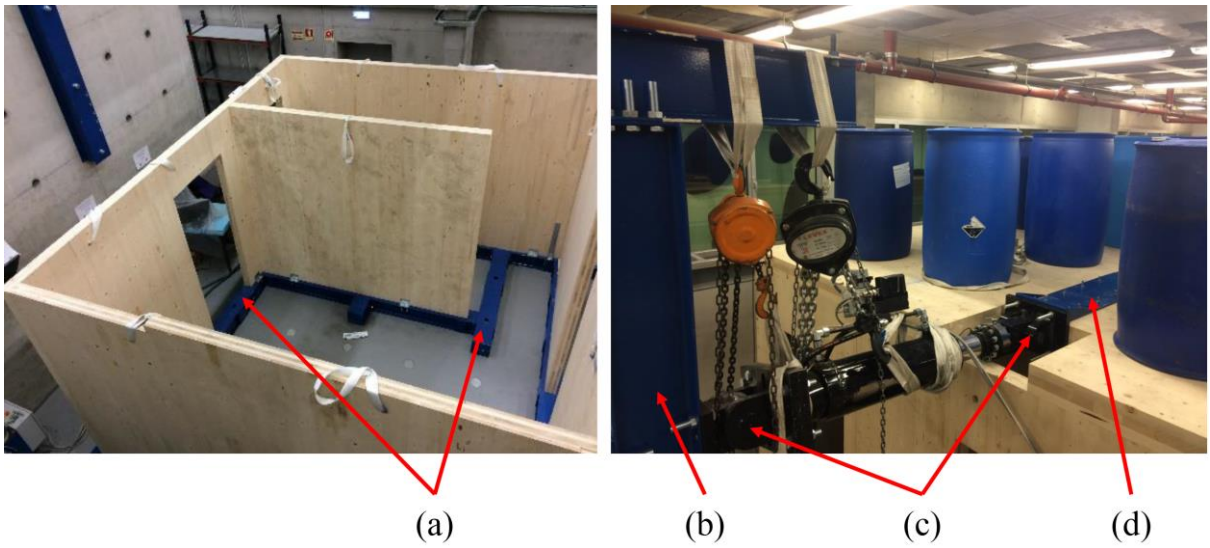

Figure 4.4 – The setup used in the tests: (a) Steel base structure; (b) Steel structure to fix the hydraulic jacks and (c) respective hinges; (d) Steel plate placed on the floors.

For the measurement of the displacement during each test, 24 LVDTs (Linear Variable Differential Transformers) were placed in demarcated positions, ensuring that not only the global deformation of the building, in each direction, was measured but also that the in-plane displacement, rotation of the floors, uplift of the walls panels and sliding were accurately registered. Figure 4.5 shows the location of: LVDTs and hydraulic jacks, applied at different levels of the building.

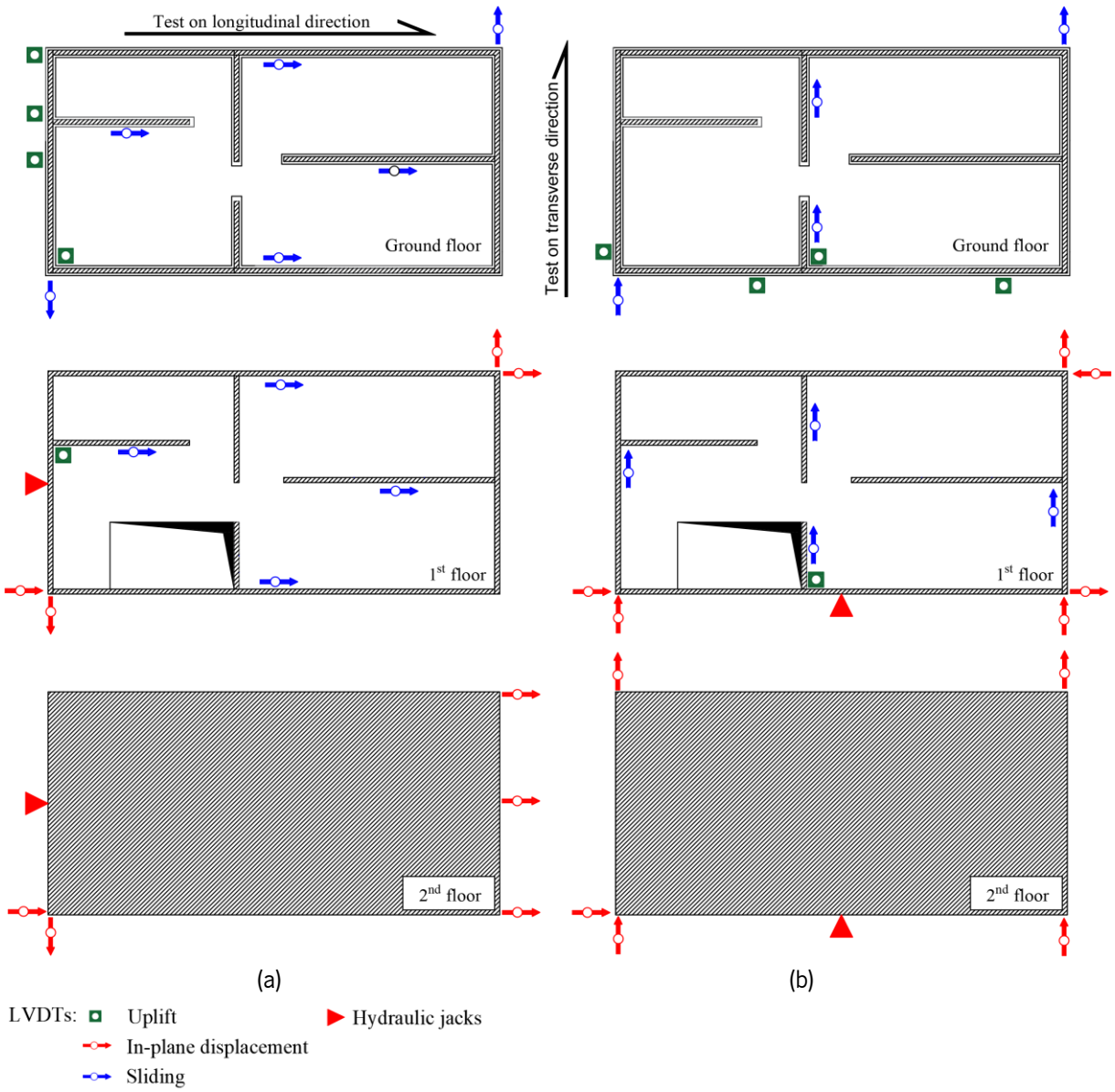

Figure 4.5 – Instrumentation used in the tests in longitudinal (a) and transverse (b) direction.

4.3.1 Frequencies estimation and definition of connectors

Connections play a prominent role in the performance of CLT buildings, and this example is no exception. The connections between the different CLT panels are crucial to ensure an adequate overall behavior of the system, keeping the different structural elements connected, while the local behavior of joints is fundamental to assure the deformability, ductility, and energy dissipation capacities needed. The connections used represented the common techniques used in practice, based on the use of angle brackets as shear connectors, hold-downs taking the uplift forces (tension), and adding screws to increase the stiffness of the connections. The metal connectors used, angle brackets and hold-downs were supplied by Simpson Strong-tie, while the screws were from Rothoblaas (see Figure 4.6). To ensure a perfect distribution of the forces introduced by the hydraulic jacks at the floors level, steel plates, screwed to the

CLT panels, were placed on both floors. Table 4.1 and Table 4.2 summarizes the different types of connections used and their locations.

HTT22 AE116 NP20/120/240 M12 & M16 CNA4.0×60

Figure 4.6 – Main metal connectors used in the tested CLT building.

Table 4.1 – Main metal connectors used in the CLT building.

Location	Type	Reference	Description
Ground floor [CLT-to-Steel]	Angle bracket	AE116	14 × CNA4.0×60 (A) 2 × M12 (B)
	Hold-down	HTT22	14 × CNA4.0×60 (A) 1 × M16 (B)
1st floor [CLT-to-CLT]	Angle bracket	AE116	14 × CNA4.0×60 (A) 7 × CNA4.0×60 (B)
	Hold-down	HTT22	14 × CNA4.0×60 (A) 1 × M16 (B)
	3 x Perforated plate	NP20/120/240	14 × CNA4.0×60 (staircase)

M12 - Threaded road Ø12 (8.8 Grade); M16 - Threaded road Ø16 (8.8 Grade)

HBS6.0×80 & HBS6.0×100 VGZ9.0×240

EVO8.0×60 HBS8.0×220

Figure 4.7 – General fasteners used in the tested CLT building.

Table 4.2 – General fasteners used in the tested CLT building.

Quantity	Location
EVO8.0×60 + M12	Steel plate-floors
2 × (HBS6.0×80) spaced to 150 mm	Wall-to-wall (spline joints)
2 × (HBS6.0×100) spaced to 150 mm	Floor-to-floor (spline joints)
HBS8.0×220 spaced to 150 mm	Wall-to-wall
VGZ9.0×240 spaced to 150 mm	Floor-to-wall

M12 - Threaded road Ø12 (8.8 Grade)

In the definition and design of the AE116 shear connections (number and location) used in the CLT building, the methodology proposed by Eurocode 8 (EC8) [51] was adopted. In this method, the horizontal forces are determined from the total mass of the building and the spectral acceleration of the building for the respective period. Horizontal forces were applied independently in longitudinal and transverse directions, where two separate analyses were carried out with the same seismic demand. The total mass

of the building admitted was 27 tons and, as the current EC8 does not provide a simplified method to define the period for CLT structures, the Rayleigh method was applied with the help of a finite element software RFEM [52] to the quantification of relative stiffness. Periods of 0.277 seconds (frequency of 3.60 Hz) and 0.385 seconds (frequency of 2.60 Hz) were obtained, for the longitudinal and transverse direction, respectively. In terms of seismic demand, the response spectrum was defined by NTC 2008 [53]. The south of Italy (Calabria) was the location chosen to obtain a spectrum with high seismic action.

Regarding the behavior factor used, a value of 2 (ductility class medium) was assumed, according to working documents aimed to prepare a new version of Eurocode 8, in particular, chapter 8 [54, 55]. Under these circumstances, a peak ground acceleration of 0.42 g was found. Thus, as both periods were in the area of constant spectral acceleration (horizontal behavior), the seismic base shear force used for the design was equal to 138 kN. On the other hand, the definition of the number and locations of the HTT22 the uplift resistance. Therefore, they were introduced near all openings and at all corners of the shear walls [32] (see Figure 4.1b and Figure 4.1c).

4.3.2 Monotonic tests

The quasi-static monotonic tests carried out consisted on the application of a displacement under a constant rate, on each floor, respecting the ISO/FDIS 21581:2010 [56]. Two hydraulic jacks were used, one on each floor, to apply the displacements under a constant rate of 0.08 mm/s and 0.04 mm/s on the second and first floor, respectively. Due to technical limitations, namely the load capacity of the hydraulic jack installed on the second floor, the criterion adopted to stop the tests was a load value of 300 kN in that hydraulic jack. Two tests were performed: one for each direction, longitudinal and transverse axes of the building.

4.3.3 Cyclic test

The cyclic test was also based on the loading procedure standardized by ISO/FDIS 21581:2010 [56], but was applied only in the transverse direction. Therefore, contrary to what happened with the monotonic tests, the loading procedure was, here, performed by force control, in which 0.90 kN/s was admitted on the 1st floor and 1.80 kN/s on the 2nd floor. Consequently, on the cyclic test, in which the need for a greater displacement of the hydraulic jacks occurred, the limitation was given by the maximum displacement of the 1st hydraulic floor of 100 mm (50 mm positive and 50 mm negative). Concerning the values to be reached for each step, this was achieved based on the ultimate displacement. Due to the

lack of definition of this value, a final displacement equal to the total height of the building divided by fifteen (*H/15*), according to the standard [56], was admitted. Since this factor is quite conservative, the number of cycles of the fourth and fifth steps of the loading procedure was changed to three (see Figure 4.8). Concerning the inserted connections, they were equal to the ones used in the monotonic test in the transverse direction, although all AE116 and HTT22 connections used were removed and new ones were introduced.

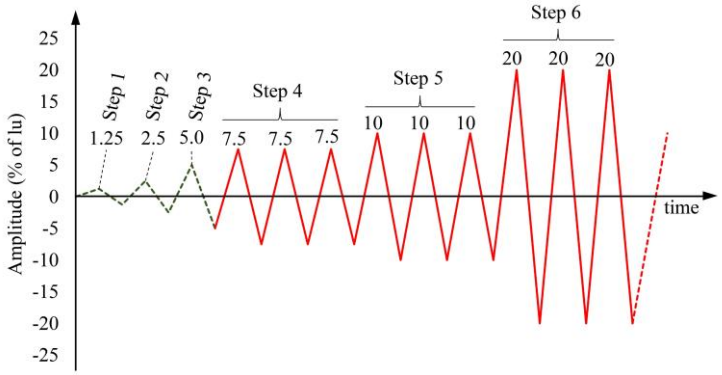

Figure 4.8 – Loading procedure defined by ISO/FDIS 21581:2010 for cyclic tests [56].

4.4 Results and discussion

Here, the main results obtained in the experimental program are described and discussed. Two experiments have been performed under monotonic loading and one under cyclic loading, and the results were separated into four groups: hydraulic jacks response, load-deformation response and damages observed.

4.4.1 Hydraulic jacks response

Figure 4.9 shows the experimental curves of the force achieved by each of the hydraulics during the time of each of the tests. It is important to note that monotonic tests were stopped when the criterion of the limitation for the load applied by the hydraulic jack of the 2nd floor (300 kN) was reached. Contrarily to the monotonic tests, for the cyclic test, due to the greater need for displacement, the hydraulic jack of the 1st floor determined the stopping criterion, because it has only 100 mm of maximum displacement (50 mm for each loading direction). However, due to the loss of displacements in the introduced hinges of the setup, the maximum displacement reached on the 1st floor was 30 mm.

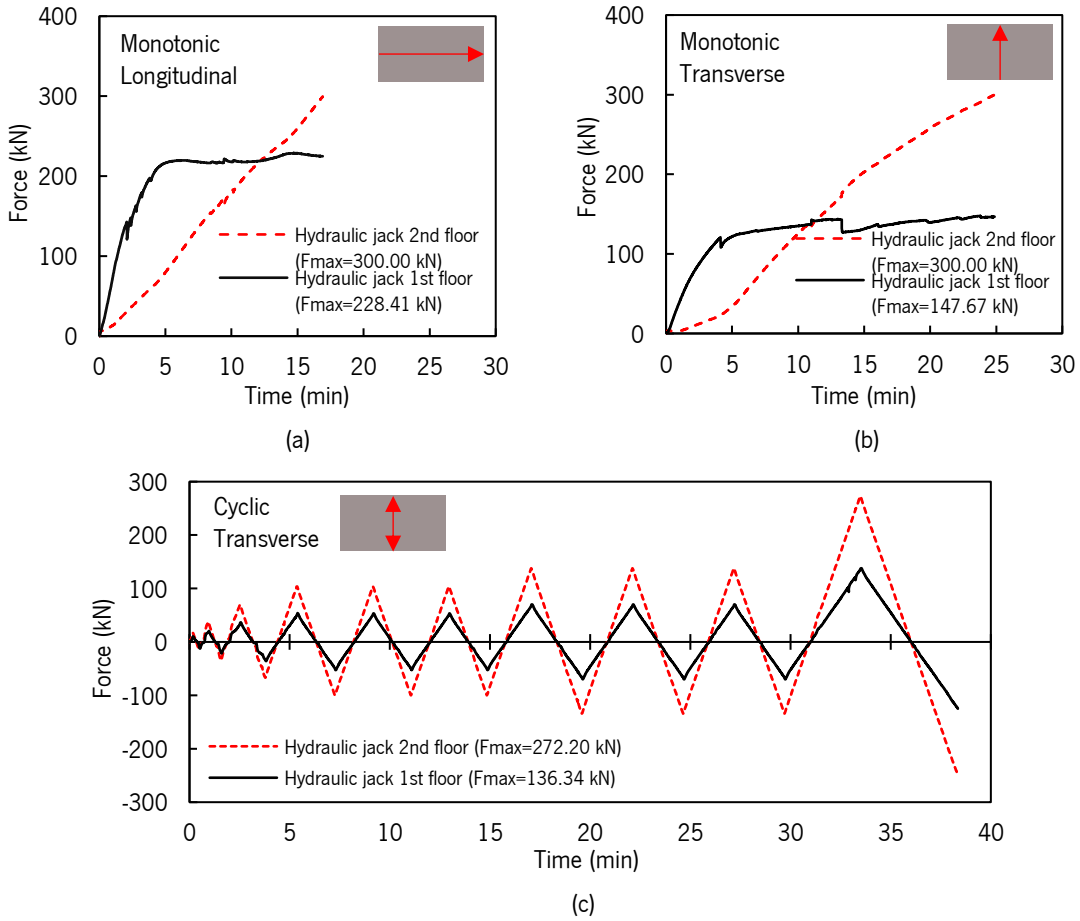

Figure 4.9 – Force versus time on the hydraulic jacks on the floors during the performed tests: (a) Monotonic test in the longitudinal direction; (b) Monotonic test in the transverse direction; (c) Cyclic test in the transverse direction.

The analysis of the graphs of the monotonic tests presented in Figure 4.9 showed a higher load-carrying capacity of the hydraulic jack of the 1st floor, as expected, with the longitudinal direction being the stiffest. Besides, through the monotonic tests, it is possible to observe the damage (plasticization) of the metal connectors on the ground floor (around five minutes in both tests). However, the same behavior did not happen on the connectors of the 1st floor due to the limitation of the hydraulic jack of the 2nd floor. The cyclic test performed, in comparison with the monotonic tests, did not reach the same load capacity for both the 1st and 2nd floor hydraulic jacks.

4.4.2 Load-deformation response

Figure 4.10 shows the maximum displacements found at different levels relative to rocking, sliding, and in-plane displacement (see caption of Figure 4.5). However, it is important to note that the rocking deformation values of 0.3 mm are relative to the verification of the uplift of the steel base structure to the laboratory concrete slab.

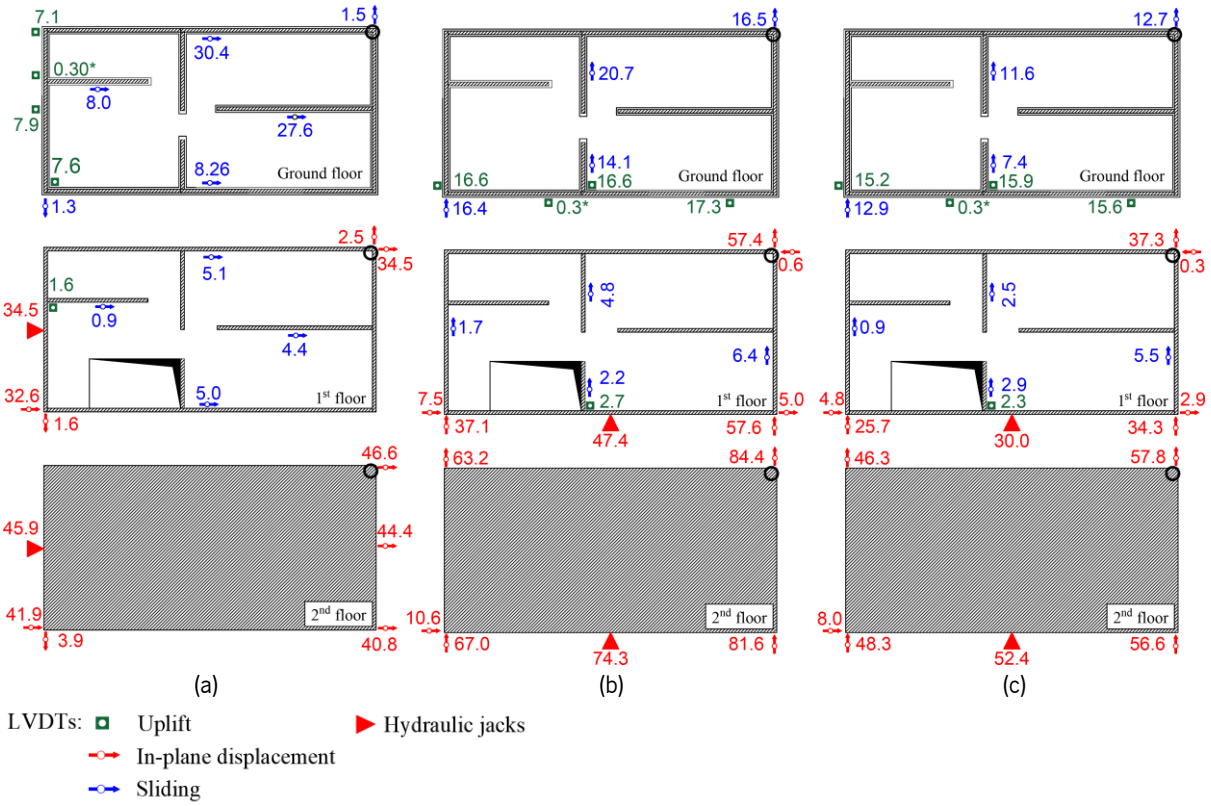

Figure 4.10 – Maximum displacements (mm) recorded during the tests: (a) Monotonic test in the longitudinal direction; (b) Monotonic test in the transverse direction; (c) Cyclic test in the transverse direction.

Similarly, but in more detail, to better understand the behavior of the building, Table 3.3 and Figure 4.11 show the lateral deflection of the building at different levels for the center of the facades A-A' and C-C' (location of the hydraulic jacks) and the farthest point concerning the hydraulic jacks, the region where more significant displacements were obtained (intersection of facade B-B' and D-D').

Table 4.3 – Lateral deflection (% of story height) measured during the tests performed

	Test	(a) Monotonic Longitudinal	(b) Monotonic Transverse	(c) Cyclic Transverse
Location: ▶ – Hydraulic jacks				
1st story	Sliding	0.32	0.56	0.30
	Rocking	0.31	0.66	0.63
	In-plane displacement	1.37	1.88	1.19
2nd story	Sliding	0.03	0.09	0.12
	Rocking	0.06	0.11	0.09
	In-plane displacement	1.82	2.95	2.08
Location: ○ – intersection of facades B-B 'and D-D'				
1st story	Sliding	1.21	0.66	0.50
	In-plane displacement	1.37	2.28	1.48
2nd story	Sliding	0.20	0.25	0.22
	In-plane displacement	1.85	3.35	2.29

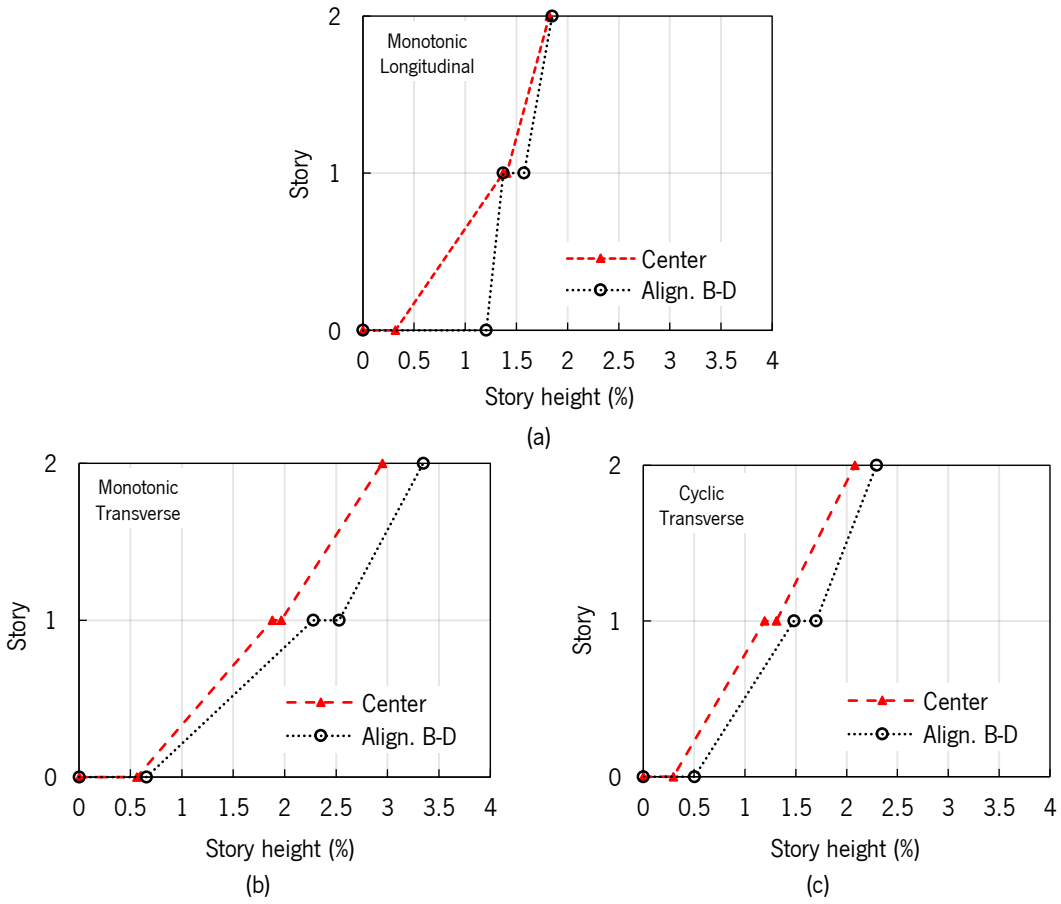

Figure 4.11 – Lateral deflection of the building at different levels: (a) Monotonic test in the longitudinal direction; (b) Monotonic test in the transverse direction; (c) Cyclic test in the transverse direction.

By analyzing Figure 4.10, Figure 4.11, and Table 3.3, it is possible to point out that transverse direction generally obtained greater sliding, rocking, and in-plane wall displacement. It is important to note that, the longitudinal direction stiffer, it presented a greater slip of the base. On the other hand, the smaller values of displacement in the cyclic test when compared to the monotonic one, in the same direction, resulted from the lower load reached during the cyclic test in the transverse direction. So, it is possible to conclude that the longitudinal direction obtained a greater sliding behavior, and with this, more friction between the panels and the steel base was verified. About the transverse direction, as a consequence of a less in-plane stiffness, the rocking was more evident. To better understand the behavior of the building, as suggested by Popovski [10], it is important to point out the sliding occurred on the ground floor and the 1st floor. This slip results from the stiffness differences between the steel base and the 1st floor walls. Although on a smaller scale, it also happens between the 1st and 2nd floor walls. On the other hand, the in-plane displacement, which represents most of the lateral displacement, occurred due to the shear and flexural deformations and due to the global rocking of the CLT panels. Consequently, overlapping the force-displacement curves (see Figure 4.12) of the tests performed, the standard ASTM E2126:2012 [57] has been applied to quantify the parameters of the elastic shear stiffness (K_e), yield load (P_{yield}) and yield

displacement (Δ_{yield}), as can be seen in Table 4.4. In the case of the cyclic test, for the application of this standard, the positive envelope curve has been used, as can be seen in Figure 4.12. The load values reached in each hydraulic jack are also listed. The results of the comparison between the monotonic and cyclic tests in the transverse direction were added in Table 4.4 for the same load magnitude.

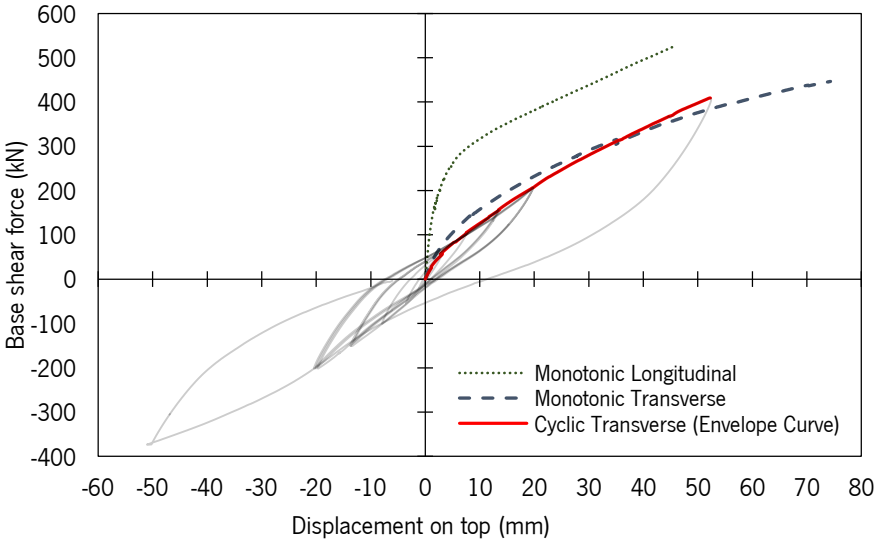

Figure 4.12 – Base shear force-displacement on top of the CLT building registered during the tests performed.

Table 4.4 – Mechanical parameters with the application of the ASTM E2126:2012 [57].

Tests	P_{peak} (kN)	Δ_{peak} (mm)	P_{yield} (kN)	Δ_{yield} (mm)	K_e (N/mm)
Monotonic Longitudinal	528.4	45.9	408.8	5.6	63241
Monotonic Transverse	447.7	74.3	347.5	19.2	14911
Monotonic Transverse[(a)]	409.0	60.1	328.3	21.4	15312
Cyclic Transverse	409.0	52.3	328.8	29.1	9910

(a) Load magnitude of the cyclic test.

By looking at Figure 4.12 and Table 4.4, one can demonstrate that the CLT building is stiffer in the longitudinal direction when compared to the transverse direction, with a significant increase of the load capacity of the structure in that direction. On the other hand, when analyzing the tests in the transversal direction, the cyclic test presents lower values of resistance. Regarding the comparison between the monotonic and cyclic test in the transverse direction with the same load magnitude, the results shows the decrease of the resistance of the cyclic test. This decrease can be considered normal given that the cyclic test is more aggressive to the structure, which a decrease in the maximum displacement (around 13%), yielding displacement (around 36%), and elastic shear stiffness (around 35%).

4.4.3 Damages observed

The damages observed during the tests were very similar for all the tests performed, being the difference given by the level of damage imposed on the building and in particular, in the connectors. As expected, the damages observed during the test, in the transverse direction, were more severe because this loading

direction is the one with less stiffness. On the other hand, with the longitudinal direction being the stiffest, practically insignificant damages was found between the walls of the 2nd floor and the 1st floor. In this context, as the building suffered rocking, the first visible damage were concentrated at the base corresponding to the hydraulic jacks' locations (see Figure 4.13).

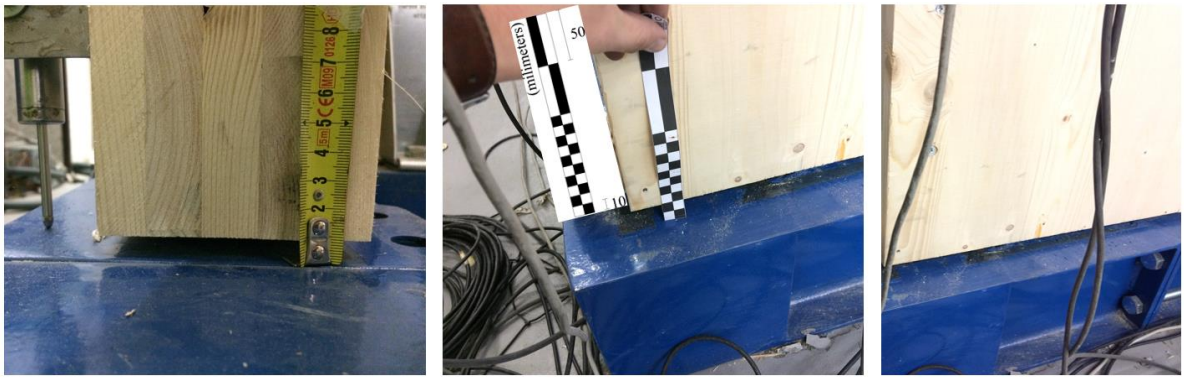

(a) (b) (c)

Figure 4.13 – Rocking of the building: (a) Monotonic longitudinal direction; (b) Monotonic transverse direction; (c) Cyclic transverse direction.

In terms of in-plane walls displacements, where no connectors (angle-brackets and hold-downs) have been inserted, the building suffered a significant lateral translation in internal walls (see Figure 4.14).

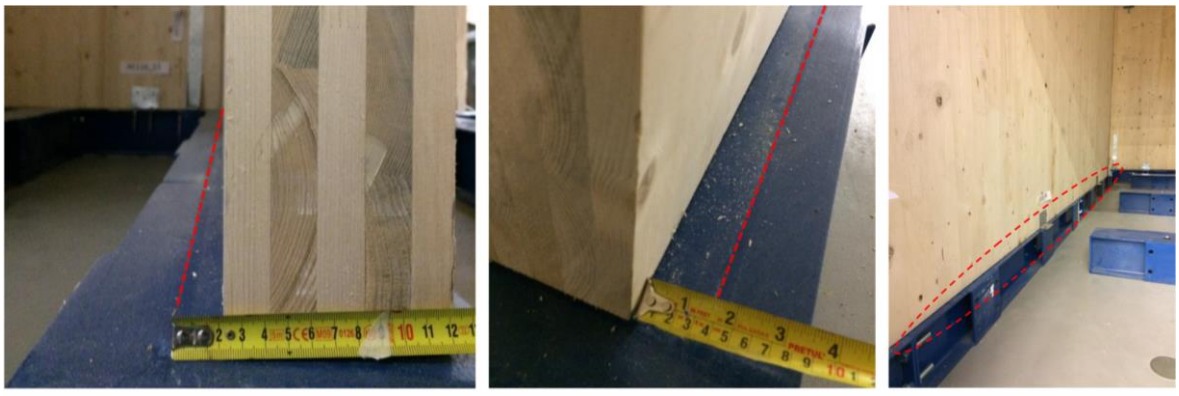

(a) (b) (c)

Figure 4.14 – Translation of the internal walls: (a) Monotonic longitudinal direction; (b) Monotonic transverse direction; (c) Cyclic transverse direction.

The severest damage observed was located in the metal connectors (AE116 and HTT22). Those connectors have been damaged as a consequence of sliding, rotation, and uplift of the CLT panels. Figure 4.15 shows the damage observed in the AE116 connectors, where it is possible to see more serious uplift damage in the tests under transverse direction. However, it is important to note that the screws that connect the steel structure of the base were virtually undamaged.

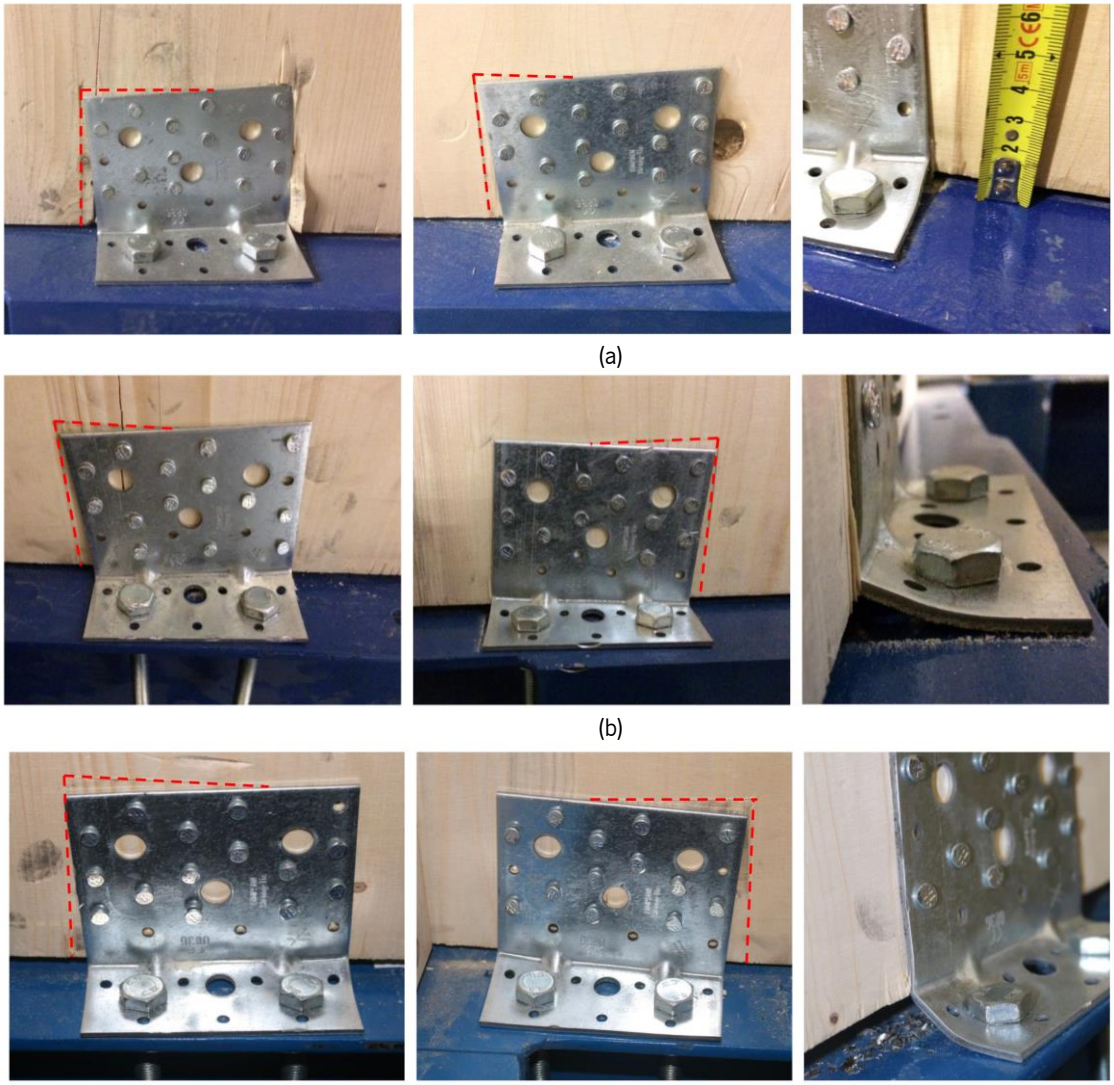

(a)

(b)

(c)

Figure 4.15 – Damages observed in the AE116 connectors: (a) Monotonic longitudinal direction; (b) Monotonic transverse direction; (c) Cyclic transverse direction.

In the case of damages observed between floors, the uplift, and sliding of the CLT panels of the second floor, compared to the ones on the first floor, were visible in the transverse direction, as shown in Figure 4.16.

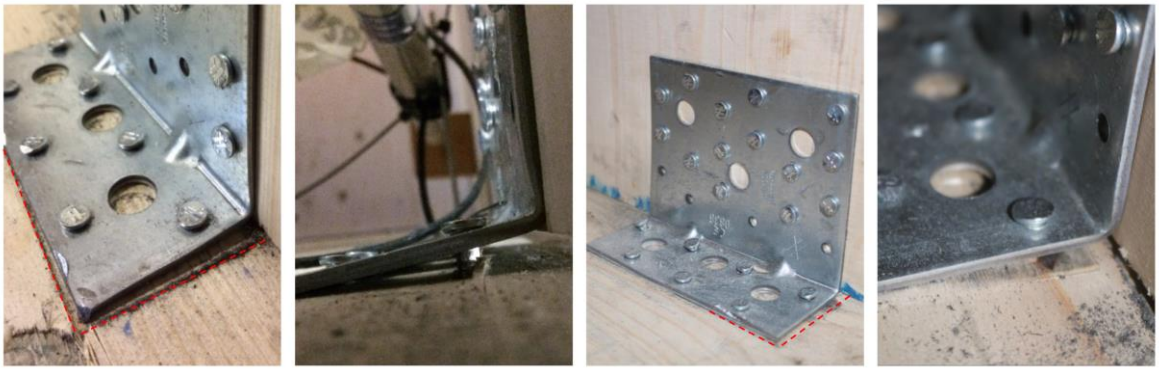

(a) (b)

Figure 4.16 – Damages observed in the AE116 connectors between floors: (a) Monotonic transverse direction; (b) Cyclic transverse direction.

On the other hand, in the case of the HTT22 connectors, it was possible to visualize uplift damages. In this case, because the center of mass is different from the center of stiffness, and therefore, a plane rotation of the building occurred, the hold-downs presented out-of-plane rotation (see Figure 4.17).

(a) (b)

Figure 4.17 – Damages observed in the HTT22 connectors: (a) Monotonic transverse direction; (b) Cyclic transverse direction.

Finally, as a consequence of less in-plane stiffness of the transverse direction, in the monotonic test, the lintels over the openings on the ground floor wall in the façade B-B' (see Figure 4.18) fissured by tension perpendicular to the grain.

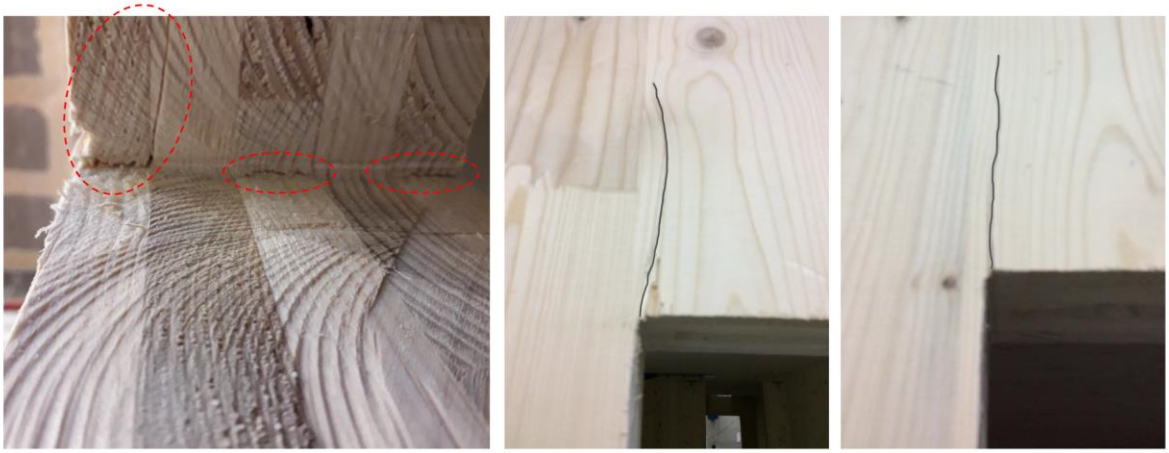

(a) (b) (c)

Figure 4.18 – Cracks on the top left corner of the openings 1500x2000 (a and b) and 900x2000 (c) on the ground floor wall in the facade B-B' during the monotonic transverse test

4.5 Final remarks

A non-symmetric 2-story full-scale platform-type CLT building with large openings was tested. The performance, at global and local levels, in each loading direction, was analyzed. In the longitudinal direction, since the structure was stiffer than the other direction, no significant damage was registered. This can be explained by the technical limitation of the hydraulic jack used on the second floor. In the first monotonic test, under a lateral load in the longitudinal direction of the building, the damages observed

were concentrated in the metal connectors (angle-brackets and hold-downs), with signs of sliding, rotation, and uplift on the ground floor. In the transverse direction, where the structure had short shear walls, more damage was observed. The rocking of the overall structure was visible, and the lintels over the larger openings cracked by tension perpendicular to the grain. Finally, yet significantly, in the cyclic test in the transverse direction, the damage was very similar to the monotonic test in the same direction, but in the former, more severe damage was observed in the angle brackets on the first floor. Although the building's load capacity was not reached in the tests performed, it was possible to verify accumulated damage in the building, where it is evident in the metal connectors.

Chapter 5

Finite element model prediction of the 2-story CLT building

5.1 Introduction

The interest in numerical models to predict the seismic response is growing. and plays an essential role in assisting the seismic design [58]. However, many of these numerical models are complex and the time to obtain results is usually long [59]. Actually, it is intended to find simpler numerical models that offer better applicability and reduced time analysis.

In this way, to help to implement pushover analysis of the CLT constructions, the experimental tests of Chapter 4 have been predicted through commercial software Dlubal RFEM [52]. Pushover analysis is a non-linear analysis to assess the structural capacity under increasing lateral loads until the failure of the structure. With this, it is possible to see the capacity curves by the base shear force versus displacement of a control point on the structure. In the finite element model, some simplifications have been carried out. In this section, firstly, the parameters of the finite element model used to predict the real behavior of the CLT structure are described and, finally, a comparison between the finite element model and the experimental campaign is presented.

5.2 Finite element model

Two finite element models have been created, one for the longitudinal direction (y-axis) and one for the transverse direction (x-axis), where the reason is related to the location of the metal connectors in each test performed in the experimental campaign. For a better understanding of the model, those description is divided into three groups: building design, structural supports, and load cases and calculation parameters.

5.2.1 Building design

The first step is related to the definition of the CLT panels (floors and walls) and their mechanical properties. They were defined through rectangular surfaces, where it was important to define the material as laminate. Regarding the design of the building, as an important step in the finite element model, it was the disconnection of the building stories. The simplification was carried out to reproduce the real behavior of the shear connectors AE116 and uplift connectors HTT22. Thus, the separation was performed with a spacing of 0.1 m as shown in Figure 5.1.

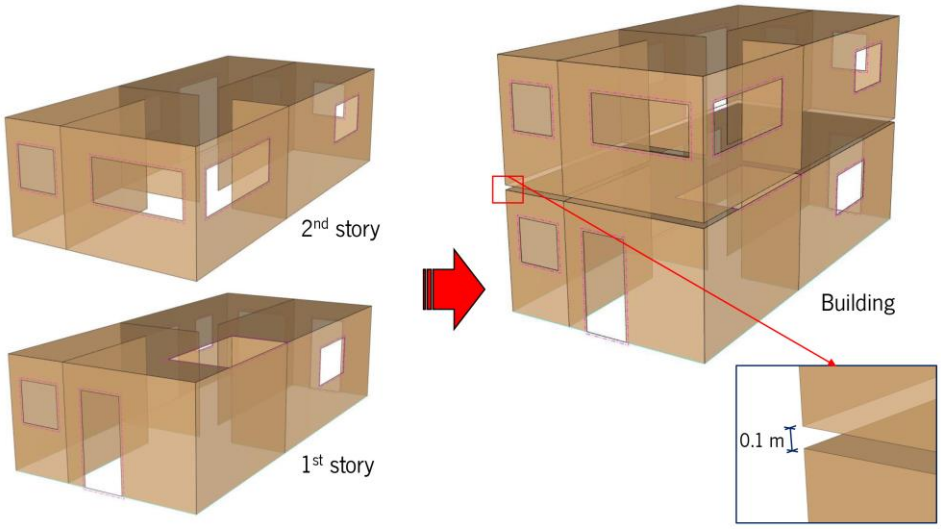

Figure 5.1 – Methodology adopted to disconnect the stories to promote the simulation of the metal connectors.

Once the panels and openings were defined, the mechanical properties of the CLT were defined through the RF-LAMINATE module. The module quantifies the stiffness matrix for each layer and generates a global panel matrix stiffness. Then, the global matrix is transferred to RFEM. The material properties adopted in the RF-LAMINATE module are listed in Table 5.1.

Table 5.1 – Material properties (N/mm²) adopted in the RF-LAMINATE module [6].

Manufacturer		**Stora Enso**
Modulus of Elasticity		
Parallel to the grain direction (E_x)	$E_{0,mean}$	12500
Perpendicular to the grain direction (E_y)	$E_{90,mean}$	0.0
Shear Modulus		
Parallel to the grain direction (G_x)	G_{mean}	690.0
Perpendicular to the grain direction (G_y)	$G_{r,mean}$	50.0

5.2.2 Definition of supports

After the definitions of the geometry of the CLT panels and their mechanical properties, this step is related to the introduction of the building supports on the ground (Steel to CLT) and between the floors (CLT to CLT). Two types of supports were introduced at the ground: Linear supports to represent the connection of the ground steel structure and the 1st story wall panels without metal connectors; and, nodal supports to represent the metal connectors AE116 and HTT22. Regarding the linear supports, as in the experimental analysis performed (Chapter 4), strong evidence of friction was identified. Therefore, two different hypotheses, with and without friction were considered. The hypothesis without friction (see Figure 5.2a), only the connection of the steel structure and CLT panels have been considered and. On the other hand, the hypothesis with friction (see Figure 5.2b), the unique difference was the addition of

the friction coefficient μ=0.4, value used by Dujic et al. [45]. However, the boundary conditions of the linear and nodal supports were performed with the global axes, as shown in Figure 5.2.

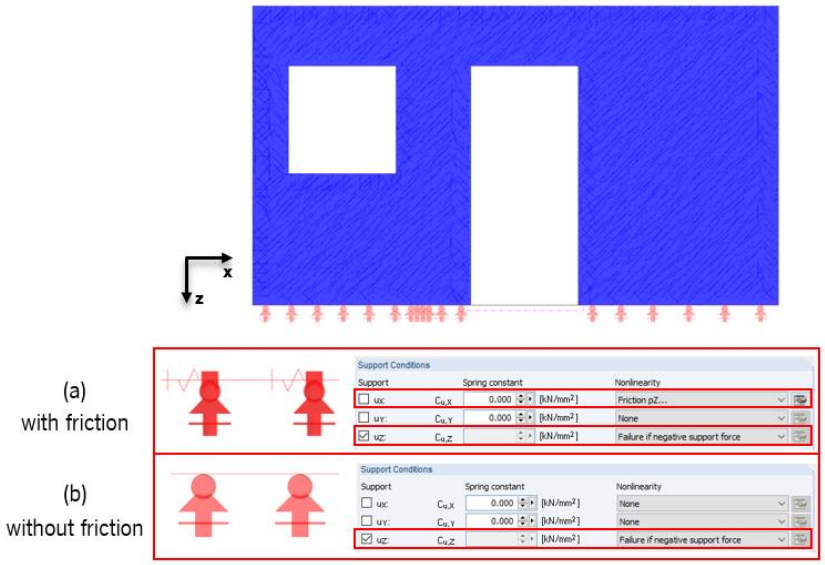

Figure 5.2 – Line supports with (a) and without (b) consideration of friction.

In the definition of the nodal supports, representing the metal connectors, it is important to introduce a small rigid vertical bar located on the same place of the metal connectors (AE116 and HTT22): the upper node is connected to the wall; and the remainder connected to nodal support (see Figure 5.3). In this context, each nodal support represents a connector where only two types are required: one for the HTT22 connector; and one for the AE116 connector. Therefore, to introduce the force-displacement diagrams of each connector, the results of Chapter 3 have been used, where the average curves (results of steel ground) of the experimental campaign performed at the University of Minho (UM) have been used.

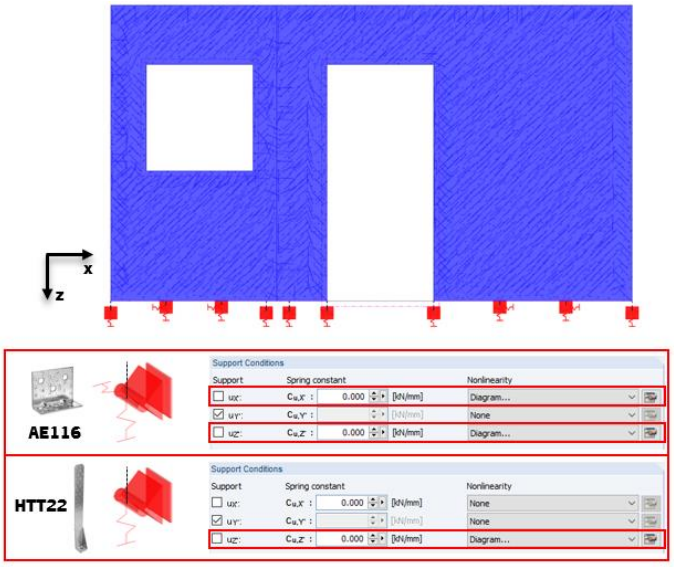

Figure 5.3 – Rigid bar and its nodal support

For a comparison of the different curves of the metal connectors, as analyzed and defined in chapter 3, the following experimental curves were used: 1st LEC of the standard EN 12512 [5] (see Figure 5.4a); EEEP curve of the standard EN 121512 [5] (see Figure 5.4b); and the bilinear curve of the standard EN 12512:2001 (see Figure 5.4c). However, due to software limitations to simulate the degradation that connectors showedin the cyclic tests performed (Chapter 3), the values after the peak load was not included.

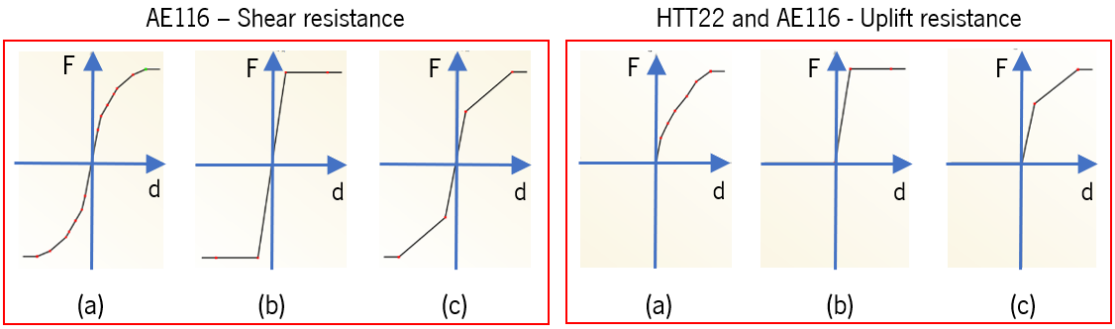

Figure 5.4 – Types of experimental curves used in the model. (a) 1ºLEC, (b) EEEP curve, and (c) Bilinear curve.

Regarding the supports between floors, with the separation of the stories previously made, it was necessary to introduce two types of rigid vertical bars along the walls. One type for the representation of the interface between stories (CLT to CLT) and another for the addition of metal connectors (AE116 and HTT22). In this way, for the first case, the bars have been inserted with the nodes connected to the upper and lower line of the walls (see Figure 5.5a), where the maximum spacing of 200 mm has been admitted. To avoid convergence problems, all members must be connected, at least, by two finite element nodes each surface. On the other hand, for metal connectors, the process was the same, but the bar needs to be inside of the walls (see Figure 5.5b). Regarding the dimension of the bars, 100 mm were admitted into each wall.

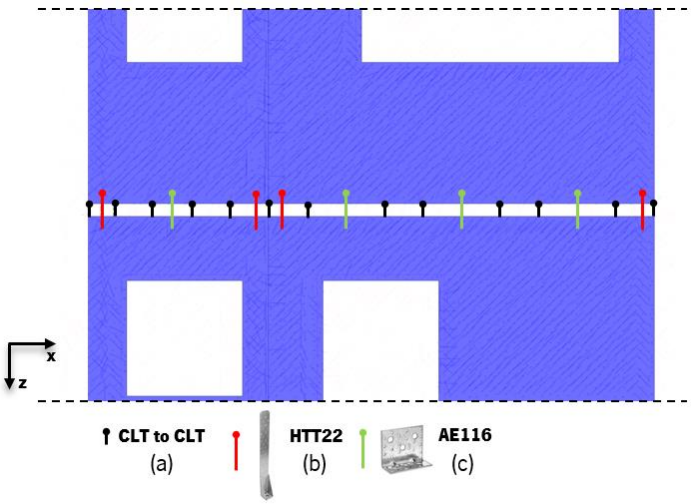

Figure 5.5 – Support between floors.

Defined the rigid bars, three hinge conditions were defined: one for the interface CLT to CLT; and the other two for defining the behavior of the metal connectors AE116 and HTT22. For the CLT to CLT interface (see Figure 5.6a), such as linear supports at the ground, only the CLT contact has been considered. On the other hand, in the definition of the hinge conditions for the metal connectors (see Figure 5.6b), the corresponding force-displacement curves (metal connectors with timber base) have been added, where the results were relative to specimen's analysis with CLT base (Chapter 3). Thus, the hinge conditions have been applied only to the upper node. However, due to the simplification of story disconnection, it was impossible to consider the friction between stories.

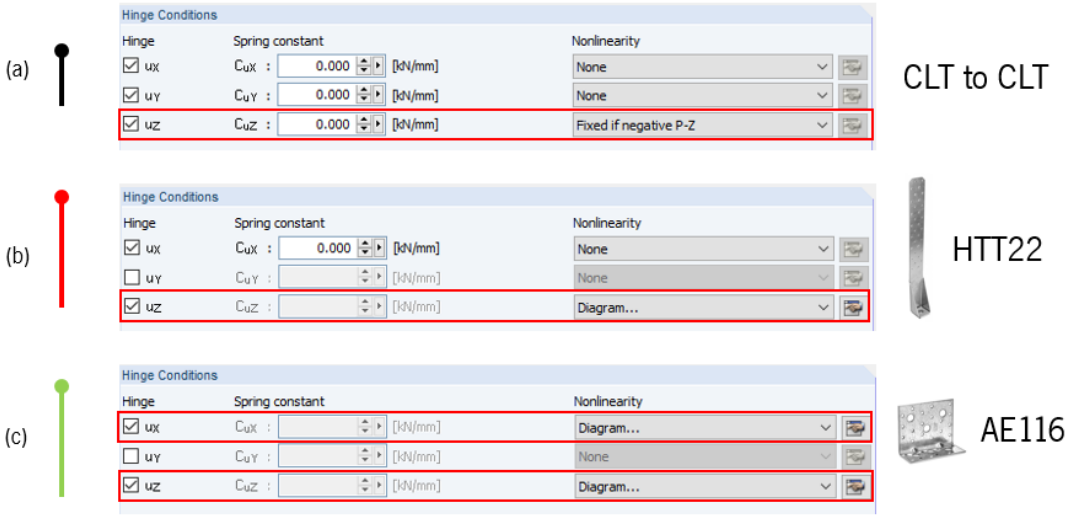

Figure 5.6 – Support between CLT floors with metal connectors

Finally, for the definition of the remaining fasteners (wall-to-wall and floor-to-wall), not being the main responsible for the resistance to lateral loads, they were introduced by rigid line hinges at the wall-to-wall and floor-to-wall intersections.

5.2.3 Definition of load cases and calculation parameters

After the model geometry, material properties, and supports, the next step was the introduction of loads. Two load cases were applied: one for vertical loads and one for horizontal loads. The vertical loads include all permanent loads applied to the structure, including the weight of the water drums used in the experimental campaign (Chapter 4). The horizontal loads, representative of the hydraulic jacks, nodal loads were introduced in the location of each hydraulic jack (see Figure 5.7), equal to horizontal loads carried out in the experimental campaign. It is important to note that the predicted tests have been performed with force control.

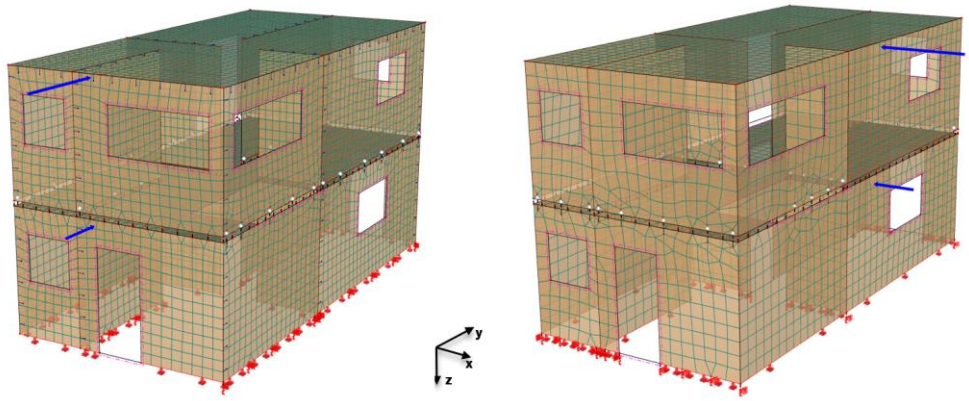

(a) (b)

Figure 5.7 – Location of the horizontal nodal loads applied in (a) longitudinal and (b) transverse direction.

5.3 Results and discussion

The main results obtained in the numerical analysis to predict the experimental campaign are described and discussed in this chapter. However, due to the location of the AE116 and HTT22 connectors applied in the experimental tests, two finite element models were created: one for the longitudinal direction; and, other for the transverse direction. The force-displacement adopted for the metal connectors AE116 and HTT22 are the average curve obtained from the cyclic tests performed at the University of Minho (three different curves were analyzed: 1st LEC of EN 12512 [5], EEEP curve of EN 12512 [5] and the bilinear curve of EN 121512:2001). The results were separated into the different tests performed on the experimental campaign: 1) monotonic longitudinal direction; 2) monotonic transverse direction; and, 3) cyclic transverse direction. To describe the numeric models analyzed, the force-displacement curves with: the respective mechanical properties; the application of the standard ASTM E2126:2012 [57]; the lateral deflection at different levels; and, the level of damage imposed on the most requested metal connectors, have been discussed. However, it is important to note that the comparison between the results has been made with the same displacement reached in the experimental tests.

5.3.1 Monotonic longitudinal direction

As expected, the analysis of Figure 5.8 and Table 5.2 shows the finite element model with friction presents results closer to experiments. The most significant difference between both models, with and without friction, is related to the elastic stiffness. Regarding the different curves used to simulated the metal connectors, the 1st LEC curves of EN 12512 [5] and the bilinear curves of EN 12512:2001 are close and present the highest reliability of the results. On the other hand, the EEEP curve of EN 12512 [5] obtained a brittle failure, where the ultimate displacement of the experimental campaign was not reached.

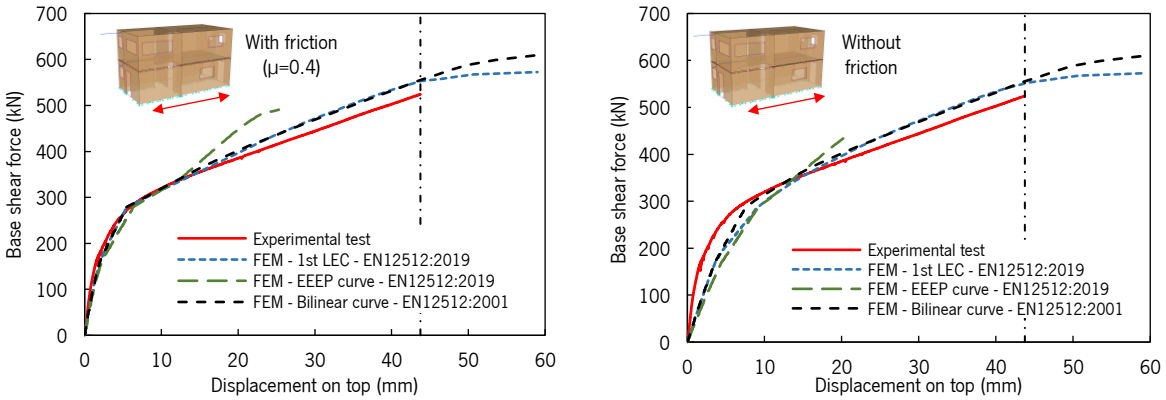

Figure 5.8 – Force-displacement curves in the monotonic longitudinal direction (a) with and (b) without friction.

Table 5.2 – Mechanical parameters of the monotonic longitudinal direction tests with and without friction.

	Tests	F_{max} (kN)	V_u (mm)	F_y (kN)	V_y (mm)	K (N/mm)
Experimental test		**524.3**	**45.9**	**405.0**	**4.8**	**74052**
With friction	FEM – 1st LEC [5]	552.8	45.9	422.5	5.6	69063
	Δ (%)	5.4	0.0	4.3	16.1	-6.7
	FEM – EEEP curve [5]	490.8	25.3	373.6	5.1	70071
	Δ (%)	-6.4	-42.2	-7.8	5.1	-5.4
	FEM – Bilinear curve [34]	555.0	45.9	422.0	5.3	74000
	Δ (%)	5.9	0.0	4.2	10.2	-0.1
Without friction	FEM – 1st LEC [5]	552.8	45.9	429.8	9.1	44200
	Δ (%)	5.4	0.0	6.1	87.9	-40.3
	FEM – EEEP curve [5]	433.8	20.2	343.9	8.7	39409
	Δ (%)	-17.3	-53.8	-15.1	80.7	-46.8
	FEM – Bilinear curve [34]	555.0	45.9	433.4	9.1	46250
	Δ (%)	5.9	0.0	7.0	88.7	-37.5

Δ – Difference between the experimental test.

Regarding the lateral deflection of the building, as can be seen in Figure 5.9, the finite element model presents a higher slip on the different levels (ground floor and 1st floor). However, as it was impossible to consider friction between floors, the difference may be related to this effect. Regarding the in-plane displacement, the values are very close to the experimental test.

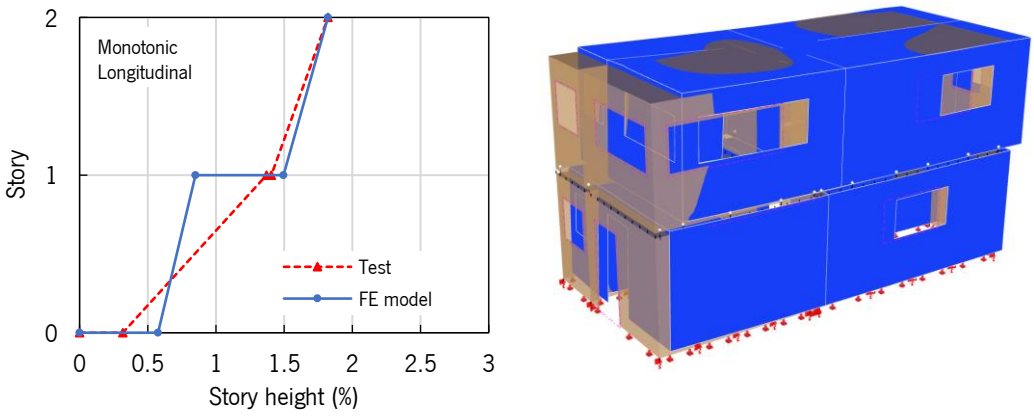

Figure 5.9 – Lateral deflection of the building in height in the monotonic longitudinal direction.

Looking at the most requested metal connectors, the Figure 5.10 shows the uplift behavior on the ground floor of the HTT22 connector located on the internal wall of the facade A-A' and the AE116 connector located on facade D-D' (near the intersection of the facades A-A' and D-D') and, on the other hand, the shear behavior of the connector AE116 located on facade D-D' (near the intersection of the facades B-B' and D-D') on the ground floor and 1st floor. The vertical dashed line (1) represents the position for the same displacement range of the experimental campaign and the force-displacement curves are relative to the average curves of the tests performed at the University of Minho (Chapter 3) and inserted in the model. As expected, graphs analysis show the higher loading of the shear connectors AE116, where the uplift resistance still presents a high safety margin.

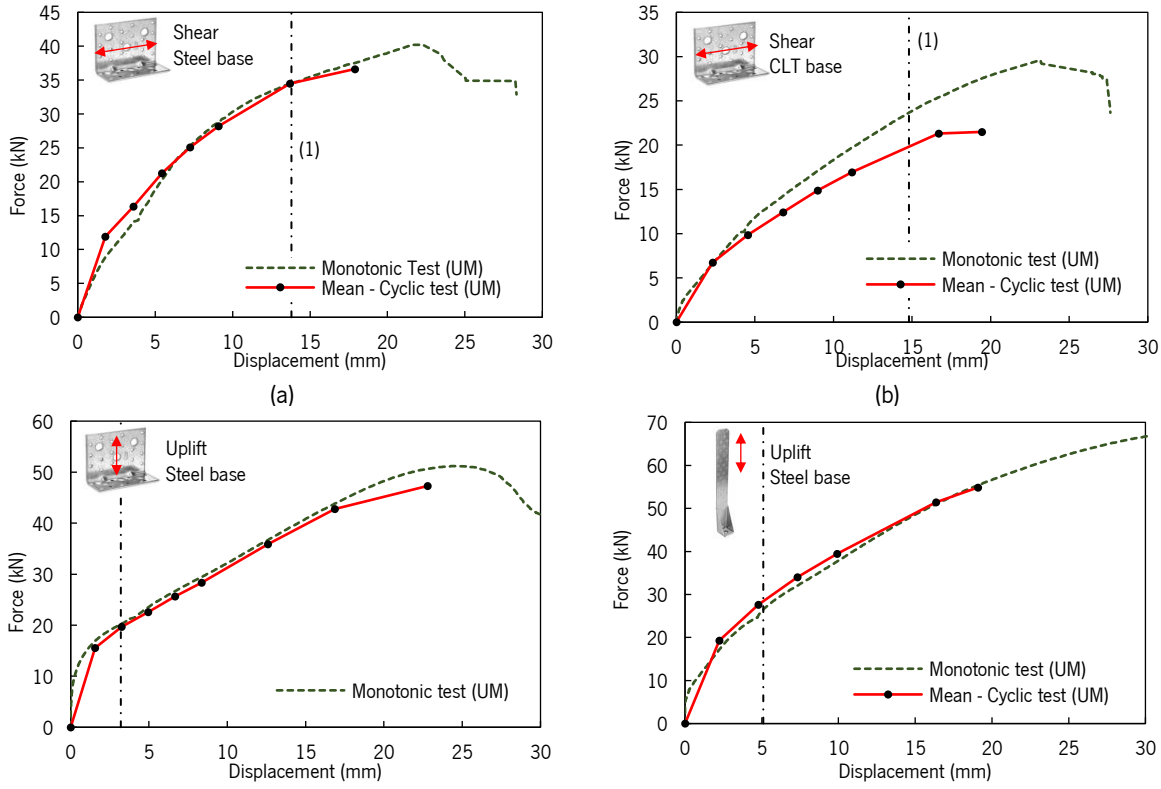

Figure 5.10 – Force versus displacement curves: AE116 shear strength with steel (a) and CLT base (b), AE116 uplift strength with steel base (c) and HTT2 uplift strength with steel base (d).

5.3.2 Monotonic transverse direction

By analyzing Figure 5.11 and Table 5.3, as in the experimental campaign, the presence of friction between the panels resulted in smaller differences compared to the finite element model with and without friction. Similar to the longitudinal direction, the curves with evident proximity are the 1st LEC curves of EN 12512 [5] and the bilinear curves of EN 12512:2001, where the EEEP curves even reaching displacement values similar to the experimental campaign are the furthest from reality.

However, it is important to note that the displacement reached through the EEEP curves was related to the residual resistance of the connectors.

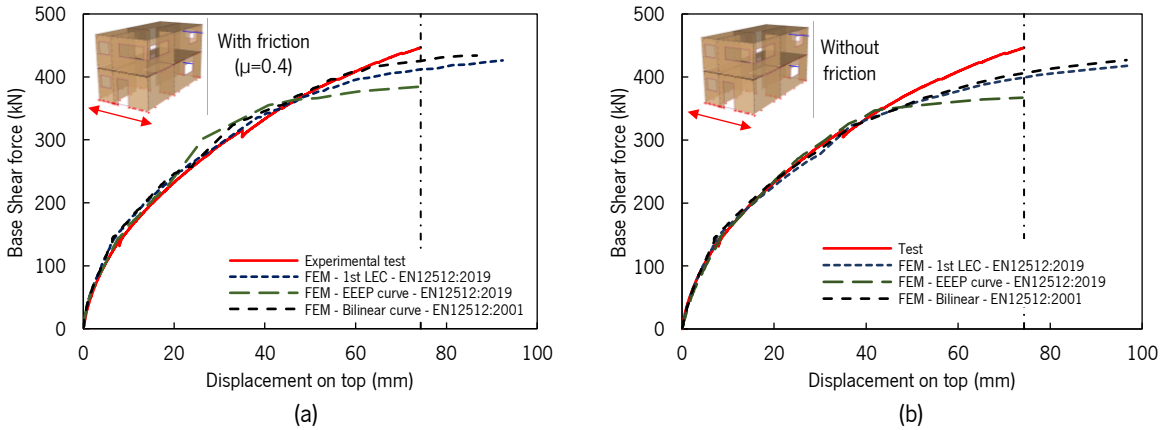

Figure 5.11 – Force-displacement curves in the monotonic transverse direction (a) with and (b) without friction.

Table 5.3 – Mechanical parameters of the monotonic transverse direction tests with and without friction.

Tests		F_{max} (kN)	V_u (mm)	F_y (kN)	V_y (mm)	K (N/mm)
Experimental test		**446.5**	**74.3**	**347.5**	**19.2**	**14911**
With friction	FEM – 1st LEC [5]	412.0	74.3	344.8	19.5	14892
	Δ (%)	-7.7	0.0	-0.8	1.6	-0.1
	FEM – EEEP curve [5]	384.6	74.1	343.6	20.1	14235
	Δ (%)	-13.9	-0.3	-1.1	5.0	-4.5
	FEM – Bilinear curve [34]	425.3	74.3	356.1	20.5	14500
	Δ (%)	-4.7	0.0	2.5	7.1	-2.8
Without friction	FEM – 1st LEC [5]	400.0	74.3	332.1	19.9	14634
	Δ (%)	-10.4	0.0	-4.4	4.0	-1.9
	FEM – EEEP curve [5]	367.1	74.0	323.8	18.5	15729
	Δ (%)	-17.8	-0.5	-6.8	-3.3	5.5
	FEM – Bilinear curve [34]	406.0	74.3	334.2	19.3	15225
	Δ (%)	-9.1	0.0	-3.8	1.0	2.1

Δ – Difference between the experimental test.

Regarding the lateral deflection of the building (see Figure 5.12), one can observe the smaller difference compared to the longitudinal direction, where the most significant difference is again given by the slip, which results in higher values of the experimental campaign.

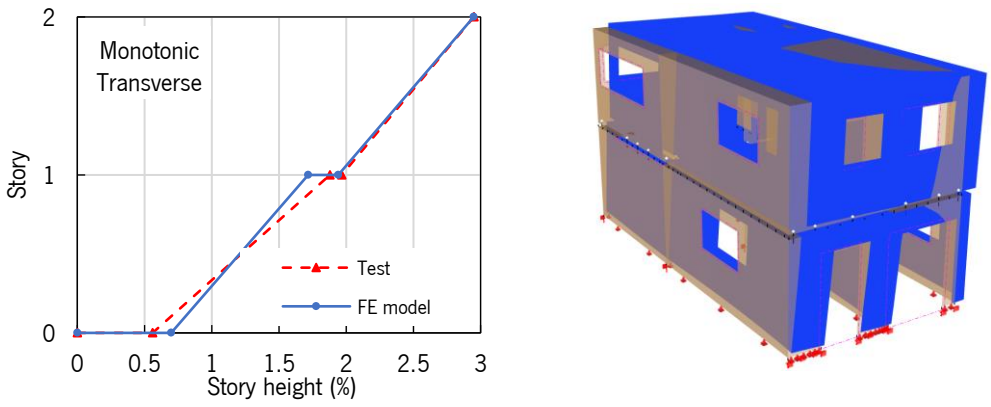

Figure 5.12 – Lateral deflection of the building in height in the monotonic transverse direction.

For transverse direction, the most requested connectors, AE116 and HTT22 at the ground floor, under uplift actions are located on the A-A' facade (near the intersection of the facades A-A' and C-C') and the connectors AE116, under shear actions are located on the internal wall in contact with the facade D-D' for the ground floor and 1st floor. In the same way as the previous analysis, the vertical dashed line (1) represents the position for the same displacement range of the experimental campaign and the force-displacement curves are relative to the average curves of the tests performed at the University of Minho (Chapter 3) and inserted in the model (see Figure 5.13). As might be expected, looking at the graphs of Figure 5.13, as more use of the metal connectors. However, as in the longitudinal direction, the shear action was more requested.

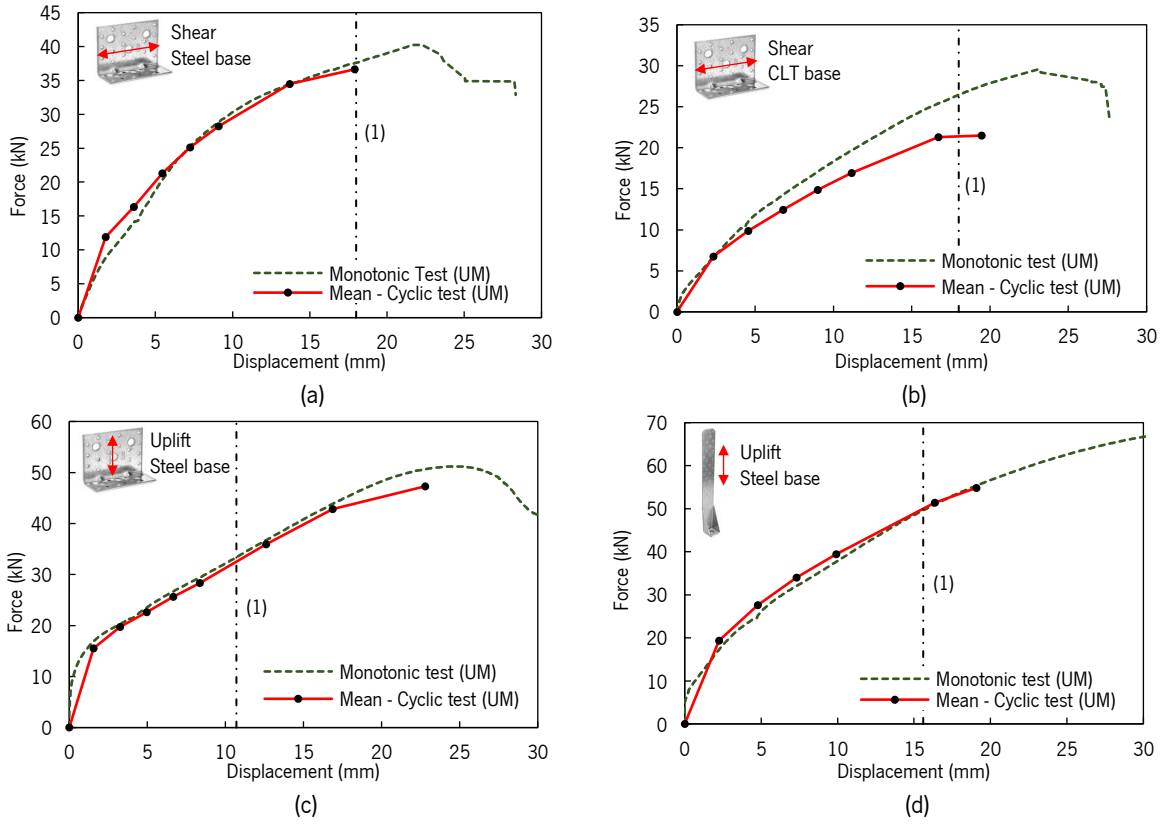

Figure 5.13 – Force versus displacement curves: AE116 shear strength with steel (a) and CLT base (b), AE116 uplift strength with steel base (c) and HTT2 uplift strength with steel base (d).

5.3.3 Cyclic transverse direction

Finally, in the same direction, but with the envelope curve of the experimental cyclic test, Figure 5.14 and Table 5.4 show higher differences between the model with and without friction. This difference is more significant in the load-carrying capacity of the structure. This effect can be considered reasonable since the cyclic load conduct to a greater presence of friction. However, due to the hydraulic limitations already reported in chapter 4, with the reduced displacement reached, all analyzes were able to obtain

the expected displacement. However, it is possible to conclude again that the analysis with EEEP curves is less reliable.

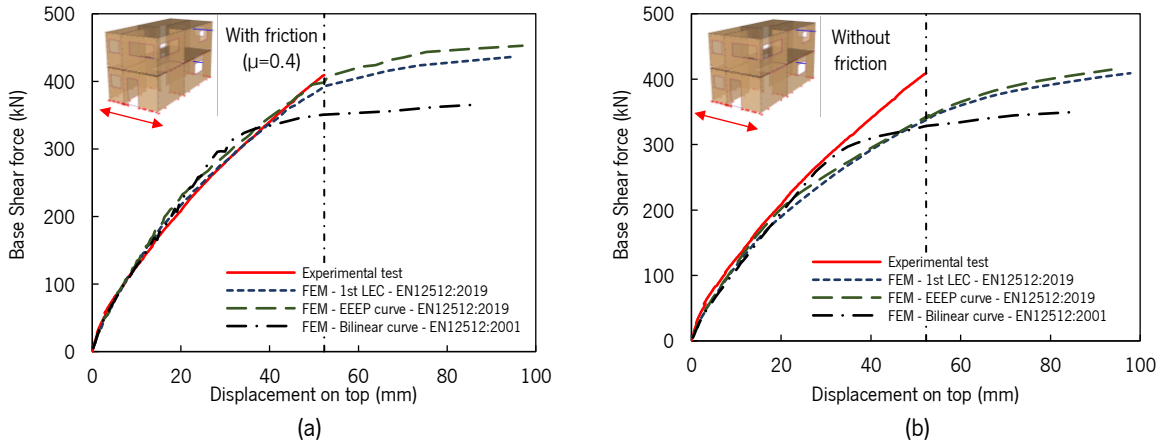

Figure 5.14 – Force-displacement curves of the cyclic transverse direction (a) with and (b) without friction.

Table 5.4 – Mechanical parameters of the cyclic transverse direction tests with and without friction.

Tests		F_{max} (kN)	V_u (mm)	F_y (kN)	V_y (mm)	K (N/mm)
Experimental test		**409.0**	**52.3**	**329.8**	**26.3**	**10225**
With friction	FEM – 1st LEC [5]	392.6	52.3	322.0	26.3	11210
	Δ (%)	-4.0	0.0	-2.4	-0.3	9.6
	FEM – EEEP curve [5]	350.6	52.3	321.5	25.9	11063
	Δ (%)	-14.3	0.0	-2.5	-1.6	8.2
	FEM – Bilinear curve [34]	398.3	52.3	335.4	27.0	11490
	Δ (%)	-2.6	0.0	1.7	2.3	12.4
Without friction	FEM – 1st LEC [5]	339.5	52.3	277.4	25.3	9893
	Δ (%)	-17.0	0.0	-15.9	-3.8	-3.2
	FEM – EEEP curve [5]	344.9	52.3	282.2	24.6	10551
	Δ (%)	-15.7	0.0	-14.4	-6.8	3.2
	FEM – Bilinear curve [34]	328.7	52.3	299.6	28.3	9667
	Δ (%)	-19.6	0.0	-9.2	7.3	-5.5

Δ – Difference between the experimental test.

Looking at lateral deflection in Figure 5.15, once again it was possible to verify that the model presents higher slip values, where higher values between floors were obtained compared to the monotonic test in the same direction.

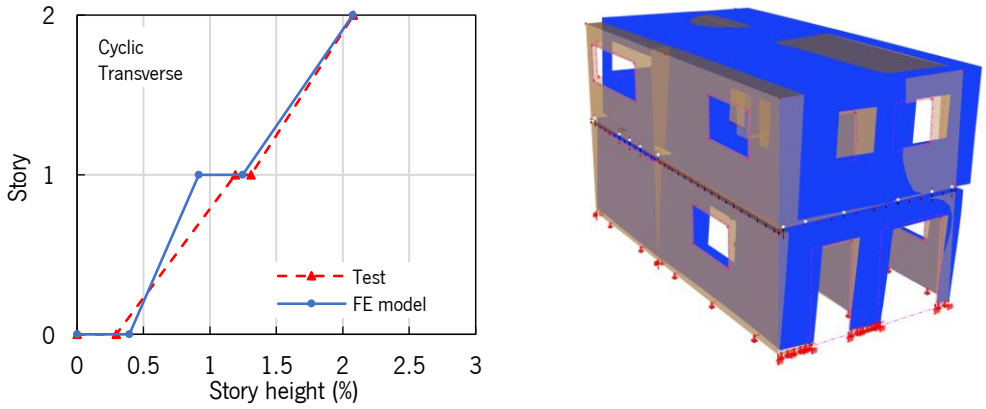

Figure 5.15 – Lateral deflection of the building at different heights in the cyclic transverse direction.

For the same connectors of the previous analysis, by analyzing the graphs of Figure 5.16, it is possible to verify, as expected, minor use of the metal connectors. However, it is important to note that the most requested connector is related to the AE116 under shear loads on the 1st floor (Figure 5.16b).

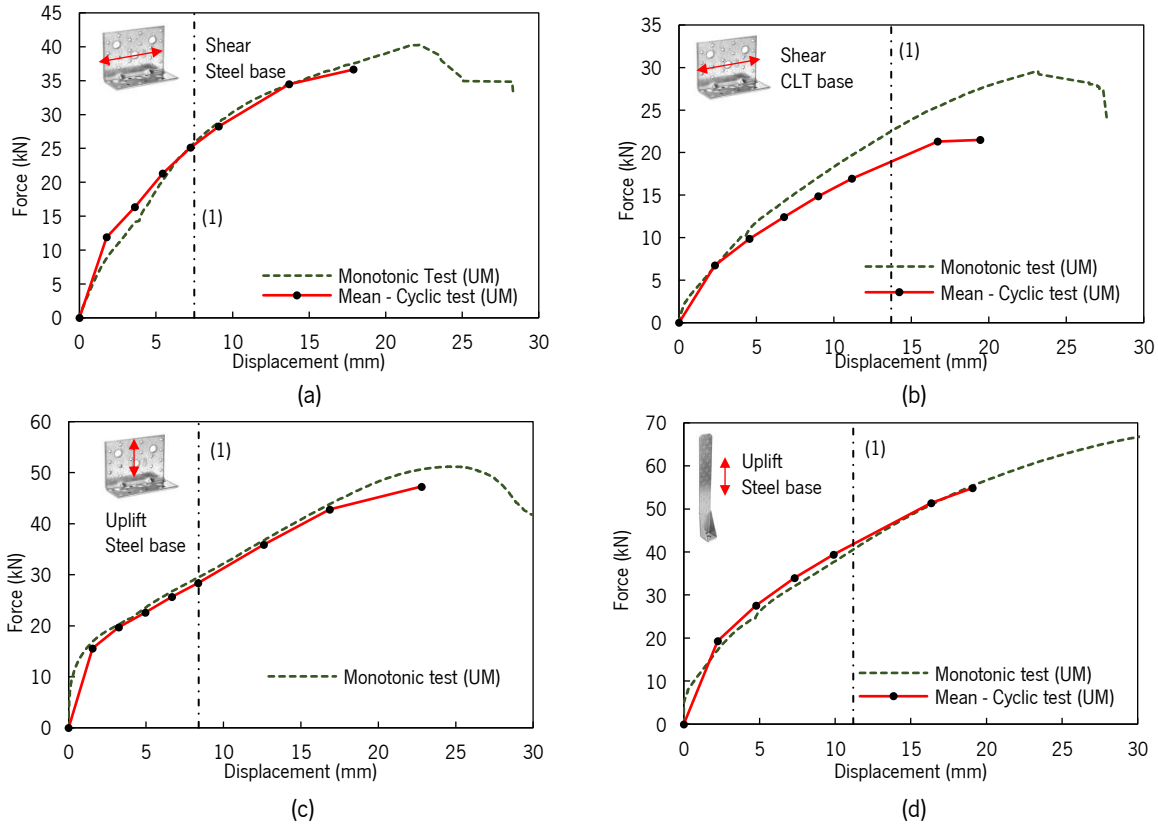

Figure 5.16 – Force versus displacement curves: AE116 shear strength with steel (a) and CLT base (b), AE116 uplift strength with steel base (c) and HTT2 uplift strength with steel base (d).

5.4 Final remarks

A commercial FEM software was used for the prediction of the 2-story CLT building analyzed in chapter 4. The results of the metal connectors (presented in chapter 3) played an important role in the final results. The steps adopted for the prediction of the building behavior were described, and then, the comparison between FE models and the experimental campaign (presented in chapter 4) has been carried out. The results were quite good, with the numeric results close to the experimental ones. The models where friction was considered, better represent the reality: on longitudinal direction the friction was important to obtain the real elastic stiffness; and, on the other hand, in the transverse direction was more important to get the load capacity. Regarding lateral deformation, the results are close to the experimental results. However, as the friction between the first floor panels was not considered for the reasons already mentioned above, the values are mostly quite different from reality.

Chapter 6

Pushover analysis with the aid of Eurocode 8 Annex B (N2 method)

6.1 Introduction

Given the complexity of seismic design through dynamic analysis and the high uncertainties that simplified methodologies can reveal, the simplicity of the pushover analysis has been widely used over time especially for low to moderate-high buildings [60-65]. It is a non-linear static analysis with the application of horizontal forces or displacements, to study the lateral resistance of the structure. Thus, it is possible to visualize the evolution of the damage of the structure and visualize brittle zones that the structure may have. However, to design a structure for a given seismic zone, the pushover analysis does not allow the quantification of these results. In this way, Fajfar and Fischinger [66-69] have developed a methodology called the N2 method (present in Eurocode 8 Annex B [51]), where it is possible to compare the capacity curve with an elastic response spectrum. It is a method generally applied to reinforced concrete and steel structures and, for this reason, there are few studies for timber buildings [61, 62, 70].

This chapter aims to apply the pushover analysis with the help of the N2 method to two study cases. That is, to increase the pushover analysis studies for low- and mid-rise CLT structures and to quantify the seismic performance applying the N2 method. The study cases are related to the building present in Chapter 4 and the second one has been created to provide a larger plan dimension and the study of different masses. To cover different seismic demand levels, three countries were chosen (Portugal, Italy, and Turkey), where four horizontal elastic response spectra have been selected for each. Regarding the numerical models, they followed the assumptions described in Chapter 5, where the experimental curves assumed for the metal connectors used were related to the bilinear curves quantified through EN 12512:2001 [34] and presented in Chapter 3. It is important to note that friction between panels was not included in the numerical modeling.

Therefore, through preliminary analyses, it was possible to observe that the response to the performance of lateral loads are controlled by the angle brackets (AE116), with the shear connectors always reaching the failure first than the uplift ones (HTT22). In this way, the analyses have been performed for different spacings of the AE116. Regarding the thickness and number of layers of the CLT panels assumed in the models, they have been related to the design of the Ultimate Limit State according to Eurocode 5 [1].

6.2 Methodology used for the numerical analysis of the CLT structures

This section presents the pushover analysis based on the N2 method proposed by Fajfar and Fischinger [66-69], applied to the seismic design of CLT buildings. This methodology is described in Eurocode 8 (Annex B) [51], which consists of transforming a Multi Degree of Freedom (MDOF) system into a Single Degree of Freedom (SDOF) system, to represent the first mode behavior. With this, it is possible to determine the performance point of the structure, based on the target displacement in the capacity curve for elastic response spectrum demand.

For a better understanding of the design procedure, the building studied in Chapter 4 has been used as a case study, and the response of that CLT building under loading in the transverse direction was studied.

6.2.1 Step 1 – Lateral load pattern

Adopting the methodology used in the finite element method of the building presented and described in Chapter 5, after this, the first step, to apply the pushover analysis, is related to the need to define the lateral load pattern. According to Eurocode 8 [51], the loads must be applied at the location of the masses in the model. Therefore, they should be applied on the floors, which presents a high mass concentration. In terms of the distribution of the lateral loads, it can be carried out through a “uniform” pattern, which depends on the mass present on the floors. On the other hand, it can be performed through the “modal” pattern, where it is performed proportionally to the lateral forces determined in the elastic analysis [51]. However, due to the impossibility of quantifying the modes shapes using RFEM software, the “modal” load pattern has been defined through a triangular distribution (see Figure 6.1), which presents a behavior close to the “modal” pattern [71]. That said, through a preliminary analysis for both load patterns, it was possible to observe a higher base shear force with lower displacement capacity (higher elastic stiffness) in the "uniform" load pattern, as happened in the pushover analysis performed by Johannes Hummel [61]. In terms of the application of the N2 method, it showed that the load patterns result in similar performance values, where the triangular load pattern presented low convergence issues. Under these circumstances, the analysis performed in this chapter was performed only for the triangular load model (see Figure 6.1). However, it is important to note that for the final seismic design, it is necessary to verify both patterns.

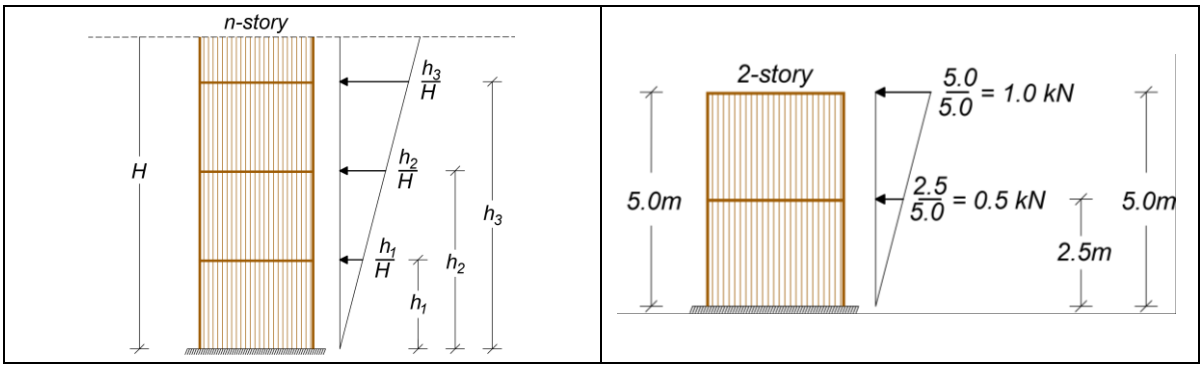

(a) (b)

Figure 6.1 – Lateral load pattern for pushover analysis. (a) General description; (b) application example.

6.2.2 Step 2 – Pushover analysis

This step is relative to the application of a pushover analysis, which is relative to a non-linear static analysis under constant gravity loads and incremental horizontal loads until structure failure. Thus, the capacity curve is defined by the relation between base shear force (F_b) and the displacement control (D_{Top}), which is located on the top of the building at the center of gravity (see Figure 6.2).

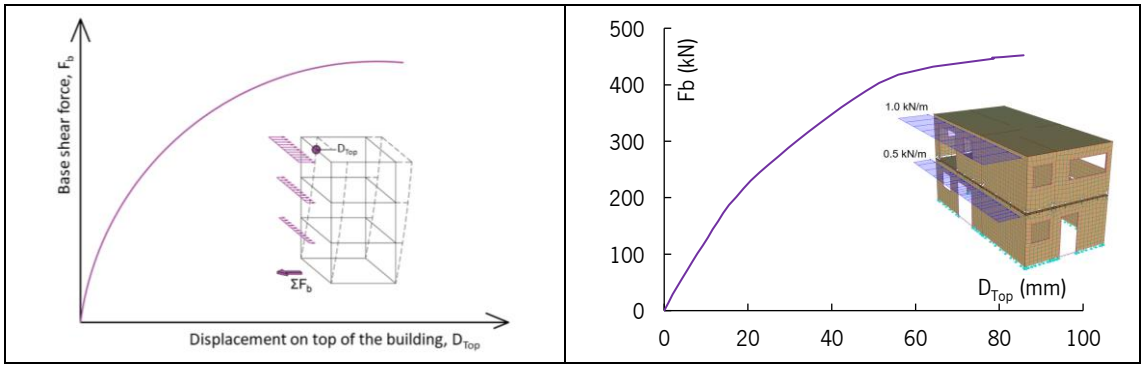

(a) (b)

Figure 6.2 – The capacity curve of pushover analysis. (a) General description; (b) application example.

6.2.3 Step 3 – Equivalent Single Degree of Freedom (SDOF) system

This step is related to the transformation of an equivalent Multi Degree of Freedom (MDOF) system to an equivalent Single Degree of Freedom (SDOF) system. In this way, through Annex B of Eurocode 8 [51], it is necessary the quantification of the transformation factor Γ (Equation 6.1), where the mass of an equivalent SDOF m^* (Equation 6.2) and normalized displacements Φ_i (see Figure 6.3) are required. Under these circumstances, normalized displacements are quantified as the lateral load pattern (step 1), and the equivalent mass is relative to the mass of each floor (see Figure 6.3a). Once the transformation factor is defined, the force F^* and displacement d^* of the equivalent SDOF system is quantified through the equations $F^* = \frac{F_b}{\Gamma}$ and $d^* = \frac{D_{Top}}{\Gamma}$, respectively. In relation to the case selected as example, the CLT building of Chapter 4, equal masses were assumed for both floors (see Figure 6.3b).

Transformation factor to SDOF system: $$\Gamma = \frac{m^*}{\sum m_i \Phi_i^2} \quad (6.1)$$

Equivalent mass of SDOF system: $$m^* = \sum m_i \Phi_i \quad (6.2)$$

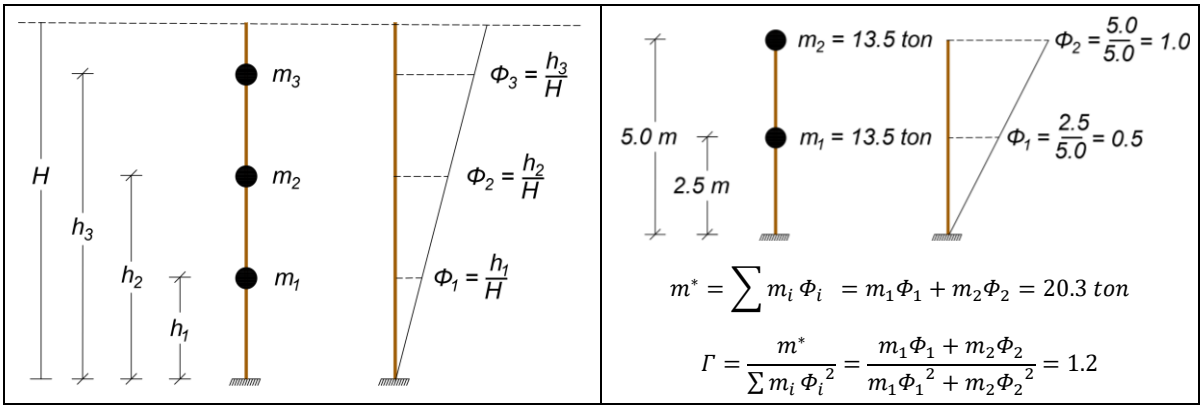

(a) (b)

Figure 6.3 – Modal parameters applied in the method. (a) General description; (b) application example.

6.2.4 Step 4 – Equivalent bilinear capacity curve of the SDOF system

The following step is related to the definition of the equivalent bilinear capacity curve and the respective period T^*. According to Eurocode 8 [51], this curve is defined by the yield force corresponding to the maximum force, where the slope of the elastic behavior is defined by the same area of the equivalent SDOF system and the equivalent bilinear capacity curve (see Figure 6.4a). However, in timber structures, it is common to admit elastic behavior until 40% of the maximum force [61], where the horizontal plastic range is defined by the same area of the equivalent SDOF system and the equivalent bilinear capacity curve (see Figure 6.4b). For example, according to the standards for timber connections EN 12512 [5, 34] and timber buildings ASTM E2126:2012 [57], the slop of elastic stiffness is defined by 40% of the maximum force [61]. In terms of ultimate displacement d^*_u, it has been defined by the failure of the structure.

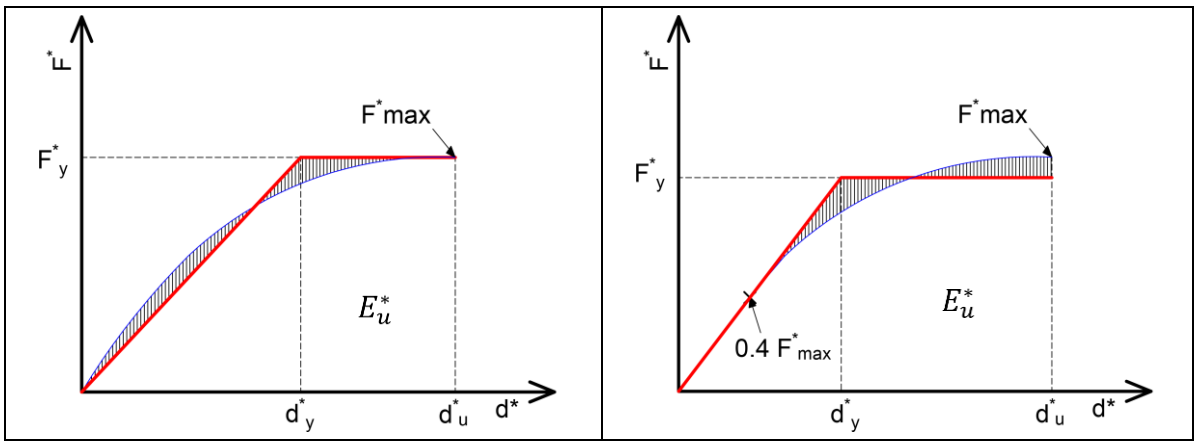

(a) (b)

Figure 6.4 – Equivalent bilinear capacity curve, according to annex B of Eurocode 8 (a) and commonly applied for timber structures (b).

Defined the equivalent bilinear capacity curve, the yielding displacement d^*_y and period T^* of the idealized SDOF system is given by:

Yielding displacement of the equivalent SDOF system:
Where E^*_u is the deformation energy up to the d^*_u.

$$d^*_y = 2\left(d^*_u - \frac{E^*_u}{F^*_y}\right) \quad (6.3)$$

Period of the equivalent SDOF system:

$$T^* = 2\pi\sqrt{\frac{m^* \times d^*_y}{F_y{}^*}} \quad (6.4)$$

For a better comparison between the two methods of quantification of the equivalent bilinear capacity curve exposed in Figure 6.4, Figure 6.5 presents their application to the adopted example. Regarding the comparison between the cases, it is possible to verify that the method defined by Eurocode 8 [51] (see Figure 6.5a), as expected, resulted in a reduction of the elastic stiffness with a reduced plastic range, where it presents a behavior quite far from tests. Thus, the analysis has been performed for the second case, in the definition of the elastic stiffness through 40% of the maximum force.

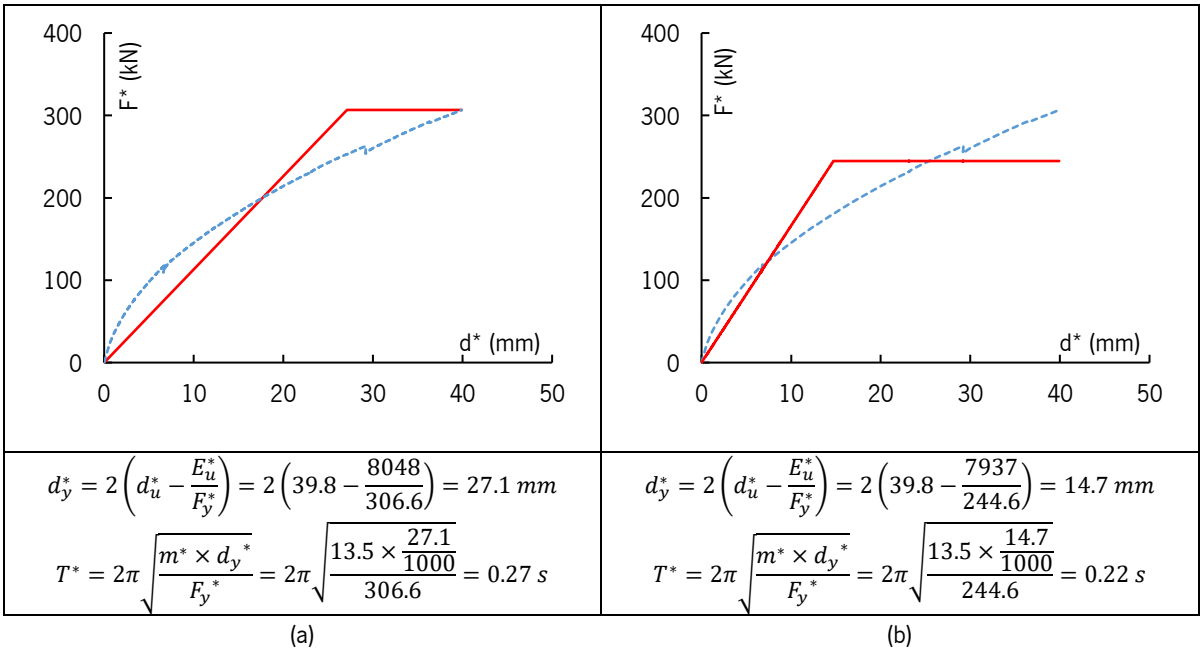

Figure 6.5 – Application example of an Equivalent bilinear capacity curve according to annex B of Eurocode 8 (a) and the method commonly applied for timber structures (b).

6.2.5 Step 5 – Demand spectra and performance displacement point

The last step is related to the quantification of the performance point of the structure through the intersection of the equivalent bilinear capacity curve of SDOF in the horizontal elastic response spectrum. In this way, firstly, it is necessary to transform the vertical axis of the equivalent bilinear capacity curve of SDOF into elastic acceleration (Equation 6.5) and, after this, the selection of a horizontal elastic response

spectrum. However, it is important to point out that the horizontal axis of the response spectrum has also to be transformed into elastic displacement (Equation 6.6).

Elastic acceleration response of bilinear curve:

$$S_e = \frac{F^*}{m^*} \tag{6.5}$$

Elastic displacement response spectrum:

$$d_e^* = S_e(T^*)\left[\frac{T^*}{2\pi}\right]^2 \tag{6.6}$$

In this way, the target displacement can be quantified graphically by the intersection of the elastic spectrum response and the equivalent bilinear capacity curve or, on the other hand, by applying the Annex B of Eurocode 8 [51], where it can be quantified by the simplified expressions defined for short periods (Figure 6.6a) and medium or long periods (Figure 6.6b). The parameter that defines the period domain is given by T_C.

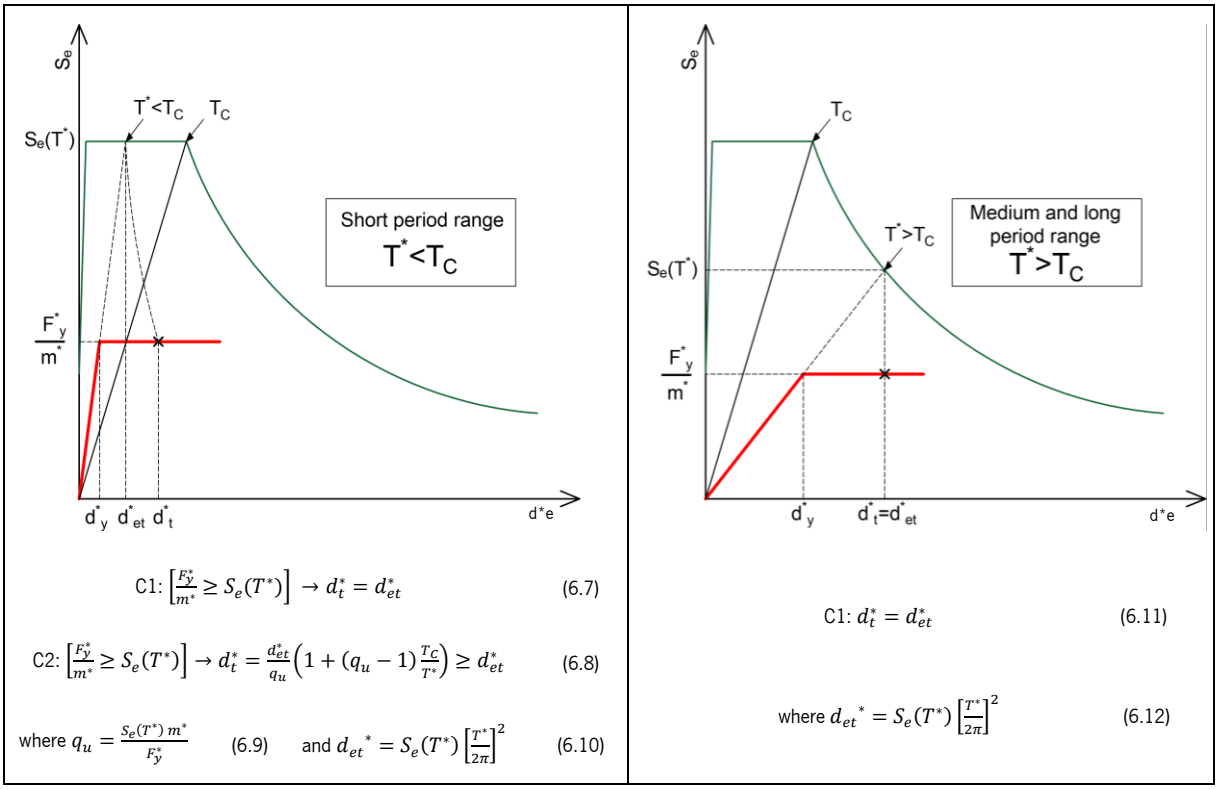

C1: $\left[\frac{F_y^*}{m^*} \geq S_e(T^*)\right] \rightarrow d_t^* = d_{et}^*$ (6.7)

C2: $\left[\frac{F_y^*}{m^*} \geq S_e(T^*)\right] \rightarrow d_t^* = \frac{d_{et}^*}{q_u}\left(1 + (q_u - 1)\frac{T_C}{T^*}\right) \geq d_{et}^*$ (6.8)

where $q_u = \frac{S_e(T^*)\, m^*}{F_y^*}$ (6.9) and $d_{et}{}^* = S_e(T^*)\left[\frac{T^*}{2\pi}\right]^2$ (6.10)

(a)

C1: $d_t^* = d_{et}^*$ (6.11)

where $d_{et}{}^* = S_e(T^*)\left[\frac{T^*}{2\pi}\right]^2$ (6.12)

(b)

Figure 6.6 – Target displacement for the equivalent SDOF system for (a) short period range and; (b) medium and long period range.

Finally, it concerns the transformation of the displacement from the SDOF system to the MDOF system, where the following equation can quantify it:

Target displacement on MDOF system:

$$d_t = \Gamma d^*{}_t \tag{6.13}$$

Within the process, applying on both examples (equivalent bilinear capacity curves according to Eurocode 8 and the common method applied to timber structures), Figure 6.7 shows the performance (target) point of the structure for each example. The seismic demand was related to the horizontal elastic response spectrum defined by Eurocode 8 [51] for Lisbon, Portugal location, where the parameters are described in Table 6.4, as Spectrum S4.

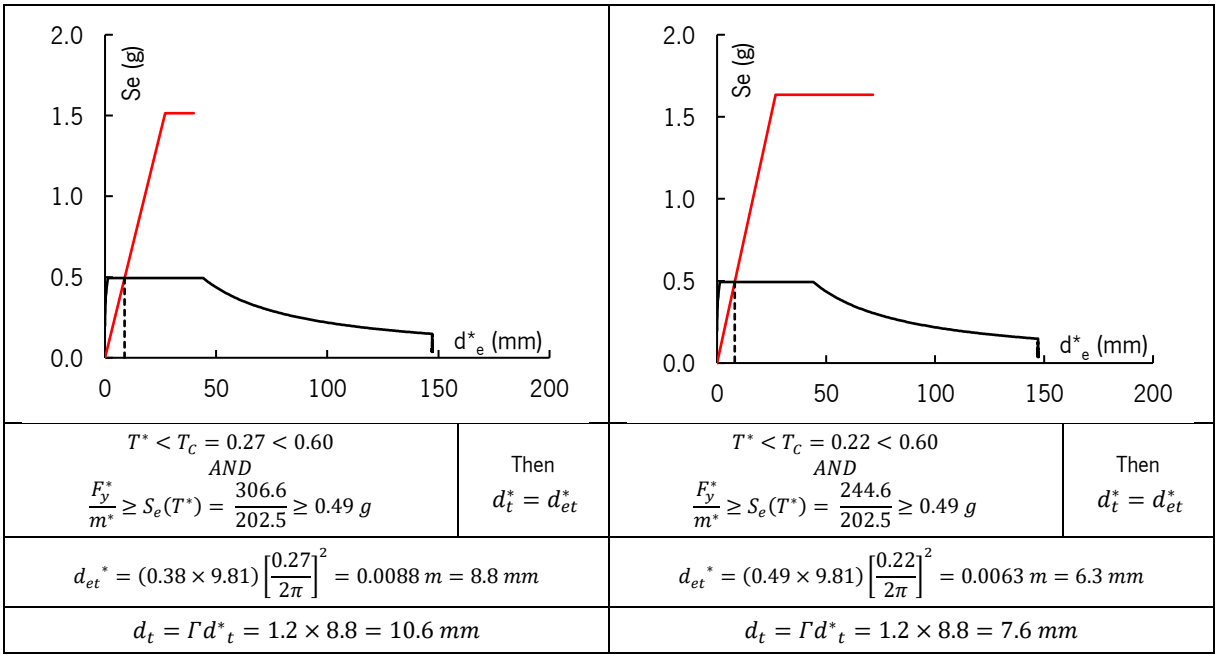

Figure 6.7 – Application examples of the target displacement for the equivalent SDOF system. Annex B of Eurocode 8 (a) commonly applied for timber structures (b).

Analyzing Figure 6.7, it is possible to observe that the two studied cases present the target displacement in the elastic state. Thus, it is possible to conclude that, for this seismic demand, the damage is practically null [72]. Regarding the differences between the two cases, the target displacement for the method presented in Annex B of Eurocode 8 shows a higher value compared to the method commonly applied to wooden structures.

6.3 Test procedures

With the description of the pushover analysis applied in this chapter, here the main variables of this analysis are described. The numerical analysis was performed using two study cases considering 2-story to 10-story to analyze low-rise and mid-rise CLT buildings and the main variables were separated into four groups: buildings, horizontal elastic spectrums response selected, metal connectors AE116 and HTT22 inserted in the tests and evaluation method.

6.3.1 Study cases

Two study cases have been studied. The study case 1 is related to the building of chapter 4 with a floor plan of 4.5 m x 9 m and with a story height of 2.5 m. In relation to case study 2, it was chosen to represent a more common building, where it has a larger in-plan dimension, symmetrical building plan and greater height between the floors compared to study case 1. The building as a floor plan of 18 m x 18 m and with a story height of 3 m. Interior walls with their respective openings were introduced to represent a real building, and the floors contained two openings for the elevators and one for the staircase. The CLT panels have been designed based on the ultimate limit state and service limit state, according to Eurocode 5 [1], where the CLT admitted was from the company Stora Enso of spruce species. In terms of thickness of the panels, 200 mm (5 layers of 50 mm) were inserted for all floors, 120 (3 layers of 40 mm) for the 1st story walls, and 100 (5 layers of 20 mm) for the remaining stories. The plans of the building and the facades with their respective openings are present in Figure 6.8.

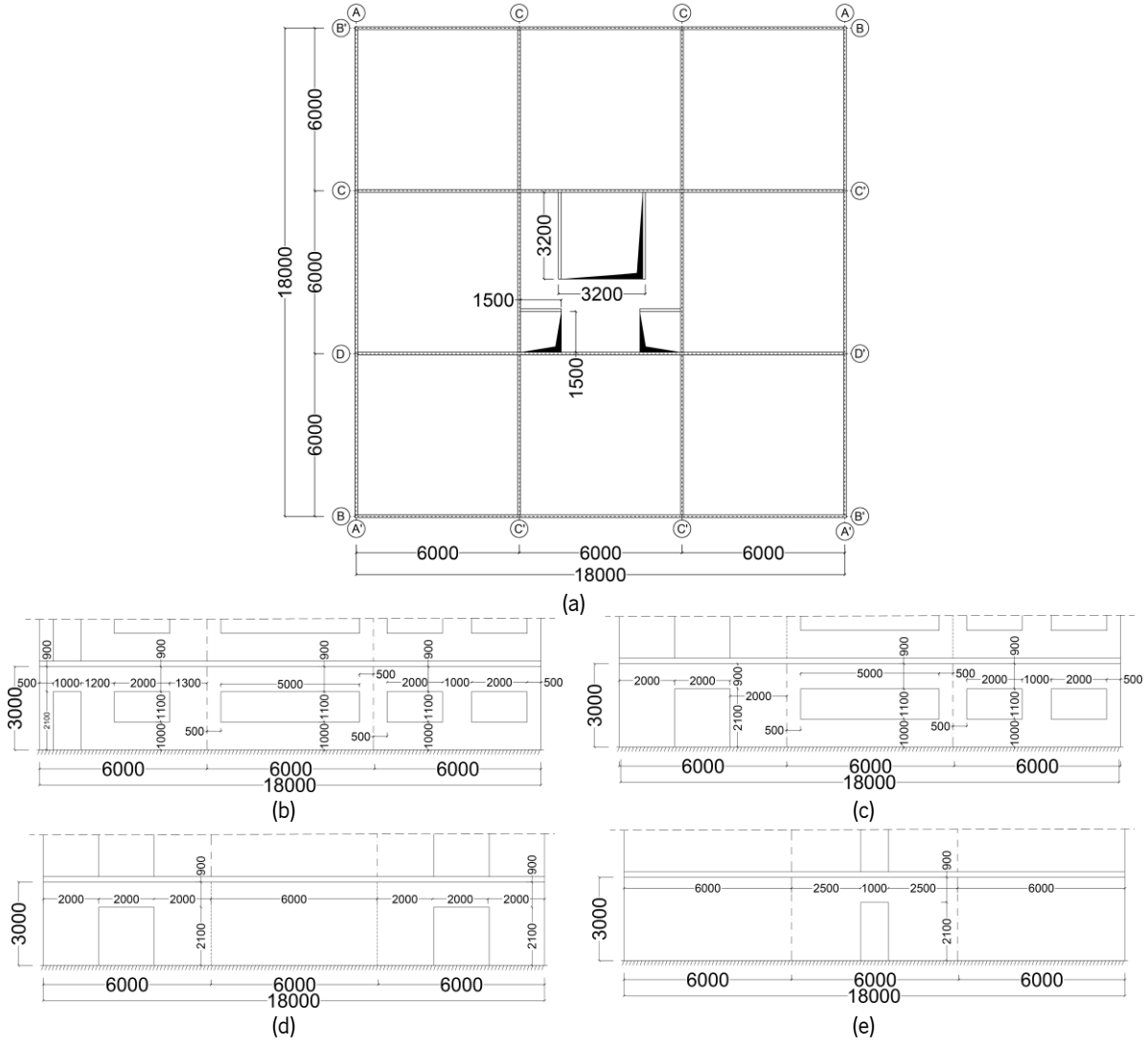

Figure 6.8 – Building plan (a) and facades of A-A' (b), B-B' (c), C-C' (d) and D-D'(e). (dimensions in mm).

Regarding the vertical loads inserted on the floors, paying particular attention to the acoustic behavior, three structural assemblies with different weights were studied. The structural assemblies have been based on solutions that the company DANOSA [73] provides while the acoustic resistance Dn,w (Airborne sound insulation) and Ln,w (Weighted normalized impact sound pressure level) of each floor was quantified applying the Portuguese standard [74, 75].

In this context, the structural assemblies with the application of the combination for seismic design (Eurocode 8 [51]) are described below. It is important to note that the assumed weights were collected in available technical tables [73, 76], and the assumed live-loads are related to category A of Eurocode 1 [50].

- Structural assembly 1 (Dn,w > 35 dB, Ln,w < 65 dB)

The structural assembly 1 is composed only by wood and acoustic layers, representing the lightest solution. In terms of acoustic resistance, according to Portuguese standard [74, 75], it is a solution that does not meet the requirements for living spaces and can, therefore, be only applied to separate storage areas and overlapping technical areas. Table 6.1 shows the structural assembly materials and the loads assumed in the analysis.

Table 6.1 – Structural assembly 1.

Number	Description	Units	Combination (Psd) $G_{k,j}$	Combination (Psd) $\Psi_{2,i} \cdot Q_{k,i}$
1	CLT panels [6]	kN/m³	5.0	-
2	Acoustic layer (for example FONODAM 900® [73] of 3.9 mm)	kN/m³	0.4	-
3	OSB [77] of 18+18 mm	kN/m³	5.5	-
4	Acoustic layer (for example CONFORDAN® [73] of 3 mm)	kN/m³	0.4	-
5	Final coating (for example timber floor [76])	kN/m²	0.2	-
-	Partition walls [76]	kN/m²	0.6	-
-	Live-load [50]	kN/m²	-	(0.8 x 0.3) x 2.0
	Total without CLT (≈ 50 mm)	**kN/m²**	**≈ 1.0**	**0.5**
				Psd **≈ 1.5**

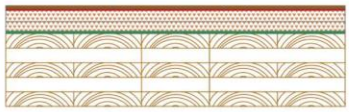

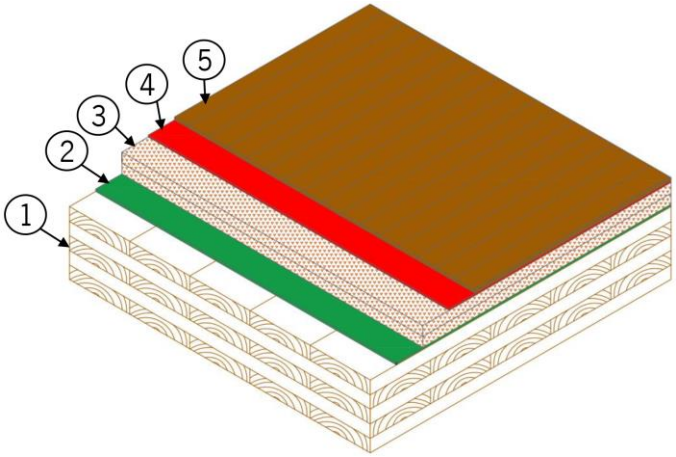

- Structural assembly 2 (Dn,w>40 dB, Ln,w<60 dB)

For structural assembly 2, the differences are related to the change of an acoustic layer and the substitution of the non-structural layer of OSB by lightweight concrete with expanded clay. In terms of acoustic resistance, an increase of the resistance was obtained with structural assembly 1. Now, this solution meets the requirements for vertical circulation paths, offices, commercial and service buildings, or other similar enclosed spaces. Table 6.2 shows the structural assembly materials and the loads assumed in the analysis.

Table 6.2 – Structural assembly 2.

Number	Description	Units	Combination (Psd) $G_{k,j}$	Combination (Psd) $\Psi_{2,i} \cdot Q_{k,i}$
1	CLT panels [6]	kN/m³	5.0	-
2	Acoustic layer (for example IMPACTODAM® 10 [73] of 10 mm)	kN/m³	0.3	-
3	Lightweight concrete with expanded clay [76] of 50 mm	kN/m³	12.0	-
4	Acoustic layer (for example CONFORDAN® [73] of 3 mm)	kN/m³	0.4	-
5	Final coating (for example timber floor [76])	kN/m²	0.2	-
-	Partition walls [76]	kN/m²	0.6	-
-	Live-load [50]	kN/m²	-	(0.8 x 0.3) x 2.0
	Total without CLT (≈ 70 mm)	**kN/m²**	**≈ 1.5**	**0.5** ***Psd*** **≈ 2.0**

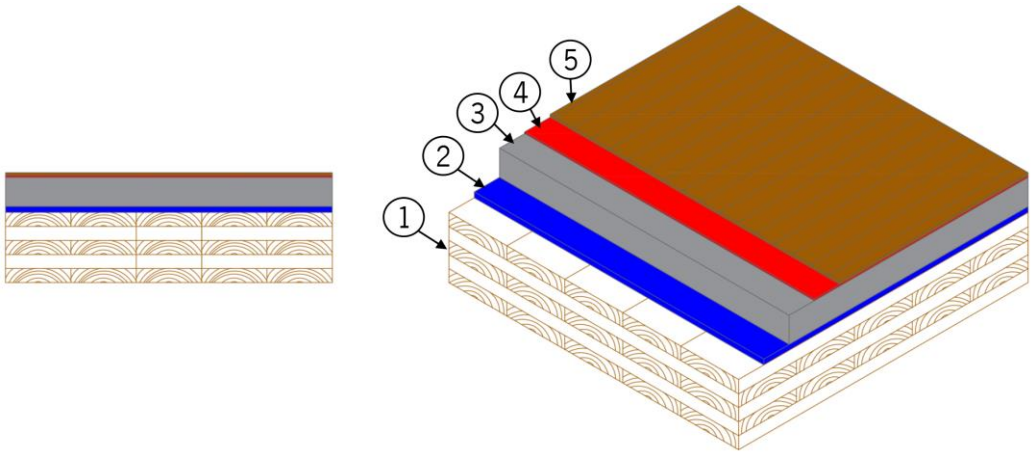

- Structural assembly 3 (Dn,w>50 dB, Ln,w<57 dB)

Finally, assembly 3, represents a solution with greater thickness and weight, as result of the addition of 50 mm of filling mortar. In consequence, this solution presents the highest acoustic resistance, meeting the requirements for residential and similar, school and similar, and hospital and similar buildings. Table 6.3 shows the structural assembly materials and the loads assumed in the models.

Table 6.3 – Structural assembly 3.

Number	Description	Units	Combination (Psd) $G_{k,j}$	Combination (Psd) $\Psi_{2,i} \cdot Q_{k,i}$
1	CLT panels [6]	kN/m³	5.0	-
2	Lightweight concrete with expanded clay [76] of 60 mm	kN/m³	12.0	-
3	Acoustic layer (for example IMPACTODAN® 5 [73] of 5 mm)	kN/m³	0.3	-
4	Filling mortar of 50 mm [76]	kN/m³	7.0	-
5	Acoustic layer (for example CONFORDAN® [73] of 3 mm)	kN/m³	0.4	-
6	Final coating (for example timber floor [76])	kN/m²	0.2	-
-	Partition walls [76]	kN/m²	0.6	-
-	Live-load [50]	kN/m²	-	(0.8 x 0.3) x 2.0
	Total without CLT (≈ 125 mm)	**kN/m²**	**≈ 2.0**	**0.5**
			Psd **≈ 2.5**	

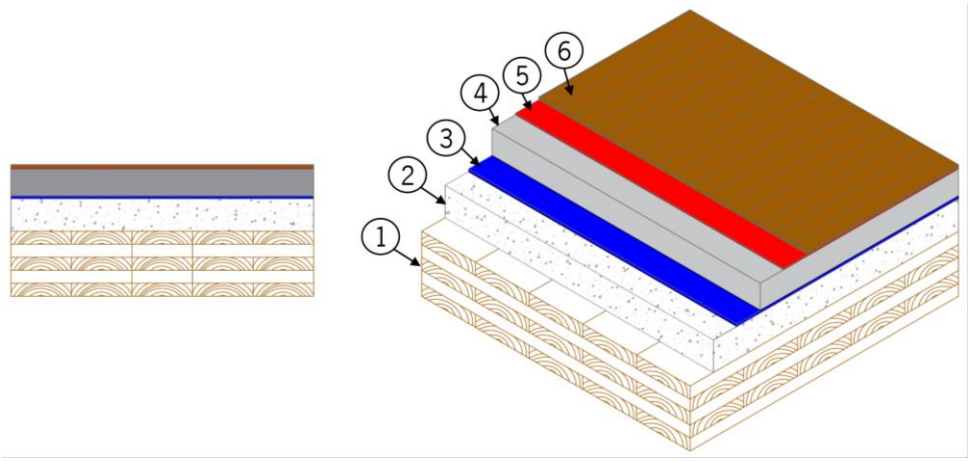

6.3.2 Seismic hazard

To perform the seismic design of the selected study cases, different horizontal elastic response spectra have been chosen. To cover a wide range of seismicity, from a moderate to high seismic activity, three countries were chosen: Portugal, Italy, and Turkey. As can be seen in Figure 6.9, Portugal presents the lowest peak ground acceleration (moderate), and Turkey presents the highest peak ground acceleration (high hazard).

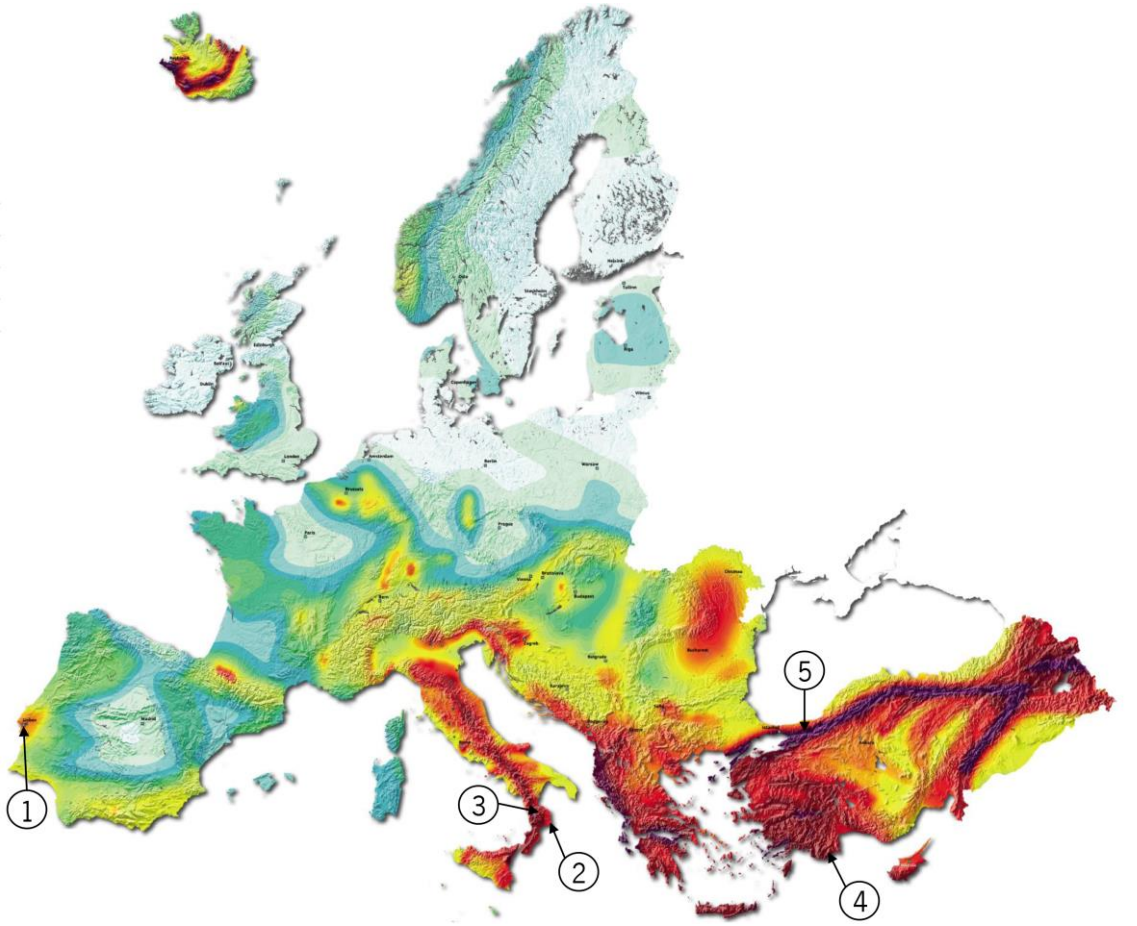

1. Lisbon, Portugal (38°45'11.2"N 9°10'59.1"W);
2. Cutro, Crotone, Italy (38°58'48.0"N 16°57'32.4"E);
3. San Gioganni in Fiore CS, Italy (39°20'31.2"N 16°35'24.0"E);
4. Belenli, Kaş/Antalya, Turkey (36°10'20.7"N 29°43'06.9"E);
5. Yeşilyurt, Başiskele/Kocaeli, Turkey (40°43'15.6"N 29°57'03.7"E).

Figure 6.9 – Hazard map of the selected locations [78].

Regarding the soil conditions, an important parameter in seismic analysis, two ground types were assumed A ($v_{s,30}$>800) and B (360>$v_{s,30}$>800) [51]. The response spectra were defined through the national regulations used for each country. Thus, Table 6.4 shows the parameters, and Figure 6.10, the graphs of the horizontal elastic response spectra adopted in the analysis.

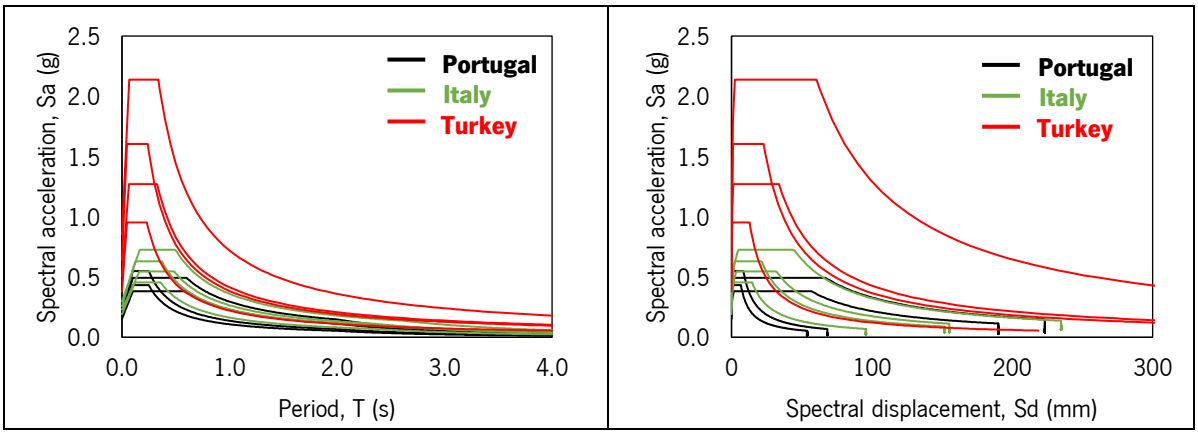

Figure 6.10 – Horizontal elastic response spectra selected.

Table 6.4 – Parameters of the horizontal elastic response spectra selected.

Location (see Figure 6.9)		Standard	Spectrum	Soil	T_c (s)	**Sd (mm) of T_c**	PGA (g)
Portugal	1	Eurocode 8 [51]	S1	A (Near)	0.25	**6.7**	0.17
	1		S2	B (Near)	0.25	**8.5**	0.22
	1		S3	A (Far)	0.60	**34.2**	0.15
	1		S4	B (Far)	0.60	**44.2**	0.20
Italy	2	NTC 2008 [53]	S1	A	0.36	**14.7**	0.19
	3		S2	B	0.37	**21.5**	0.26
	2		S3	B	0.48	**31.3**	0.23
	3		S4	A	0.49	**43.4**	0.30
Turkey	4	AFAD 2018 [79]	S1	A (B in [79])	0.23	**12.8**	0.38
	5		S2	B (C in [79])	0.24	**22.9**	0.64
	4		S3	A (B in [79])	0.33	**33.8**	0.50
	5		S4	B (C in [79])	0.34	**60.5**	0.86

6.3.3 Metal connectors AE116 and HTT22 inserted in the tests

As mentioned, one of the variables studied in the analysis of this chapter is related to the AE116 shear connectors location and spacings. In the study case 1, the CLT building of Chapter 4, a spacing of one AE116 shear connector every 3.0 m, 1.5 m, and 0.75 m were adopted. However, due to the short length of the walls in the transverse direction and to avoid structural disorders, the 3.0 m spacing was not studied in this direction. On the other hand, in study case 2, as it presents a more substantial mass floors, which results in higher demand, the analysis has been performed assuming a spacing of one AE116 connector every 1.5 m, 1.0 m, and 0.5 m. The HTT22 connectors, main responsible for the uplift resistance, were introduced near all openings and at all corners of the shear walls.

To identify the soft-story mechanism of the buildings, a preliminary pushover analysis was performed, assuming the same number of metal connectors for all stories. As expected, given the greater strength of the AE116 connectors on the foundation, the 1st floor presented a soft-story mechanism (see Figure 6.11) as a consequence of the failure of the AE116 shear connectors.

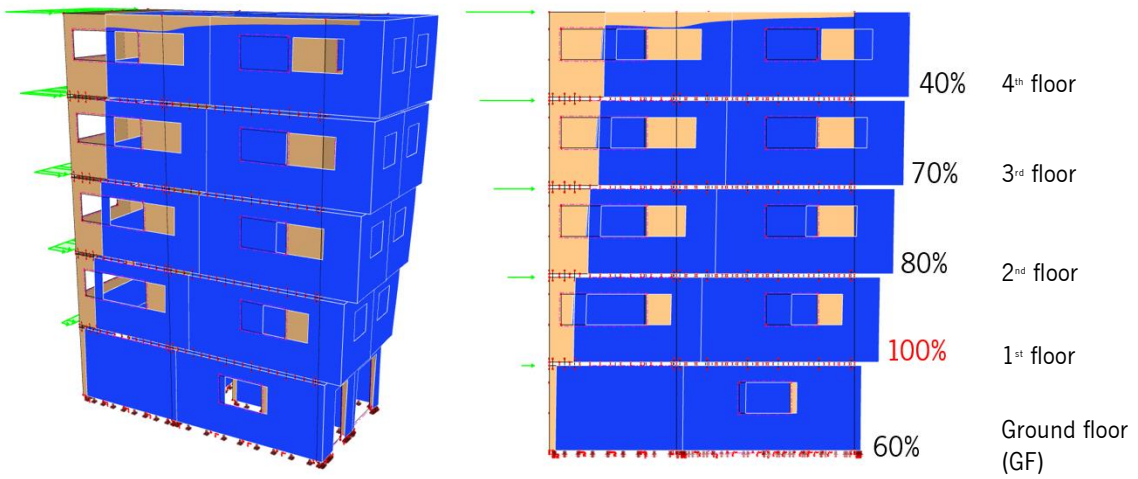

Figure 6.11 – Soft-story failure mechanisms of the 5-story building, study case 1, Longitudinal direction. (note that the plotted percentage values concern the load-carrying capacity reached).

In this context and to obtain better flexibility and rational use of the metal connectors, the number of AE116 connectors has been reduced on the remaining levels, percentage to reach around 100% of the load capacity of the AE116 metal connectors at all floors (see Figure 6.11). Table 6.5 shows the percentages used for each level in the numerical analysis based on preliminary analysis aimed to prevent the soft-story mechanism.

Table 6.5 – Percentage of AE116 connectors for each level

Building	Floor									
	GF	1st	2nd	3th	4th	5th	6th	7th	8th	9th
2-story	1.0	1.0	–	–	–	–	–	–	–	–
3-story	0.7	1.0	0.7	–	–	–	–	–	–	–
4-story	0.7	1.0	0.8	0.5	–	–	–	–	–	–
5-story	0.6	1.0	0.8	0.7	0.4	–	–	–	–	–
6-story	0.6	1.0	0.9	0.7	0.5	0.3	–	–	–	–
7-story	0.6	1.0	0.9	0.8	0.7	0.5	0.3	–	–	–
8-story	0.6	1.0	0.9	0.8	0.7	0.6	0.4	0.3	–	–
9-story	0.6	1.0	0.9	0.9	0.8	0.7	0.5	0.4	0.3	–
10-story	0.6	1.0	0.9	0.9	0.8	0.7	0.6	0.5	0.4	0.3

6.3.4 Evaluation method

To evaluate the structural performance of the different selected cases studies, three states were defined for the results of the N2 method: elastic range, plastic range, and failure (see Figure 6.12). The elastic range where the damage is practically null; plastic range where the damage already exists and the level of damage depends on the location of the target displacement; and failure, which means that the building has great structural weaknesses when subjected to lateral loads. Figure 6.12 shows an example for the case of medium and long period periods ($T^*>T_c$) for different horizontal elastic response spectra.

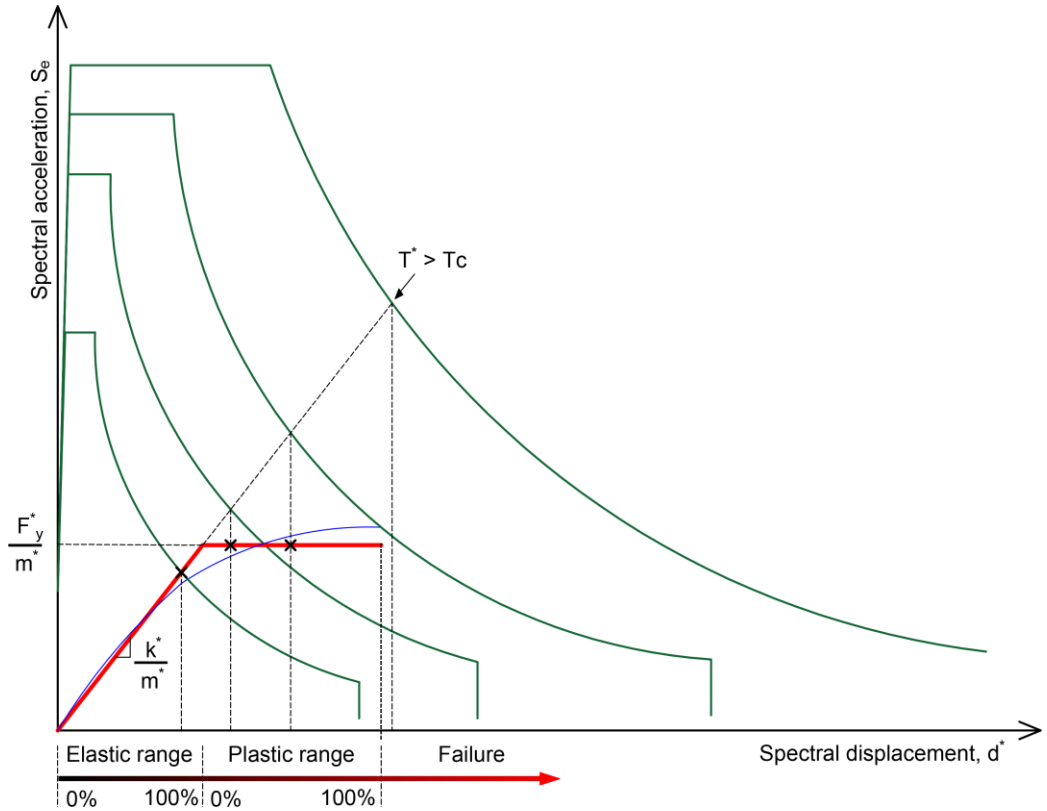

Figure 6.12 – Example of quantifying structural performance points [51, 72].

6.4 Results and discussion

Two different buildings, considering that the number of stories varies from 2 to 10, have been analyzed. The first building (study case 1) is related to the experimental program of Chapter 4, where the transverse and longitudinal directions have been evaluated. As the building contained just two stories, the addition of the different stories was related to the repetition of the second one. On the other hand, the second building (study case 2) presents higher in the plan area and story height, with openings for elevators and staircase, where three different floor masses were evaluated. For simplification, only analysis of 2-story, 4-story, 8-story, and 10-story are described and discussed.

6.4.1 Study case 1 – CLT building of Chapter 4

The study case 1 corresponds to the building studied in Chapter 4, representing the simplest example, as it has only 4.5x9.1 m in plan with a story height of 2.5 m. However, both directions were analyzed as a representation of a building with a 4.5 m façade and a 9.1 m façade. Regarding the mass of the floors, as it presents very similar values, a constant value of 13.5 tons per floor was admitted. In this way, considering the case of a 2-story building, the capacity curves and the main mechanical parameters obtained through the pushover analysis with the application of the standard ASTM E2126:2012 [57] are shown in Figure 6.13.

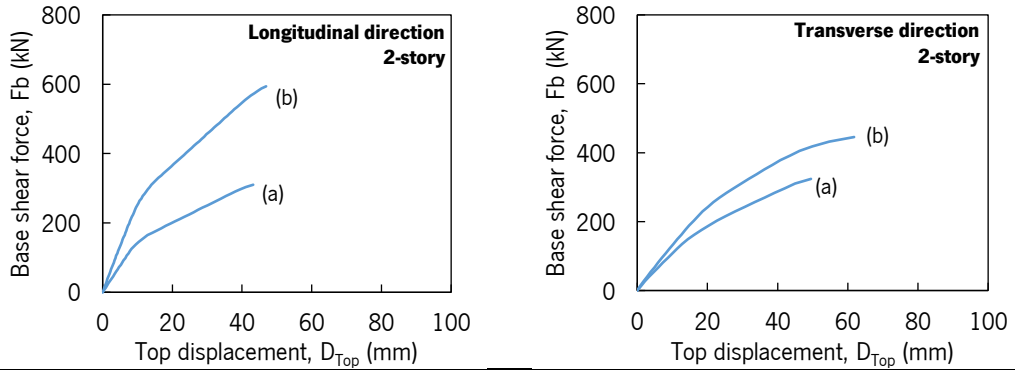

Direction	Tests	F_{max} (kN)	K(N/mm)	F_y (kN)	V_y (mm)	D_{Top} (mm)
Longitudinal (9.1 m)	(a) AE116 spaced to 3.00 m	310.2	15131	242.9	16.1	43.2
	(b) AE116 spaced to 1.50 m	594.0	25548	466.5	18.3	46.9
Transverse (4.5 m)	(a) AE116 spaced to 1.50 m	324.0	10588	268.4	25.3	49.5
	(b) AE116 spaced to 0.75 m	445.5	12802	386.6	30.2	61.8

Figure 6.13 – Capacity curves from non-linear pushover analysis and main mechanical parameters (study case 1–2-story).

By analyzing Figure 6.13, in agreement whit what was observed during the experimental campaign of the building presented in Chapter 4, the longitudinal direction is stiffer even for the spacing of 3.0 meters when compared to the transverse direction. By analyzing only the AE116 tests spaced at 1.50 m in both directions, it is possible to observe high differences between the mechanical parameters. However, it is important to note that the ultimate displacement (D_u) of both tests is similar. Once the capacity curves were obtained, the structural performance of each direction was determined by the N2 method. In this way, Figure 6.14 shows the equivalent bilinear capacity curves (SDOF system) and the horizontal elastic spectrum of each country, and Table 6.6, the target displacement parameters that best define the structural behavior. However, for a better comparison between results in Figure 6.14, the spectral acceleration value of 1 g is dashed.

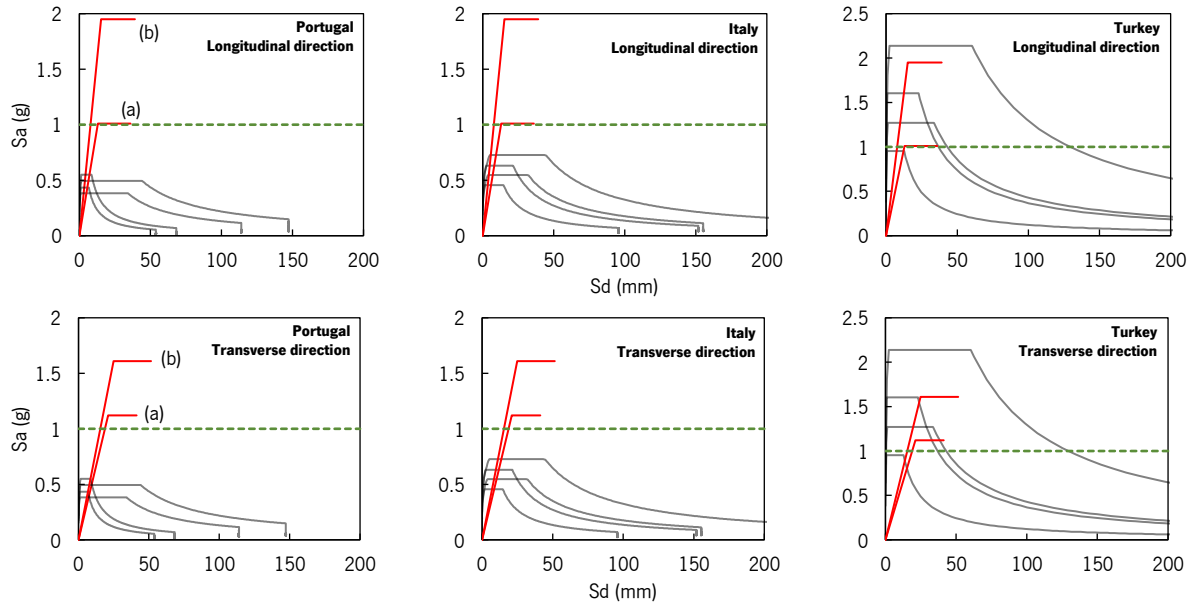

Figure 6.14 – Quantification of performance points for each country selected (study case 1–2-story).

Table 6.6 – Parameters of performance selected for each country (study case 1–2-story).

Direction:		Longitudinal			Transverse		
Country	Spectrum	Spaced to (m)	d_t (mm)	Location of d_t (%)	Spaced to (m)	d_t (mm)	Location of d_t (%)
Portugal	S1	3.00	6.7	42.0% of ①	1.50	9.1	35.8% of ①
	S2	3.00	8.6	53.3% of ①	1.50	11.5	45.4% of ①
	S3	3.00	6.0	37.1% of ①	1.50	8.6	34.1% of ①
	S4	3.00	7.7	47.9% of ①	1.50	11.2	44.0% of ①
Italy	S1	3.00	7.1	44.2% of ①	1.50	10.3	40.6% of ①
	S2	3.00	9.8	61.2% of ①	1.50	14.3	56.3% of ①
	S3	3.00	8.5	53.0% of ①	1.50	12.4	48.8% of ①
	S4	3.00	11.3	70.5% of ①	1.50	16.4	64.8% of ①
Turkey	S1	3.00	14.8	92.4% of ①	1.50	20.0	79.0% of ①
	S2	3.00	19.8	13.8% of ②	1.50	28.7	14.0% of ②
	S3	3.00	25.0	32.8% of ②	1.50	34.8	39.1% of ②
	S4	3.00	33.3	63.5% of ②	0.75	39.7	30.0% of ②

① - elastic range; ② - Plastic range; KO – Failure; d_t – target displacement for the MDOF system.

The analysis of Figure 6.14 and Table 6.6 shows that Portugal and Italy present all target displacements in the elastic range. On the other hand, Turkey presents some results in the plastic range, and the spectrum S4 for transverse direction does not have structural safety for a AE116 shear connectors 1.5m spacing. However, it is important to note that for the longitudinal direction, the spacing of 3.0 m is sufficient for obtaining structural safety for all spectra responses.

In the case of a 4-story building, the capacity curves and the main mechanical parameters with the application of the standard ASTM E2126:2012 [57] are shown in Figure 6.15. For a better comparison of capacity curves, the previous capacity curves (2-story building) are in dashed lines.

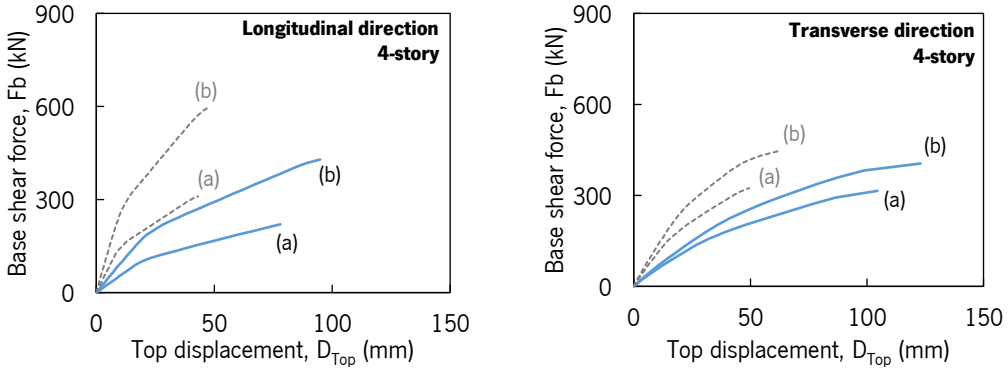

Direction	Tests	F_{max} (kN)	K(N/mm)	F_y (kN)	V_y (mm)	D_{Top} (mm)
Longitudinal (9.1 m)	(a) AE116 spaced to 3.00 m	220.0	5366	174.0	32.4	78.0
	(b) AE116 spaced to 1.50 m	429.0	8919	336.9	37.8	94.9
Transverse (4.5 m)	(a) AE116 spaced to 1.50 m	315.0	5143	268.5	52.2	104.5
	(b) AE116 spaced to 0.75 m	405.0	5895	355.1	60.2	123.0

Figure 6.15 – Capacity curves from non-linear pushover analysis and main mechanical parameters (study case 1–4-story).

The increase in the number of stories resulted in a reduction of strength, being the largest difference related to the elastic stiffness (K). Likewise, due to the increased height of the building, which results in greater flexibility, the ultimate displacements (D_{Top}) have been much higher. Within the process, applying

the N2 method, Figure 6.16 shows the equivalent bilinear capacity curves and the response spectra for each country and Table 6.7 the performance points selected.

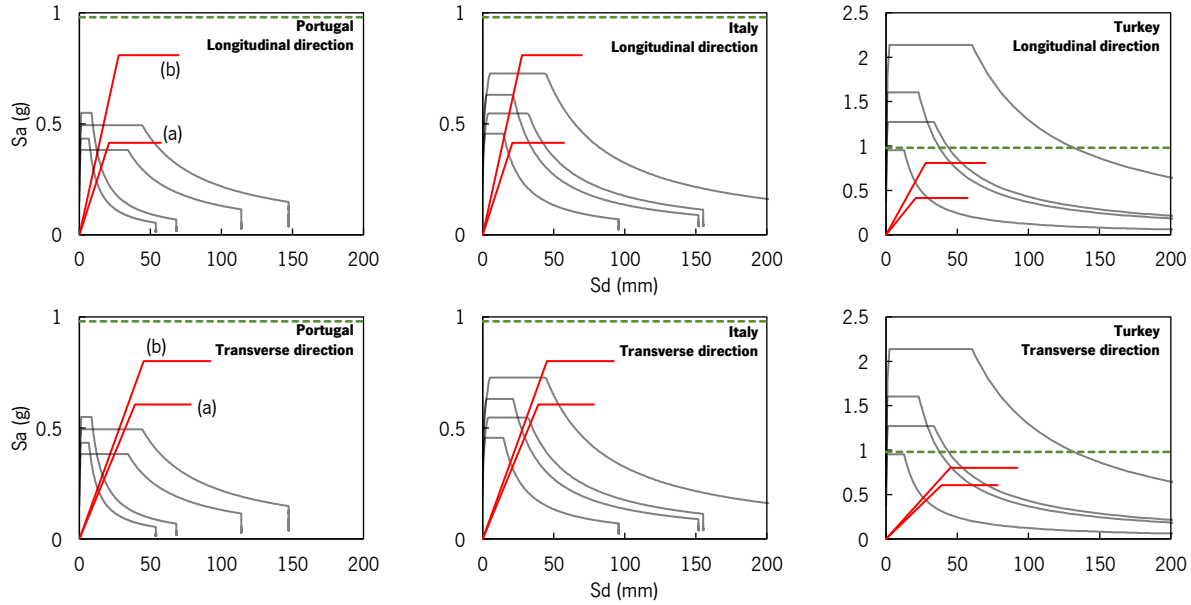

Figure 6.16 – Quantification of performance points for each country selected (study case 1–4-story).

Table 6.7 – Parameters of performance selected for each country (study case 1–4-story).

Direction:		Longitudinal			Transverse		
Country	Spectrum	Spaced to (m)	d_t (mm)	Location of d_t (%)	Spaced to (m)	d_t(mm)	Location of d_t (%)
Portugal	S1	3.00	16.8	51.9% of ①	1.50	18.3	35.1% of ①
	S2	3.00	21.3	65.8% of ①	1.50	23.2	44.5% of ①
	S3	3.00	26.1	80.5% of ①	1.50	33.0	63.1% of ①
	S4	3.00	33.7	02.8% of ②	1.50	42.6	81.5% of ①
Italy	S1	3.00	25.5	78.5% of ①	1.50	27.7	53.1% of ①
	S2	3.00	36.2	08.3% of ②	1.50	39.4	75.5% of ①
	S3	3.00	37.3	10.8% of ②	1.50	44.9	86.0% of ①
	S4	3.00	49.6	37.8% of ②	1.50	61.0	16.8% of ②
Turkey	S1	3.00	37.8	11.9% of ②	1.50	38.2	73.1% of ①
	S2	3.00	65.7	73.0% of ②	1.50	66.4	27.1% of ②
	S3	1.50	55.4	30.9% of ②	1.50	71.6	37.2% of ②
	S4	1.50	92.1	95.0% of ②	0.75	120.5	96.1% of ②

① - elastic range; ② - Plastic range; KO – Failure; d_t – target displacement for the MDOF system.

Analyzing Figure 6.16 and Table 6.7 can be immediately observed in the reduction of the spectral acceleration of the plastic range (F^*_y/m^*). However, the decrease of the elastic stiffness and the increase of ultimate displacement evidenced in Figure 6.15, resulted in changes in the performance of the building. In the longitudinal direction, the performance parameters show a higher demand, where the spacings of S3 and S4 for Turkey had to be decreased to 1.5 m. On the other hand, in the transverse direction, in general, all the tests show the performance points similar to a 2-story building, where the spectrum response S4 of Turkey shows a performance close to failure.

For a 6-story building, the capacity curves and the main mechanical parameters with the application of the standard ASTM E2126:2012 [57] are shown in Figure 6.17. It is important to mention that a reduction of the AE116 shear connector spacing to 0.75 m was necessary for the longitudinal direction.

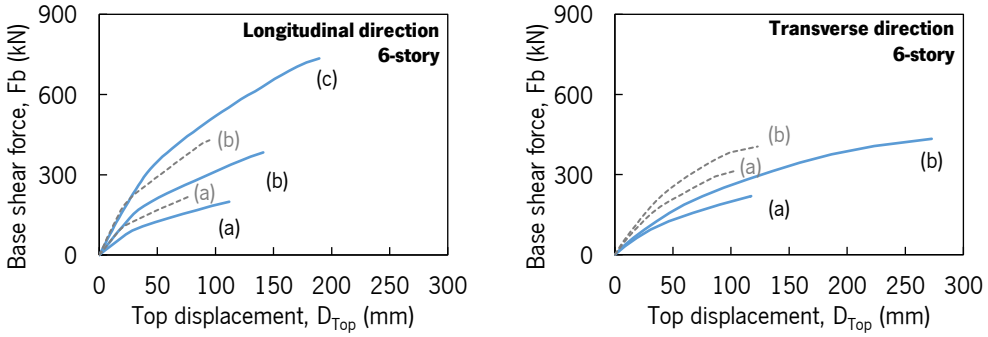

Direction	Tests	F_{max} (kN)	K(N/mm)	F_y (kN)	V_y (mm)	D_{Top} (mm)
Longitudinal (9.1 m)	(a) AE116 spaced to 3.0 m	199.1	3301	162.1	49.1	111.9
	(b) AE116 spaced to 1.5 m	383.5	5164	305.2	59.1	141.2
	(c) AE116 spaced to 0.75 m	735.0	7534	593.8	78.8	189.4
Transverse (4.5 m)	(a) AE116 spaced to 1.5 m	219.2	3101	187.6	60.5	117.3
	(b) AE116 spaced to 0.75 m	433.8	3225	370.9	115.0	272.7

Figure 6.17 – Capacity curves from non-linear pushover analysis and main mechanical parameters (study case 1–6-story).

Figure 6.17 presents for comparison purposes, in-dash the capacity curves of the 4-story building. It can be seen that the values of load-carrying capacity are close, except for the case AE116, in which spaced at 1.50 m for the transverse direction. In the same way, due to the greater flexibility of the building, lower values of elastic stiffness are presented (differences between 63% to 83%) and higher values of ultimate displacement (differences between 30% to 55%) are achieved. Analyzing the 0.75 m spacing for the longitudinal direction, a significant increase of strength occurred compared to the 1.5 m spacing. However, it is important to note that the elastic stiffness for the transverse direction for 1.5 m and 0.75 m spacing is similar. Thereby, Figure 6.18 shows the equivalent bilinear capacity curves and the response spectra for each country, and Table 6.8, the parameters of performance selected.

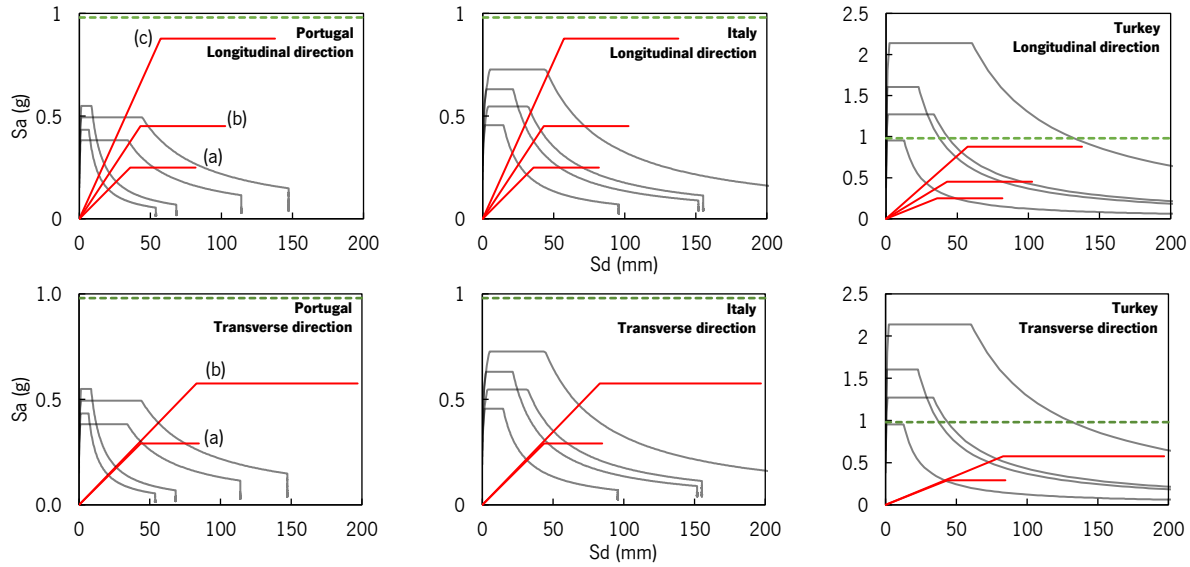

Figure 6.18 – Quantification of performance points for each country selected (study case 1–6-story).

Table 6.8 – Parameters of performance selected for each country (study case 1–6-story).

Direction:		Longitudinal			Transverse		
Country	Spectrum	Spaced to (m)	d_t(mm)	Location of d_t (%)	Spaced to (m)	d_t(mm)	Location of d_t (%)
Portugal	S1	3.00	28.0	57.1% of ①	1.50	29.2	48.3% of ①
	S2	3.00	35.6	72.4% of ①	1.50	37.1	61.3% of ①
	S3	3.00	59.4	16.4% of ②	1.50	61.9	02.5% of ②
	S4	3.00	76.7	44.0% of ②	1.50	80.0	34.3% of ②
Italy	S1	3.00	42.5	86.5% of ①	1.50	44.3	73.2% of ①
	S2	3.00	60.4	18.0% of ②	1.50	63.0	04.4% of ②
	S3	3.00	68.8	31.3% of ②	1.50	71.7	19.7% of ②
	S4	3.00	93.5	70.6% of ②	1.50	97.4	65.0% of ②
Turkey	S1	3.00	58.1	14.3% of ②	1.50	61.3	01.4% of ②
	S2	3.00	101.0	82.6% of ②	1.50	106.6	81.2% of ②
	S3	1.50	90.8	38.6% of ②	0.75	110.7	96.3% of ①
	S4	0.75	129.6	46.0% of ②	0.75	192.3	49.0% of ②

① - elastic range; ② - Plastic range; KO – Failure; d_t – target displacement for the MDOF system.

The analysis of Figure 6.18 allows for verifying the substantial increase of the plastic range state for the spacing of 0.75 m in the transverse direction. Regarding the longitudinal direction, with a spacing of 0.75m, as expected, there was an increase in resistance compared to 3.0 m and 1.5 m spacing. Looking at Table 6.8, it is possible to verify that the response spectrum S4 of the longitudinal direction and the response spectrum S3 of the transverse direction of Turkey have been reduced to 0.75 m spacing.

For the 8-story building, the capacity curves and the main mechanical parameters with the application of the standard ASTM E2126:2012 [57] are shown in Figure 6.19.

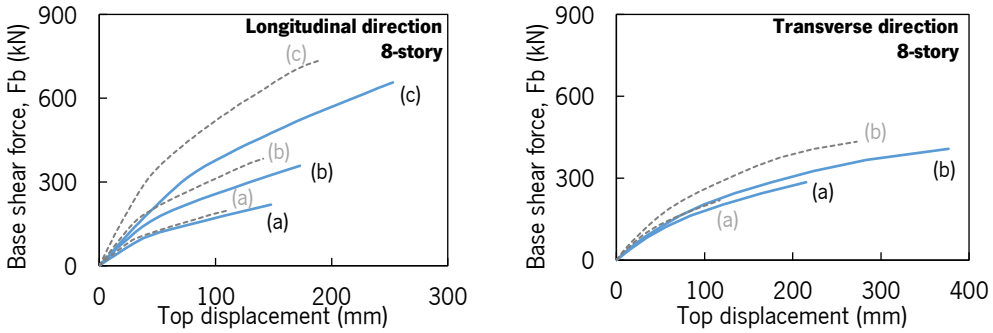

Direction	Tests	F_{max} (kN)	K(N/mm)	F_y (kN)	V_y (mm)	D_{Top} (mm)
Longitudinal (9.1 m)	(a) AE116 spaced to 3.00 m	218.8	2652	177.7	67.0	147.8
	(b) AE116 spaced to 1.50 m	358.0	3735	288.4	77.2	172.8
	(c) AE116 spaced to 0.75 m	656.3	4301	534.4	124.3	252.8
Transverse (4.5 m)	(a) AE116 spaced to 1.50 m	285.4	2208	245.0	111.0	215.2
	(b) AE116 spaced to 0.75 m	407.7	2259	352.0	155.8	376.8

Figure 6.19 – Capacity curves from non-linear pushover analysis and main mechanical parameters (study case 1–8-story).

The analysis of Figure 6.19 shows the similarity in terms of load-carrying capacity and an increase in the displacement values compared to the previous analysis (6-story), where the major differences are related to the AE116 spaced to 0.75 m for longitudinal direction. Applying the N2 method, Figure 6.20 shows the equivalent bilinear capacity curves and the response spectra for each country, and Table 6.9, the parameters of performance selected.

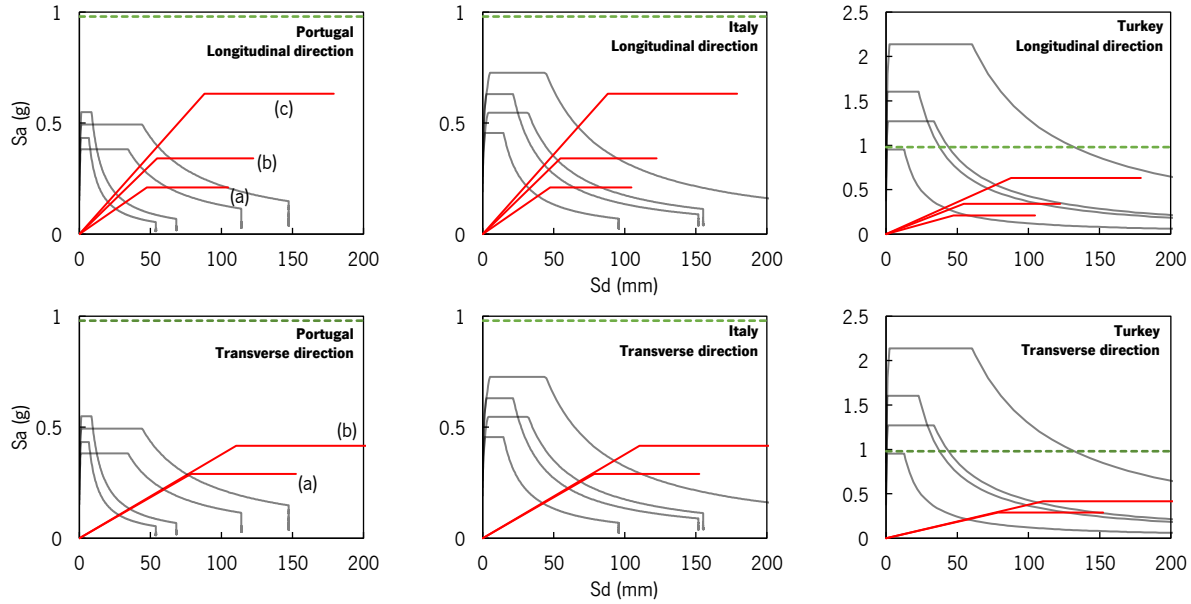

Figure 6.20 – Quantification of performance points for each country selected (study case 1–8-story).

Table 6.9 – Parameters of performance selected for each country (study case 1–8-story).

Direction:		Longitudinal			Transverse		
Country	Spectrum	Spaced to (m)	d_t(mm)	Location of d_t (%)	Spaced to (m)	d_t(mm)	Location of d_t (%)
Portugal	S1	3.00	36.3	54.2% of ①	1.50	39.9	35.9% of ①
	S2	3.00	46.1	68.7% of ①	1.50	50.6	45.6% of ①
	S3	3.00	76.9	12.3% of ②	1.50	84.4	76.0% of ①
	S4	3.00	99.4	40.0% of ②	1.50	109.0	98.3% of ①
Italy	S1	3.00	55.0	82.1% of ①	1.50	60.3	54.4% of ①
	S2	3.00	78.3	13.9% of ②	1.50	85.9	77.4% of ①
	S3	3.00	89.1	27.3% of ②	1.50	97.7	88.1% of ①
	S4	3.00	121.1	66.9% of ②	1.50	132.8	20.9% of ②
Turkey	S1	3.00	74.2	09.0% of ②	1.50	85.0	76.6% of ①
	S2	3.00	117.4	42.0% of ②	1.50	147.3	34.9% of ②
	S3	1.50	129.1	76.8% of ②	0.75	155.2	99.6% of ①
	S4	0.75	202.6	60.9% of ②	0.75	270.1	51.7% of ②

① - elastic range; ② - Plastic range; KO – Failure; d_t – target displacement for the MDOF system.

Analyzing Figure 6.20 and Table 6.9, it is possible to verify that the results are similar to the previous analysis, where, in general, all the analyzes present better performance of the building because it resulted in a smaller reduction in the slope of the elastic stiffness and the increase of the plastic range state. Finally, for a 10-story building, the capacity curves and the main mechanical parameters with the application of the standard ASTM E2126:2012 are shown in Figure 6.21.

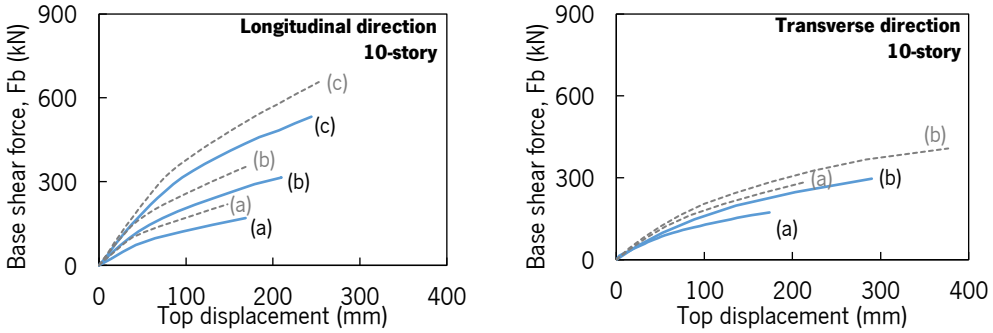

Direction	Tests	F_{max} (kN)	K(N/mm)	F_y (kN)	V_y (mm)	D_{top} (mm)
Longitudinal (9.1 m)	(a) AE116 spaced to 3.00 m	169.4	1716	143.8	83.8	168.6
	(b) AE116 spaced to 1.50 m	314.6	2629	262.5	99.9	209.9
	(c) AE116 spaced to 0.75 m	532.4	3686	445.3	120.8	244.3
Transverse (4.5 m)	(a) AE116 spaced to 1.50 m	173.3	1768	143.8	81.3	173.9
	(b) AE116 spaced to 0.75 m	297.0	1773	262.4	148.0	290.0

Figure 6.21 – Capacity curves from non-linear pushover analysis and main mechanical parameters (study case 1–10-story).

Analyzing Figure 6.21, it is possible to verify that, unlike the previous analyzes, the ultimate displacement decreased in transverse direction tests and in the test AE116 spaced to 0.75 m in the longitudinal direction. Thereby, Figure 6.22 shows the equivalent bilinear capacity curves and the response spectra for each country, and Table 6.10, the parameters of performance selected.

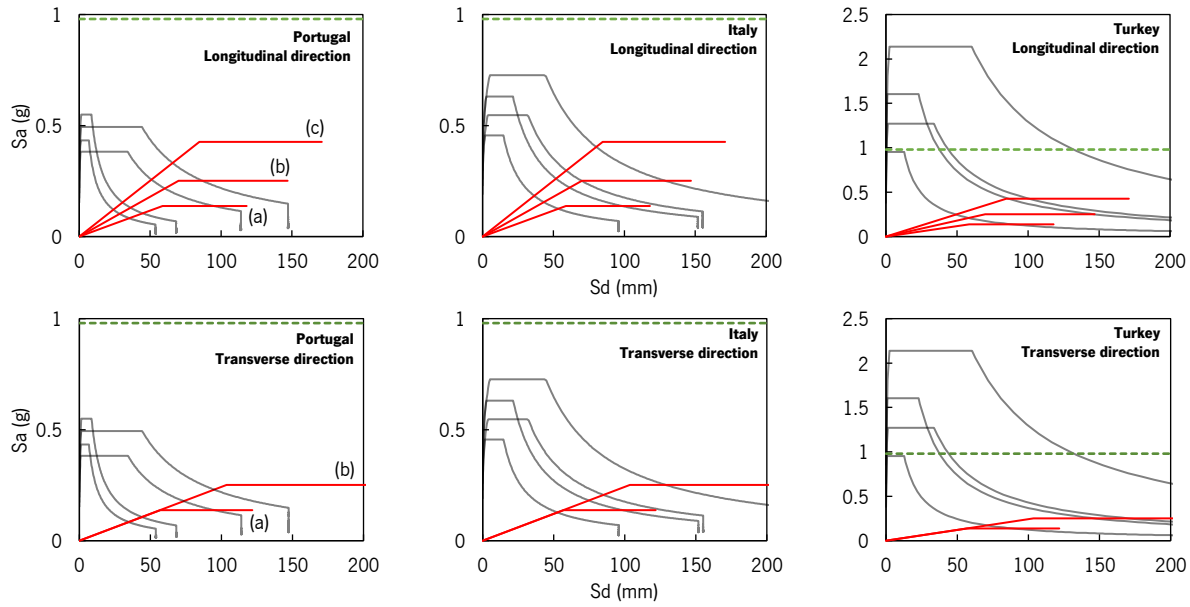

Figure 6.22 – Quantification of performance points for each country selected (study case 1–10-story).

Table 6.10 – Parameters of performance selected for each country (study case 1–10-story).

Direction:		Longitudinal			Transverse		
Country	Spectrum	Spaced to (m)	d_t(mm)	Location of d_t (%)	Spaced to (m)	d_t(mm)	Location of d_t (%)
Portugal	S1	3.00	50.7	60.5% of ①	1.50	49.6	61.1% of ①
	S2	3.00	64.4	76.8% of ①	1.50	63.0	77.4% of ①
	S3	3.00	107.4	27.9% of ②	1.50	105.1	25.7% of ②
	S4	3.00	138.8	64.8% of ②	1.50	135.7	58.8% of ②
Italy	S1	3.00	76.8	91.7% of ①	1.50	75.1	92.4% of ①
	S2	3.00	109.3	30.1% of ②	1.50	106.9	27.7% of ②
	S3	3.00	124.4	47.9% of ②	1.50	121.7	43.6% of ②
	S4	1.50	136.7	33.5% of ②	0.75	166.2	12.8% of ②
Turkey	S1	3.00	103.5	23.2% of ②	1.50	104.6	25.2% of ②
	S2	1.50	145.5	41.5% of ②	0.75	181.6	23.6% of ②
	S3	1.50	157.5	52.3% of ②	0.75	195.8	33.6% of ②
	S4	0.75	241.1	97.4% of ②	**0.75**	**340.2**	**KO**

① - elastic range; ② - Plastic range; KO – Failure; d_t – target displacement for the MDOF system.

Figure 6.22 and Table 6.10 show, as expected that the location of the target displacement increased for all response spectra. However, it is important to note that for the transverse direction for spectrum S4 (Turkey), the 0.75 m spacing for the AE116 shear connectors does not meet the structural safety. Under these circumstances, the spacing would have to be reduced or another shear connector, with a higher load-carrying capacity should be used.

6.4.2 Study case 2

The study case 2 represents a CLT building with a plan of 18x18 m, a story height of 3 m, and was selected to represent a more current structure. In comparison with study case 1, this building presents a higher floor area and story height, and in addition to the staircase opening, two elevator openings have been included. Beyond these, to study different masses on the floors, three different structural assemblies have been defined with different masses. Figure 6.23 presents the capacity curves and the main mechanical parameters with the application of the standard ASTM E2126:2012 [57] for a 2-story building. However, it is important to note that given the proximity of the capacity curves of the different structural assemblies (different masses on the floors studied), only the structural assembly 3 (2.5 kN/m² + CLT panels) is shown in Figure 6.23.

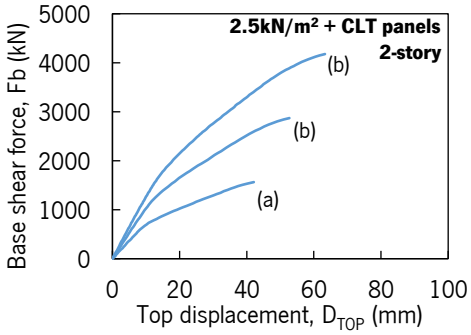

Tests	F_{max} (kN)	K (N/mm)	F_y (kN)	V_y (mm)	D_{top} (mm)
(a) AE116 spaced to 1.5 m	1563.1	71230	1244.0	17.5	42.1
(b) AE116 spaced to 1.0 m	2869.9	100627	2329.9	23.2	52.7
(b) AE116 spaced to 0.5 m	4176.8	121114	3415.0	28.2	63.3

Figure 6.23 – Capacity curves from non-linear pushover analysis and the main mechanical parameter considering assembly 3 (study case 2–2-story).

As expected, the load-carrying capacity and elastic stiffness increased significantly when compared with study case 1 (see Figure 6.23). On the other hand, the smaller values of displacement resulted from the low flexibility of the building. In this way, applying the N2 method, Figure 6.24 shows the equivalent bilinear capacity curves and the horizontal elastic response spectrum of each country and Table 6.11 the location of the target displacement. In the same way of study case 1, for better comparison between results in Figure 6.24, the spectral acceleration value of 1 g is dashed.

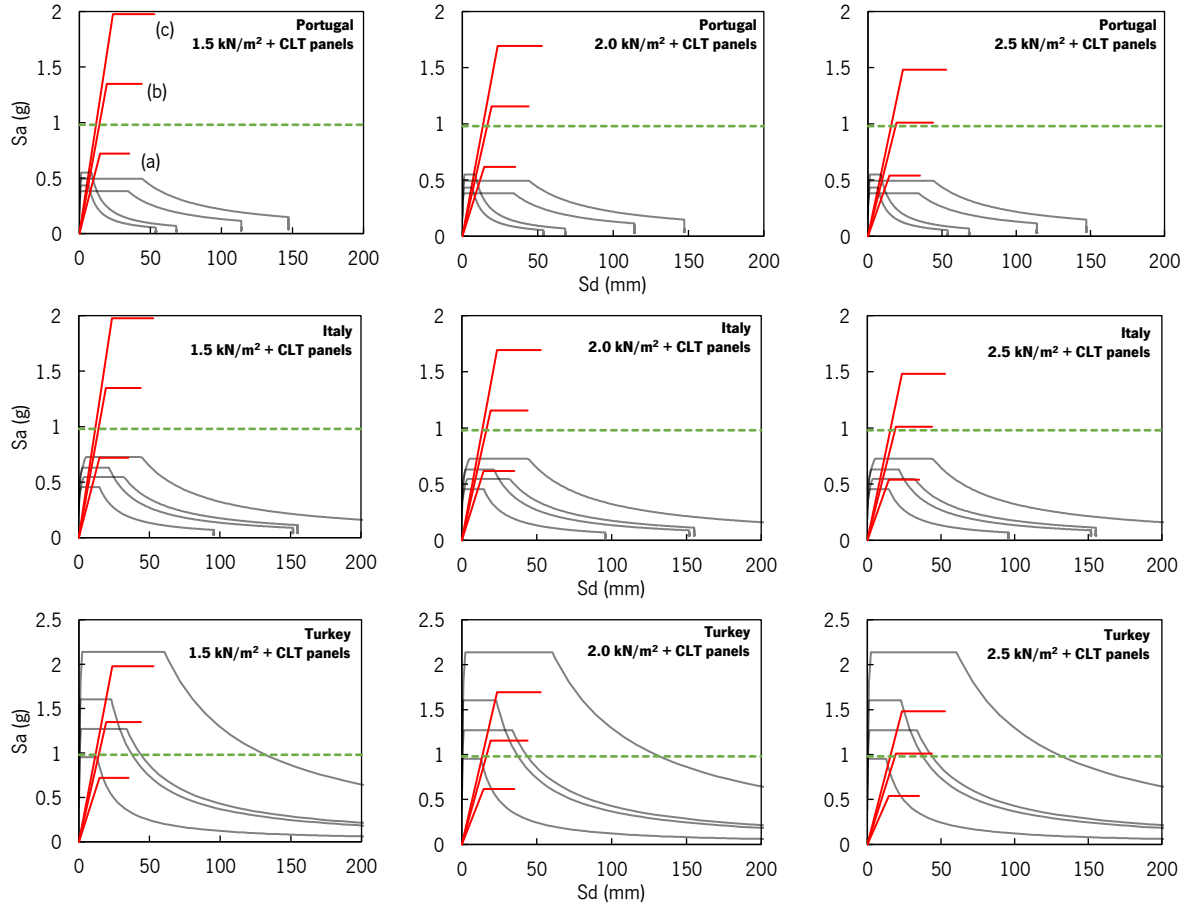

Figure 6.24 – Quantification of performance points for each country selected (study case 2–2-story).

Table 6.11 – Parameters of performance selected for each country (study case 2–2-story).

Country:			Portugal		Italy		Turkey	
Loads		Spectrum	Spaced to (m)	Location of d_t (%)	Spaced to (m)	Location of d_t (%)	Spaced to (m)	Location of d_t (%)
Assembly 1	1.5 kN/m² + CLT	S1	1.50	53.7% of ①	1.50	63.3% of ①	1.50	16.4% of ②
		S2	1.50	68.2% of ①	1.50	87.6% of ①	1.50	54.3% of ②
		S3	1.50	53.1% of ①	1.50	76.0% of ①	1.50	80.7% of ②
		S4	1.50	68.6% of ①	1.50	00.7% of ②	1.00	45.9% of ②
Assembly 2	2.0 kN/m² + CLT	S1	1.50	58.5% of ①	1.50	73.8% of ①	1.50	14.0% of ②
		S2	1.50	74.2% of ①	1.50	01.6% of ②	1.50	75.1% of ②
		S3	1.50	61.9% of ①	1.50	88.6% of ①	1.50	76.5% of ②
		S4	1.50	80.0% of ①	1.50	12.6% of ②	1.00	66.6% of ②
Assembly 3	2.5 kN/m² + CLT	S1	1.50	62.7% of ①	1.50	84.4% of ①	1.50	26.1% of ②
		S2	1.50	79.5% of ①	1.50	11.9% of ②	1.50	96.0% of ②
		S3	1.50	70.8% of ①	1.50	00.9% of ②	1.00	40.9% of ②
		S4	1.50	91.5% of ①	1.50	24.5% of ②	1.00	87.3% of ②

① - elastic range; ② - Plastic range; KO – Failure; d_t – target displacement for the MDOF system.

Analyzing Figure 6.24 and Table 6.11, for the selected response spectrum for Portugal and Italy, the 1.5 m spacing is more than sufficient to ensure structural safety. However, for Turkey, due to the low displacement reached, the spectrum S4 for all structural assemblies and the spectrum S3 for structural assembly 3 (2.5 kN/m² + CLT panels) does not present structural safety for 1.5 m spacing. Evaluated the 2-story building, Figure 6.25 shows the capacity curves for the 4-story building and the main

mechanical parameters with the application of the standard ASTM E2126:2012 [57]. In the same way of study case 1, for a better comparison of capacity curves, the previous capacity curves (2-story building) are in dashed lines.

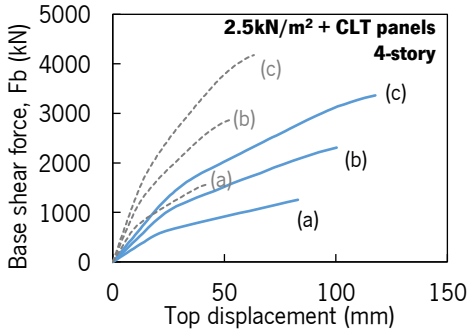

Tests	F_{max} (kN)	K(N/mm)	F_y (kN)	V_y (mm)	D_{Top} (mm)
(a) AE116 spaced to 1.5 m	1254.4	28769	983.5	34.2	83.0
(b) AE116 spaced to 1.0 m	2308.3	42564	1842.1	43.3	100.4
(c) AE116 spaced to 0.5 m	3362.3	52379	2690.0	51.4	117.7

Figure 6.25 – Capacity curves from non-linear pushover analysis and main mechanical parameters (study case 2–4-story).

The analysis of Figure 6.25 shows that the tests performed present an accentuated decrease of the elastic stiffness and an increase in ultimate displacement compared to the previous analysis (2-story). Figure 6.26 shows the equivalent bilinear capacity curves and the horizontal elastic spectrum of each country and Table 6.12 the target displacement selected.

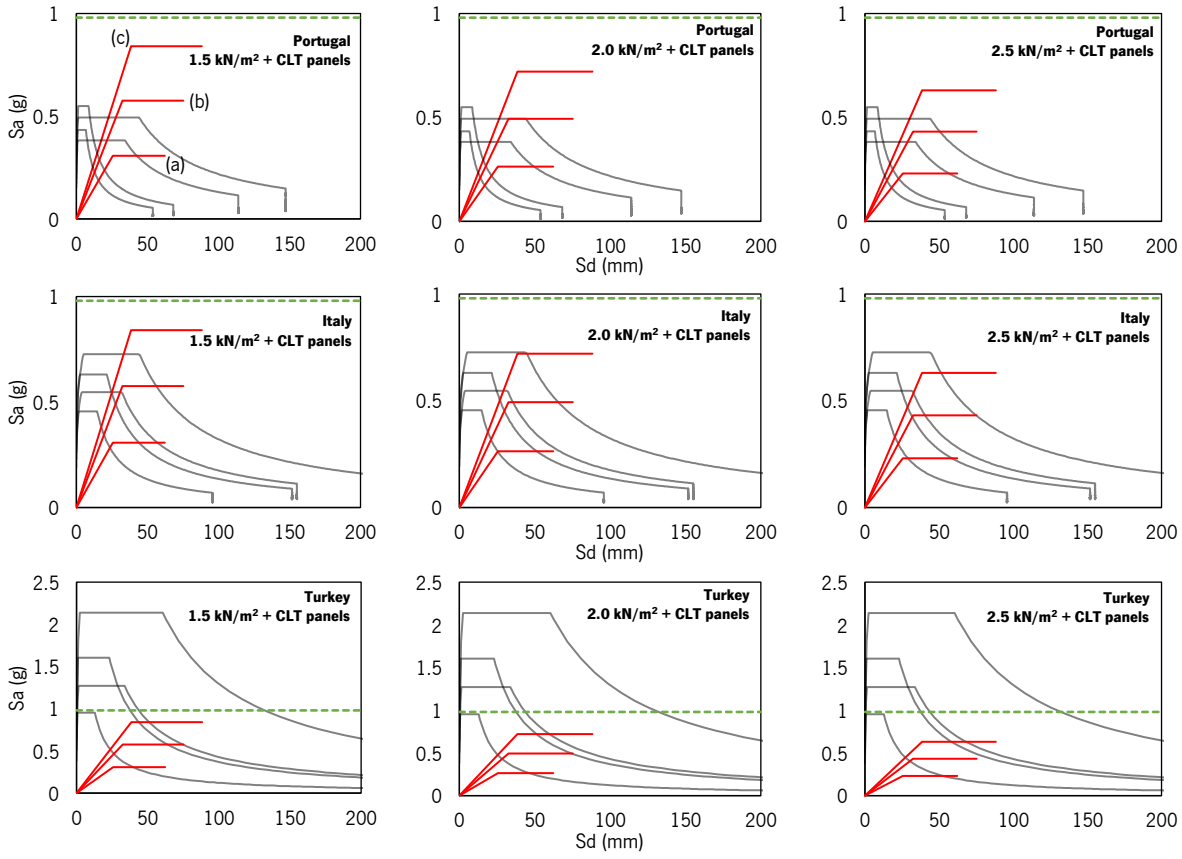

Figure 6.26 – Quantification of performance points for each country selected (study case 2–4-story).

Table 6.12 – Parameters of performance selected for each country (study case 2–4-story).

Country:			Portugal		Italy		Turkey	
Loads		Spectrum	Spaced to (m)	Location of d_t (%)	Spaced to (m)	Location of d_t (%)	Spaced to (m)	Location of d_t (%)
Assembly 1	1.5 kN/m² + CLT	S1	1.50	61.8% of ①	1.50	93.6% of ①	1.50	21.8% of ②
		S2	1.50	78.4% of ①	1.50	23.2% of ②	1.00	45.8% of ②
		S3	1.50	17.1% of ②	1.50	36.1% of ②	1.00	36.8% of ②
		S4	1.50	42.5% of ②	1.50	74.2% of ②	0.50	88.7% of ②
Assembly 2	2.0 kN/m² + CLT	S1	1.50	66.3% of ①	1.50	00.3% of ②	1.50	28.1% of ②
		S2	1.50	84.1% of ①	1.50	30.0% of ②	1.00	51.9% of ②
		S3	1.50	28.3% of ②	1.50	43.9% of ②	1.00	42.5% of ②
		S4	1.50	57.0% of ②	1.50	84.7% of ②	0.50	94.8% of ②
Assembly 3	2.5 kN/m² + CLT	S1	1.50	71.2% of ①	1.50	05.5% of ②	1.50	33.6% of ②
		S2	1.50	91.3% of ①	1.50	37.4% of ②	1.00	35.9% of ②
		S3	1.50	88.5% of ①	1.50	52.2% of ②	1.00	47.1% of ②
		S4	1.50	66.4% of ②	1.00	39.4% of ②	**0.50**	**KO**

① - elastic range; ② - Plastic range; KO – Failure; d_t – target displacement for the MDOF system.

Analyzing Figure 6.26, it is possible to observe that the spectral acceleration of the plastic range decreased significantly, where all equivalent bilinear capacity curves present values below 1g, as happened in the study case 1. On the other hand, Table 6.12 shows that Portugal already presents target displacements on plastic range state, in Italy, spectrum S4 for structural assembly 3 has been reduced to 1.0 m spacing, and in Turkey, the response spectrum S4 in structural assembly 3, for the minimum analyzed spacing, presents no structural safety.

Figure 6.27 shows the capacity curves and main mechanical parameters with the application of the standard ASTM E2126:2012 [57], for a 6-story building.

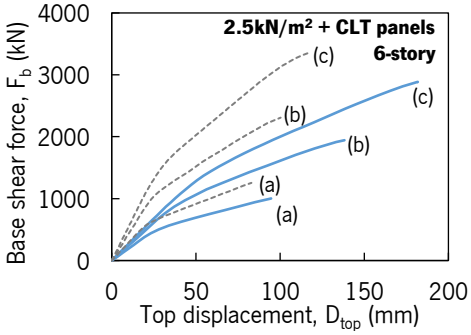

Tests	F_{max} (kN)	K(N/mm)	F_y (kN)	V_y (mm)	D_{Top} (mm)
(a) AE116 spaced to 1.5 m	997.0	19104	816.0	42.7	93.2
(b) AE116 spaced to 1.0 m	1943.4	24037	1602.0	66.6	138.3
(c) AE116 spaced to 0.5 m	2884.6	26218	2335.5	89.1	181.8

Figure 6.27 – Capacity curves from non-linear pushover analysis and main mechanical parameters (study case 2–6-story).

Based on Figure 6.27, it is possible to verify a decrease in the resistance, where the most significant differences are related to the elastic stiffness. However, as expected, the ultimate displacement increased. Figure 6.28 shows the equivalent bilinear capacity curves and the horizontal elastic spectrum of each country, and Table 6.13, the target displacement selected.

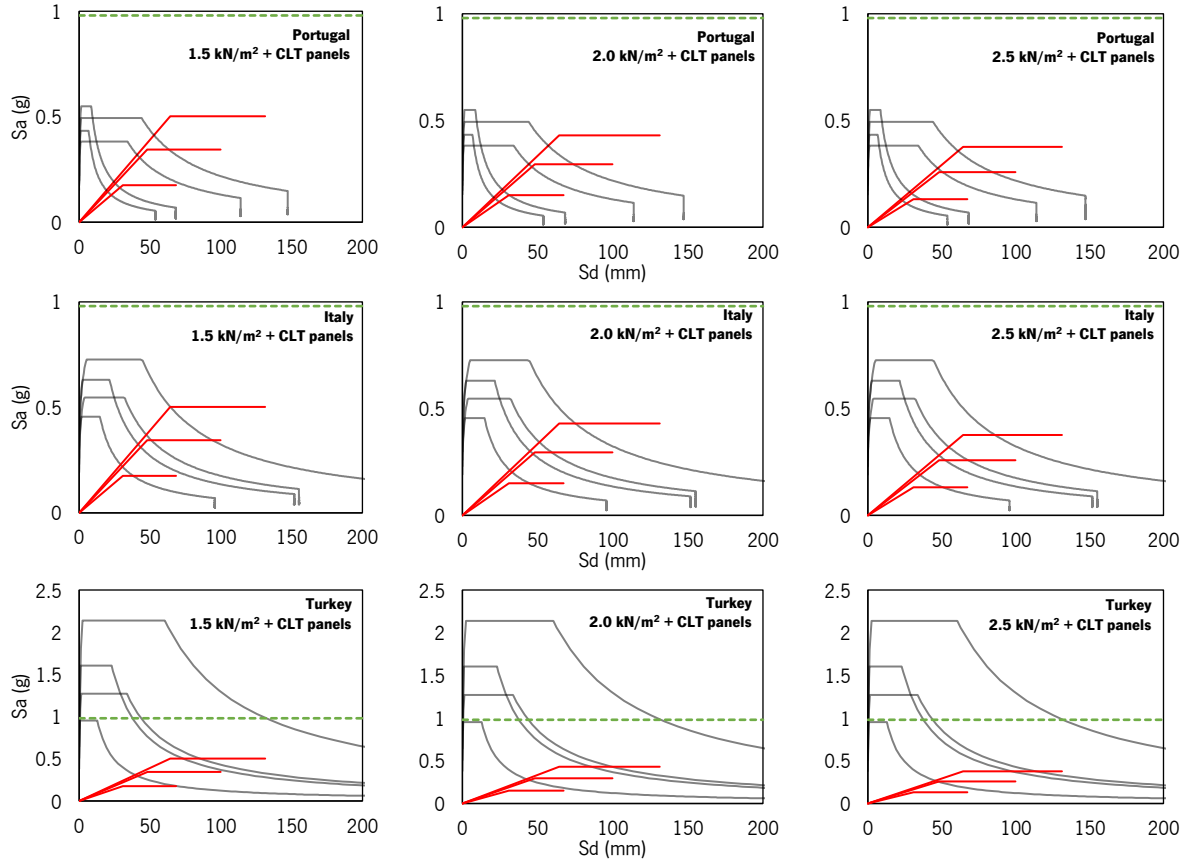

Figure 6.28 – Quantification of performance points for each country selected (study case 2–6-story).

Table 6.13 – Parameters of performance selected for each country (study case 2–6-story).

Country:			Portugal		Italy		Turkey	
Loads		Spectrum	Spaced to (m)	Location of d_t (%)	Spaced to (m)	Location of d_t (%)	Spaced to (m)	Location of d_t (%)
Assembly 1	1.5 kN/m² + CLT	S1	1.50	74.4% of ①	1.50	10.4% of ②	1.50	47.3% of ②
		S2	1.50	94.4% of ①	1.50	49.3% of ②	1.00	56.7% of ②
		S3	1.50	47.0% of ②	1.50	67.3% of ②	1.00	45.6% of ②
		S4	1.50	84.6% of ②	1.00	37.0% of ②	**0.50**	**KO**
Assembly 2	2.0 kN/m² + CLT	S1	1.50	80.1% of ①	1.50	18.0% of ②	1.50	53.8% of ②
		S2	1.50	01.3% of ②	1.50	61.3% of ②	1.00	70.6% of ②
		S3	1.50	58.8% of ②	1.50	81.5% of ②	1.00	58.6% of ②
		S4	1.00	22.3% of ②	1.00	47.4% of ②	**0.50**	**KO**
Assembly 3	2.5 kN/m² + CLT	S1	1.50	84.9% of ①	1.50	24.2% of ②	1.50	65.2% of ②
		S2	1.50	06.5% of ②	1.50	70.1% of ②	1.00	83.2% of ②
		S3	1.50	67.5% of ②	1.50	91.5% of ②	1.00	70.2% of ②
		S4	1.00	31.1% of ②	1.00	58.1% of ②	**0.50**	**KO**

① - elastic range; ② - Plastic range; KO – Failure; d_t – target displacement for the MDOF system.

In Figure 6.28, itis possible to verify, again, a high decrease of the spectral acceleration of the plastic range state and an increase of the ultimate displacement compared to the previous analysis. Regarding Table 6.13, it can be seen that for structural assembly 3 and response spectrum S4 of Portugal, it has necessary to reduce to 1.0 m. Similarly, for structural assembly 1 and 2, for the spectrum S4 of Italy, the same change has been also carried out. Looking at Turkey's demands, all spectra S4 do not present

structural safety for the minimum spacing analyzed. Figure 6.29 shows the capacity curves and main mechanical parameters with the application of the standard ASTM-E2126:2012 [57] for an 8-story building.

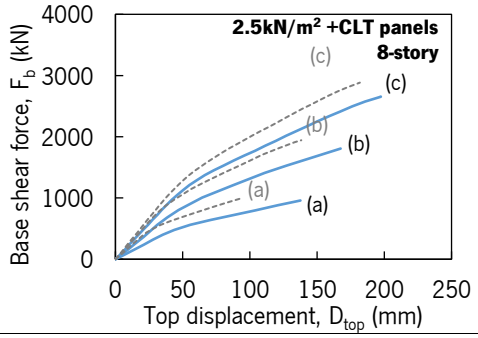

Tests	F_{max} (kN)	K(N/mm)	F_y (kN)	V_y (mm)	D_{Top} (mm)
(a) AE116 spaced to 1.5 m	959.2	11382	791.0	69.5	137.6
(b) AE116 spaced to 1.0 m	1807.4	17503	1491.1	85.2	167.5
(c) AE116 spaced to 0.5 m	2655.6	22743	2133.0	93.8	197.4

Figure 6.29 – Capacity curves from non-linear pushover analysis and main mechanical parameters (study case 2–8-story).

Analyzing in Figure 6.29, it is possible to verify that the results load-carrying capacity is similar to the 6-story analysis, as occurred in the same number of stories in the study case 1. However, it is also possible to verify the increase in displacements. Figure 6.30 shows the equivalent bilinear capacity curves and the horizontal elastic spectrum of each country, and Table 6.14, the spacing recommended, and the location of the target displacement.

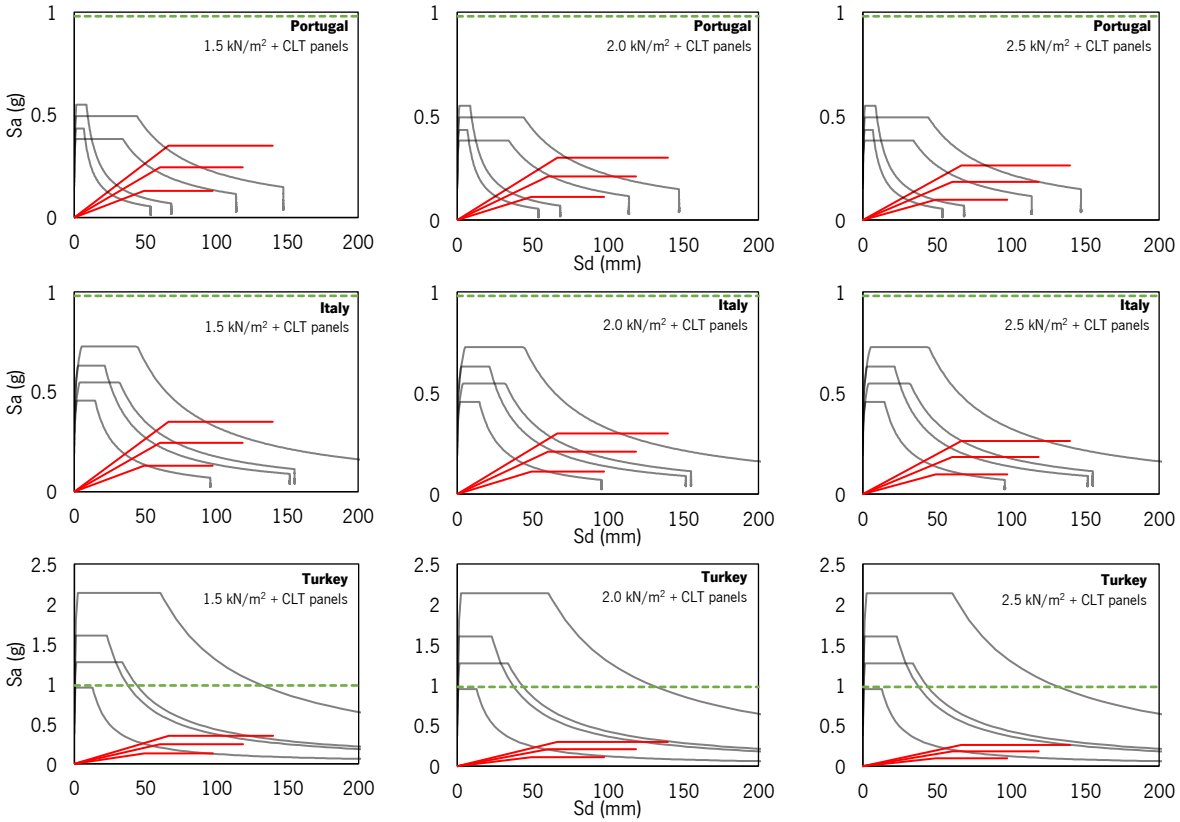

Figure 6.30 – Quantification of performance points for each country selected (study case 2–8-story).

Table 6.14 – Parameters of performance selected for each country (study case 2–8-story).

Country:			Portugal		Italy		Turkey	
Loads		Spectrum	Spaced to (m)	Location of d_t (%)	Spaced to (m)	Location of d_t (%)	Spaced to (m)	Location of d_t (%)
Assembly 1	1.5 kN/m² + CLT	S1	1.50	67.9% of ①	1.50	02.8% of ②	1.50	43.5% of ②
		S2	1.50	86.1% of ①	1.50	47.2% of ②	1.00	81.5% of ②
		S3	1.50	44.6% of ②	1.50	67.8% of ②	1.00	67.9% of ②
		S4	1.00	23.2% of ②	1.00	50.8% of ②	**0.50**	**KO**
Assembly 2	2.0 kN/m² + CLT	S1	1.50	73.2% of ①	1.50	11.2% of ②	1.50	54.0% of ②
		S2	1.50	92.9% of ①	1.50	59.0% of ②	1.00	92.1% of ②
		S3	1.50	02.4% of ②	1.00	19.1% of ②	1.00	77.3% of ②
		S4	1.00	33.2% of ②	1.00	63.1% of ②	**0.50**	**KO**
Assembly 3	2.5 kN/m² + CLT	S1	1.50	78.4% of ①	1.50	19.1% of ②	1.50	63.7% of ②
		S2	1.50	99.5% of ①	1.50	70.3% of ②	1.00	85.6% of ②
		S3	1.50	09.1% of ②	1.00	26.9% of ②	0.50	52.7% of ②
		S4	1.00	11.7% of ②	1.00	73.6% of ②	**0.50**	**KO**

① - elastic range; ② - Plastic range; KO – Failure; d_t – target displacement for the MDOF system.

Figure 6.30 and Table 6.14 shows that better performance of the structure was verified for all selected cases, as happened in for the study case 1. However, it is important to note that for structural assembly 3 the spacing has been reduced to 1.0 m and 0.5 m for the response spectrum S3 of Italy and Turkey, respectively. Figure 6.31 shows the capacity curves and main mechanical parameters with the application of the standard ASTM E2126:2012 [57] for a 10-story building.

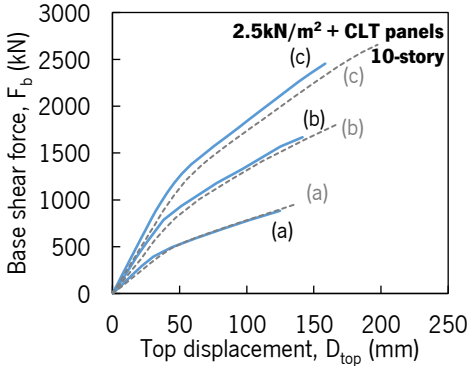

Tests	F_{max} (kN)	K_s (N/mm)	F_y (kN)	D_y (mm)	D_{Top} (mm)
(a) AE116 spaced to 1.5 m	882.7	13123	730.6	55.7	124.7
(b) AE116 spaced to 1.0 m	1668.2	20919	1402.9	67.1	141.6
(c) AE116 spaced to 0.5 m	2453.8	26871	1972.0	73.4	158.4

Figure 6.31 – Capacity curves from non-linear pushover analysis and main mechanical parameters (study case 2–10-story).

Unlike all previous analyzes, the increase of the number of stories led to an increment of the elastic stiffness (see Figure 6.31). However, as happened in the study case 1, the ultimate displacements decreased when the number of stories increases. Figure 6.32 shows the equivalent bilinear capacity curves and the horizontal elastic spectrum of each country and Table 6.15 the spacing recommended and location of the target displacement.

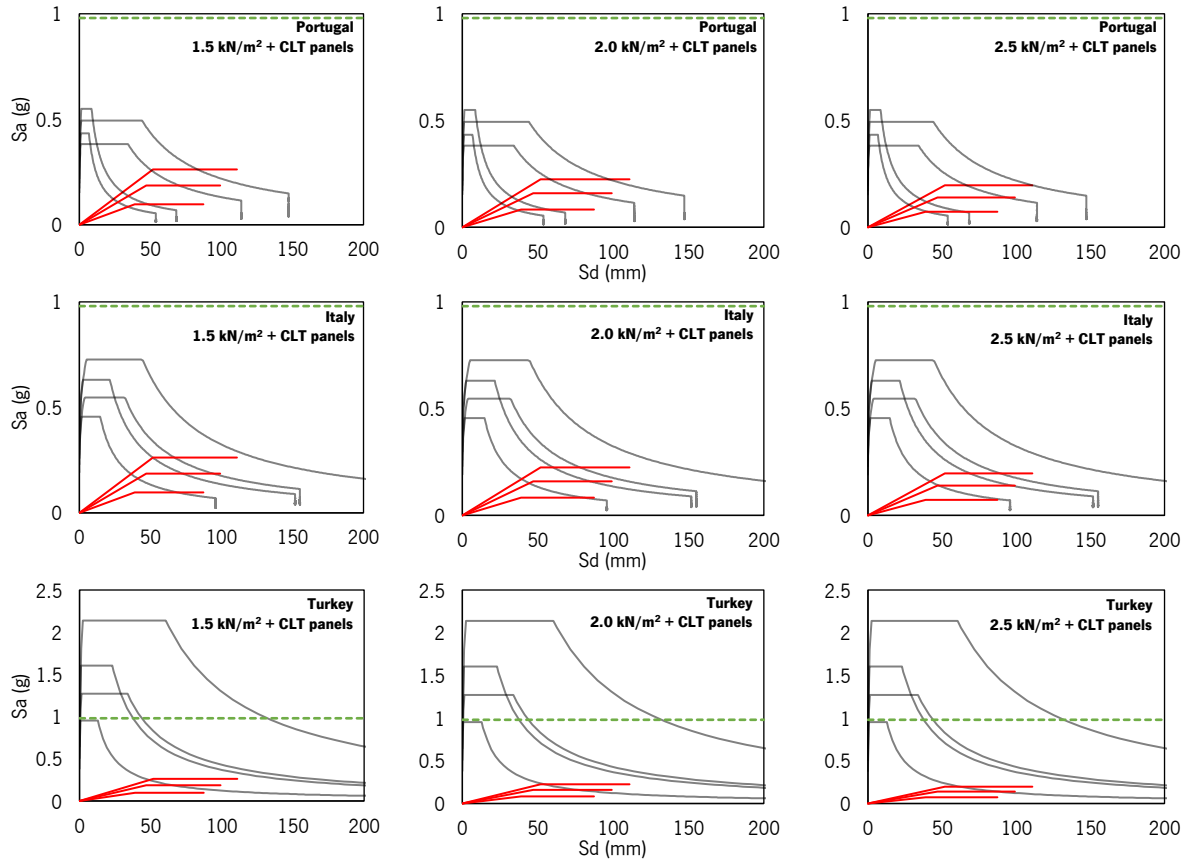

Figure 6.32 – Quantification of performance points for each country selected (study case 2–10-story).

Table 6.15 – Parameters of performance selected for each country (study case 2–10-story).

Country:			Portugal		Italy		Turkey	
Loads		Spectrum	Spaced to (m)	Location of d_t (%)	Spaced to (m)	Location of d_t (%)	Spaced to (m)	Location of d_t (%)
Assembly 1	1.5 kN/m² + CLT	S1	1.50	88.1% of ①	1.50	26.9% of ②	1.50	66.7% of ②
		S2	1.50	09.4% of ②	1.00	22.9% of ②	0.50	76.2% of ②
		S3	1.50	69.7% of ②	1.00	38.6% of ②	0.50	64.3% of ②
		S4	1.00	53.4% of ②	1.00	84.6% of ②	**0.50**	**KO**
Assembly 2	2.0 kN/m² + CLT	S1	1.50	95.3% of ①	1.50	35.7% of ②	1.50	78.7% of ②
		S2	1.50	16.8% of ②	1.00	32.0% of ②	0.50	83.2% of ②
		S3	1.50	81.9% of ②	1.00	48.9% of ②	0.50	70.8% of ②
		S4	1.00	64.9% of ②	0.50	59.5% of ②	**0.50**	**KO**
Assembly 3	2.5 kN/m² + CLT	S1	1.50	01.7% of ②	1.50	44.1% of ②	1.00	34.5% of ②
		S2	1.50	23.8% of ②	1.00	39.8% of ②	0.50	97.6% of ②
		S3	1.00	37.6% of ②	1.00	57.7% of ②	0.50	84.3% of ②
		S4	1.00	74.8% of ②	0.50	69.0% of ②	**0.50**	**KO**

① - elastic range; ② - Plastic range; KO – Failure; d_t – target displacement for the MDOF system.

Based on Figure 6.32 and Table 6.15, due to the decrease of ultimate displacement verified on capacity curves (see Figure 6.31), Italy and Turkey underwent many changes, in which the 0.5 m spacing was found for almost all analyzes for Turkey.

6.5 Final remarks

The development of this chapter aimed to evaluate two buildings by applying the pushover analysis with the help of the N2 method, using different response spectra for Portugal, Italy, and Turkey. The first building is related to the one experimentally analyzed in Chapter 4 and the other was created to increase the floor area of the building and study different floor masses. Moreover, the value of the spacing of the AE116 shear connector was one of the variables studied in this analysis.

In order to avoid soft-story, a preliminary pushover analysis was carried out in order to obtain greater flexibility and rationalize the use of the shear connectors. After the analysis, it has been possible to conclude that the basis of the analysis is always given by the 1st floor, with the reduction carried out on the remaining floors.

Analyzing the two studies case, the pushover analysis allowed to conclude, as expected, a greater load capacity and greater stiffness for the study case 2.

Based on the pushover analysis performed and applying N2 method, it was possible to conclude that Portugal represents the safer location (lower seismicity location), where spacing of 1.0 m for the AE116 is sufficient to ensure safety for all selected spectra. On the other hand, Turkey, due to the high seismicity of the selected spectra, various cases are not safe, being a possible solution to reduce the spacing of the connector or the use of a more resistant shear connector.

Chapter 7

Conclusions and recommendations

7.1 Conclusions

Simple numerical models to predict the structure's behavior are of utmost importance for the design of structures. However, when the issue is dealing with structures subjected to seismic loads, numerical analyzes must take into account the material nonlinearities, where usually involve some difficulties resulting from their complexity. To circumvent this complexity and provide more simple design methodologies, experimental analyzes play an extremely important role in the study of all materials used in each construction.

The development of this thesis aimed to evaluate CLT structures under seismic loads, where experimental and numerical approaches were adopted.

In the first phase, to assess the typical connectors of the CLT construction (angle brackets and hold-downs), an experimental evaluation was performed to analyze the current version and new proposal for the revision of EN 12512. The test results obtained with this work helped to validate the test setups used at the University of Minho, given the similarity with the results obtained by the company Simpson Strong-Tie.

The new proposal of the EN 12512 standard presents values quite different from the current version. These results can be considered normal because the new proposal presents a different view than the current one. However, it is important to note that the proposal of the standard presents more detailed and rigorous analysis, and, on the other hand, the current standard presents very general information.

For metal connectors with and without acoustic layer, the differences are quite significant and bad for the acoustic layer, which leads to the recommendation that it should be avoided in areas with high seismicity.

After the experimental analysis of the metal connectors, a 2-story CLT building was tested under monotonic and cyclic lateral loads. The building showed great signs of friction on the stiffer direction (longitudinal direction) and, on the other hand, in the transverse direction, the largest rocking for

only have 4.5 meters of the resisting facade. Also, as expected, it was possible to see that the metal connectors have a great responsibility for resistance to the lateral loads.

After the experimental approach, a numerical analysis was carried out using the commercial software Dlubal RFEM. The modeling pointed out results quite identical to the experimental tests. The largest differences were related to the friction values between the CLT floors. As expected, the longitudinal direction obtained better results in the model considering the friction, given that greater signs of friction were seen between the panels and the foundation in the experimental campaign. Regarding the transverse direction, as it had only 4.5 meters of facade, due to the global rocking effect of the building, it resulted in close results with and without friction for the monotonic test.

Afterward, and using the calibrated model, a pushover numerical analysis has been performed to apply to the N2 method. Two different buildings were studied, assuming various response spectra for Portugal, Italy, and Turkey. The building analyzed experimentally on Chapter 4 and another one representing a building with a larger floor area and story height and with different structural assemblies of the floors were studied. The results were very encouraging, as it was possible to obtain important data for the seismic project of CLT buildings. Among them, it was possible to identify the recommended number of shear connectors for CLT buildings; percentage of connectors to be inserted per floor to avoid soft story; and it was found once again that the shear connectors play an important role, being the first element of failure.

7.2 Recommendations

Given all the work done within the thesis and literature review, it is possible to establish recommendations for the seismic design of CLT buildings. In particular, here some recommendations for a seismic design through commercial software are (see Figure 7.1):

- Introduction of the metal connectors curve of 1st LEC according to the new proposal in the revision of the EN 12512 [5] or the bilinear according to EN 12512:2001 for greater reliability of the final results;
- The shear strength of the HTT22 uplift resistance connectors and the uplift resistance of the AE116 connector between CLT floors can be negligible;
- Finally, with the numerical analysis of Chapter 6, recommended tables of spacing of the AE116 shear connector have been defined, where they were made based on the weight on the floors and the facade length (see Table 7.1 to Table 7.5). However, it is important to note that the tables are only for structural pre-design and require the validation of results through seismic

design, and the values given represent values for the 1st floor, where the reduction in other levels can be performed as presented in Table 6.5 of Chapter 6.

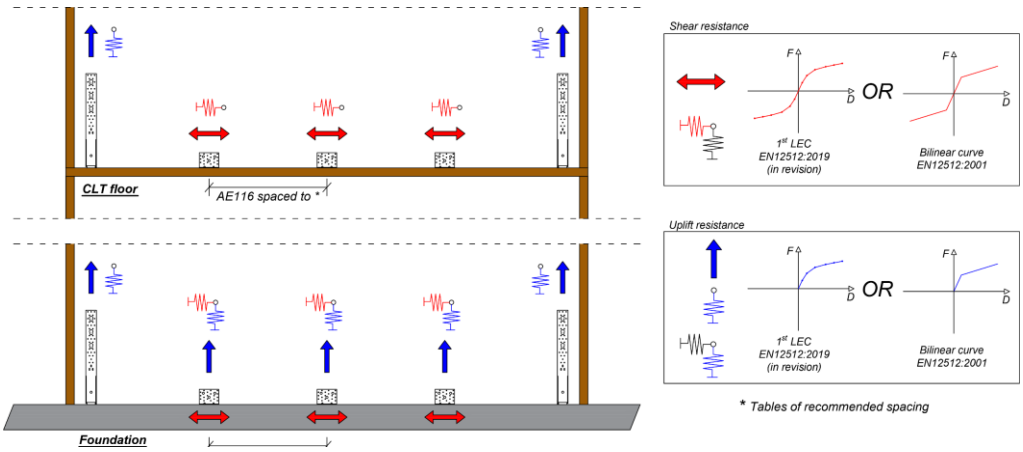

Figure 7.1 – Recommendations for the seismic analysis of CLT buildings.

Table 7.1 – Recommended spacing for angle bracket AE116, 9.1 meters of façade, floors with 2 kN/m² + CLT.

Building with:	Recommended spacing for angle bracket AE116 (m) for each response spectrum											
	Portugal				Italy				Turkey			
	S1	S2	S3	S4	S1	S2	S3	S4	S1	S2	S3	S4
2-story	3.00	3.00	3.00	3.00	3.00	3.00	3.00	3.00	3.00	3.00	3.00	3.00
3-story	3.00	3.00	3.00	3.00	3.00	3.00	3.00	3.00	3.00	3.00	1.50	1.50
4-story	3.00	3.00	3.00	3.00	3.00	3.00	3.00	3.00	3.00	3.00	1.50	1.50
5-story	3.00	3.00	3.00	3.00	3.00	3.00	3.00	3.00	3.00	3.00	1.50	0.75
6-story	3.00	3.00	3.00	3.00	3.00	3.00	3.00	3.00	3.00	3.00	1.50	0.75
7-story	3.00	3.00	3.00	3.00	3.00	3.00	3.00	3.00	3.00	3.00	1.50	0.75
8-story	3.00	3.00	3.00	3.00	3.00	3.00	3.00	3.00	3.00	3.00	1.50	0.75
9-story	3.00	3.00	3.00	3.00	3.00	3.00	3.00	1.50	3.00	1.50	1.50	0.75
10-story	3.00	3.00	3.00	3.00	3.00	3.00	3.00	1.50	3.00	1.50	1.50	0.75

Table 7.2 – Recommended spacing for angle bracket AE116, 4.5 meters of façade, floors with 2 kN/m² + CLT.

Building with:	Recommended spacing for angle bracket AE116 (m) for each response spectrum											
	Portugal				Italy				Turkey			
	S1	S2	S3	S4	S1	S2	S3	S4	S1	S2	S3	S4
2-story	1.50	1.50	1.50	1.50	1.50	1.50	1.50	1.50	1.50	1.50	1.50	0.75
3-story	1.50	1.50	1.50	1.50	1.50	1.50	1.50	1.50	1.50	1.50	1.50	0.75
4-story	1.50	1.50	1.50	1.50	1.50	1.50	1.50	1.50	1.50	1.50	1.50	0.75
5-story	1.50	1.50	1.50	1.50	1.50	1.50	1.50	1.50	1.50	1.50	1.50	0.75
6-story	1.50	1.50	1.50	1.50	1.50	1.50	1.50	1.50	1.50	1.50	0.75	0.75
7-story	1.50	1.50	1.50	1.50	1.50	1.50	1.50	1.50	1.50	1.50	0.75	0.75
8-story	1.50	1.50	1.50	1.50	1.50	1.50	1.50	1.50	1.50	1.50	0.75	0.75
9-story	1.50	1.50	1.50	1.50	1.50	1.50	1.50	0.75	1.50	0.75	0.75	0.75
10-story	1.50	1.50	1.50	1.50	1.50	1.50	1.50	0.75	1.50	0.75	0.75	KO

Table 7.3 – Recommended spacing for angle bracket AE116, 18 meters of façade, floors with 1.5 kN/m² + CLT.

Building with:	Recommended spacing for angle bracket AE116 (m) for each response spectrum											
	Portugal				Italy				Turkey			
	S1	S2	S3	S4	S1	S2	S3	S4	S1	S2	S3	S4
2-story	1.50	1.50	1.50	1.50	1.50	1.50	1.50	1.50	1.50	1.50	1.00	1.00
3-story	1.50	1.50	1.50	1.50	1.50	1.50	1.50	1.50	1.50	1.00	1.00	0.5
4-story	1.50	1.50	1.5	1.50	1.50	1.50	1.50	1.50	1.50	1.00	1.00	0.5
5-story	1.50	1.50	1.50	1.50	1.50	1.50	1.50	1.50	1.50	1.00	1.00	KO
6-story	1.50	1.50	1.50	1.50	1.50	1.50	1.50	1.00	1.50	1.00	1.00	KO
7-story	1.50	1.50	1.50	1.50	1.50	1.50	1.50	1.00	1.50	1.00	1.00	KO
8-story	1.50	1.50	1.50	1.00	1.50	1.50	1.50	1.00	1.50	1.00	1.00	KO
9-story	1.50	1.50	1.50	1.00	1.50	1.50	1.00	1.00	1.50	1.00	1.00	KO
10-story	1.50	1.50	1.50	1.00	1.50	1.00	1.00	1.00	1.50	1.00	0.50	KO

Table 7.4 – Recommended spacing for angle bracket AE116, 18 meters of façade, floors with 2.0 kN/m² + CLT.

Building with:	Recommended spacing for angle bracket AE116 (m) for each response spectrum											
	Portugal				Italy				Turkey			
	S1	S2	S3	S4	S1	S2	S3	S4	S1	S2	S3	S4
2-story	1.50	1.50	1.50	1.50	1.50	1.50	1.50	1.50	1.50	1.50	1.00	1.00
3-story	1.50	1.50	1.50	1.50	1.50	1.50	1.50	1.50	1.50	1.00	1.00	0.50
4-story	1.50	1.50	1.50	1.50	1.50	1.50	1.50	1.50	1.50	1.00	1.00	0.50
5-story	1.50	1.50	1.50	1.50	1.50	1.50	1.50	1.00	1.50	1.00	1.00	KO
6-story	1.50	1.50	1.50	1.00	1.50	1.50	1.50	1.00	1.50	1.00	1.00	KO
7-story	1.50	1.50	1.50	1.00	1.50	1.50	1.50	1.00	1.50	1.00	1.00	KO
8-story	1.50	1.50	1.50	1.00	1.50	1.50	1.00	1.00	1.50	1.00	1.00	KO
9-story	1.50	1.50	1.50	1.00	1.50	1.50	1.00	1.00	1.50	1.00	1.00	KO
10-story	1.50	1.50	1.50	1.00	1.50	1.00	1.00	0.50	1.50	0.50	0.50	KO

Table 7.5 – Recommended spacing for angle bracket AE116, 18 meters of façade, floors with 2.5 kN/m² + CLT.

Building with:	Recommended spacing for angle bracket AE116 (m) for each response spectrum											
	Portugal				Italy				Turkey			
	S1	S2	S3	S4	S1	S2	S3	S4	S1	S2	S3	S4
2-story	1.50	1.50	1.50	1.50	1.50	1.50	1.50	1.50	1.50	1.50	1.00	1.00
3-story	1.50	1.50	1.50	1.50	1.50	1.50	1.50	1.50	1.50	1.00	1.00	0.50
4-story	1.50	1.50	1.50	1.50	1.50	1.50	1.50	1.00	1.50	1.00	1.00	KO
5-story	1.50	1.50	1.50	1.50	1.50	1.50	1.50	1.00	1.50	1.00	1.00	KO
6-story	1.50	1.50	1.50	1.00	1.50	1.50	1.50	1.00	1.50	1.00	1.00	KO
7-story	1.50	1.50	1.50	1.00	1.50	1.50	1.50	1.00	1.50	1.00	1.00	KO
8-story	1.50	1.50	1.50	1.00	1.50	1.50	1.00	1.00	1.50	1.00	0.50	KO
9-story	1.50	1.50	1.50	1.00	1.50	1.50	1.00	1.00	1.00	1.00	0.50	KO
10-story	1.50	1.50	1.00	1.00	1.50	1.00	1.00	0.50	1.00	0.50	0.50	KO

7.3 Suggestions for future works

The different analysis presented during the thesis can be complemented and enriched with the following suggested studies:

- Creation of a database with all tests results of metal connectors under lateral loads;

- To perform experimental analysis on the different metal connectors available, considering variables like the presence of acoustic layer, assessing the effect of resistance;
- Replicate the experimental analysis of the building in chapter 4, but in this case, the failure of the building will be the most important, to visualize more degradation of the elements;
- Prediction of the 2-story CLT building experimentally analyzed in other commercial software;
- Consideration of friction between CLT floors to improve prediction performed;
- Study of the behavior of CLT buildings with the presence of reinforced concrete cores (e.g., elevator box).

References

[1] EN 1995-1:2004, Eurocode 5: Design of timber structures - Part 1-1: General - Common rules and rules for buildings. Brussels: CEN; 2004.

[2] Gagnon S, Pirvu C. CLT Handbook: Cross-Laminated Timber. Canadian Edition; 2011.

[3] Karacabeyli E, Douglas B, CLT Handbook: Cross-Laminated Timber. US Edition; 2013.

[4] Brandner R, Flatscher G, Ringhofer A, Schickhofer G, Thiel A. Cross laminated timber (CLT): overview and development. European Journal of Wood and Wood Products 2016. 74 (3). 331-351. https://doi.org/10.1007/s00107-015-0999-5.

[5] A proposal for the revision of the European Standard EN 12512, Timber structures - Test methods - Cycling testing of timber connections and assemblages for seismic design, Version n. 20190312, 2019.

[6] Stora Enso CLT, Stora Enso Wood Products GmbH; 2017

[7] Augustin M. Handbook 1 - Timber Structures. Wood Based Panels. Leonardo Da Vinci Pilot Project. Educational Materials for Designing and Testing of Timber Structures. TEMTIS 2008. pp. 63-99.

[8] Uibel T, Blaß HJ. Load carrying capacity of joints with dowel type fasteners in solid wood panels. Proc., CIB-W18 Meeting 2006, International Council for Building/Conseil International du Bâtiment, Rotterdam, Netherlands; 2006.

[9] Unterwieser H, Schickhofer GR. Characteristic values and test configurations of CLT with focus on selected properties. Focus Solid Timber Solution-European Conf. Cross Laminated Timber (CLT). Cost Conf., Technical Univ. of Graz, Graz, Austria; 2013.

[10] BS EN 368:2001, Wood-based panels - Glued laminated timber — Performance requirements and minimum production requirements; 2001.

[11] Stadthaus, 24 Murray Grove, London. TRADA Tecnology 2009.

[12] Forté – Building australias first timber Highrise. Wood Solutions Presentation Atlanta Conference 2013.

[13] Bridport House, London. Stora Enso Wood Products GmbH 2011.

[14] Abrahamsen R, Malo KA. Structural design and assembly of "Treet" - A 14-storey timber residential building in Norway, WCTE 2014 - World Conference on Timber Engineering; 2014

[15] Harley T, White G, Dowdall A, Bawcombe J, McRobie A, Steinke R. Dalston Lane - The World's Tallest CLT building, WCTE 2016 - World Conference on Timber Engineering; 2016.

[16] Jackson Q, Mansfield J. 25 King - Presentation to AIRAH. Aurecon and Lendlease 2019.

[17] Franke S. Mechanical Properties of Beech CLT. World Conference on Timber Engineering WCTE2016, Vienna, Austria 2016.

[18] Winter S, Kreuzinger H, Mestek P. Teilprojekt 15 - Flächen aus Brettstapel. TU München 2009.

[19] EN 338 – Structural timber – Strength classes. Office for Official Publications of the European Communities. Brussels, Belgium; 2009

[20] BBS characteristics, Binderholz CLT BBS; 2019.

[21] Cross-laminated timber, KLH; 2019.

[22] Izzi M, Casagrande D, Bezzi S, Pasca D, Follesa M, Tomasi R. Seismic behaviour of Cross-Laminated Timber structures: A state-of-the-art review. Engineering Structures 2018. 170 https://doi.org/10.1016/j.engstruct.2018.05.060.

[23] Ceccotti A, Follesa M. Seismic behavior of multi-story X-Lam buildings, in: Int. Workshop on Earthquake Engineering on Timber Structures. 2006. 81-95.

[24] Ceccotti A, Sandhaas C, Okabe M, Yasumura M, Minowa C, Kawai N. SOFIE project - 3D shaking table test on a seven-storey full-scale cross-laminated building. Earthquake Engineering & Structural Dynamics 2013. 42 (13) 2003–21. https://doi.org/10.1002/EQE.2309.

[25] Mohammad M, Gagnon S, Karacabeyli E, Popovsky M. Innovative Mid-Rise Timber Structures Offer New Opportunities for Designers. (S. E. Association, Ed.) SEAOC 2011 2011. pp. 1-12.

[26] Costa AC, Candeias PX, Flatscher G, Schickhofer GR. Seismic perfomance of multi-storey timber buildings: TUGraz building. Series Report, Lisbon, Portugal; 2013a.

[27] Popovski M, Gavric I, Schneider J. Performance of two-storey CLT house seubjected to lateral loads. Proceedings of the 12th World Conference on Timber Engineering WCTE 2014, Quebec, Canada. 2014. https://doi.org/10.13140/RG.2.1.3582.9280.

[28] Popovski M, Gavric I. Performance of a 2-Story CLT House Subjected to Lateral Loads. Journal of Structural Engineering 2016. 142 (4) E4015006. https://doi.org/10.1061/(ASCE)ST.1943-541X.0001315.

[29] Yasumura M, Kobayashi K, Okabe M, Miyake T, Matsumoto K. Full-Scale Tests and Numerical Analysis of Low-Rise CLT Structures under Lateral Loading. Journal of Structural Engineering 2015. 142 E4015007. 10.1061/(ASCE)ST.1943-541X.0001348.

[30] Ceccotti A, Lauriola MP, Pinna M, Sandhaas C. SOFIE Project - Cyclic Tests on Cross-Laminated Wooden Panels. Proceedings of the 9th World Conference on Timber Engineering, August 6-10, Portland, Oregon; 2006a.

[31] Dujic B, Klobcar S, Zarnic R. Influence of openings on shear capacity of wooden walls. Proc., 40th CIB-W18 Meeting, Ingenieurholzbau und Baukonstruktionen, Karlsruhe Institute of Technology, Germany. 2007.

[32] Popovski M, Schneider J, Schweinsteiger M. Lateral load resistance of cross-laminated wood panels. 11th World Conf. on Timber Engineering WCTE 2010, A. Ceccotti and J.-W. van de Kuilen, eds., Riva del Garda, Italy. 2010.

[33] Seim W, Hummel J, Flatscher G, Schickhofer G. CLT Wall elements under cyclic loading-Details for anchorage and connection. Proc., COST Action FP1004 Conf. on the State-of-the Art in CLT Research, Univ. of Bath, North East Somerset, U.K. 2013.

[34] EN 12512:2001. Timber structures - Test methods - Cyclic testing of joints made with mechanical fasteners

[35] Gavric I, Fragiacomo M, Ceccotti A. Cyclic behavior of CLT wall systems : experimental tests and analytical prediction models. ASCE Journal of Structural Engineering 2015c. 1–14.

[36] Málaga-Chuquitaype C, Skinner J, Dowdall A, Kernohan J. Response of CLT shear walls under cyclic loads. World Conference on Timber Engineering, Vienna, Austria. 2016.

[37] Gavric I, Ceccotti A, Fragiacomo M. Experimental cyclic tests on cross-laminated timber panels and typical connections. Proc., 14th ANIDIS Conf., Politecnico di Bari, Italy. 2011.

[38] Gavric I, Fragiacomo M, Ceccotti A, Cyclic behaviour of typical metal connectors for cross-laminated (CLT) structures. ed., ed. Vol. 48. 2014.

[39] ISO 16670:2003, ISO/FDIS 21581, Timber structures - Joints made with mechanical fasteners - Quasi-static reversed-cyclic test method, 2003.

[40] EN 26891:2001 - Timber structures - Joints made with mechanical fasteners - General principles for the determination of strength and deformation characteristics, 2001

[41] Aranha CA. Experimental and Numerical Assessment of the Seismic Behaviour of Log and Cross-Laminated Timber Systems. Ph.D. thesis, University of Minho, Portugal; 2016.

[42] Pozza L, Ferracuti B, Massari M, Savoia M. Axial – Shear interaction on CLT hold-down connections – Experimental investigation. Engineering Structures 2018. 160 10.1016/j.engstruct.2018.01.021.

[43] SAP2000 V.11, Computers and Structures Inc., Berkeley, CA, USA; 2007.

[44] Follesa M, Christovasilis IP, Vassallo D, Fragiacomo M, Ceccotti A. Seismic design of multi-storey CLT buildings according to Eurocode 8. Int. J. Earthquake Eng. 2013. 4 pp. 27–53.

[45] Dujic B, Strus K, Zarnic R, Ceccotti A. Prediction of dynamic response of a 7-storey massive XLam wooden building tested on a shakink table. WCTE Wold Conference on Timber Engineering; 2010.

[46] Rinaldin G, Fragiacomo M. Non-linear simulation of shaking-table tests on 3- and 7-storey X-Lam timber buildings. Engineering Structures 2016. 113 133. 10.1016/j.engstruct.2016.01.055.

[47] Sylodyn acoustic layer, Vibration Isolation Sylodyn - Elastomer, ATIS; 2017

[48] I. Gavric, M. Fragiacomo, A. Ceccotti. Cyclic behaviour of typical metal connectors for cross-laminated (CLT) structures. Materials and Structures 2015. 48 6. 1841. 10.1617/s11527-014-0278-7.

[49] Technical Brochure Lvl by Stora Enso, 2018., LVL by Stora Enso, Technical brochure. ed., ed. Vol. 2018.

[50] EN 1991-1:2002, Eurocode 1: Actions on structures - Part 1-1: General actions - Densities, self-weight, imposed loads for buildings. Brussels: CEN; 2002.

[51] EN 1998-1:2004. Eurocode 8: Design of structures for earthquake resistance - Part 1: General rules, seismic actions and rules for buildings. Brussels: CEN; 2004.

[52] Dlubal software GmbH®. Structural Engineering Software for Analysis and Design, Version 5.20.02. 2019.

[53] NTC 2008, Norme Tecniche per le Costruzioni. DM 14 gennaio 2008, G.U. n. 29, 4 febbraio, n. 30, 2008.

[54] Follesa M, Fragiacomo M, Casagrande D, Tomasi R, Piazza M, Vassallo D, Rossi S. The new version of chapter 8 of Eurocode 8. World Conference Timber Engineering. WCTE 2016 2016.

[55] Follesa M, Fragiacomo M, Casagrande D, Tomasi R, Piazza M, Vassallo D, Canetti D, Rossi S. The new provisions for the seismic design of timber buildings in Europe. Engineering Structures 2018. 168 736-747. https://doi.org/10.1016/j.engstruct.2018.04.090.

[56] ISO/FDIS 21581, Timber structures - Static and cyclic lateral load test methods for shear walls, 2010.

[57] ASTM E2126-11, Standard Test Methods for Cyclic (Reversed) Load Test for Shear Resistance of Vertical Elements of the Lateral Force Resisting Systems for Buildings, 2012.

[58] Raheem SA, Zaher AA, Taha A, Omar M. Effects of numerical modeling simplification on seismic design of buildings. Coupled Systems Mechanics 2018. 7 731-753. 10.12989/csm.2018.7.6.731.

[59] Demir A, Başaran H, Bağci M. A comparative assessment of existing structure by performance based analyses 2014.

[60] Jabbar S, Husssain M. Pushover Analysis of G+5 Reinforced Concrete Building in Basrah. 2018. 10.21172/ijiet.111.10.

[61] Hummel J, Displacement-based seismic design for multi-storey cross laminated timber buildings. ed., ed. Vol. 2017.

[62] Mergos P, Beyer K. Displacement-Based Seismic Design of Symmetric Single-Storey Wood-Frame Buildings with the Aid of N2 Method. Frontiers in Built Enviornment 2015. 1 10.3389/fbuil.2015.00010.

[63] Leslie R, Naveen AP, A Study on Pushover Analysis using Capacity Spectrum Method based on Eurocode 8, 16th World Conference on Earthquake Engineering, 16WCEE 2017; 2017.

[64] Naveen AP, Syed S, Leslie R. A study on pushover analysis using eurocode based capacity spectrum method, International Journal of Scientific & Engineering Research; 2014

[65] Alguhane TM, Khalil AHH, Fayed MN, Ismail AAA. Pushover Analysis of Reinforced Concrete Buildings Using Full Jacket Technics: A Case Study on an Existing Old Building in Madinah, World Academy of Science, Engineering and Technology International Journal of Civil and Environmental Engineering; 2016

[66] FAJFAR, P, FISCHINGER, M. - N2 – A method for non-linear seismic analysis of regular buildings: Proceedings of the 9th World Conference in Earthquake Engineering. Tokyo-Kyoto, Japan, 1988. Vol.5, 111-116.

[67] Peter F. A Nonlinear Analysis Method for Performance-Based Seismic Design. Earthquake Spectra - EARTHQ SPECTRA 2000. 16 10.1193/1.1586128.

[68] Fajfar P. Capacity spectrum method based on inelastic demand spectra. Earthquake Engineering & Structural Dynamics 1999. 28 9. 979-993.

[69] Fajfar P, Gaspersic P. The N2 Method for the seismic damage analysis of RC buildings. Earthquake Engineering & Structural Dynamics 1996. 25 1. 31-46. 10.1002/(sici)1096-9845(199601)25:1<31::aid-eqe534>3.0.co;2-v.

[70] Fragiacomo M, Dujic B, Sustersic I. Elastic and ductile design of multi-storey crosslam massive wooden buildings under seismic actions. Engineering Structures. 2011. 33 11. 10.1016/j.engstruct.2011.05.020.

[71] Coutinho D, Marques M, Delgado R. Comparação de modelos com não linearidade concentrada ou distribuída na análise "pushover" de edfícios de betão armado. 2008.

[72] Cosenza E, Vecchio Cd, Ludovico Md, Dolce M, Moroni C, Prota A, Renzi E, The Italian guidelines for seismic risk classification of constructions: technical principles and validation. ed., ed. Vol. 2018.

[73] DANOSA, www.danosa.com, Retrieved 3 September 2019.

[74] Regulamento Geral do Ruído (RGR), aprovado pelo DL n.º 9/2007, de 17 de Janeiro.

[75] Regulamento dos Requisitos Acústicos dos Edifícios (RRAE), aprovado pelo Decreto-Lei n.º 129/2002, de 11 de Maio e alterado pelo Decreto-Lei n.º 96/2008 de 9 de junho.

[76] Tabelas Técnicas. Tabelas Técnicas, J. S. Brazão Farinha e A. Correia dos Reis, edição P. O. B., 1992. 1992.

[77] BS EN 12369-1:2001, Wood-based panels - Characteristic values for structural design - Part 1: OSB, particleboards and fibreboards; 2001.

[78] Giardini D., J. Woessner L. Mapping Europe's Seismic Hazard 2014; EOS, 95(29): 261-262.

[79] AFAD - Disaster & Emergency Management Authority Presidential of Earthquake Department, Earthquake Hazard Map of Turkey; 2018.

Annex A - Metal connectors analyzed at University of Minho

ID: **AE116_ LSC1**

Type: AE116 Simpson Strong-Tie
Test Load: Cyclic
Protocol: EN 12512 [5]
Rate [mm/s]: 0.275/1.25
$V_{y,EEEP,m}$ [mm]: 9.4
$K_{deg,min}$: 0.60

Notes:
Base support: Steel plate
Test direction: Shear/Lateral
AE116 + 14 x CNA Annular ring nails (Ø4x60 mm) + 2 Threaded road 8.8 Ø12

Results

Maximum Load	$F_{max,c}$	34.4	[kN]
EEEP Ultimate displacement	$V_{u,EEEP,c}$	17.5	[mm]
Failure type	-	(i)	[-]
EEEP Stiffness	$K_{EEEP,c}$	5678	[kN/m]
EEEP Yield displacement	$V_{y,EEEP,c}$	4.9	[mm]
EEEP Yield force	$F_{y,EEEP,c}$	29.0	[kN]
EEEP Ductility	$D_{EEEP,c}$	3.5	[-]
Design degradation factor	k_{deg}	0.73	[-]

Comments:
Test: Cyclic 1
Setup: University of Minho

(i) Failure

Step	1st Cycle			2nd Cycle			3rd Cycle		
	V_{max} [mm]	$F_{(Vmax)}$ [kN]	V_{eq} [%]	V_{max} [mm]	$F_{(Vmax)}$ [kN]	V_{eq} [%]	V_{max} [mm]	$F_{(Vmax)}$ [kN]	V_{eq} [%]
1	1.6	11.7	4.2	-	-	-	-	-	-
2	3.3	16.6	3.7	-	-	-	-	-	-
3	5.0	21.1	7.5	-	-	-	-	-	-
4	6.7	24.5	3.9	-	-	-	-	-	-
5	8.4	27.0	4.0	-	-	-	-	-	-
6	12.8	32.6	3.4	13.1	29.5	3.8	13.1	28.7	4.2
7	17.5	34.4	3.7	17.9	28.8	3.7	17.9	25.0	3.6

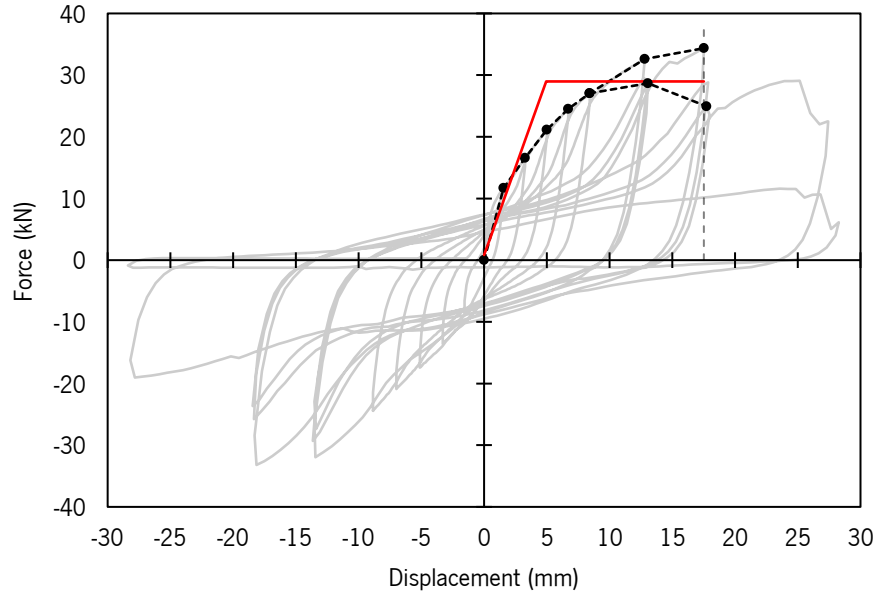

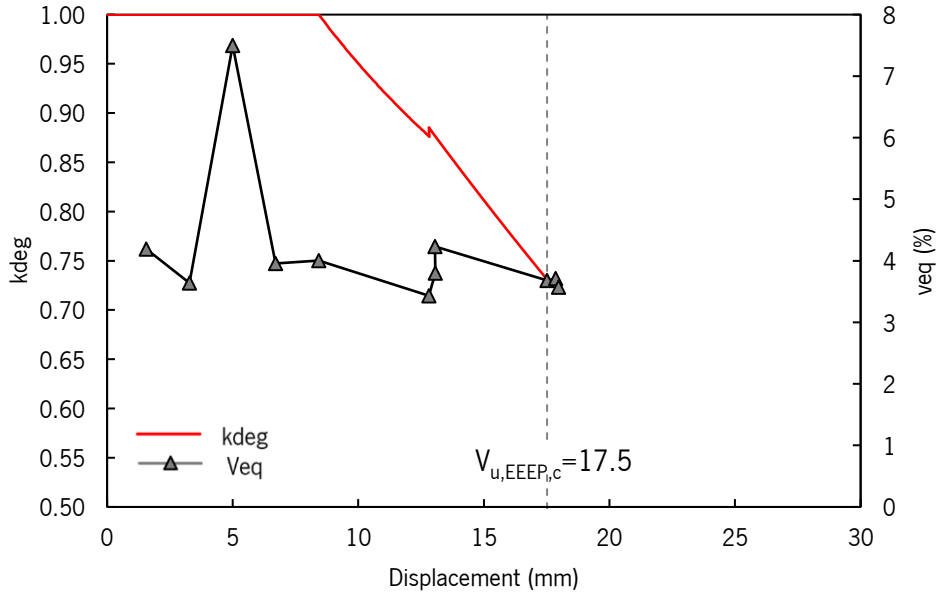

Failure mechanism:

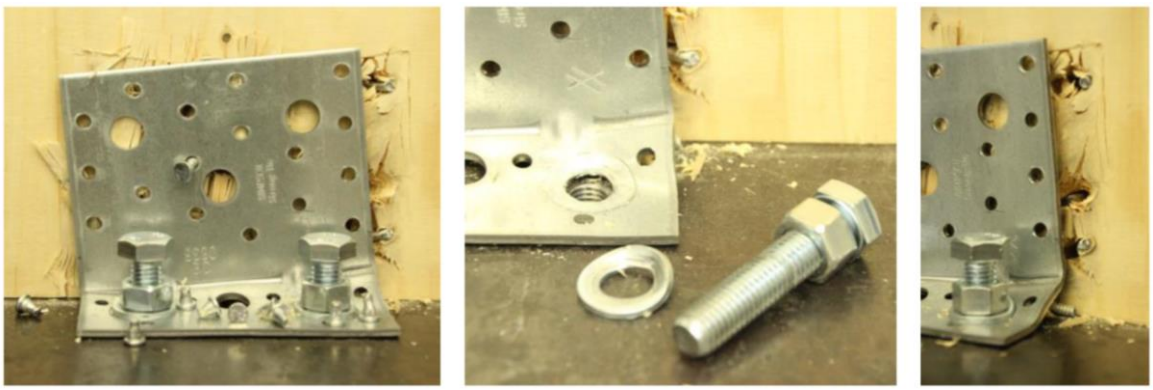

ID: **AE116_LSC2**

Type: AE116 Simpson Strong-Tie
Test Load: Cyclic
Protocol: EN 12512 [5]
Rate [mm/s]: 0.275/1.25
$V_{y,EEEP,m}$ [mm]: 9.4
$K_{deg,min}$: 0.60

Notes:
Base support: Steel plate
Test direction: Shear/Lateral
AE116 + 14 x CNA Annular ring nails (Ø4x60 mm) + 2 Threaded road 8.8 Ø12

Results

Maximum Load	$F_{max,c}$	38.2	[kN]
EEEP Ultimate displacement	$V_{u,EEEP,c}$	18.4	[mm]
Failure type	-	(iv)	[-]
EEEP Stiffness	$K_{EEEP,c}$	6418	[kN/m]
EEEP Yield displacement	$V_{y,EEEP,c}$	4.7	[mm]
EEEP Yield force	$F_{y,EEEP,c}$	29.9	[kN]
EEEP Ductility	$D_{EEEP,c}$	3.9	[-]
Design degradation factor	k_{deg}	0.60	[-]

Comments:
Test: Cyclic 2
Setup: University of Minho

(iv) K_{deg}<0.6

Step	1st Cycle			2nd Cycle			3rd Cycle		
	V_{max} [mm]	$F_{(Vmax)}$ [kN]	V_{eq} [%]	V_{max} [mm]	$F_{(Vmax)}$ [kN]	V_{eq} [%]	V_{max} [mm]	$F_{(Vmax)}$ [kN]	V_{eq} [%]
1	1.9	12.1	6.0	-	-	-	-	-	-
2	3.8	16.7	4.0	-	-	-	-	-	-
3	5.7	21.5	3.9	-	-	-	-	-	-
4	7.5	25.6	4.0	-	-	-	-	-	-
5	9.4	29.0	4.1	-	-	-	-	-	-
6	14.2	35.8	3.6	14.2	32.0	3.9	14.1	30.9	4.4
7	18.9	38.5	3.9	18.9	29.1	3.7	18.8	22.6	3.1

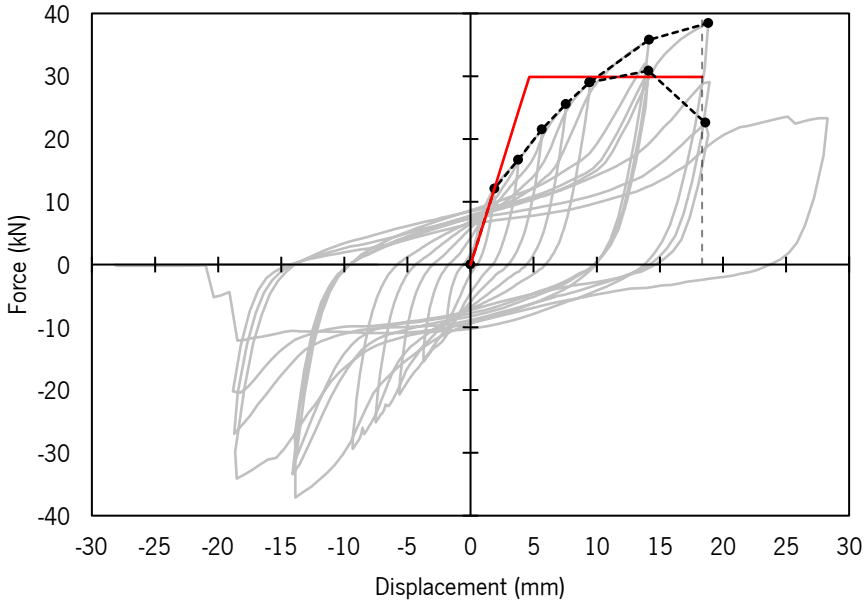

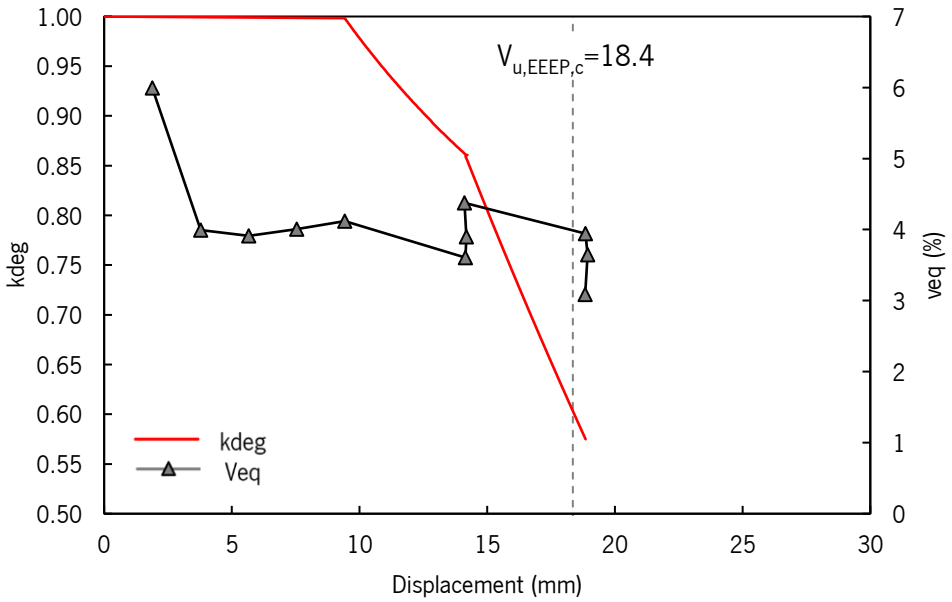

Failure mechanism:

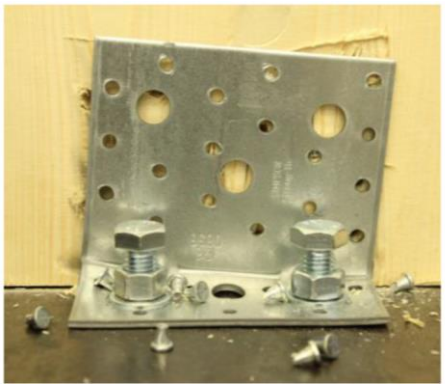

ID: **AE116_LSC3**

Type: AE116 Simpson Strong-Tie
Test Load: Cyclic
Protocol: EN 12512 [5]
Rate [mm/s]: 0.275/1.25
$V_{y,EEEP,m}$ [mm]: 9.4
$K_{deg,min}$: 0.60

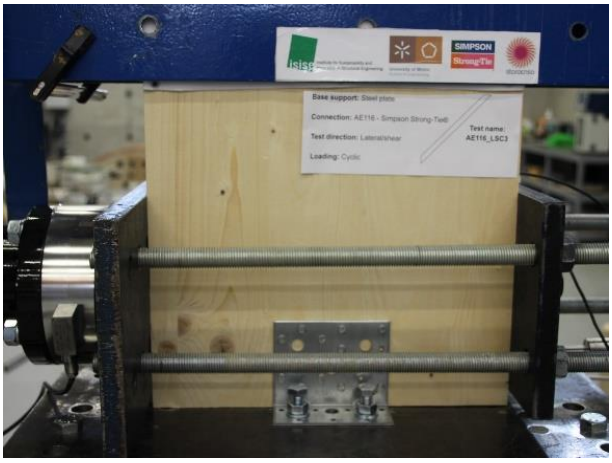

Notes:
Base support: Steel plate
Test direction: Shear/Lateral
AE116 + 14 x CNA Annular ring nails (Ø4x60 mm) + 2 Threaded road 8.8 Ø12

Results

Maximum Load	$F_{max,c}$	37.4	[kN]
EEEP Ultimate displacement	$V_{u,EEEP,c}$	17.8	[mm]
Failure type	-	(iv)	[-]
EEEP Stiffness	$K_{EEEP,c}$	4081	[kN/m]
EEEP Yield displacement	$V_{y,EEEP,c}$	7.4	[mm]
EEEP Yield force	$F_{y,EEEP,c}$	31.6	[kN]
EEEP Ductility	$D_{EEEP,c}$	2.4	[-]
Design degradation factor	k_{deg}	0.6	[-]

Comments:
Test: Cyclic 3
Setup: University of Minho

(iv) K_{deg}<0.6

Step	1st Cycle			2nd Cycle			3rd Cycle		
	V_{max} [mm]	$F_{(Vmax)}$ [kN]	V_{eq} [%]	V_{max} [mm]	$F_{(Vmax)}$ [kN]	V_{eq} [%]	V_{max} [mm]	$F_{(Vmax)}$ [kN]	V_{eq} [%]
1	1.9	11.9	5.4	-	-	-	-	-	-
2	3.8	15.8	3.5	-	-	-	-	-	-
3	5.7	21.2	3.7	-	-	-	-	-	-
4	7.5	25.2	4.0	-	-	-	-	-	-
5	9.4	28.6	4.1	-	-	-	-	-	-
6	14.1	35.0	3.6	14.2	31.8	3.8	14.1	30.8	4.2
7	18.9	38.0	3.8	18.9	27.2	3.3	18.8	20.9	2.8

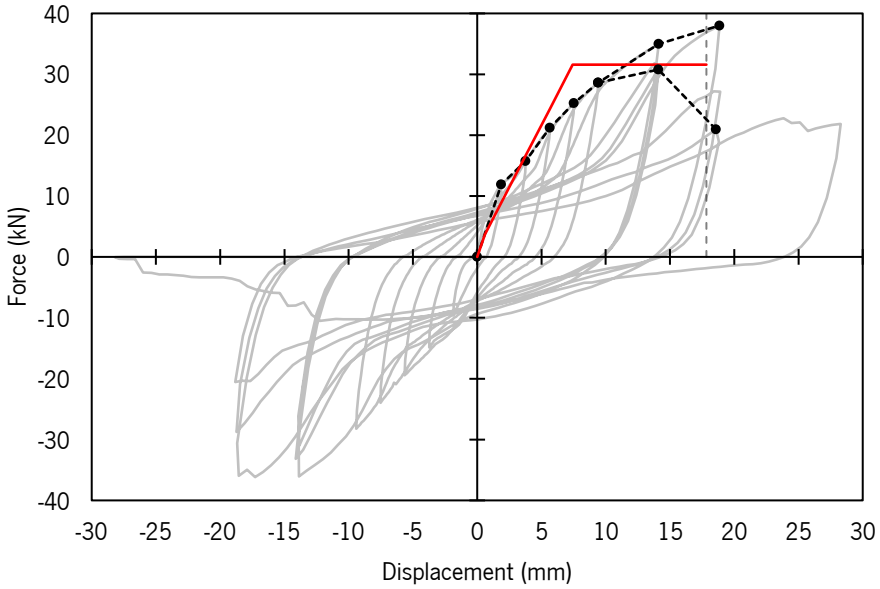

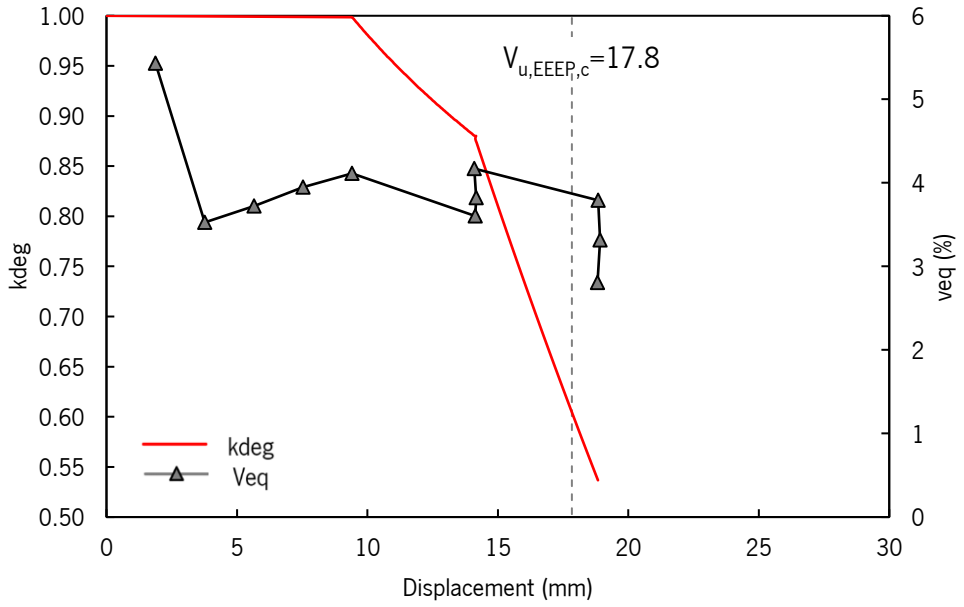

Failure mechanism:

ID: **AE116_LTC1**

Type: AE116 Simpson Strong-Tie
Test Load: Cyclic
Protocol: EN 12512:2018 [5]
Rate [mm/s]: 0.275/1.25
$V_{y,EEEP,m}$ [mm]: 11.0
$K_{deg,min}$: 0.60

Notes:
Base support: CLT 100 C5S C24
Test direction: Shear/Lateral
AE116 + 14 x CNA Annular ring nails (Ø4x60) mm) + 7 x CNA Annular ring nails (Ø4x60)

Results

Maximum Load	$F_{max,c}$	21.0	[kN]
EEEP Ultimate displacement	$V_{u,EEEP,c}$	18.1	[mm]
Failure type	-	(iv)	[-]
EEEP Stiffness	$K_{EEEP,c}$	2064	[kN/m]
EEEP Yield displacement	$V_{y,EEEP,c}$	8.1	[mm]
EEEP Yield force	$F_{y,EEEP,c}$	17.3	[kN]
EEEP Ductility	$D_{EEEP,c}$	2.2	[-]
Design degradation factor	k_{deg}	0.60	[-]

Comments:
Test: Cyclic 1
Setup: University of Minho

(iv) K_{deg}<0.6

Step	1st Cycle			2nd Cycle			3rd Cycle		
	V_{max} [mm]	$F_{(Vmax)}$ [kN]	V_{eq} [%]	V_{max} [mm]	$F_{(Vmax)}$ [kN]	V_{eq} [%]	V_{max} [mm]	$F_{(Vmax)}$ [kN]	V_{eq} [%]
1	2.3	6.3	6.1	-	-	-	-	-	-
2	4.6	9.4	5.1	-	-	-	-	-	-
3	6.8	12.2	5.3	-	-	-	-	-	-
4	9.0	14.6	5.5	-	-	-	-	-	-
5	11.2	16.5	5.6	-	-	-	-	-	-
6	16.8	21.0	4.6	16.6	18.8	5.7	16.8	17.2	7.2
7	22.2	19.5	5.1	21.9	10.2	4.0	22.0	10.6	5.9

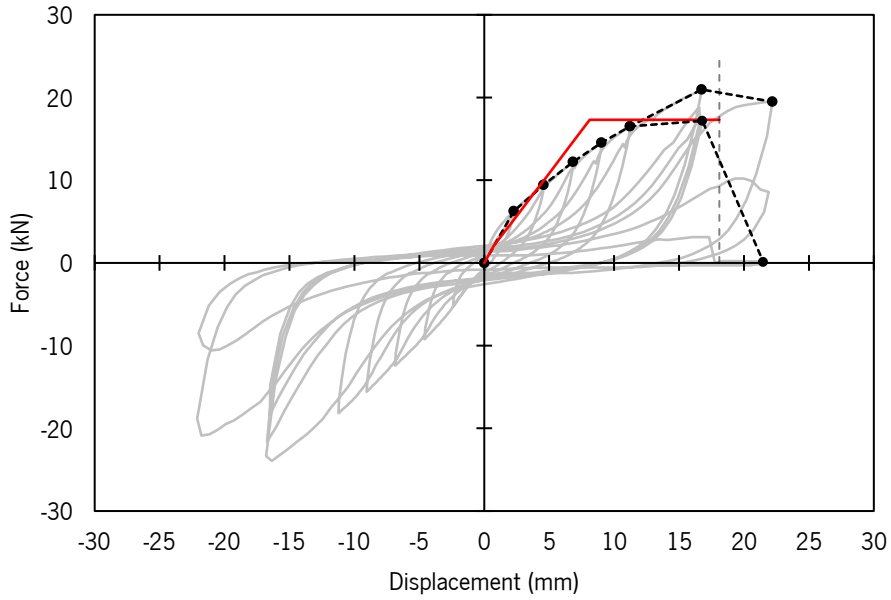

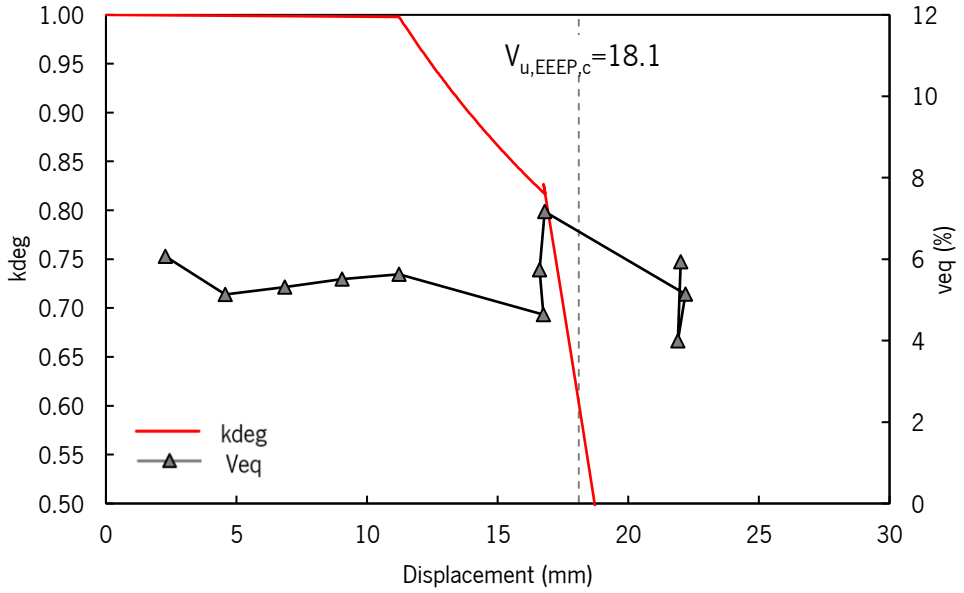

Failure mechanism:

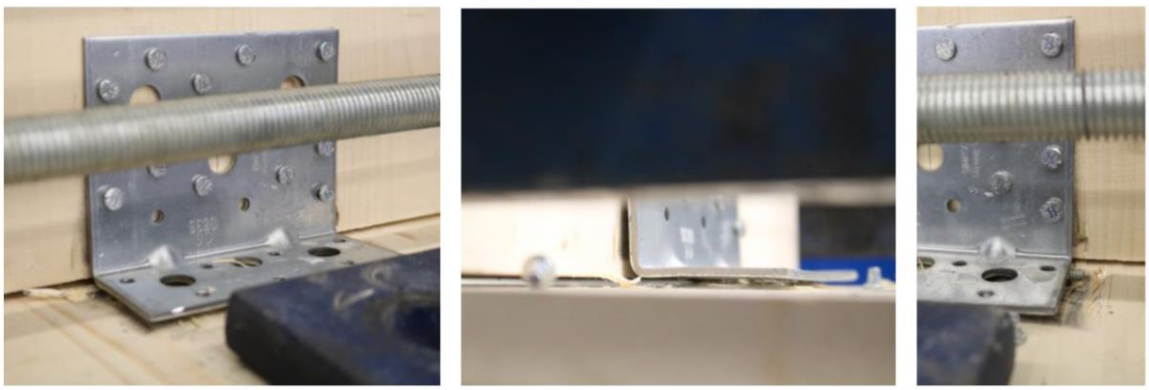

ID: **AE116_LTC2**

Type: AE116 Simpson Strong-Tie
Test Load: Cyclic
Protocol: EN 12512 [5]
Rate [mm/s]: 0.275/1.25
$V_{y,EEEP,m}$ [mm]: 11.0
$K_{deg,min}$: 0.60

Notes:
Base support: CLT 100 C5S C24
Test direction: Shear/Lateral
AE116 + 14 x CNA Annular ring nails (Ø4x60 mm) + 7 x CNA Annular ring nails (Ø4x60)

Results

Maximum Load	$F_{max,c}$	22.1	[kN]
EEEP Ultimate displacement	$V_{u,EEEP,c}$	21.6	[mm]
Failure type	-	(iv)	[-]
EEEP Stiffness	$K_{EEEP,c}$	2644	[kN/m]
EEEP Yield displacement	$V_{y,EEEP,c}$	6.8	[mm]
EEEP Yield force	$F_{y,EEEP,c}$	18.3	[kN]
EEEP Ductility	$D_{EEEP,c}$	3.2	[-]
Design degradation factor	k_{deg}	0.6	[-]

Comments:
Test: Cyclic 2
Setup: University of Minho

(iv) K_{deg}<0.6

Step	1st Cycle			2nd Cycle			3rd Cycle		
	V_{max} [mm]	$F_{(Vmax)}$ [kN]	V_{eq} [%]	V_{max} [mm]	$F_{(Vmax)}$ [kN]	V_{eq} [%]	V_{max} [mm]	$F_{(Vmax)}$ [kN]	V_{eq} [%]
1	2.3	7.4	5.4	-	-	-	-	-	-
2	4.6	10.6	4.7	-	-	-	-	-	-
3	6.8	12.8	4.4	-	-	-	-	-	-
4	9.0	15.2	4.6	-	-	-	-	-	-
5	11.2	17.1	4.7	-	-	-	-	-	-
6	16.7	21.4	4.2	16.5	19.6	5.0	16.7	17.4	6.0
7	22.1	22.2	4.9	22.1	15.6	5.4	22.0	13.0	5.8

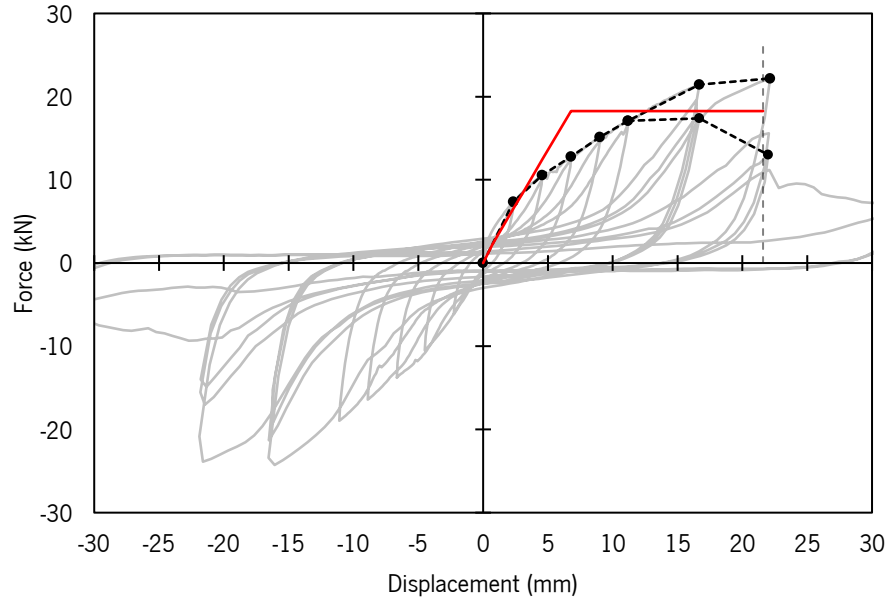

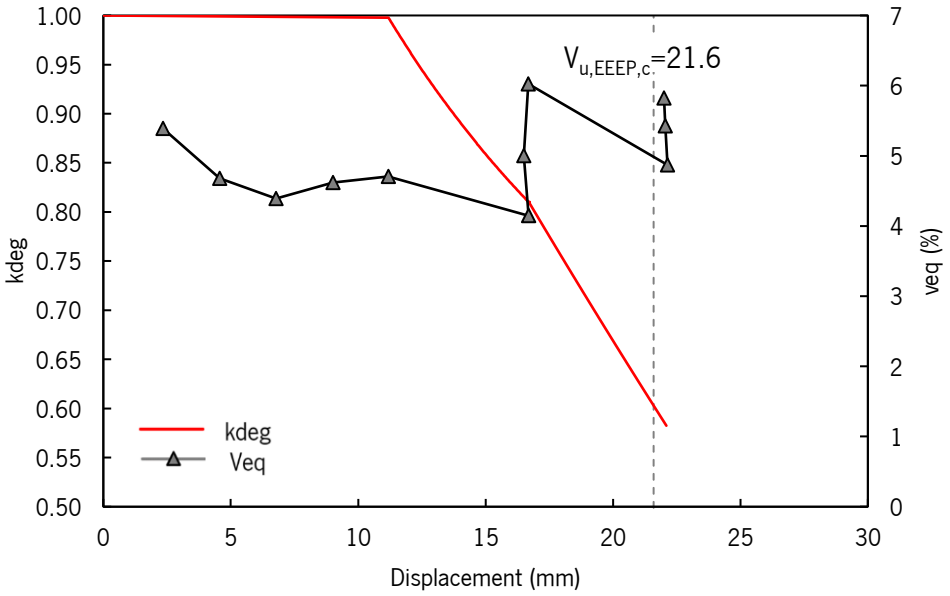

Failure mechanism:

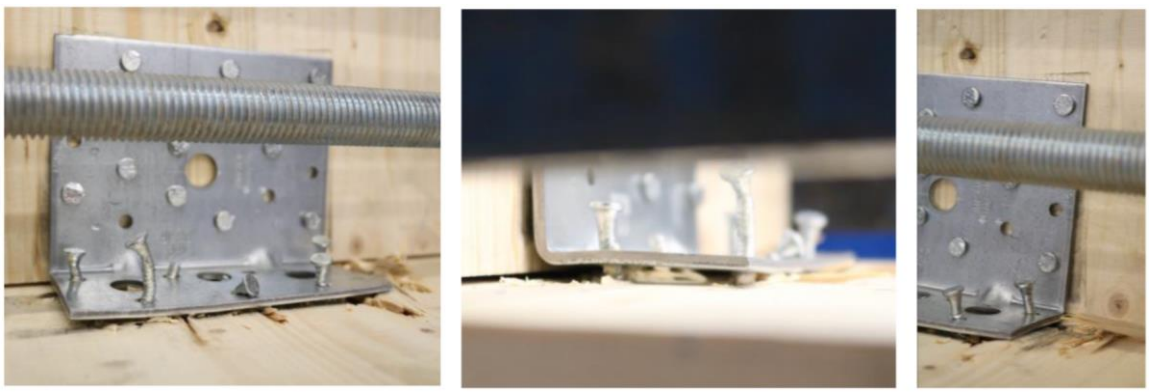

ID: **AE116_LTC3**

Type: AE116 Simpson Strong-Tie
Test Load: Cyclic
Protocol: EN 12512 [5]
Rate [mm/s]: 0.275/1.25
$V_{y,EEEP,m}$ [mm]: 11.0
$K_{deg,min}$: 0.60

Notes:
Base support: CLT 100 C5S C24
Test direction: Shear/Lateral
AE116 + 14 x CNA Annular ring nails (Ø4x60 mm) + 7 x CNA Annular ring nails (Ø4x60)

Results

Maximum Load	$F_{max,c}$	21.8	[kN]
EEEP Ultimate displacement	$V_{u,EEEP,c}$	18.6	[mm]
Failure type	-	(iv)	[-]
EEEP Stiffness	$K_{EEEP,c}$	2140	[kN/m]
EEEP Yield displacement	$V_{y,EEEP,c}$	8.2	[mm]
EEEP Yield force	$F_{y,EEEP,c}$	18.1	[kN]
EEEP Ductility	$D_{EEEP,c}$	2.3	[-]
Design degradation factor	k_{deg}	0.6	[-]

Comments:
Test: Cyclic 3
Setup: University of Minho

(iv) K_{deg}<0.6

Step	1st Cycle			2nd Cycle			3rd Cycle		
	V_{max} [mm]	$F_{(Vmax)}$ [kN]	V_{eq} [%]	V_{max} [mm]	$F_{(Vmax)}$ [kN]	V_{eq} [%]	V_{max} [mm]	$F_{(Vmax)}$ [kN]	V_{eq} [%]
1	2.3	7.4	5.4	-	-	-	-	-	-
2	4.6	10.6	4.7	-	-	-	-	-	-
3	6.8	12.8	4.4	-	-	-	-	-	-
4	9.0	15.2	4.6	-	-	-	-	-	-
5	11.2	17.1	4.7	-	-	-	-	-	-
6	16.7	21.4	4.2	16.5	19.6	5.0	16.7	17.4	6.0
7	22.1	22.2	4.9	22.1	15.6	5.4	22.0	13.0	5.8

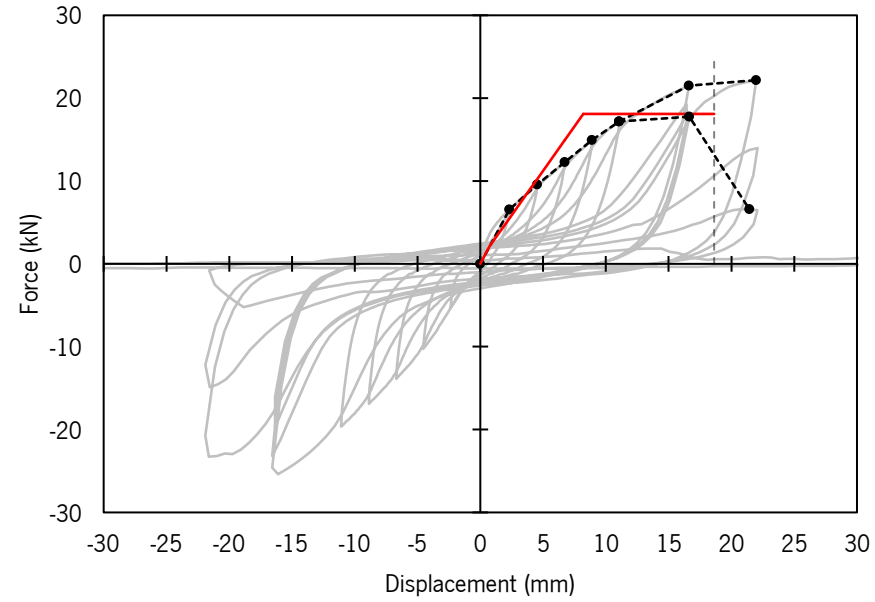

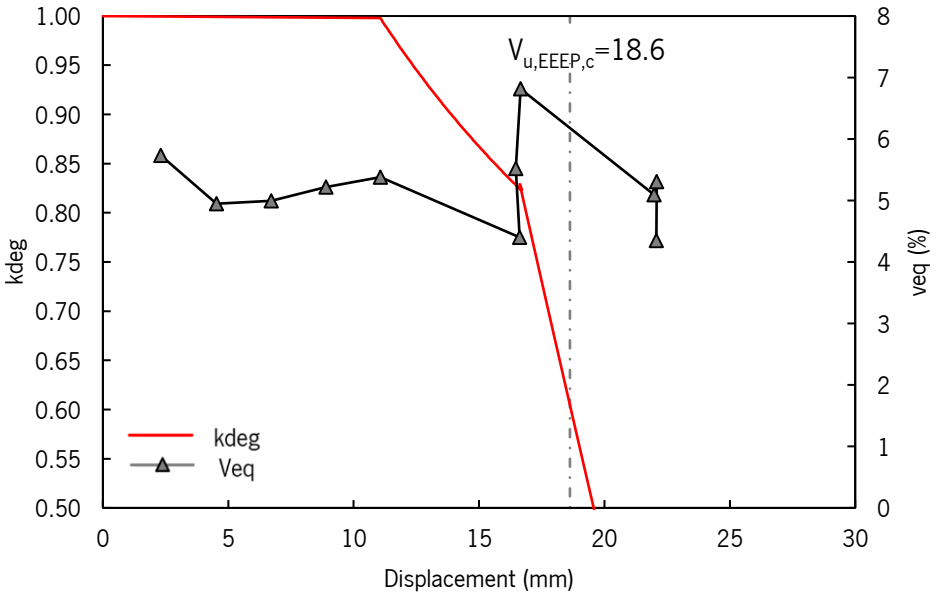

Failure mechanism:

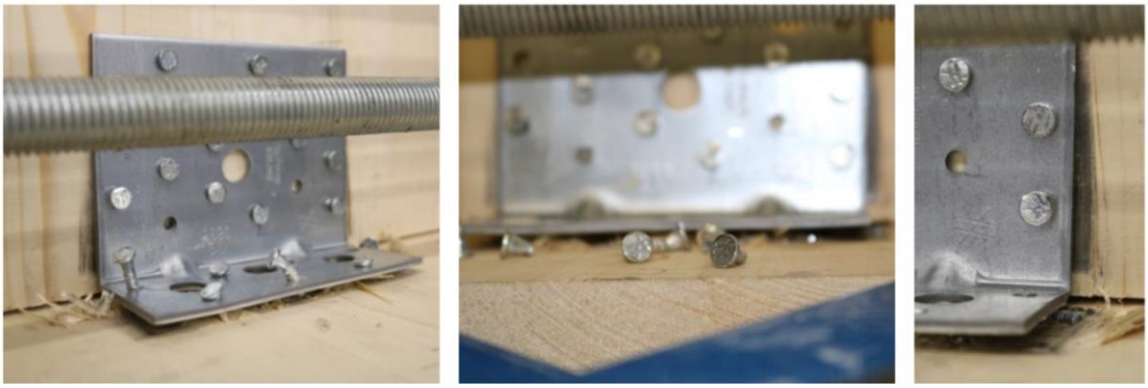

ID: **AE116_USC1**

Type: AE116 Simpson Strong-Tie
Test Load: Cyclic
Protocol: EN 12512 [5]
Rate [mm/s]: 0.275/1.25
$V_{y,EEEP,m}$ [mm]: 8.9
$K_{deg,min}$: 0.60

Notes:
Base support: steel plate
Test direction: Uplift/Tension
AE116 + 14 x CNA Annular ring nails (Ø4x60 mm) + 2 Threaded road 8.8 Ø12

Results

Maximum Load	$F_{max,c}$	45.9	[kN]
EEEP Ultimate displacement	$V_{u,EEEP,c}$	22.7	[mm]
Failure type	-	(iv)	[-]
EEEP Stiffness	$K_{EEEP,c}$	4465	[kN/m]
EEEP Yield displacement	$V_{y,EEEP,c}$	7.6	[mm]
EEEP Yield force	$F_{y,EEEP,c}$	36.4	[kN]
EEEP Ductility	$D_{EEEP,c}$	3.0	[-]
Design degradation factor	k_{deg}	0.60	[-]

Comments:
Test: Cyclic 1
Setup: University of Minho

(iv) K_{deg}<0.6

Step	1st Cycle			2nd Cycle			3rd Cycle		
	V_{max} [mm]	$F_{(Vmax)}$ [kN]	V_{eq} [%]	V_{max} [mm]	$F_{(Vmax)}$ [kN]	V_{eq} [%]	V_{max} [mm]	$F_{(Vmax)}$ [kN]	V_{eq} [%]
1	1.6	14.2	10.6	-	-	-	-	-	-
2	3.3	18.7	8.8	-	-	-	-	-	-
3	5.0	21.6	8.8	-	-	-	-	-	-
4	6.7	24.5	8.8	-	-	-	-	-	-
5	8.4	27.1	8.5	-	-	-	-	-	-
6	12.7	34.3	6.8	12.8	30.8	8.5	12.7	30.5	9.1
7	16.9	41.1	7.6	17.1	36.4	9.3	17.2	32.8	8.9
8	25.6	46.1	6.2	26.1	29.9	8.6	26.2	24.8	8.8

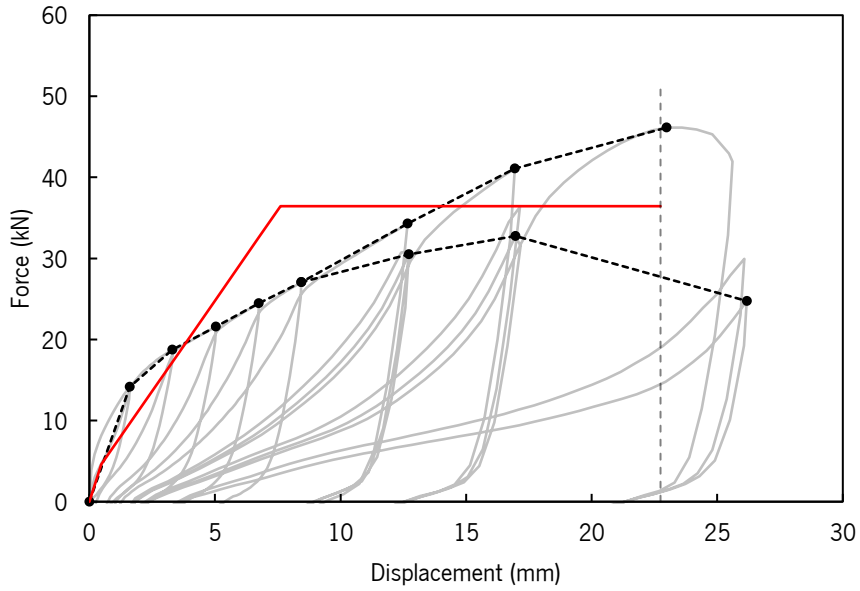

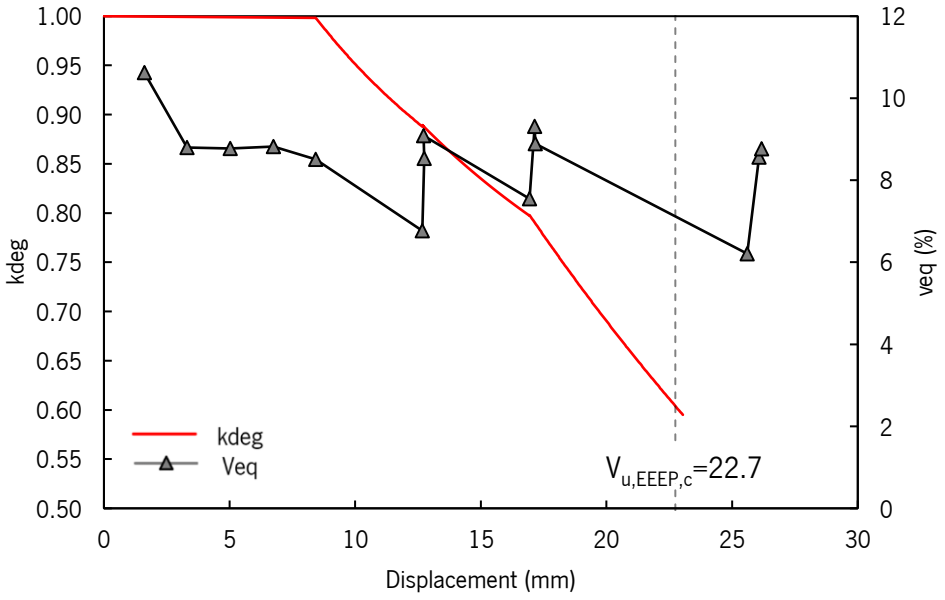

Failure mechanism:

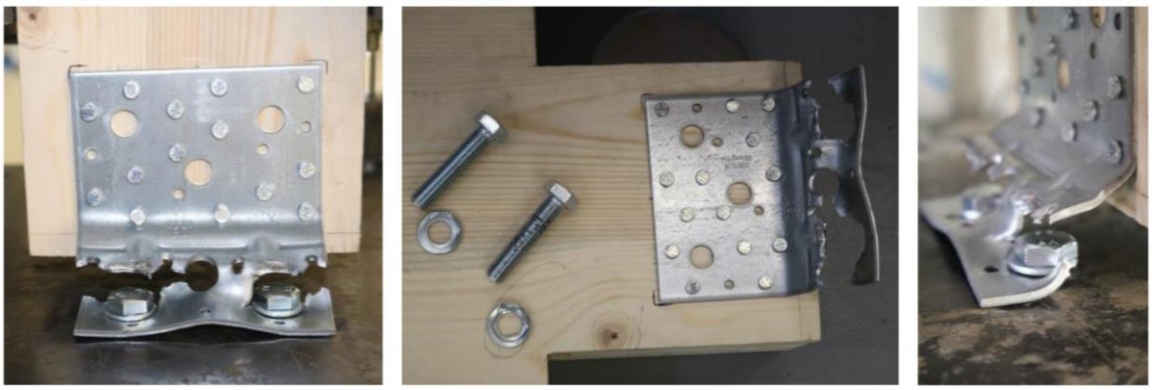

ID: **AE116_USC2**

Type: AE116 Simpson Strong-Tie
Test Load: Cyclic
Protocol: EN 12512 [5]
Rate [mm/s]: 0.275/1.25
$V_{y,EEEP,m}$ [mm]: 8.9
$K_{deg,min}$: 0.60

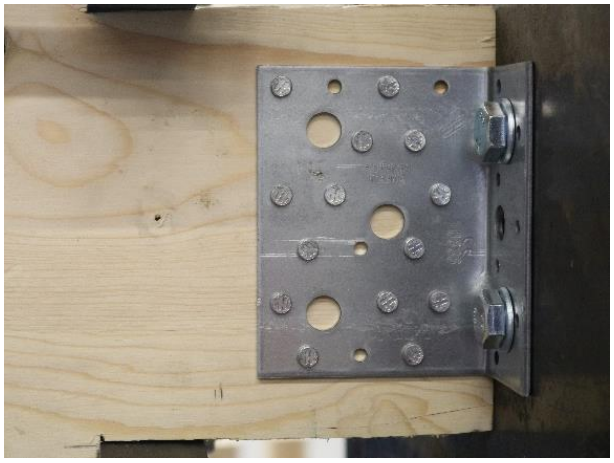

Notes:
Base support: steel plate
Test direction: Uplift/Tension
AE116 + 14 x CNA Annular ring nails (Ø4x60 mm) + 2 Threaded road 8.8 Ø12

Results

Maximum Load	$F_{max,c}$	52.6	[kN]
EEEP Ultimate displacement	$V_{u,EEEP,c}$	23.8	[mm]
Failure type	-	(iv)	[-]
EEEP Stiffness	$K_{EEEP,c}$	5149	[kN/m]
EEEP Yield displacement	$V_{y,EEEP,c}$	7.4	[mm]
EEEP Yield force	$F_{y,EEEP,c}$	40.8	[kN]
EEEP Ductility	$D_{EEEP,c}$	3.2	[-]
Design degradation factor	k_{deg}	0.60	[-]

Comments:
Test: Cyclic 2
Setup: University of Minho

(iv) K_{deg}<0.6

Step	1st Cycle			2nd Cycle			3rd Cycle		
	V_{max} [mm]	$F_{(Vmax)}$ [kN]	V_{eq} [%]	V_{max} [mm]	$F_{(Vmax)}$ [kN]	V_{eq} [%]	V_{max} [mm]	$F_{(Vmax)}$ [kN]	V_{eq} [%]
1	1.5	16.7	21.3	-	-	-	-	-	-
2	3.2	20.8	17.2	-	-	-	-	-	-
3	4.9	23.8	18.8	-	-	-	-	-	-
4	6.6	27.0	19.2	-	-	-	-	-	-
5	8.3	29.8	18.5	-	-	-	-	-	-
6	12.5	37.3	14.5	12.6	33.5	19.4	12.6	32.9	20.6
7	16.8	44.6	16.4	17.0	39.5	21.6	17.0	35.4	21.4
8	25.3	54.2	15.9	25.8	41.0	22.8	26.0	30.7	20.0

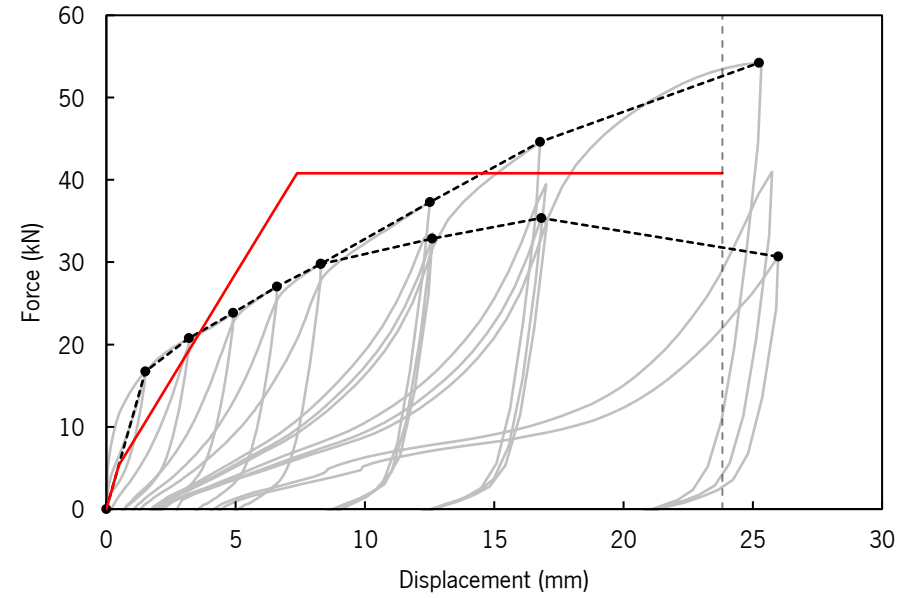

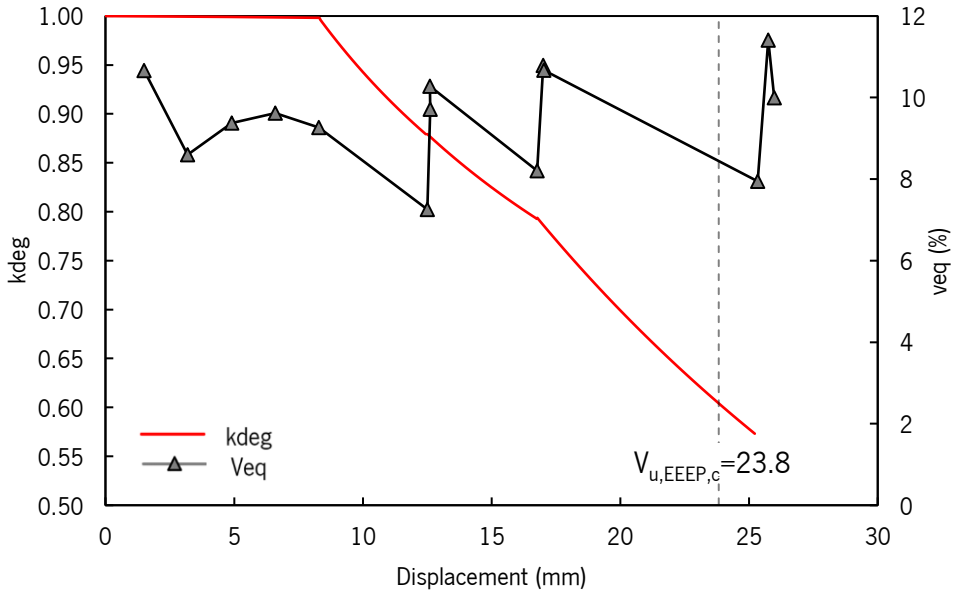

Failure mechanism:

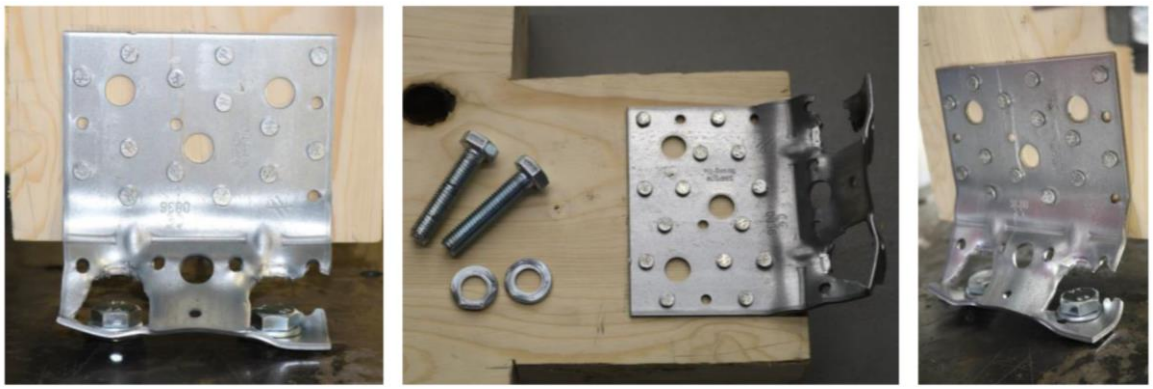

ID: **AE116_USC3**

Type: AE116 Simpson Strong-Tie
Test Load: Cyclic
Protocol: EN 12512 [5]
Rate [mm/s]: 0.275/1.25
$V_{y,EEEP,m}$ [mm]: 8.9
$K_{deg,min}$: 0.60

Notes:
Base support: steel plate
Test direction: Uplift/tension
AE116 + 14 x CNA Annular ring nails (Ø4x60 mm) + 2 Threaded road 8.8 Ø12

Results

Maximum Load	$F_{max,c}$	43.3	[kN]
EEEP Ultimate displacement	$V_{u,EEEP,c}$	21.8	[mm]
Failure type	-	(i)	[-]
EEEP Stiffness	$K_{EEEP,c}$	7263	[kN/m]
EEEP Yield displacement	$V_{y,EEEP,c}$	4.6	[mm]
EEEP Yield force	$F_{y,EEEP,c}$	34.9	[kN]
EEEP Ductility	$D_{EEEP,c}$	4.7	[-]
Design degradation factor	k_{deg}	0.67	[-]

Comments:
Test: Cyclic 3
Setup: University of Minho

(i) Failure

Step	1st Cycle			2nd Cycle			3rd Cycle		
	V_{max} [mm]	$F_{(Vmax)}$ [kN]	V_{eq} [%]	V_{max} [mm]	$F_{(Vmax)}$ [kN]	V_{eq} [%]	V_{max} [mm]	$F_{(Vmax)}$ [kN]	V_{eq} [%]
1	1.5	15.8	20.9	-	-	-	-	-	-
2	3.2	19.6	17.0	-	-	-	-	-	-
3	4.9	22.4	17.7	-	-	-	-	-	-
4	6.6	25.5	17.9	-	-	-	-	-	-
5	8.4	28.2	17.1	-	-	-	-	-	-
6	12.6	36.1	13.7	12.8	32.2	17.2	12.7	31.9	18.7
7	16.9	42.8	15.5	17.1	37.1	19.2	17.2	32.7	18.3
8	25.7	43.3	12.1	26.0	30.5	17.5	26.1	25.8	17.5

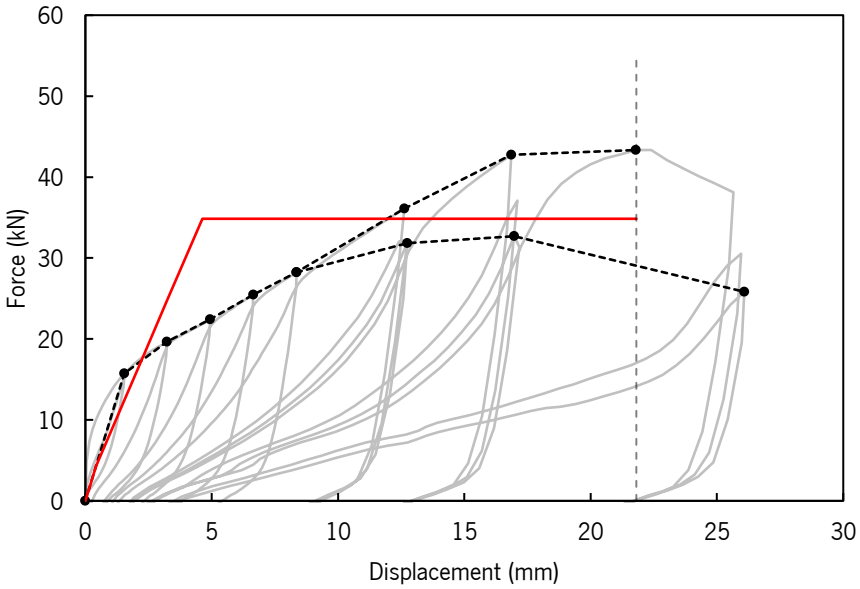

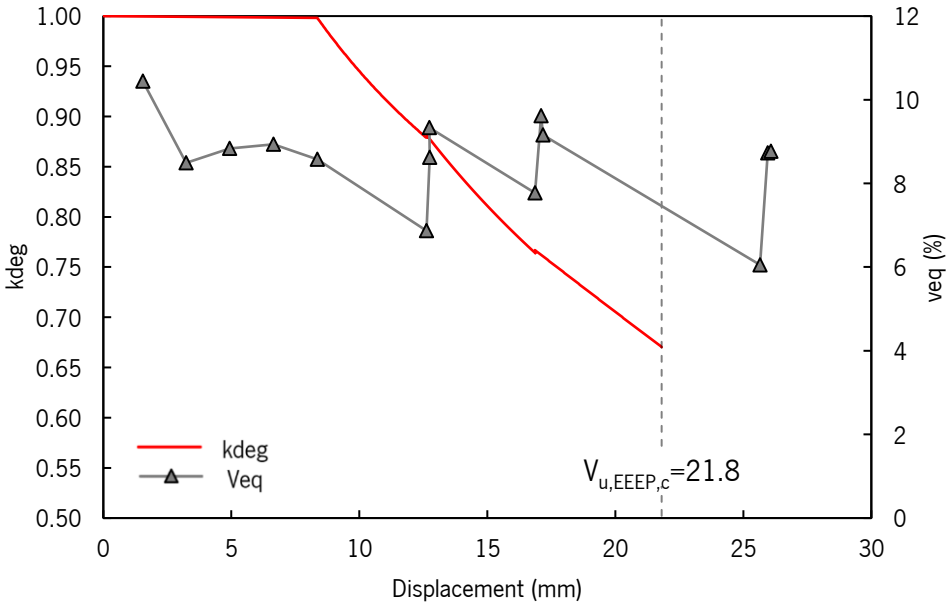

Failure mechanism:

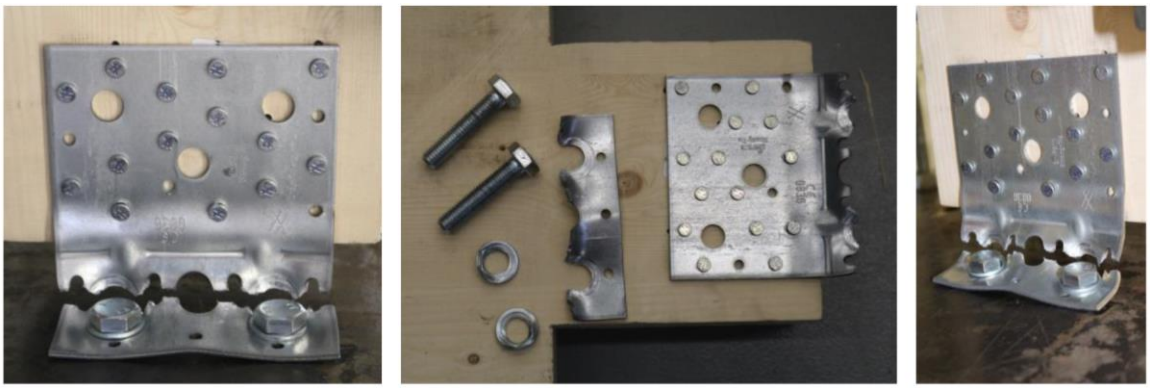

ID: **AE116_UTC1**

Type: AE116 Simpson Strong-Tie
Test Load: Cyclic
Protocol: EN 12512 [5]
Rate [mm/s]: 0.275/1.25
$V_{y,EEEP,m}$ [mm]: 1.7
$K_{deg,min}$: 0.60

Notes:
Base support: CLT 100 C5S C24
Test direction: Uplift/Tension
AE116 + 14 x CNA Annular ring nails (Ø4x60 mm) + 7 x CNA Annular ring nails (Ø4x60)

Results

Maximum Load	$F_{max,c}$	12.9	[kN]
EEEP Ultimate displacement	$V_{u,EEEP,c}$	5.5	[mm]
Failure type	-	(i)	[-]
EEEP Stiffness	$K_{EEEP,c}$	6314	[kN/m]
EEEP Yield displacement	$V_{y,EEEP,c}$	1.7	[mm]
EEEP Yield force	$F_{y,EEEP,c}$	11.4	[kN]
EEEP Ductility	$D_{EEEP,c}$	3.2	[-]
Design degradation factor	k_{deg}	0.78	[-]

Comments:
Test: Cyclic 1
Setup: University of Minho

(i) Failure

Step	1st Cycle			2nd Cycle			3rd Cycle		
	V_{max} [mm]	$F_{(Vmax)}$ [kN]	V_{eq} [%]	V_{max} [mm]	$F_{(Vmax)}$ [kN]	V_{eq} [%]	V_{max} [mm]	$F_{(Vmax)}$ [kN]	V_{eq} [%]
1	0.3	3.2	19.6	-	-	-	-	-	-
2	0.6	4.7	14.2	-	-	-	-	-	-
3	0.9	5.8	12.9	-	-	-	-	-	-
4	1.2	6.9	13.8	-	-	-	-	-	-
5	1.5	8.1	15.0	-	-	-	-	-	-
6	2.3	10.5	14.8	2.3	10.1	25.5	2.3	9.6	26.3
7	3.2	12.5	15.8	3.2	11.7	31.0	3.1	9.7	28.7
8	4.8	12.9	10.6	4.8	11.6	35.6	4.8	10.9	39.5
9	6.5	11.6	11.7	6.5	9.9	33.4	6.5	9.4	35.2

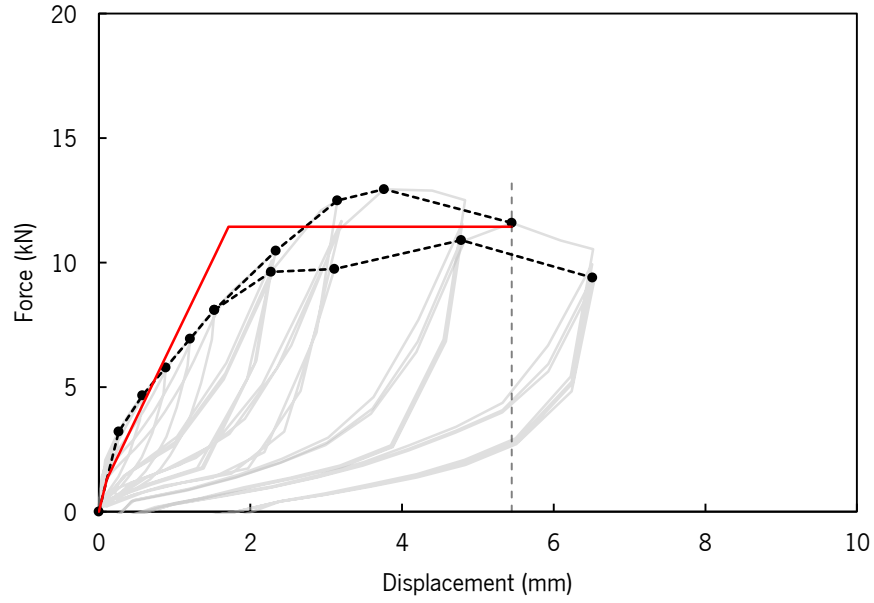

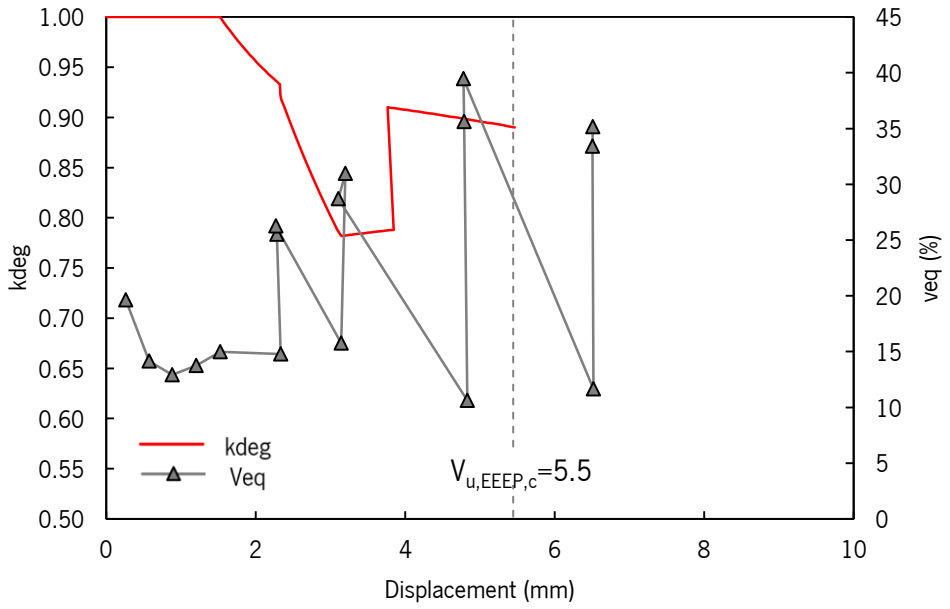

Failure mechanism:

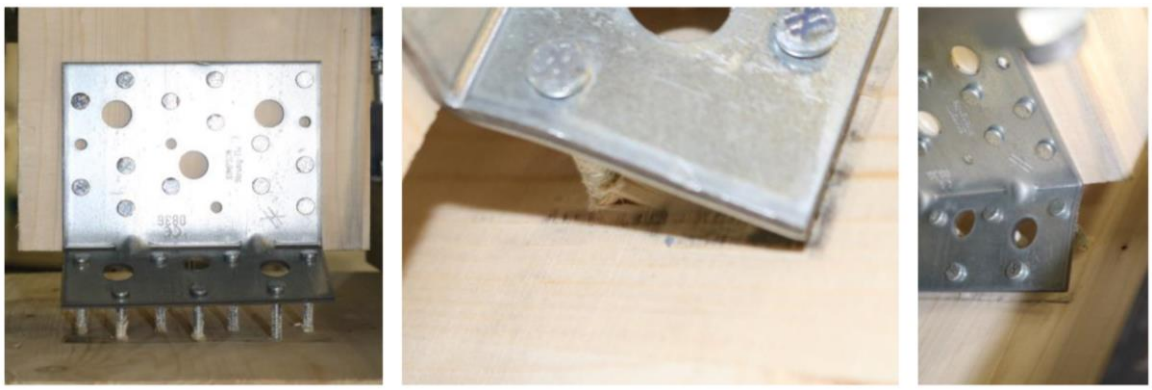

ID: **AE116_UTC2**

Type: AE116 Simpson Strong-Tie
Test Load: Cyclic
Protocol: EN 12512 [5]
Rate [mm/s]: 0.275/1.25
$V_{y,EEEP,m}$ [mm]: 1.7
$K_{deg,min}$: 0.60

Notes:
Base support: CLT 100 C5S C24
Test direction: Uplift/Tension
AE116 + 14 x CNA Annular ring nails (Ø4x60 mm) + 7 x CNA Annular ring nails (Ø4x60)

Results

Maximum Load	$F_{max,c}$	16.2	[kN]
EEEP Ultimate displacement	$V_{u,EEEP,c}$	7.1	[mm]
Failure type	-	(i)	[-]
EEEP Stiffness	$K_{EEEP,c}$	5634	[kN/m]
EEEP Yield displacement	$V_{y,EEEP,c}$	2.4	[mm]
EEEP Yield force	$F_{y,EEEP,c}$	14.3	[kN]
EEEP Ductility	$D_{EEEP,c}$	2.9	[-]
Design degradation factor	k_{deg}	0.85	[-]

Comments:
Test: Cyclic 2
Setup: University of Minho

(i) Failure

Step	1st Cycle			2nd Cycle			3rd Cycle		
	V_{max} [mm]	$F_{(Vmax)}$ [kN]	V_{eq} [%]	V_{max} [mm]	$F_{(Vmax)}$ [kN]	V_{eq} [%]	V_{max} [mm]	$F_{(Vmax)}$ [kN]	V_{eq} [%]
1	0.3	2.9	27.8	-	-	-	-	-	-
2	0.6	4.5	23.1	-	-	-	-	-	-
3	0.9	6.0	22.2	-	-	-	-	-	-
4	1.2	7.3	20.4	-	-	-	-	-	-
5	1.5	8.3	20.2	-	-	-	-	-	-
6	2.4	10.7	18.5	2.3	10.4	34.1	2.3	10.1	36.5
7	3.3	13.3	20.9	3.2	12.8	37.9	3.1	11.2	36.6
8	4.8	16.1	14.5	4.8	15.2	38.5	4.8	14.6	41.8
9	6.5	16.2	12.8	6.4	13.4	35.7	6.5	13.8	44.6

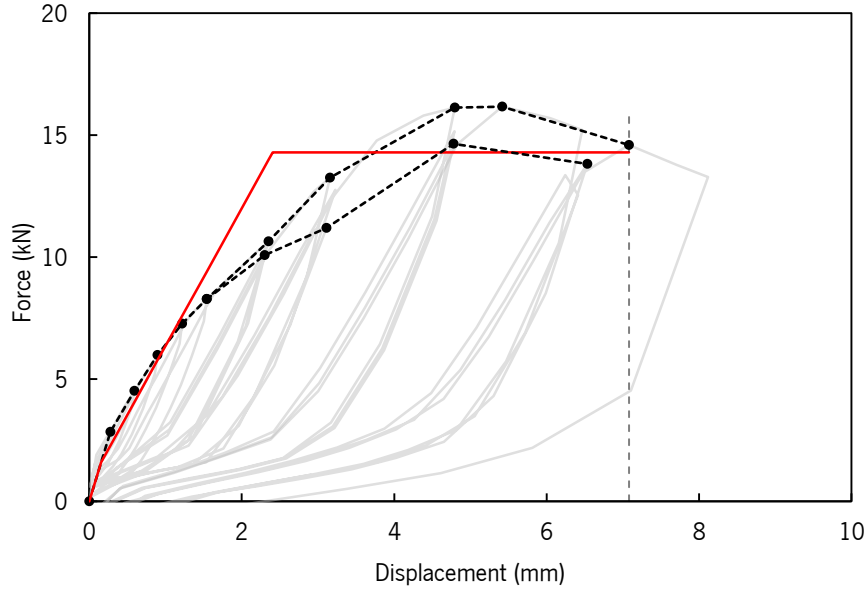

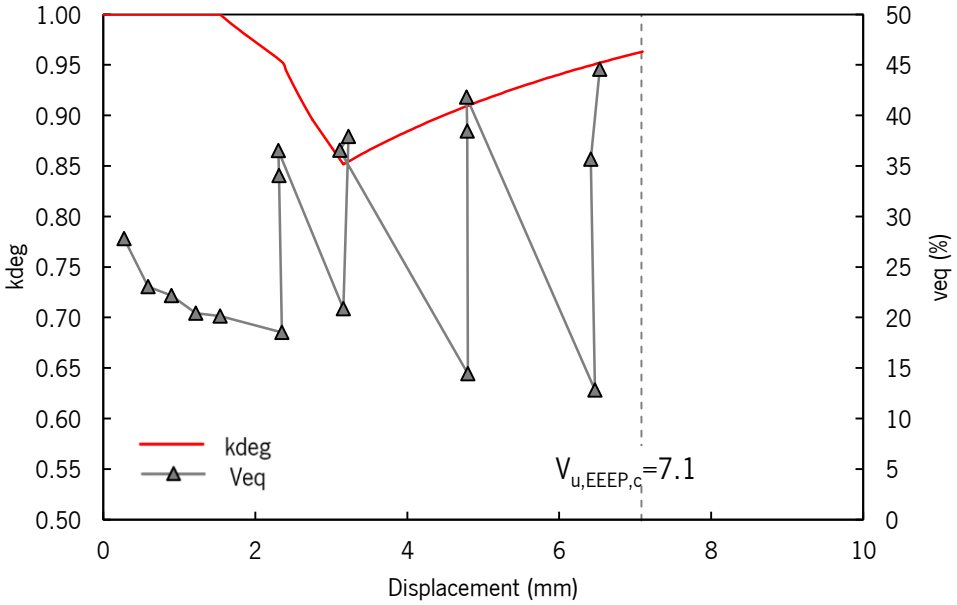

Failure mechanism:

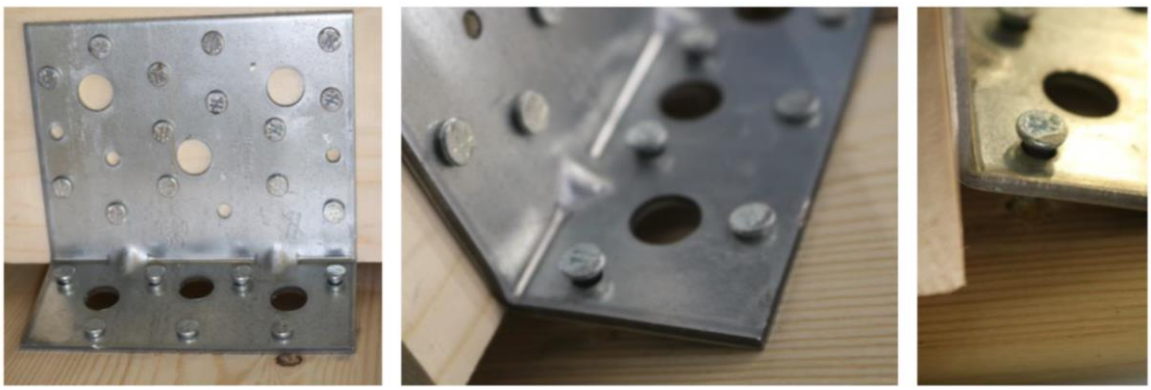

ID: **AE116_UTC3**

Type: AE116 Simpson Strong-Tie
Test Load: Cyclic
Protocol: EN 12512 [5]
Rate [mm/s]: 0.275/1.25
$V_{y,EEEP,m}$ [mm]: 1.7
$K_{deg,min}$: 0.60

Notes:
Base support: CLT 100 C5S C24
Test direction: Uplift/Tension
AE116 + 14 x CNA Annular ring nails (Ø4x60 mm) + 7 x CNA Annular ring nails (Ø4x60)

Results

Maximum Load	$F_{max,c}$	16.9	[kN]
EEEP Ultimate displacement	$V_{u,EEEP,c}$	6.7	[mm]
Failure type	-	(i)	[-]
EEEP Stiffness	$K_{EEEP,c}$	7658	[kN/m]
EEEP Yield displacement	$V_{y,EEEP,c}$	1.9	[mm]
EEEP Yield force	$F_{y,EEEP,c}$	15.1	[kN]
EEEP Ductility	$D_{EEEP,c}$	3.6	[-]
Design degradation factor	k_{deg}	0.81	[-]

Comments:
Test: Cyclic 3
Setup: University of Minho

(i) Failure

Step	1st Cycle			2nd Cycle			3rd Cycle		
	V_{max} [mm]	$F_{(Vmax)}$ [kN]	V_{eq} [%]	V_{max} [mm]	$F_{(Vmax)}$ [kN]	V_{eq} [%]	V_{max} [mm]	$F_{(Vmax)}$ [kN]	V_{eq} [%]
1	0.3	3.7	24.4	-	-	-	-	-	-
2	0.5	5.6	15.9	-	-	-	-	-	-
3	0.8	7.0	13.5	-	-	-	-	-	-
4	1.1	8.4	13.7	-	-	-	-	-	-
5	1.4	9.5	14.5	-	-	-	-	-	-
6	2.1	11.8	13.4	2.1	11.5	24.6	2.0	11.0	25.6
7	2.9	14.3	15.4	2.9	13.5	28.4	2.8	11.5	26.0
8	4.5	16.9	11.7	4.4	15.7	30.0	4.4	15.1	32.7
9	6.1	16.9	12.3	6.1	14.2	27.1	6.2	15.0	34.9

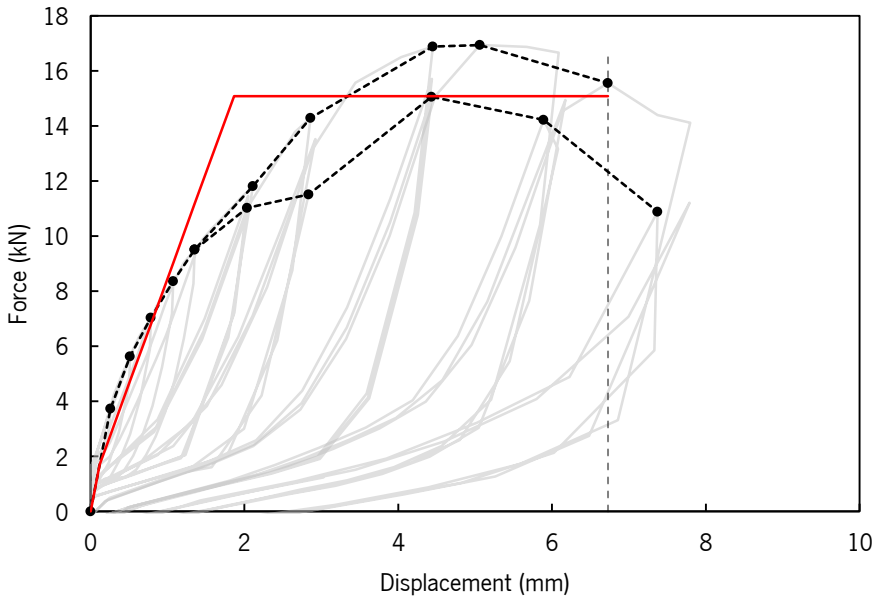

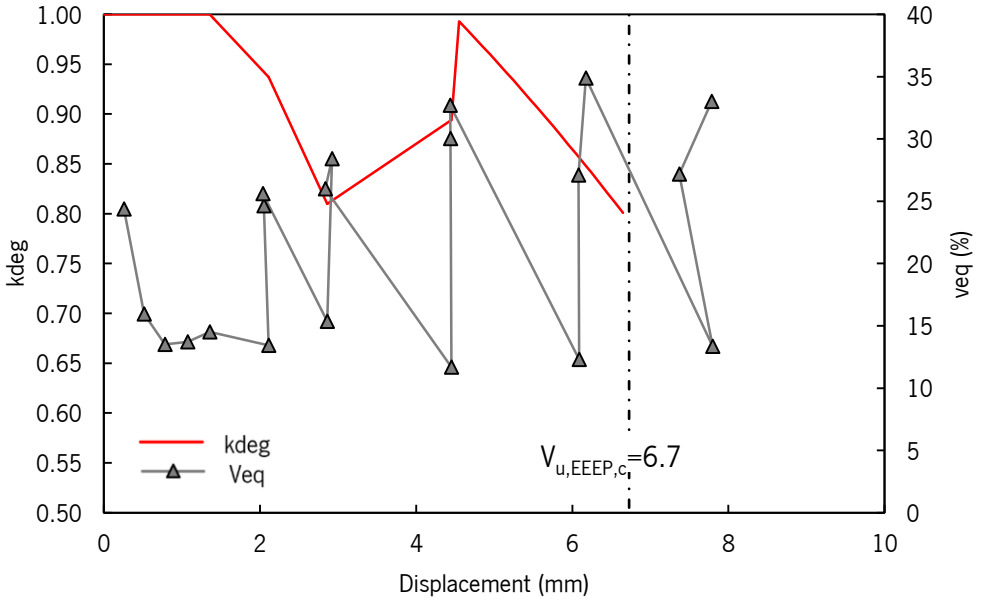

Failure mechanism:

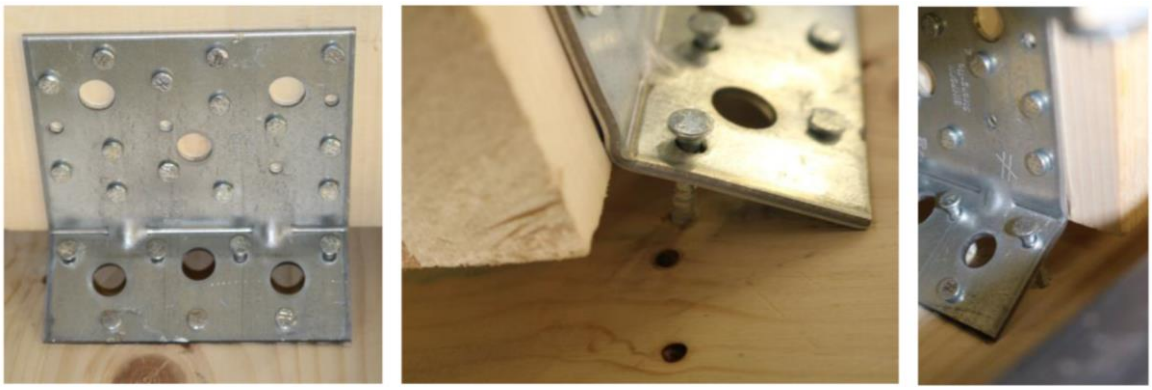

ID: **HTT22_UTC1**

Type: HTT22 Simpson Strong-Tie
Test Load: Cyclic
Protocol: EN 12512 [5]
Rate [mm/s]: 0.275/1.25
$V_{y,EEEP,m}$ [mm]: 13.5
$K_{deg,min}$: 0.60

Notes:
Base support: CLT 100 C5S C24
Test direction: Uplift/Tension
HTT22 + 15 x CNA Annular ring nails (Ø4x60 mm) + 1 Threaded road 8.8 Ø16

Results

Maximum Load	$F_{max,c}$	53.8	[kN]
EEEP Ultimate displacement	$V_{u,EEEP,c}$	18.9	[mm]
Failure type	-	(i)	[-]
EEEP Stiffness	$K_{EEEP,c}$	5870	[kN/m]
EEEP Yield displacement	$V_{y,EEEP,c}$	6.9	[mm]
EEEP Yield force	$F_{y,EEEP,c}$	42.4	[kN]
EEEP Ductility	$D_{EEEP,c}$	2.7	[-]
Design degradation factor	k_{deg}	0.91	[-]

Comments:
Test: Cyclic 1
Setup: University of Minho

(i) Failure

Step	1st Cycle			2nd Cycle			3rd Cycle		
	V_{max} [mm]	$F_{(Vmax)}$ [kN]	V_{eq} [%]	V_{max} [mm]	$F_{(Vmax)}$ [kN]	V_{eq} [%]	V_{max} [mm]	$F_{(Vmax)}$ [kN]	V_{eq} [%]
1	2.2	17.6	23.0	-	-	-	-	-	-
2	4.7	25.6	13.2	-	-	-	-	-	-
3	7.2	32.4	14.2	-	-	-	-	-	-
4	9.8	37.7	14.9	-	-	-	-	-	-
5	16.2	50.2	10.6	-	-	-	-	-	-
6	18.9	53.8	18.9	19.0	52.1	33.3	19.0	49.1	35.2

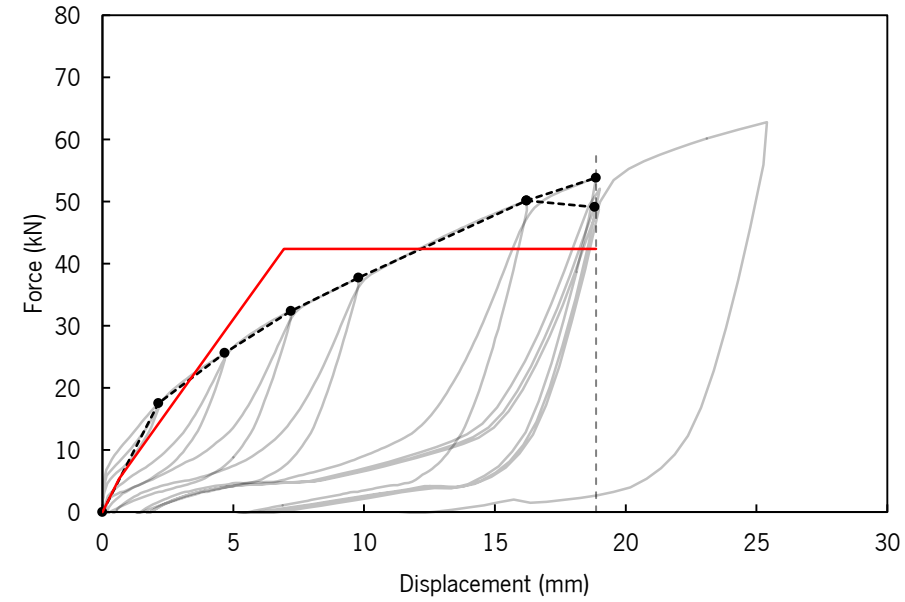

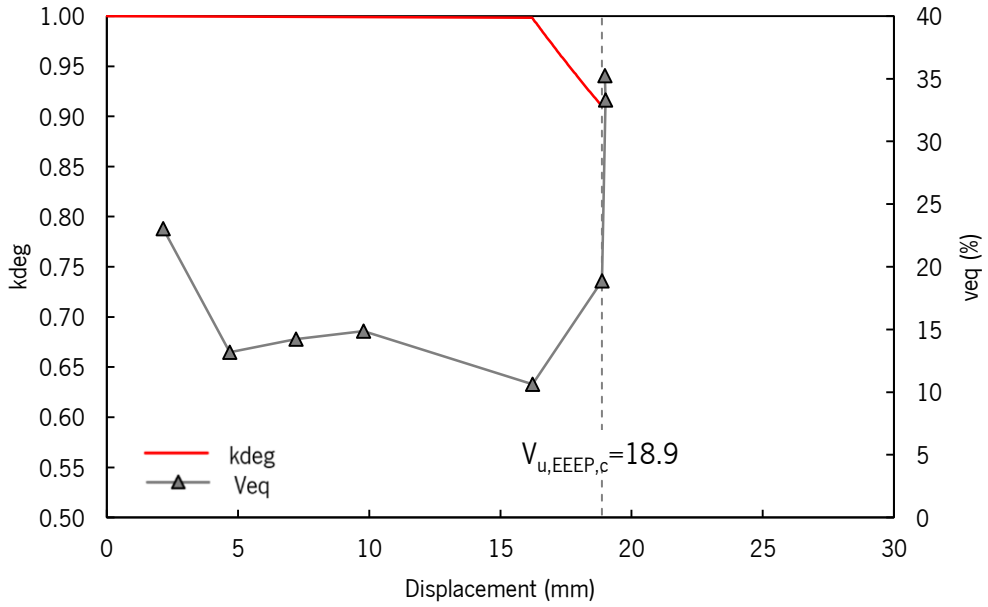

Failure mechanism:

ID: **HTT22_UTC2**

Type: HTT22 Simpson Strong-Tie
Test Load: Cyclic
Protocol: EN 12512 [5]
Rate [mm/s]: 0.275/1.25
$V_{y,EEEP,m}$ [mm]: 13.5
$K_{deg,min}$: 0.60

Notes:
Base support: CLT 100 C5S C24
Test direction: Uplift/Tension
HTT22 + 15 x CNA Annular ring nails (Ø4x60 mm) + 1 Threaded road 8.8 Ø16

Results

Maximum Load	$F_{max,c}$	55.9	[kN]
EEEP Ultimate displacement	$V_{u,EEEP,c}$	18.9	[mm]
Failure type	-	(i)	[-]
EEEP Stiffness	$K_{EEEP,c}$	6205	[kN/m]
EEEP Yield displacement	$V_{y,EEEP,c}$	6.9	[mm]
EEEP Yield force	$F_{y,EEEP,c}$	44.4	[kN]
EEEP Ductility	$D_{EEEP,c}$	2.7	[-]
Design degradation factor	k_{deg}	0.88	[-]

Comments:
Test: Cyclic 2
Setup: University of Minho

(i) Failure

Step	1st Cycle			2nd Cycle			3rd Cycle		
	V_{max} [mm]	$F_{(Vmax)}$ [kN]	V_{eq} [%]	V_{max} [mm]	$F_{(Vmax)}$ [kN]	V_{eq} [%]	V_{max} [mm]	$F_{(Vmax)}$ [kN]	V_{eq} [%]
1	2.3	18.2	24.1	-	-	-	-	-	-
2	4.7	27.2	14.1	-	-	-	-	-	-
3	7.3	34.0	14.3	-	-	-	-	-	-
4	9.8	39.7	15.2	-	-	-	-	-	-
5	16.2	52.3	10.5	-	-	-	-	-	-
6	18.9	55.9	18.4	19.0	53.9	34.0	18.9	50.9	35.9

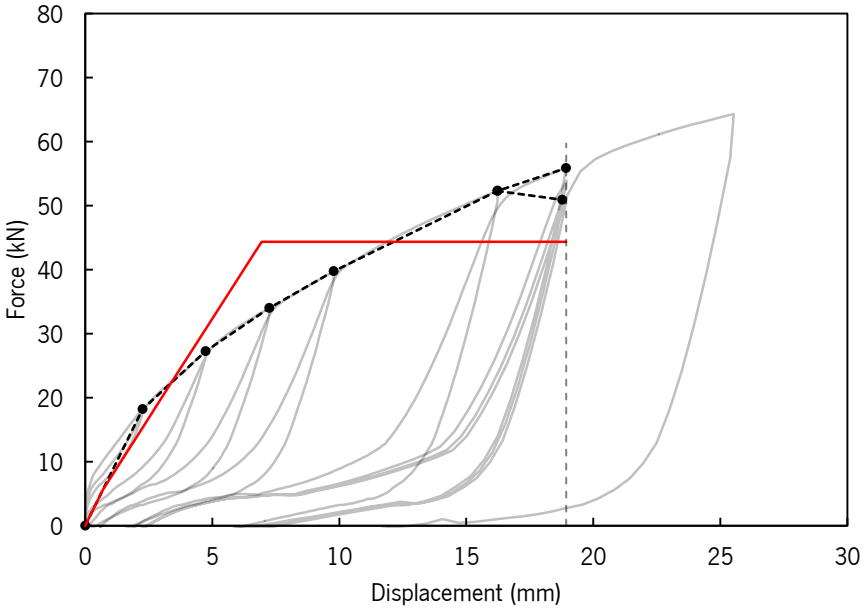

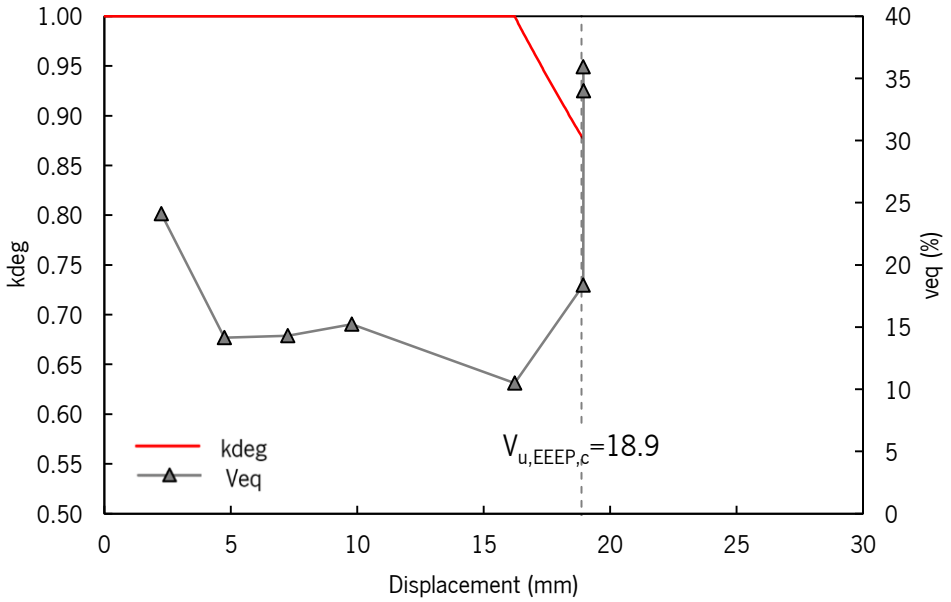

Failure mechanism:

ID: **HTT22_UTC3**

Type: HTT22 Simpson Strong-Tie
Test Load: Cyclic
Protocol: EN 12512 [5]
Rate [mm/s]: 0.275/1.25
$V_{y,EEEP,m}$ [mm]: 13.5
$K_{deg,min}$: 0.60

Notes:
Base support: CLT 100 C5S C24
Test direction: Uplift/Tension
HTT22 + 15 x CNA Annular ring nails (Ø4x60 mm) + 1 Threaded road 8.8 Ø16

Results

Maximum Load	$F_{max,c}$	54.8	[kN]
EEEP Ultimate displacement	$V_{u,EEEP,c}$	19.4	[mm]
Failure type	-	(i)	[-]
EEEP Stiffness	$K_{EEEP,c}$	7293	[kN/m]
EEEP Yield displacement	$V_{y,EEEP,c}$	5.9	[mm]
EEEP Yield force	$F_{y,EEEP,c}$	44.0	[kN]
EEEP Ductility	$D_{EEEP,c}$	3.3	[-]
Design degradation factor	k_{deg}	0.90	[-]

Comments:
Test: Cyclic 3
Setup: University of Minho

(i) Failure

Step	1st Cycle			2nd Cycle			3rd Cycle		
	V_{max} [mm]	$F_{(Vmax)}$ [kN]	V_{eq} [%]	V_{max} [mm]	$F_{(Vmax)}$ [kN]	V_{eq} [%]	V_{max} [mm]	$F_{(Vmax)}$ [kN]	V_{eq} [%]
1	2.3	22.2	12.7	-	-	-	-	-	-
2	4.9	29.9	11.3	-	-	-	-	-	-
3	7.5	35.6	12.3	-	-	-	-	-	-
4	10.1	40.9	14.9	-	-	-	-	-	-
5	16.6	51.8	10.2	-	-	-	-	-	-
6	19.4	54.9	18.1	19.6	52.7	31.8	19.5	49.6	33.1

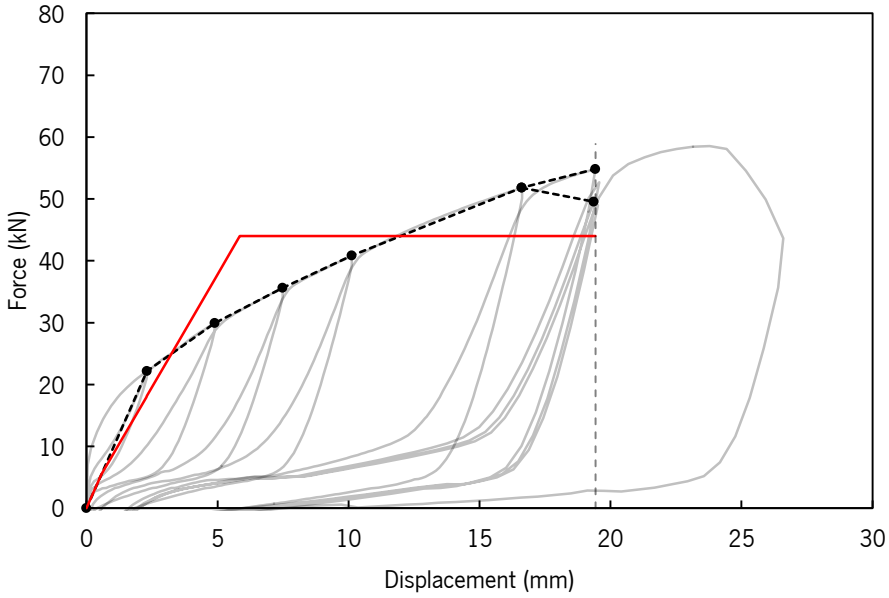

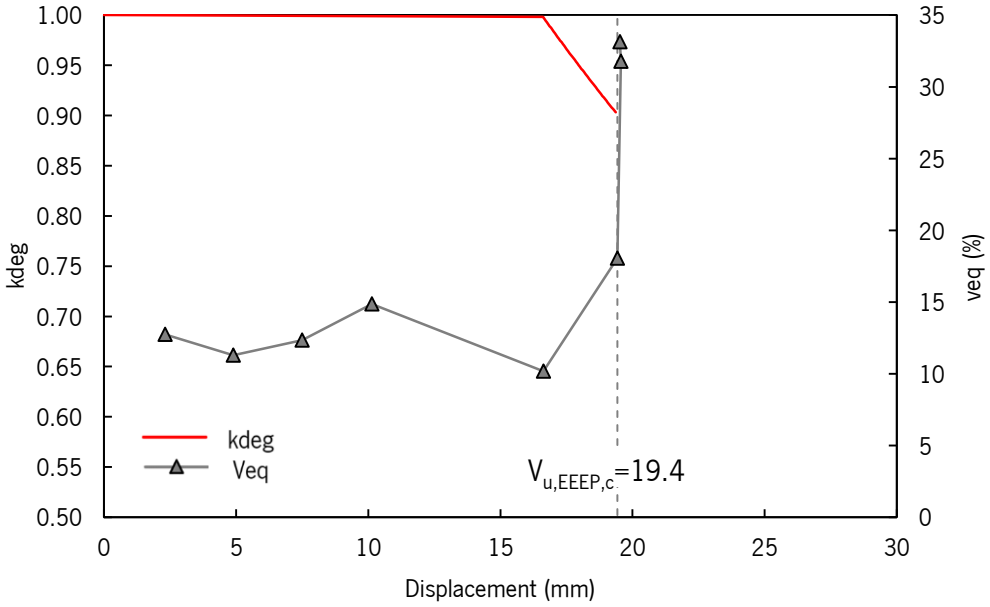

Failure mechanism:

ID: **HTT22E_UTC1**

Type: HTT22E Simpson Strong-Tie
Test Load: Cyclic
Protocol: EN 12512 [5]
Rate [mm/s]: 0.275/1.25
$V_{y,EEEP,m}$ [mm]: 6.1
$K_{deg,min}$: 0.60

Notes:
Base support: CLT 100 C5S C24
Test direction: Uplift/Tension
HTT22 + 15 x CNA Annular ring nails (Ø4x60 mm) + 1 Threaded road 8.8 Ø16

Results

Maximum Load	$F_{max,c}$	72.2	[kN]
EEEP Ultimate displacement	$V_{u,EEEP,c}$	23.3	[mm]
Failure type	-	(i)	[-]
EEEP Stiffness	$K_{EEEP,c}$	7383	[kN/m]
EEEP Yield displacement	$V_{y,EEEP,c}$	7.6	[mm]
EEEP Yield force	$F_{y,EEEP,c}$	60.2	[kN]
EEEP Ductility	$D_{EEEP,c}$	3.1	[-]
Design degradation factor	k_{deg}	0.92	[-]

Comments:
Test: Cyclic 1
Setup: University of Minho

(i) Failure

Step	1st Cycle			2nd Cycle			3rd Cycle		
	V_{max} [mm]	$F_{(Vmax)}$ [kN]	V_{eq} [%]	V_{max} [mm]	$F_{(Vmax)}$ [kN]	V_{eq} [%]	V_{max} [mm]	$F_{(Vmax)}$ [kN]	V_{eq} [%]
1	1.1	16.2	22.1	-	-	-	-	-	-
2	2.2	23.4	16.6	-	-	-	-	-	-
3	3.4	28.7	15.1	-	-	-	-	-	-
4	4.6	33.9	16.5	-	-	-	-	-	-
5	5.9	38.6	17.9	-	-	-	-	-	-
6	9.1	49.0	12.9	9.0	47.2	31.3	9.0	45.1	30.4
7	12.2	58.2	14.5	12.3	55.7	31.9	12.4	54.5	34.7
8	18.8	68.3	10.9	18.9	63.3	30.4	19.0	63.2	34.7
9	26.5	36.7	5.9	26.8	30.1	26.1	26.8	26.9	32.9

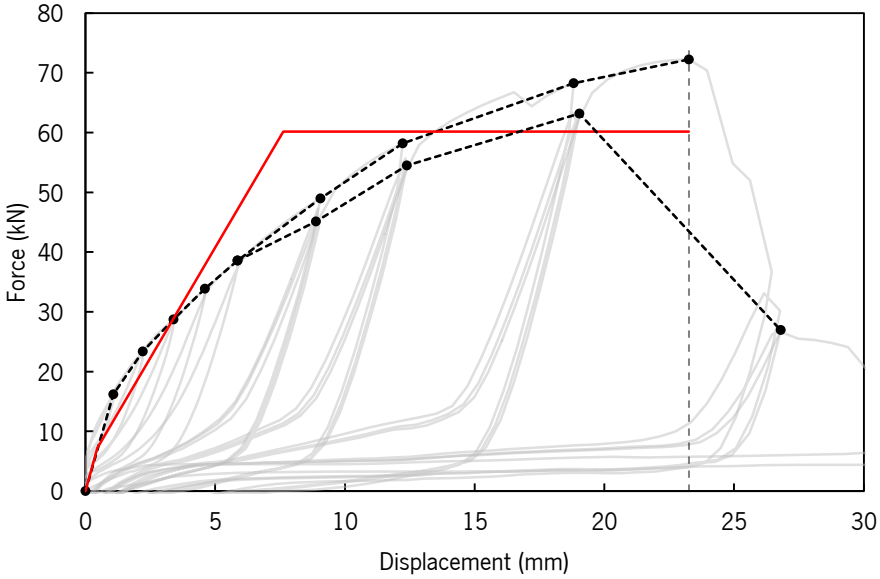

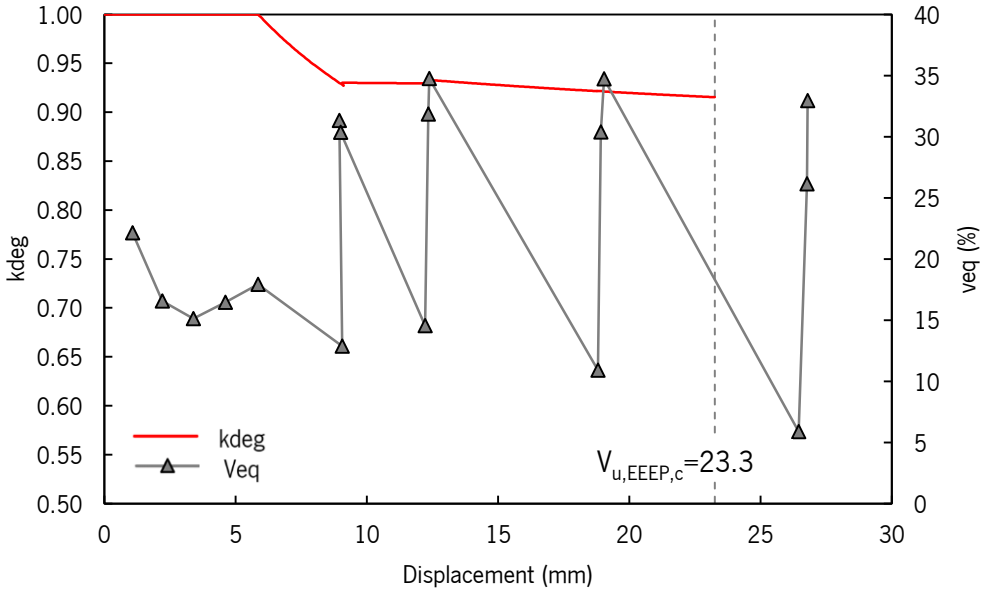

Failure mechanism:

ID: **HTT22E_UTC2**

Type: HTT22E Simpson Strong-Tie
Test Load: Cyclic
Protocol: EN 12512 [5]
Rate [mm/s]: 0.275/1.25
$V_{y,EEEP,m}$ [mm]: 6.1
$K_{deg,min}$: 0.60

Notes:
Base support: CLT 100 C5S C24
Test direction: Uplift/Tension
HTT22 + 15 x CNA Annular ring nails (Ø4x60 mm) + 1 Threaded road 8.8 Ø16

Results

Maximum Load	$F_{max,c}$	61.7	[kN]
EEEP Ultimate displacement	$V_{u,EEEP,c}$	19.4	[mm]
Failure type	-	(i)	[-]
EEEP Stiffness	$K_{EEEP,c}$	9042	[kN/m]
EEEP Yield displacement	$V_{y,EEEP,c}$	4.9	[mm]
EEEP Yield force	$F_{y,EEEP,c}$	50.3	[kN]
EEEP Ductility	$D_{EEEP,c}$	3.9	[-]
Design degradation factor	k_{deg}	0.92	[-]

Comments:
Test: Cyclic 2
Setup: University of Minho

(i) Failure

Step	1st Cycle			2nd Cycle			3rd Cycle		
	V_{max} [mm]	$F_{(Vmax)}$ [kN]	V_{eq} [%]	V_{max} [mm]	$F_{(Vmax)}$ [kN]	V_{eq} [%]	V_{max} [mm]	$F_{(Vmax)}$ [kN]	V_{eq} [%]
1	1.2	19.7	16.8	-	-	-	-	-	-
2	2.4	24.8	14.2	-	-	-	-	-	-
3	3.7	29.5	15.3	-	-	-	-	-	-
4	4.9	33.8	17.4	-	-	-	-	-	-
5	6.2	38.2	19.8	-	-	-	-	-	-
6	9.4	46.8	13.7	9.3	45.0	35.4	9.4	42.7	39.9
7	12.7	54.3	15.4	12.8	51.8	37.5	12.8	50.5	41.0
8	19.4	61.8	11.0	19.4	56.4	32.9	19.5	56.0	38.0

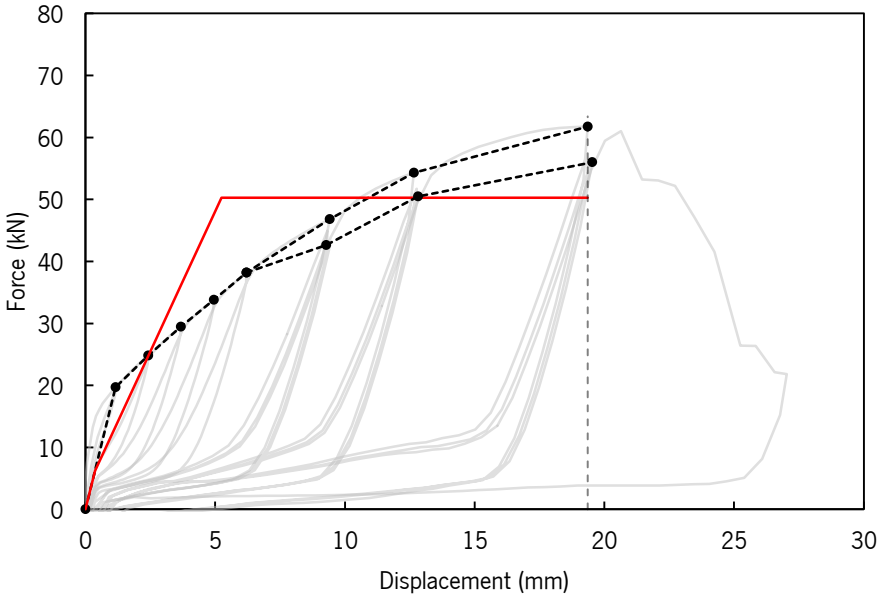

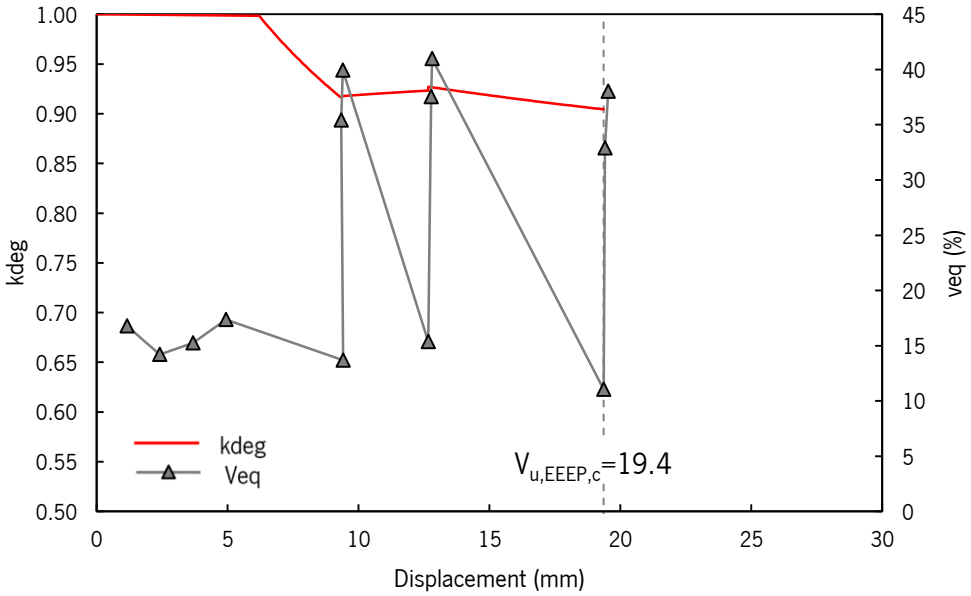

Failure mechanism:

ID: **HTT22E_UTC3**

Type: HTT22E Simpson Strong-Tie
Test Load: Cyclic
Protocol: EN 12512 [5]
Rate [mm/s]: 0.275/1.25
$V_{y,EEEP,m}$ [mm]: 6.1
$K_{deg,min}$: 0.60

Notes:
Base support: CLT 100 C5S C24
Test direction: Uplift/Tension
HTT22 + 15 x CNA Annular ring nails (Ø4x60 mm) + 1 Threaded road 8.8 Ø16

Results

Maximum Load	$F_{max,c}$	63.5	[kN]
EEEP Ultimate displacement	$V_{u,EEEP,c}$	19.4	[mm]
Failure type	-	(i)	[-]
EEEP Stiffness	$K_{EEEP,c}$	5136	[kN/m]
EEEP Yield displacement	$V_{y,EEEP,c}$	8.7	[mm]
EEEP Yield force	$F_{y,EEEP,c}$	51.8	[kN]
EEEP Ductility	$D_{EEEP,c}$	2.2	[-]
Design degradation factor	k_{deg}	0.88	[-]

Comments:
Test: Cyclic 3
Setup: University of Minho

(i) Failure

Step	1st Cycle			2nd Cycle			3rd Cycle		
	V_{max} [mm]	$F_{(Vmax)}$ [kN]	V_{eq} [%]	V_{max} [mm]	$F_{(Vmax)}$ [kN]	V_{eq} [%]	V_{max} [mm]	$F_{(Vmax)}$ [kN]	V_{eq} [%]
1	1.2	13.6	21.5	-	-	-	-	-	-
2	2.5	19.4	16.3	-	-	-	-	-	-
3	3.8	23.8	16.1	-	-	-	-	-	-
4	5.1	28.1	17.8	-	-	-	-	-	-
5	6.4	32.6	19.6	-	-	-	-	-	-
6	9.7	42.3	14.5	9.4	40.8	32.0	9.5	39.0	33.5
7	12.8	50.7	15.6	12.8	48.5	32.6	13.0	47.5	36.4
8	19.5	63.5	12.4	19.6	57.8	28.0	19.8	56.4	33.9

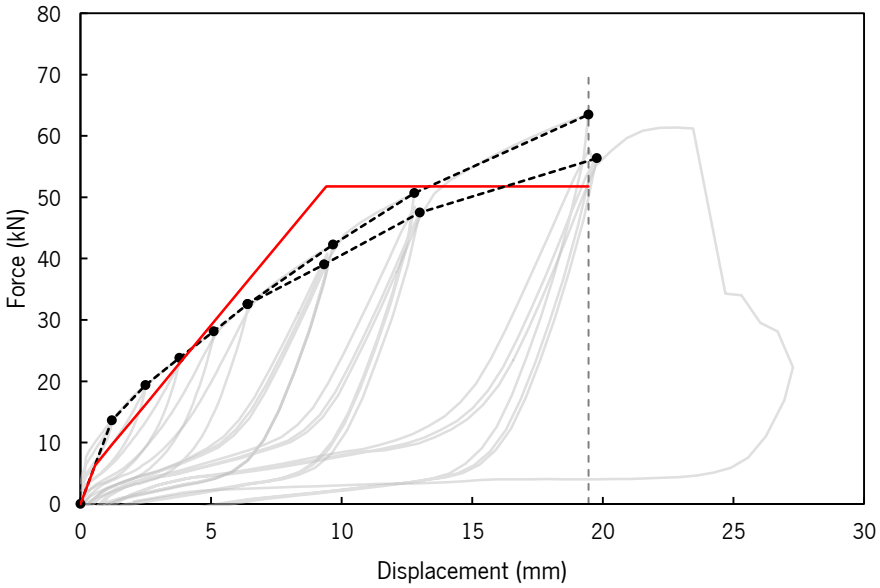

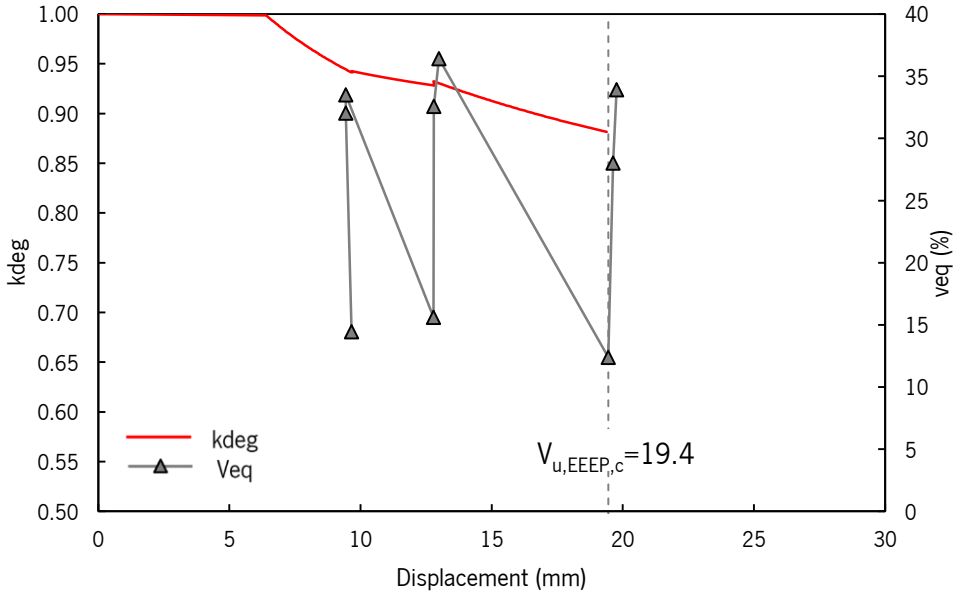

Failure mechanism: